THE DEVELOPMENT OF ABRASIVE-CORROSIVE WEAR RESISTANCE OF STEELS BY MICROSTRUCTURAL CONTROL

by

Keith Cecil Barker

A thesis submitted to the Faculty of Engineering, University of Cape Town in fulfillment of the degree of Doctor of Philosophy

Dept of Materials Engineering
University of Cape Town

February 1988

The copyright of this thesis vests in the author. No quotation from it or information derived from it is to be published without full acknowledgement of the source. The thesis is to be used for private study or non-commercial research purposes only.

Published by the University of Cape Town (UCT) in terms of the non-exclusive license granted to UCT by the author.

University of Cape Town

ABSTRACT

The performance of developmental alloyed steels with improved abrasive- corrosive wear resistant properties has been evaluated. The synergistic effect of abrasion and corrosion in the accelerated wear of steels is examined and the main parameters identified. A model of the process is proposed. The model is used to develop the optimum abrasive-corrosive wear resistance in steels for applications in the gold mines of South Africa.

A wide range of engineering steels, both commercially available and experimental, has been evaluated in laboratory simulated abrasive and abrasive-corrosive wear tests. An appraisal of the wear tests and the applicability of the results to in-service conditions has led to the development of an additional abrasive-corrosive wear test. It has been established that both the microstructure and chemical composition determine the resistance of a material to wear. Control of the microstructure by alloying and heat treatment is attempted in order to optimise the abrasive-corrosive wear resistant properties for each class of microstructure whilst maintaining adequate formability and weldability.

Abrasion of a metal surface has been shown to accelerate the rate of corrosion. Three categories of corrosion behavior are defined. A model of the abrasive-corrosive wear process is proposed to account for the behavior. The model adequately predicts the outcome to a change in system parameter, namely : an increase in the corrosivity of the water, an increase in the frequency of abrasive events, a change in the chemical composition and the degree of passivity inherent in the material. Recommendations are made to maximize the abrasive-corrosive wear resistant properties without resorting to expensive highly alloyed steels.

To satisfy the needs of the mining industry, two microstructures of note are identified: a metastable austenitic (TRIP type) steel and a 0.25% carbon lath martensitic alloyed steel. A basic chemical composition is proposed with each microstructure. The austenitic steel is shown to achieve its abrasion resistance through the high degree of work hardening it undergoes during abrasion and the high ultimate strength of the strained material. The lath martensitic steel has the necessary strength to toughness ratio for good abrasion resistance. A 20% degree of work hardening in conjunction with a bulk hardness in excess of 500 HV is prescribed for superior abrasion resistant properties in the wear system of the mines. The life time cost of the martensitic alloyed steel recommends it for applications in the gold mines of South Africa.

ACKNOWLEDGEMENTS

I wish to express my appreciation to all those who assisted me during the course of this research project, in particular:

Professor A. Ball, my supervisor, for his advice and support.

Mrs Gay Perez for her invaluable experimental assistance.

Mrs H Böhm, Mrs S Betz, Ms T Leveton, Ms C Lang and Ms F Barker for their help in the preparation of the final manuscript.

Mr B Greeves and Mr J Petersen for the photographic work. Mr N Dreze and Mr A Rapley for their technical assistance.

The Staff and my fellow students for their support and encouragement.

The CSIR and COMRO are gratefully acknowledged for the provision of research bursaries

This thesis was based on the results of the collaborative programme of work undertaken as part of the research and development programme of the Research Organisation of the Chamber of Mines of South Africa.

CONTENTS Page

A GLOSSARY OF SYMBOLS AND ABBREVIATIONS

bcc	body centred cubic
bct	boby centred tetragonal
E_b	breakdown potential corresponding to uniform breakdown of the passive oxide film
E_{corr}	corrosion potential
E_p	pitting potential corresponding to localised breakdown of passivity
E_x	protection potential
fcc	face centred cubic
F.F.	Ferrite Factor
ΔF	difference in free energy
HV	Vickers hardness units
i	induction period (elapsed time)
J	Joules
M_d	Temperature below which a transformation to martensite will occur if induced by strain (deformation)
M_f	Temperature at which there is complete transformation to martensite (finish)
M_s	Temperature at which transformation to martensite begins on cooling (start)
n	work hardening exponent
pH	log $[H^+]^{-1}$
ppm	concentration in parts per million
Q	free energy of activation
Q_{dif}	activation energy for diffusion
Q_{dsln}	activation energy for dissolution
Q_s	activation energy and entropy for the forward reaction
r	rate of volume loss
RAR	Relative Abrasion Resistance (laboratory test)
RWRL	Relative Abrasive-Corrosive Wear Resistance (laboratory test)
RWRL#2	Relative Abrasive-Corrosive Wear Resistance (laboratory test) alternative conditions
SEM	Scanning Electron Microscope
S.H.E.	standard hydrogen electrode
t	time
TDS	Total Dissolved Solids
TRIP	Tranformation Induced Plasticity
v	accumulative volume loss

ERRATA

Throughout the text where TRIP steels is read, it should read TRIP type steels.

Chapter 3, page 82, Steels from Source F; The reader would get a more accurate account of the development of the Source F alloys from Lenel and Knott (1987): "Microstructure - Composition Relations and M_S temperatures in Fe-Cr-Mn-N alloys", Metallurgical Transactions A, 18A, 767-775. Lenel and Knott (1987); "Structure and properties of corrosion and wear resistant Cr-Mn-N steels", Metallurgical Transactions A, 18A, 847-855.

Chapter 4, page 113, last sentence; "The assumed value of 40 Joules for the toughness of the Source F alloys was conservative. The above two references put the impact toughness closer to 200 J for these alloys. This will move the relative position of these alloys in Tables 4.9 and 4.11.

Chapter 4, page 119, Table 4.15:

Material	Hardness	Toughness
3CR12 iii	250	80
F351	225	200
AISI 440B	648	5

CHAPTER 1

INTRODUCTION

1.1 WEAR

The concepts of material selection and wear must have come conjoint with mans earliest search for a "better" tool. The critical study of abrasive wear is of recent interest dating from the 1950's while research in corrosion had been active for some decades.

The principle phenomenon of wear is the removal of material from surfaces by mechanical and/or chemical processes - any embellishment on this is then defining a particular tribo-system. For example, abrasive wear is defined as the removal of solid material from a surface by the unidirectional sliding action of discrete particles of another material (Moore, 1974). Corrosive wear can be defined as the progressive loss of original material from a solid surface by its chemical interaction with the environment.

Wear in the Mining Industry is considered to be due to both mechanical abrasion and chemical corrosion although it is often used synonymously with abrasive wear which is in many cases the dominant process (Powell, 1972). The role of corrosion in the wear of metals which are continuously or intermittently abraded is often under estimated because no obvious corrosion product is observed.

1.2 MOTIVATION

The cost of mining and processing gold bearing ore is escalating continually in South Africa. Traditionally the high cost attributed to wear has been accepted as inevitable when mining gold. It is often seen as an insoluble problem which is best overcome by the use of cheap materials. The hidden costs include down-time and the repetitive and labour intensive routine replacement of worn parts (Mokken, 1977; Protheroe, 1979).

There is presently a move away from the traditional labour intensive mining methods to a mechanised mining system (Joughin, 1975). Research into mining methods to improve productivity and efficiency has high-

lighted many problem areas (Joughin, 1978). The success of the new mechanised mining systems will depend on overcoming the effects of severe wear on the reliability and economic life of the equipment (Protheroe, 1979). It is firmly believed that substantial savings can be achieved by sophistication in the choice and utilisation of materials (Mokken, 1979).

The matrix for gold is quartzite. The extreme hardness of this material (900 to 1300 HV) implies that all equipment used in the mining and transportation of this ore is subject to abrasive wear. In addition, the high relative humidity (commonly at 95%) and the poor quality of mine service waters makes corrosion the most pernicious and widespread of problems (Higginson and White, 1983). Although the conditions in the South African gold mines are particularly harsh, the need for research into wear in the Mining Industry is a world wide problem ("War on Wear" Conference IMechE, 1984).

The Research Organisation of the Chamber of Mines of South Africa (COMRO) has identified areas of particular concern in their mechanisation development program. An example related to corrosive-abrasive wear is the deterioration of the pans of shaker conveyors which are used with non-explosive mining methods to move rock underground both at the stope face and in gullies. Shaker conveyors comprise a number of individual pans usually 2 metres long which can be welded together to reach a length of 80 metres. In operation the rock is accelerated down-dip in contact with the pan, which is then pulled up-dip, allowing the rock to slide over the pan as static friction is overcome. Repetition of this cycle results in a net down-dip motion of the rock (Protheroe, 1979). The mild steel pans exhibited a classic low-stress gouging abrasion wear mechanism with a large corrosion contribution to the overall wear process (Noël, 1981).

Previous investigations have identified the importance of understanding the wear mechanisms (Allen, Protheroe and Ball, 1981), highlighted the importance of the microstructure of a steel in containing wear (Harris, 1983) and identified the role played by corrosion (Noël, 1981). Protheroe, Ball and Heathcock (1982) have highlighted the need for a limited number of low cost, general engineering steels which are resistant to both general corrosion and abrasion by quartzite, irrespective of the nature or type of abrasion. These steels would find application throughout the gold mining industry and be used for both internal and external parts of machines subject to abrasion with or without corrosion.

1.3 THE APPROACH TAKEN

The need for one or more general purpose abrasion and corrosion resistant steel has been identified. The practical requirements and characteristics of such a steel are according to Protheroe, Ball and Heathcock, (1982) :

a) a resistance to general corrosion in the underground environment.

b) a high resistance to abrasion by quartzite.

c) a toughness sufficient for general structural engineering applications (minimum Charpy impact energy of 35 Joules).

d) an ability to undergo simple heat treatments so as to alter the hardness and toughness.

e) be reasonably formable, machinable and weldable.

f) the cost should be kept as low as possible.

A wide range of materials are readily available for use in either abrasive or corrosive wear applications but none of these materials have yet proved adequate in meeting the combination of requirements specific to the mining industry of South Africa (Allen, Ball and Noël, 1984). Consequently, an alternative approach through microstructural design has been undertaken in which new alloy compositions are formulated to provide the necessary operational benefits (Protheroe, Ball and Heathcock, 1982; Allen, Ball and Noël, 1984; Bee, Peters, Atkinson and Garrett, 1985). In meeting this demand for new steels, a collaborative program of research in alloy development has been orchestrated by COMRO with various universities, steel manufacturers and overseas research institutions.

1.4 OBJECTIVES

Two important aspects of any alloy development programme is the testing and evaluation of materials as they become available, and to understand fully the mechanisms giving rise to the problem under consideration. The objectives of this dissertation are divided into three parts.

1. To evaluate the performance of potential abrasive-corrosive wear resistant alloys for mining applications

   by (a) comparing the performance of experimental and commercial steels with propriety wear resistant steels;

   (b) ranking the materials with respect to dry abrasion resistance and abrasion-corrosion resistance.

2. To develop an understanding of the synergistic effects of abrasion and corrosion in the wear of steels

   by (a) determining the influence the microstructure, alloying content, fabrication route and heat treatment have on a materials wear performance;

   (b) investigating the material's resistance to corrosion and how this may be affected by the process of abrasion, the abraded surface, the period of corrosion, and the environment;

   (c) relating the properties of the material to its wear resistance and identifing the salient features of a superior wear resistant steel.

3. To design a superior abrasive-corrosive wear resistant steel which meets the requirements listed in section 1.3.

A programme has therefore been established towards solving the problem of abrasive-corrosive wear through material selection and design. This research should make it possible to understand the major mechanisms which constitute the wear process and enable one to recommend alloy steels which would best control and economically extend wear life, with considerable savings to the Mining Industry.

CHAPTER 2

LITERATURE SURVEY

2.1 ABRASION

The following discussion of the abrasion wear process is limited for simplicity to dry, two-body abrasive wear. The emphasis will be on low-stress gouging abrasion (Rigney and Glaeser, 1977) as typified by the rubber wheel test (ASTM STP 615, 1976) or the pin on abrasive paper test (Mulhearn and Samuels, 1962).

2.1.1 Dry, two body Abrasive Wear

Abrasion is a form of wear mediated by hard particles. These particles can range from boulder size chunks of ore sliding down a chute to micron sized grit which have contaminated the internals of a machine. Stress is involved in any abrasive situation and the abrasives act to concentrate this stress.

In the 1950's, Krushchov and Babichev as cited in numerous reviews (Richardson, 1967; Avery, 1974, Moore, 1974) identified two processes taking place when abrasive grains make contact with the wearing surface :

a) the formation of plastically impressed grooves which do not involve metal removal; and

b) the separation of metal particles in the form of microchips.

Thus, besides the stress intensity factor there is a vertical deformation component of a hard asperity penetrating a softer surface, and a translational shearing action involving sliding of the abrasive across the surface and fracture .

Mulhearn and Samuels (1962), in studying the characteristics of abrasive papers, defined a critical attack angle above which a chip is cut by the abrasive and below which it is not. Murray, Mutton and Watson (1979) identified two mechanisms of groove formation

namely cutting and ploughing. They found that a mixed mode of groove formation (cutting and ploughing) can be expected for a wide range of abrasive shapes and materials. Generally, material removal occurs by a micro-cutting process which produces chips or other less well defined fragments. Grooves can also be formed without material removal, solely by plastic deformation. If an estimated 40% of the total groove volume (Moore, 1974) is removed as wear debris, the remainder is displaced by plastic flow to the sides to form ridges. Larsen-Basse (1968) calculated that only 15% of the groove volume for copper is removed as chips. A measure of abrasion resistance would then be associated with the pile up of material (plastic flow) in relation to the material that is removed. Any microstructural factor which permits extensive plastic flow without fracture would then improve abrasion resistance.

Moore (1980) in his reveiw on abrasive wear, observed that most models are a necessary oversimplification of a very complex process (fig. 2.1). He identified the two major mechanisms of material removal as plastic deformation and fracture (if we are to exclude environmental effects). These mechanisms operate simultaneously except at the upper and lower limits.

Simple fracture is illustrated in the scratching of brittle solids which produce median cracks normal to the surface, and lateral cracks extending from beneath the indention towards the surface. Material is lost when lateral cracks intersect each other or propagate to the surface. Microstructural features which can retard the propagation of said cracks (a measure of micro-toughness) would be necessary to prevent gross volume losses in abrasive wear.

Plastic deformation is involved with (i) the formation of grooves without direct material removal; (ii) the separation of particles in the form of wear debris or primary microchips; (iii) the shear of material to the sides of the grooves which at a later stage becomes detached to form secondary microchips. Thus ultimately material may in the latter stages be removed by fracture but plastic deformation controls the rate at which it is removed. The deformation mechanisms have been refered to as predominantly ploughing, predominantly cutting or a mixed mode of abrasion (Murray, Mutton and Watson, 1979).

The rate of abrasive wear is critically dependent on the volume of debris generated through plastic deformation and fracture processes (fig. 2.1). The type of wear debris is indicative of the mechanisms operating at the worn surface and is unique to the tribological system under examination.

Moore (1980) formulated that the volume of material removed by plastic deformation, V, is a function of

a) the probibility of wear debris formation, K_1

b) the mean proportion of groove volume removed, K_2 (ratio of volume removed to volume displaced)

c) the abrasive particle shape, K_3

d) the applied load, L

e) the surface hardness of the material, H

so that

$$V = K_1.K_2.K_3.L.H^{-1} \qquad ....(1)$$

He cited that the probibility of debris formation and proportion of groove volume removed depends on material properties other than surface hardness.

The external system variables that are introduced in equation (1) are fixed and need to be defined before considering the material parameters and those properties which could favour the route marked in fig. 2.1.

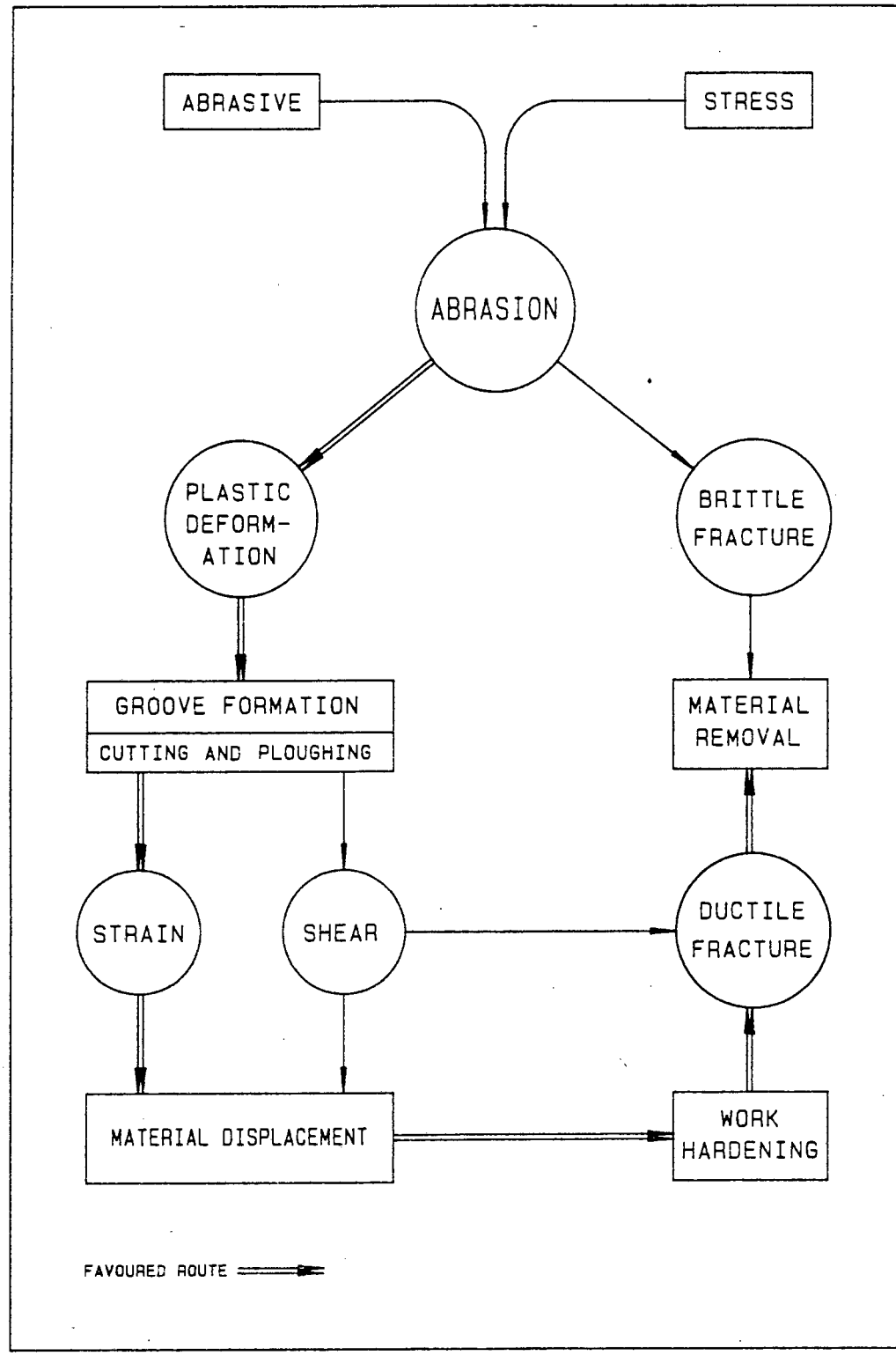

FIGURE 2.1 : An outline of the process of abrasive wear showing the favoured high energy route which would resist the loss of material

2.1.2 Properties and variables of the tribological system

To characterize any tribological system involving abrasive wear, consideration must be given to the properties of the abrasive and the other variables within the system (fig. 2.2).

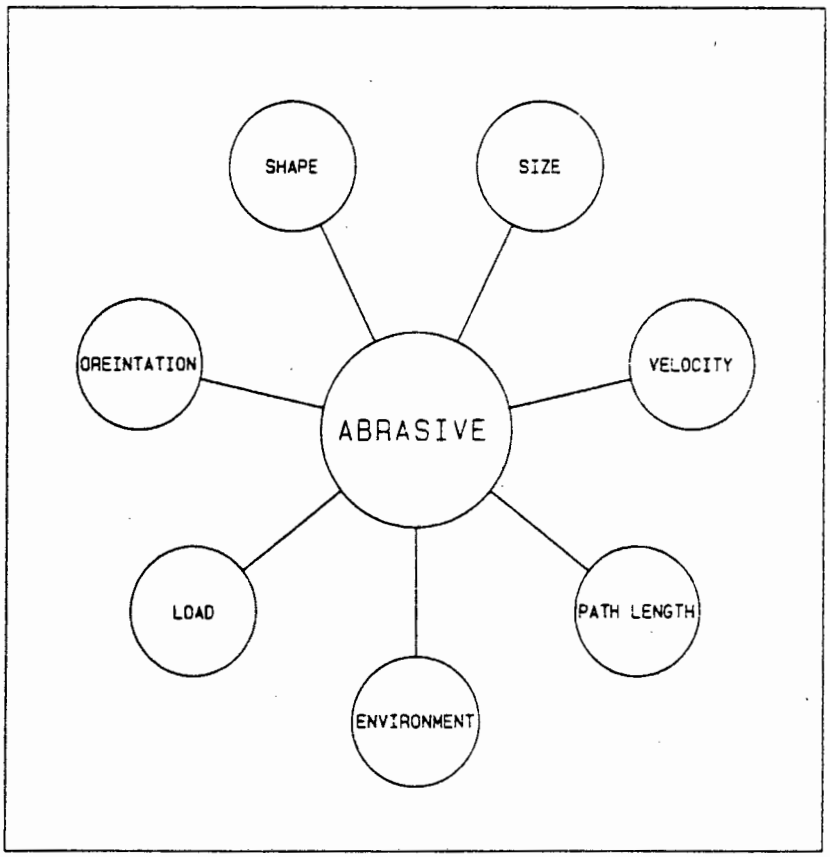

FIGURE 2.2 : External variables in a Tribological system

Moore (1974 and 1980) reviewed the properties of the abrasive. Abrasives are usually inert oxides which can fracture under stress to produce sharp angular fragments. He found that the abrasive type and its hardness relative to the abraded surface does not influence wear resistance except when the two surfaces have approximately equal hardness. The shape of the abrasive particle is important in that it influences the transition from elastic to plastic contact. Wear rate is higher for "sharp" pointed abrasives than for "blunt" rounded abrasives. Quarzite in particular does not become rounded during abrasion but fragments to produce new sharp edges. Abrasion increases as the particle becomes less platelike and thus has less chance of lying flat.

The orientation of the abrasive can influence the formation of wear debris. Mulhearn and Samuels (1962) showed that chips are only produced when the contacting face of an abrasive grain makes an angle greater than the "critical attack angle" with the wearing surface. A transition from ploughing to microchip formation occurs when the critical attack angle is exceeded. Larsen-Basse and Tanouye (1978) showed that wear rate increases with increasing grit size, becoming independent at very large grit sizes. Therefore large rocks can be treated as small grit sized point loads in the study of abrasive wear.

Larsen-Basse (1968) observed that a linear relationship exists between wear rate and abrasive path length after the running-in period. Wear rate is also directly proportional to nominal load up until the load where the abrasive is being crushed. The wear rate per unit load decreases with load and is a function of the material.

Wear has been reported to increase slightly with sliding speed in the range zero to 2.5 m/s (Moore, 1974). Larsen-Basse and Tanouye (1978) found an inverse relationship between removal rate and sliding velocity at very low velocities (0-0.1 m/s). This levels off at higher speeds and is irrespective of abrasive grit size. Allen, Protheroe and Ball (1981/1982) found austenitic stainless steels to be markedly velocity sensitive in the range 0.02 to 0.45 m/s. This was not true for other grades of stainless steel, mild steel or a proprietary abrasion resistant steel. They discussed their findings in the light of the ability of microstructures to accommodate the high strains without fracture.

Where material selection and design are the objectives, the external variables must be eliminated as far as possible. It is suggested (Rigney and Glaeser, 1977) that the nature of the abrasive test (loading, type of abrasive, etc) be as close to the service conditions as possible and remain constant for the duration of the test program. Moore (1980) warns on the dangers of selecting materials on the basis of performance data from tests that do not closely simulate the service conditions. Ball and Ward (1985) discussed this aspect and presented the procedure they followed to ensure that a representitive laboratory test facility was commissioned.

2.1.3 Relationships between materials and abrasion

Mechanical properties

Numerous workers have tried to relate abrasion resistance to a measurable mechanical property with limited success. In Moore's review (1974), elastic modulus and the elastic limit of strain were found to be inversely proportional to the wear volumes for pure metals; but this does not hold for heat treated steels. Torrance (1980) attempted to relate abrasion resistance to hardness and elastic modulus. Kwok (1982) in studying a 0.3C/3Cr/2Mn steel, found abrasion resistance increased with hardness, tensile strength and yield strength. He explained this in terms of plasic work before fracture, depth of indentation and the alternative of shear or crack initiation under an applied stress.

Zum-Gahr (1981/1982) identified the different properties of a material which would influence friction and abrasive wear. These are yeild strength under restaint or hardness, work hardening, ductility, crystal anisotropy and mechanical instability. Resistance to elastic/plastic strain or hardness together with work hardening determine the contact area between an abrasive particle and the material. Garrison and Garriga (1983) noted that bulk hardness is an inadequate measure of abrasive wear resistance. They incorporated a ploughing term into their wear rate expression and suggested that the fraction of groove ploughed is proportional to some measure of ductility.

Richardson (1967) attributed the high ductility at the abraded surface to the presence of hydrostatic pressures and compressive residual stresses. Diesburg and Borik (1974) observed how little is understood of the relationship between abrasion resistance and toughness. Surprisingly, they showed that for wrought and cast low alloy steels, a decrease in toughness improved the abrasion resistance. A notable exception is the austenitic manganese steels where a great improvement in toughness may be gained without affecting the high stress abrasion resistance found in crusher jaws. The microstructure of these steels is known to be unstable to mechanical deformation.

Studies which attempt correlations between mechanical properties and wear performance are complicated by the fact that the observed wear rates are not only controlled by metallurgical variables and the corresponding micro-mechanical properties, but also by the external service conditions.

Material Hardness

The relationship between abrasion resistance and hardness approximates to a straight line which passes through the origin for pure metals. "Bulk hardness is often used to present abrasive wear data" (Moore, 1974). This has led to the often erroneous generalization that an increase in hardness reflects an increase in wear resistance (fig. 2.3).

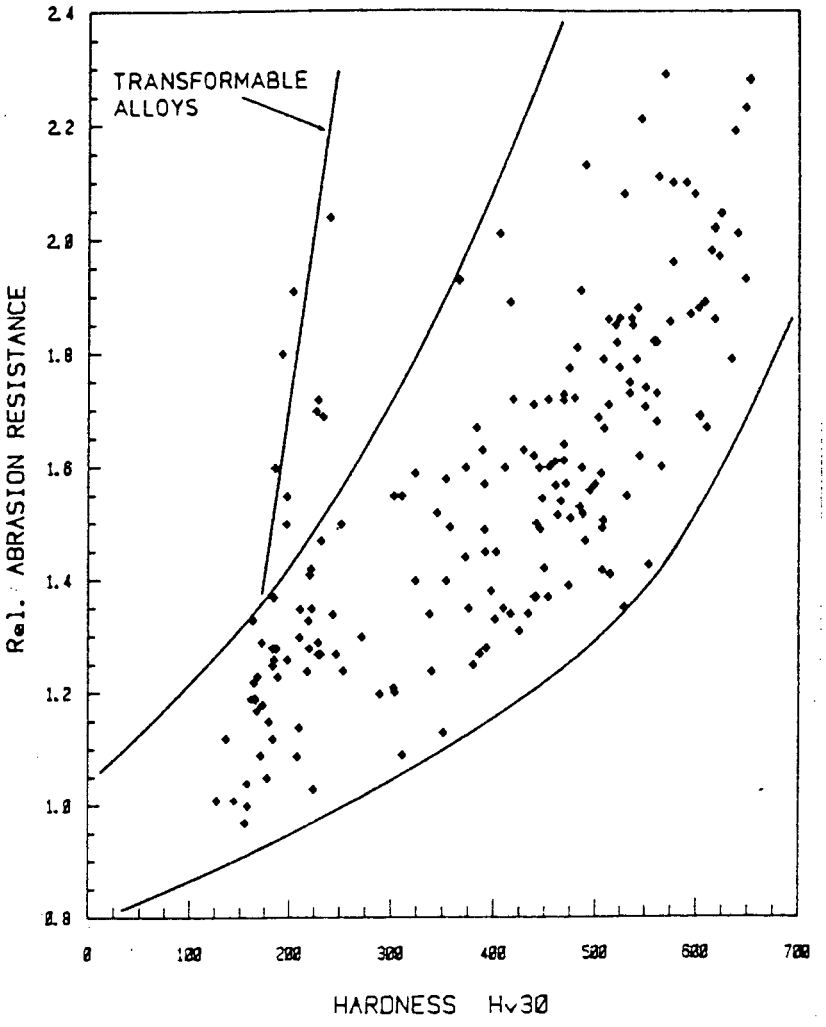

FIGURE 2.3 : Hardness is inadequate as a guide for selecting abrasion resistant materials (combined plot of all materials tested at Dept. of Materials Eng., UCT, Sept. 1985)

Rigney and Glaeser (1977) advocate caution in extending the simple hardness correlation to metals containing impurities, solutes or to more complicated microstructures. They plotted curves for heat treated steels, cold worked metals, precipitation hardened alloys and transformable steels of different initial hardnesses. These fall between the limits set by pure metals and brittle ceramics (fig. 2.4). Torrance (1980) showed that alloys hardened by heat treatment lie beneath the pure metals line on a straight line of lower gradient. Murray, Mutton and Watson (1979) showed that the relationships between different carbon steels are better described as a series of sigmoidal curves and suggested that the relatively low slopes obtained for carbon steels are indicative of a transition from ploughing to cutting as the hardness of the steel increases (fig. 2.4). Alternatively, at the same surface hardness, wear by ploughing predominates in pure metals and microchip formation predominates in hardened steels.

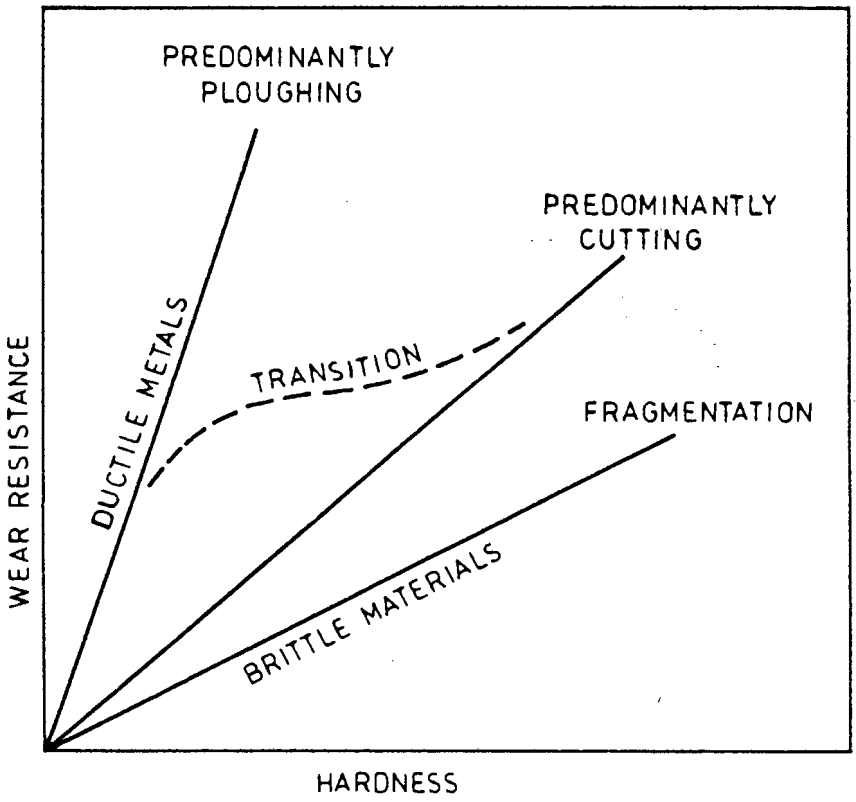

FIGURE 2.4 : Three possible relationships between metal hardness and wear resistance predicted by considering ploughing, cutting and spalling mechanisms of groove formation. The dotted curve shows the transitional behavior for steels (Murray, Mutton and Watson, 1979)

Richardson (1967) found that the surface hardness of an abraded metal is considerably higher than its bulk hardness. He suggested that the abrasion resistance of a metal might correlate better with its hardness in a very heavily worked condition. In his paper comparing shotpeening, trepanning and abrasive wear, Richardson found that within limited classes of materials, abrasion resistance may be taken as proportional to the maximum hardness. He found that the whole of the effective surface does not strain harden to the same level, although limited regions reach a maximum hardness. Correlation was found to be better, but heat-treated alloys still fell on lines of lower gradient than the pure metals. In their review, Garrison and Garriga (1983) argued that a knowledge of the surface hardness is insufficient to predict abrasion resistance.

Moore (1974) pointed out that a high degree of strain hardening occurs at the surface. That is, wear is dependent on the strength of the material in its maximum work hardened state and this would be a function of its attained surface hardness. This can only be related back to bulk hardness within a narrow group of materials where the rate of strain hardening is shown to be a function of the bulk hardness (as in the heat treatment of a plain carbon steel).

Richardson (1967) in his discussion said that the high hardness at the worn surface is achieved, in part, as a result of the elastic constraint from the surrounding material and the high hydrostatic pressure during application of the strain which inhibits fracture of the subsurface during the wear process. These physical restraints are nearly absent when a more homogeneous strain is applied, as in a tensile test for example. Richardson also pointed out that the distribution of strain around an indenting abrasive arises from the elasticity, work hardening and anisotropy of the material and from the shape of the indentor. Thus during abrasion the whole of the effective surface will not in general reach a maximum hardness although limited regions do so. The model put forward by Ball (1983) is not in complete agreement because debris is only formed once the strain exceeds the limits of the material. At a steady state the entire surface is abraded and all points have seen fracture at some time. Ball thus argues that the extreme surface is at an equal state of maximum work hardening (specific to the abrasive wear system).

Moore (1974,1980) explained the limiting strength (maximum hardness) attained at the worn surfaces in terms of metallurgical structure. He suggested it is a measure of the maximum dislocation density that can be stored by the material under the stress system developed during abrasive wear and before fracture occurs. The extent of surface hardening is large for pure metals where the nucleation of cracks is limited to dislocation interactions. On the other hand, the extent of strengthening is low for martensitic steels which have a high probability of pre-existing cracks or crack nucleation sites. He concluded that abrasive wear has to be defined more in terms of the flow and fracture properties of a material and its metallurgical structure rather than surface hardness.

Despite the inadequacies, the hardness of a material is the most important mechanical characteristic for describing the contact surface between an abrasive particle and the surface of a material. The static penetration of an abrasive particle into a softer surface runs analogous to the process of hardness testing. Thus, although hardness is an inadequate measure of abrasive wear resistance, it will continue to be used to predict results within a narrow class of materials.

Work hardening during abrasion

"Work hardening is usually considered synonymous with strain hardening" (Avery, 1974). Strain hardening is defined as an increase in hardness and strength caused by plastic deformation at temperatures below the recrystallisation temperature. Cold work is the operation of producing such deformation and the resulting permanent strain.

A measure of the work hardening ability of a material is given by the strain hardening exponent, n, determined from a tensile test and defined in the equation :

$$\text{flow stress} = (\text{strength coeff.}) \times (\text{true strain})^n \qquad \ldots.(2)$$

Moore (1974) has cited numerous workers in his review who attribute the scatter about a straight line of abrasion resistance versus hardness to the strain hardening exponent, n.

Work hardening is related to the restraint to shear or slip so pure fcc metals do not harden as extensively as bcc metals (Table 2.1). It is also a strong function of purity. The values of the work hardening exponent quoted in Table 2.1 are obtained from tensile tests at low rates of strain and for strains less than 0.3. The exponent would generally decrease with increasing strain.

TABLE 2.1 : Typical values of the work hardening exponent for pure metals and abrasion resistant steels

	Material	W.H.Exponent	Microstructure
P	Copper	0.414[a]	fcc (polycryst.)
U	Brass	0.404	fcc (polycryst.)
R	Iron	0.26	bcc (polycryst.)
E	Molybdenum	0.25	bcc (polycryst.)
S	Quatough	0.081[b]	martensite
T	Wearalloy 500	0.077	martensite
E	Roqlast AH400	0.067	martensite
E	AISI 304	0.45-0.50[c]	austenite
L	AISI 301	0.50-0.70	austenite
S	3CR12	0.173[d]	martensite/ferrite

Ref. a) Garrison (1987), b) Peters (1983), c) Peckner and Bernstein (1982), d) Brink (1983)

Investigators have estimated n by indirect means using abrasive wear data. Richardson (1967) developed a work hardening coefficient from bulk and surface hardness measurements. He found that most of the pure metals and substitutional alloys work harden by a factor of between 4 and 7, with pearlite carbon steels approximating to 4 and the purest metals having the highest strength ratio. Interstitial elements were found to reduce the work hardening capacity to as low as 1.4. Mutton and Watson (1978) identified several problems associated with mathematical modeling linking abrasion resistance to hardness and the work hardening exponent. Fundamentally abrasion is not an intrinsic material property.

The strains reached at a worn surface are extremely high compared with more conventional deformation processes. Moore and Douthwaite (1976) recorded strains of 8 for trepanning and 2.5 for abrasion

near the surface of a copper/silver solder laminated specimen. Zum--Gahr (1981/1982) found the surface of 70/30 brass worn by a sliding diamond to have deformed to a true strain of at least 3 up to a depth of 18 micrometres below the worn surface. Richardson (1967) showed that the strain at the extreme surface is apparently independent of the depth of the indentation of the abrasive particle and insensitive to the different methods of achieving surface deformation. Moore and Douthwaite (1976) reached the same conclusion. Thus the limiting material strength and the critical strain to fracture are material properties divorced from the stress-strain system.

Moore, Richardson and Attwood (1972) considered the limits of surface strength. They found that the extent of strain hardening is a maximum for pure metals and is decreased by the addition of substitutional elements. Realising that the stress-strain system under wear conditions is complex, they argued that with two thirds of the mean contact stress being hydrostatic pressure the strength limitation is imposed by ductile fracture. That is, the value of the ultimate strength is a measure of the maximum dislocation density that can be stored by the metal before ductile fracture occurs. As the initiation and growth of cracks is controlled by dislocation mobility in the material, and as work hardening is also a function of the dislocation mobility then under abrasive conditions the two are interrelated. Moore et al. (1972) were of the opinion that work hardening and dislocation multiplication would continue further if fracture were inhibited.

It can be assumed for ductile materials that wear does not start until the elastic limit has been exceeded. Avery (1974) argued that the initial impact stress will encounter a low (original) elastic limit, but any energy in excess of that will increase the elastic limit and yield strength due to work hardening. Ball (1983) described the advantage in having a material with a high work hardening capacity for abrasive wear resistance. He argued that a material with a moderate yield strength but high work hardening capacity is able to respond plastically to the impact loading associated with abrasion (fig. 2.5). He described how a rising stress--strain curve (the post yield region) reduces the chances of wear loss for a given stress distribution of abrasive strikes. Wear

would only occur after work hardening has proceeded to the limit and ductility has been exhausted. Fracture at the surface then occurs because the imposed stresses are exceeding the maximum attainable limits in material strength and strain accommodation.

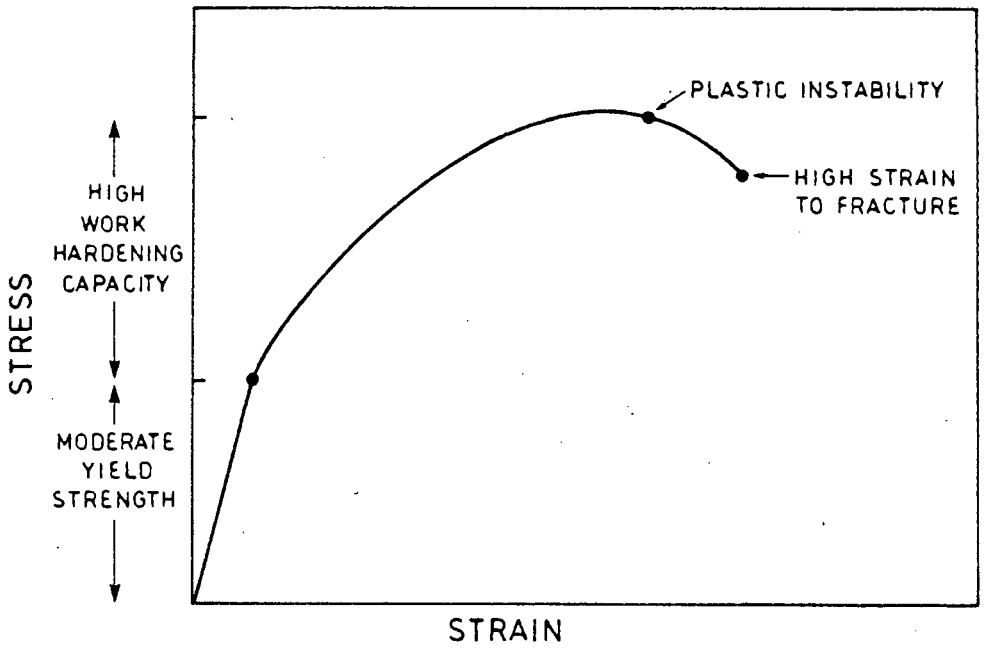

FIGURE 2.5 : Schematic stress-strain curve illustrating the good strength and ductility found in a material with a high work hardening capacity

An increase in abrasion velocity (increased rate of strain) affects the flow stress of a material by making deformation more difficult (Larsen-Basse and Tanouye, 1978). A counter influence is an increase in friction temperature leading to easier slip and deformation. The net result has an adverse effect on the work hardening exponent and abrasion resistance especially for austenitic steels (Allen, Protheroe and Ball, 1981/1982).

Prior cold work has an effect on abrasion resistance because work hardening is inherent in the abrasion process. Avery (1974) found no statistically significant benefit from prehardening by cold work under high stress abrasion, grinding or gouging conditions. Allen, Protheroe and Ball (1981/1982) found prior cold work to be detrimental to the abrasion resistance of austenitic stainless steels. Harris (1983) reported a small decrease in relative abrasion resistance for cold worked mild steel.

The accumulation of plastic strain in the surface layers during abrasion leads to different degrees of hardening depending on the material strain hardening exponent. The strain levels reached at worn surfaces are extremely high. Plastic deformation is limited by fracture; that is, a local fracture criterion governs the detachment of a swarf or debris particle. The volume of material removed by an abrading asperity is determined by the plastic flow, the tolerable amount of plastic strain, the limiting strength and the micro--fracture properties of the material in the plastically deformed region.

Microstructure

Work hardening has been found to be a maximum for pure metals but alloying does increase the materials ultimate tensile strength and micro-fracture properties. The decrease in work hardening by the addition of substitutional elements can be minimised through microstructural control. Moore, Richardson and Attwood (1972) identified four classes of materials according to their response to an applied flow stress at high and low strain.

a) Pure metals show the highest degree of strain hardening. Dislocation multiplication and mobility are controlled by dislocation interaction only; so work hardening is a function of dislocation density and purity. During fracture there are only a limited number of sites for the formation of voids or the nucleation of cracks.

b) Substitutional solid solution alloys have solute atoms which increase the material strength by solute atom/dislocation interactions. The extent of strain hardening at high strain is lower than for pure metals.

c) Interstitial atoms can support a high dislocation density and offer a powerful obstruction to dislocation movement. This imparts a high initial strength and the extent of strain hardening is limited. An increased probibility of crack nucleation and fracture.

d) The strength of precipitation and dispersion hardened alloys was found to be limited to that of their matrix. The matrix properties determine the critical stress for catastrophic coalesence of voids which lead to fracture. Strain hardening is limited.

To this should be added a fifth class, namely, transformable dual phase steels. The strain induced transformation to bct martensite from primary austenite is known to occur at the wear surface (Pearce, 1983). The transformation accounts for the extent of hardening in the immediate surface region with the initiation and propagation of cracks being suppressed during the formation of martensite (Tamura, 1982).

The materials with a fully martensitic microstructure do not fall within any one class but are a combination of all the above mentioned strengthening mechanisms. No one strengthening machanism is superior. Bryggman (1983) found that quenched and tempered carbon steels had a higher specific grooving energy (higher resistance to abrasion) than similar strengthened HSLA steels. He also observed that a ferrite-pearlite microstructure had a lower specific grooving energy than the same material in a martensitic structure. No difference in specific grooving energy was found for a quenched steel after various temperings. A duplex structure of 25% austenite in a martensitic matrix had a low specific grooving energy at large groove sizes but improved considerably for small groove sizes. Austenitic manganese steel showed good resistance to heavy gouging but was only average for smaller grooves.

In their study of the abrasion resistance of stainless steels, Allen, Protheroe and Ball (1981/1982) found the metastable austenitic alloys to have the best abrasion resistance and to be superior to some proprietary abrasion resistant steels. They rationalized this in terms of the materials capacity to accommodate the high imposed strains. They then discussed the economic alternatives of the ferritic and martensitic grades of stainless steel. It was concluded that a metastable austenite grade or a duplex ferrite--martensite grade of stainless steel may be the optimium abrasion resistant material where corrosion is also involved. The enhanced abrasion resistance of these steel types was accounted for in the

strain induced martensitic transformation and the consequent high work hardening capacity. The strength and ductility of the duplex structure was also attractive.

Allen, Ball and Noël (1984) reported that a ferrite-martensite duplex steel, 3CR12, showed poor dry abrasion resistance. They found that increasing the hardness of the martensite phase through alloying improved the abrasion resistance marginally. The alternative was to heat treat to produce a fully martensitic structure. This did improve the yeild strength and bulk hardness but the abrasion resistance was adversly affected by the decrease in fracture toughness and ductility.

Diesburg and Borik (1974) considered a tempered martensite to have the best combination of toughness and abrasion resistance for structural and constructional steels. They suggested suitable alloying additions were necessary to achieve the martensitic microstructures and insure hardenibility of thick sections. A Fe/3Cr/2Mn/0.5Mo/0.3C steel (Quatough) was found to have a good combination of tensile properties, fracture toughness and abrasion resistance (Kwok, 1982). This steel consisted of a highly dislocated lath martensite with continuous films of retained austenite and was the prefered structure over a bainitic-martensitic or a ferritic-pearlitic microstructure for wear resistance. The wear resistance was seen to decrease sharply after tempering above 300°C due to the decomposition of interlath retained austenite and the formation of carbides. Kwok (1982) also found that grain refinement through a double heat treatment improved the toughness without impairing the resistance to abrasive wear.

Zackay, Parker, Fahr and Busch (1967) developed high strength steels with enhanced ductility which undergo strain induced transformation hardening (TRIP steels). The stress-strain characteristics of these steels are typical of the form discussed by Ball (1983) in his paper on the design of abrasion resistant materials. Protheroe, Ball and Heathcock (1982) included two TRIP steels in a discussion on the development of wear resistant steels but did not present any experimental results to substantiate their argument.

Protheroe, Ball and Heathcock (1982), in their search for wear resistant steels for the gold mining industry, concluded that none of the existing low cost alloys could meet their unique set of requirements (section 1.3). They proposed a corrosion resistant martensitic type steel with some retained austenite or a corrosion resistant TRIP steel.

Bee, Peters, Atkinson and Garrett (1985) met this need by developing a Quatough type steel with the necessary higher alloying content to provide the resistance to corrosion while retaining the prescribed microstructure. The desired fine grained, dislocated lath martensite surrounded by a continuous film of retained austenite has been produced (Peters, 1983) and unpublished initial field trials were encouraging. This type of steel has been included in the present study. Ball and Böhm (1987) report on the wear performance of three candidate steels of the types proposed and these too are included in the present study.

2.1.4 Abrasion as an energy dissipating process

A fruitful approach in understanding wear is to consider an energy balance of the tribological process. Wear is then seen as a consequence of an energy transformation process. In the analysis by Uetz and Föhl (1979), it was concluded that the materials and the operating conditions should be selected to minimize that portion of the energy directed towards fracture processes and to maximise that portion of the energy transfer process associated with elastic and plastic deformation (fig. 2.1).

Fleming and Suh (1977) took a fracture mechanics approach to wear and embroidered on the delamination theory of wear as first proposed by Suh in 1973. This theory hinges around the stress intensity associated with a subsurface crack and considers the nucleation and propogation of subsurface cracks. Arising out of this theory is an appreciation that two ways of reducing wear are firstly, by reducing the subsurface deformation and the crack nucleation rate and secondly, by decreasing the crack growth rate. This highlights the roles of crystal plasticity (Hirth and Rigney, 1976) and fracture toughness (Hornbogen, 1975) in the wear of metals.

Moore (1979) assessed the energy dissipated in abrasive wear and identified four primary energy absorbing mechanisms. The major mechanism is plastic deformation. Moore pointed out that 90% of the energy expended in plastic deformation is converted to heat. The subsequent local temperature rise can lead to secondary energy absorbing mechanisms such as phase changes and thermally activated recovery and recrystallisation processes. The other primary energy dissipation processes are elastic deformation, surface molecular mechanisms and the creation of new surfaces. These latter processes together with noise and vibration are calculated to be 10^{-4} times the plastic work contribution (Moore and Douthwaite, 1976). Thus the energy expended in plastic deformation accounts for almost all of the external work (or frictional work) done in the abrasion of ductile materials.

Bryggman, Hogmark and Vingsbo (1979) have developed a simple but most effective instrument to measure the external work during formation of a single groove. With their modified impact tester they are able to measure the force and energy required to produce a single controlled groove. The energy, E, and the weight, W, of the material removed in a grooving event was found to be related through the power function $E = kW^q$ where k and q are material parameters obtained experimentally. Bryggman (1983) linked these parameters to shear stress and shear strain equivalents.

Vingsbo and Hogmark (1984) made use of the specific grooving energy term as a measure of abrasion resistance. This had the feature of being a materials parameter specific to the severity of the wear (size of groove). They found for very small grooves that the specific grooving energy exceeds the thermodynamic melting energy. They rationalized that most of the total cutting energy expended during a chip formation event is transformed to heat. By monitoring the forces during groove formation, they were also able to develop a dynamic hardness term for a number of steels.

The heat-energy present during rapid plastic deformation remains within the volume of deformed material resulting in an adiabatic temperature rise possibly exceeding 1000°C (Moore, 1980). Although melting is extremely unlikely (cited Moore, 1977) adiabatic shear is

widely reported as a predominant mechanism during abrasion. Moore and Douthwaite (1976) calculated the strain energy within the abraded surface layers to be considerably greater than for conventional deformation. These factors are considered the driving force for the observed recrystallisation of deformed material close to the worn surface. They may result in phase changes.

Bryggman (1983) studied the mechanisms of chip formation as related to alloying, microstructural differences and groove depth. The chip formation mechanism was found to be essentially common. He showed, using his quick stop pendulum, how a gradual build up of localized internal shear stress results in a primary shear zone propogating from the leading edge of the grooving tool tip to the specimen surface some distance ahead (fig. 2.6). The high strain is concentrated into a zone called the primary shear zone.

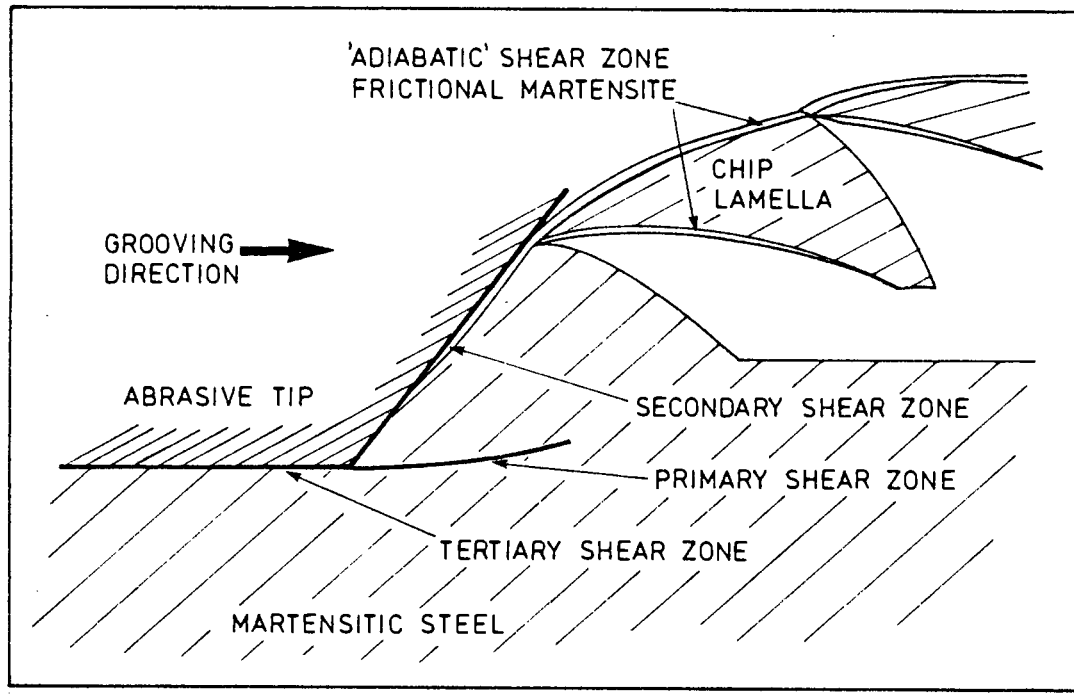

FIGURE 2.6 : Chip formation during grooving in a martensitic steel (sketched from micrographs presented by Bryggman, 1983; Vingsbo and Hogmark, 1984)

In principle, the momentary groove depth controls the spacing between successive primary shear zones. Material properties, for instance an increase in hardness, were found to reduce the spacing between nucleation of shear zones. Bryggman (1983) found the frictional layers at the bottom of the grooves to be a continuation of the primary shear zones. He then went on to develop a model which adequately explains the changes in morphology in terms of rate of localised shear strains, localised temperature rises and the density and mobility of dislocations within the primary shear zones. Vingsbo and Hogmark (1984) considered the resulting microstructures to be the equilibrium result of these previously dynamic processes.

A simple consideration of abrasion as an energy balance has highlighted the dominance of plastic deformation. The dissipation of the frictional work may lead to changes in the property of the material close to the abrading surface. These imposed changes can, with the right microstructural matrix, be put to advantage in inhibiting further gross plastic deformation and retarding the onset of fracture and thereby prevent the early onset of material loss during abrasive wear.

2.2 CORROSION

The early failure of mining equipment, as a result of corrosion, is a major problem in the South African mining industry (Mokken, 1977). Corrosion is induced by the wet operating conditions associated with an underground mining operation. It can be in the form of a general attack, for example on structural steels around the bases which rest on wet concrete floors. The alternative form, crevice or pitting corrosion, is a severe form of localized corrosion that occurs in crevices or under entrapped dirt. This latter form can greatly reduce the service life of equipment.

Corrosion is defined as the interaction of a material and its environment. For metals, corrosion is the result of metals seeking their lowest energy state which thermodynamically is the oxide for all non-precious metals. The real question about corrosion is not whether it will happen but how fast and in what form. Thus corrosion must be studied as a rate process.

2.2.1 Determining the corrosion rates of metals

Oxidation rates in dry atmospheres follow Arrhenius's exponential rate law. But in the presence of moisture, an electrochemical cell is formed and corrosion rates are orders of magnitude faster. Corrosion involves the transfer of charge from the anode to the cathode. Thus corrosion rates can be expressed as an electrical current or current density. The driving force for corrosion (as for any chemical reaction) can be quantified by the potential difference between the rest potential of the anodic and cathodic half reactions.

A polarisation curve of potential versus current density provides a unique means of describing and predicting the corrosion behaviour of a metal-solute system (Greene, 1962). Higginson (1984) has used this method to investigate the corrosivity of South African mine waters on mild steel.

The reactions at the anode and cathode can be measured or calculated to produce a polarisation curve (fig.2.7a). The dissolution of metal, M, occurs at the anode.

$$M \rightleftharpoons M^{2+} + 2e^{-} \qquad \text{(anodic half reaction)}$$

The production of hydroxyl ions takes place at the cathode for neutral aerated aqueous solutions.

$$O_2 + 2H_2O + 4e^- \rightleftharpoons 4OH^- \qquad \text{(cathodic half reaction)}$$

The complete reaction is then the formation of the oxide.

$$M^{2+} + 2OH^- \longrightarrow MO + H_2O \qquad \ldots.(3)$$

The rate of this reaction is subject to the concentration and free flow of the species. If for example, the diffusion of dissolved oxygen to the cathode was slow then corrosion would be limited by the concentration of oxygen (fig. 2.7b). The cathodic reaction would be concentration polarised or the rate of corrosion is under "cathodic control". Higginson (1984) found that the concentration of dissolved oxygen was the biggest single factor determining the rate of corrosion of mild steel in mine waters.

The resistance within a metal is usually very low so that a large current can flow between the anodic and cathodic sites. Any resistance met by the current flow in completing the electrical circuit would reduce the corrosion rate. If for example, the rate of charge transfer through the oxide layer is retarded, the anodic reaction is resistance polarised to a more noble state (fig. 2.7c).

The rate of corrosion can also be controlled by the reaction sequence at the metal-electrolyte interface. In some cases an overpotential is necessary to overcome the activation energy for a net forward reaction to occur. Conversely, the presence of impurity elements at the metal surface or ions in the electrolyte can act as catalysts. A change in pH may result in different reaction products being formed (Pourbaix, 1966). This means different anodic and cathodic reactions and a different rate of corrosion (fig. 2.7d). Higginson (1984) showed the pH dependence of mild steel in aerated mine service waters to be divided into three regions (fig 2.8). At pH values between 4 and 7 the corrosion rate is independent of pH. Below a pH of 4, the corrosion rate increases exponentially with decreasing pH. This is the pH range often found within a crevice despite the outside environment being at a neutral pH. Above a pH of 7 there is a change in the properties of the oxide scale and the corrosion rate is slightly lower but still essentially independent of pH (fig. 2.8).

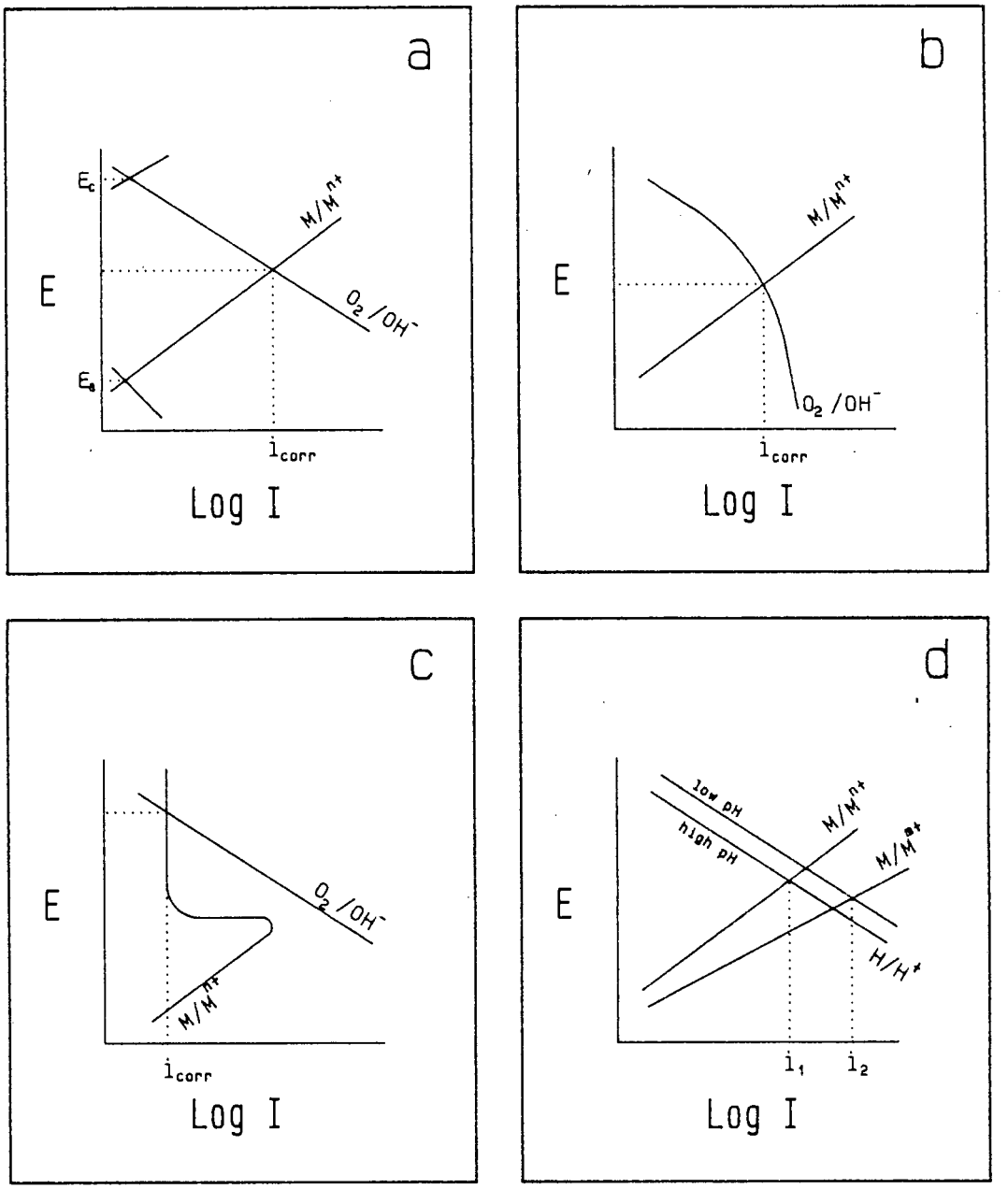

FIGURE 2.7 : Schematic polarization curves of applied potential versus current density

a) The anodic and cathodic half reactions. i_{corr} is the free corrosion rate.

b) The cathodic reaction is controlled by diffusion. Concentration polarization.

c) A passive oxide layer reduces the metal dissolution rate. Resistance polarization.

d) An increase in the acidity (h⟶l) or a change in the anodic reaction (m⟶n) may result in an increase in the corrosion current density ($i_1 < i_2$).

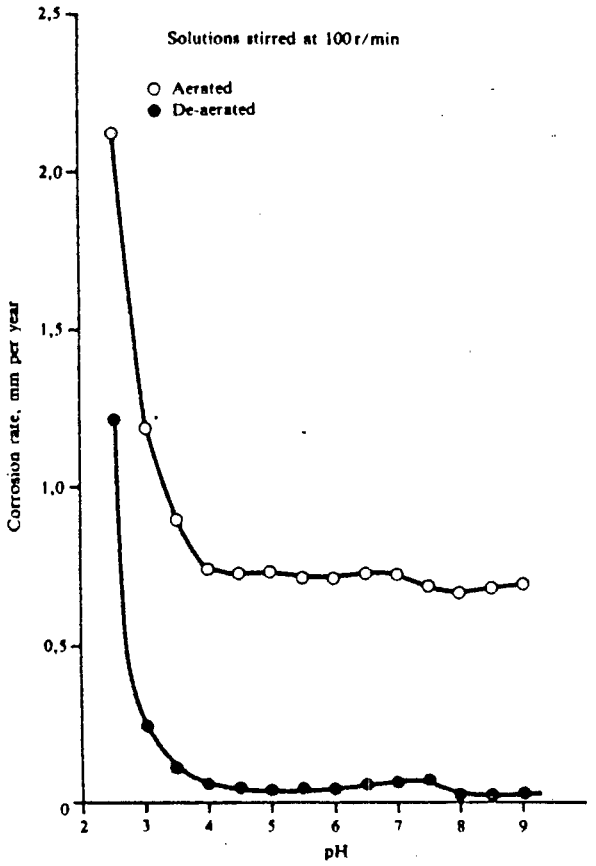

FIGURE 2.8 : Effect of pH on corrosion rate of mild steel in a synthetic mine water (Higginson, 1984)

So far no mention has been made of the size and location of the anodic and cathodic sites. For general corrosion the rate of corrosion at any specific location is the same. However, if the anode is limited to a small area with respect to the cathode, a fast rate of attack is expected. This localised attack occurs as a result of physical conditions, be they environmental, metallurgical or mechanical. Proper design of equipment enjoys a high priority in the control of localized corrosion, frequently taking precedence over material selection (Mokken, 1977). Lastly, corrosion rates can change as corrosion proceeds due to a change in the local environment at the active anodic site. Pitting is such an example.

In many industries the concept of Corrosion Monitoring is well established (Moreland and Hines, 1979; Controlling Corrosion Handbook). The advantages are to gain information on the state of the operational equipment, to link the corrosion processes to the operation variables, and to monitor or control a protection system.

2.2.2 Passivity - inhibiting corrosion

Inhibiting corrosion by protective coatings applied to the metal surface has a major disadvantage in the mines. The coatings (galvanized, rubber, paint, plastic resins, etc) are unable to withstand the extent of abrasion so their application is limited. Steels need to be inherently passive in their operating environment if their useful life is to be extended.

Uhlig in his review paper (1979) uses two definitions for passivity:

1) "A metal is passive if it substantially resists corrosion in a given environment resulting from marked anodic polarisation." A metal in the passive state has a corrosion potential appreciably more noble than its potential in the active state. Or, the metal becomes passive when the potential of the polarised anode area has closely approached the potential of the cathode area.

2) "A metal is passive if it substantially resists corrosion in a given environment despite a marked thermodynamic tendency to react." Metals passive by this definition exhibit low corrosion rates because of reaction-product films acting as surface diffusion barriers. These films are usually thicker than films characterised under the first definition.

Passivity involves a protective oxide film between the metal anode site and the electrolyte. An early theory to explain passivity was the electron configuration theory (Uhlig, 1979). Two further theories, one based on reaction velocities and rate of metal dissolution and the other, the oxide film theory based on unusual stoichiometric iron oxides have been proposed, but these have been superceded by the current adsorption theory.

The adsorption theory ascribes passivity to reduced reaction kinetics at the metal-passive film interface (or alternately the passive film-electrolyte interface) instead of limited ionic or atomic mobility through the oxide film. This theory proposes that once the affinity of the metal surface for oxygen has been satisfied, the absorbed film blocks the progress of further chemical reactions

(Fontana and Greene, 1982). The chemisorbed film will reduce the value of the exchange current density thereby increasing the anodic polarisation characteristics of the metal. The adsorbed films become non-stoichiometric metal oxides as they grow in thickness with time. Eventually stoichiometric oxides nucleate from the less stable non-stoichiometric compositions. Uhlig (1979) observes that the properties of passivity that persist after this transformation are likely to result from a diffusion barrier film (definition 2) rather than by reduced reaction kinetics (definition 1).

Cathodic polarisation can destroy passivity by reducing the concentration of adsorbed oxygen and by supplying interstitial hydrogen which would impair chemisorption of oxygen. Chloride ions destroy passivity by destabilising the oxide film growth such that the film formation rate is surpassed by the metal dissolution rate at a break in the film resulting in a decrease in anodic polarisation (Cieslak and Duquette, 1984). This kinetic interaction is seen to occur at or above a well defined potential called the pitting potential. Crevice corrosion, on the other hand, can initiate at a more active potential due to passivity being destroyed following a change in the solution composition of the crevice away from that of the bulk of the electrolyte. This shift in local conditions can be in the form of a decrease in pH, lack of dissolved oxygen or by increasing the chloride concentration in a crevice (Turnbull, 1983).

Metallurgical aspects of passivation

Passivation of steel can only be achieved through alloying (Hashimoto, Asami, Naka and Masumoto, 1979). A growing trend in the mines is to use alloyed and stainless steels in areas which were traditionally thought to be highly abrasive (Mokken, 1977; Furze, 1987). Much work has been done recently on the effectiveness of the alloying elements on corrosion resistance. The Americans are motivated to find a partial substitute for chromium in corrosion resistant steels (Floreen, 1982). In the design of an abrasive-corrosive wear resistant steel it is necessary to consider the influence the major elements have on imparting passivity to the steel.

Stainless steels basically derive their passive characteristics from chromium in solid solution usually above 11 wt% Cr. Chromium alloyed to iron moves the primary passivation potential, E_{pp} (fig. 2.9) in the active direction (more negative potential) and reduces the passive current density, i_{pass} (Chen and Stephens, 1979). Increasing the chromium content of iron-chrome alloys in de-aerated synthetic sea water raises the pitting potential, E_p (Pessal and Lui, 1971). Chromium is an essential ingredient in the design of an abrasive-corrosive wear resistant steel (fig. 2.10).

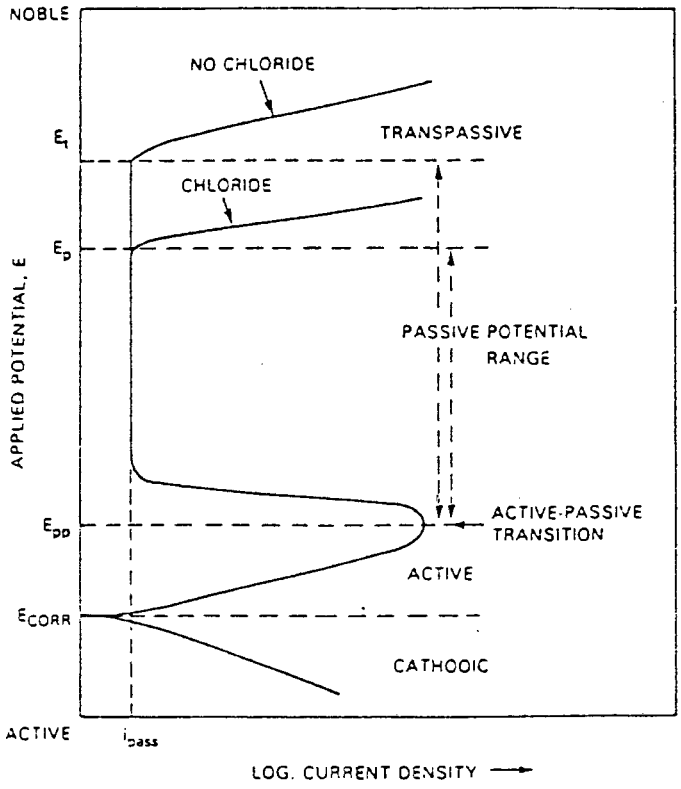

FIGURE 2.9 : A schematic polarization curve for a stainless steel showing passivity in a sulphuric acid solution (Sedriks, 1984). The features of the graph are refered to in the text

Molybdenum has a strong beneficial influence on passivity by increasing the pitting potential (Bond and Lizlovs, 1968) and resisting the onset of crevice corrosion in marine environments (Sedriks, 1982). Hashimoto et al. (1979) attribute this to an initially more active dissolution rate as a precursor to passive film formation. The passive MoO_2 film remains stable under very acidic conditions (Wu, Rui-Cheng, Hüi-Zhong and Pourbaix, 1984).

Nickel improves the corrosion resistance of low carbon high chromium steels in less oxidising atmospheres. The pitting resistance of austenitic stainless steels increases when the nickel content is raised from 14% to 39% (Bond and Lizlovs, 1968). The substitution of manganese for nickel in the 18-8 austenitic stainless steels has been tried with marginal success. The presence of 5 to 15% manganese in 18Cr/5Ni steels decrease their ability to passivate and their resistance to pitting in chloride and nitrate solutions (Lunarska et al., 1975). Greene and Wilde (1970) noted an increase in the critical anodic current density, i_{max}, with an increase in manganese for type 304 stainless steel. It remains uncertain whether manganese can be substituted for nickel without adversely affecting the corrosion resistance in the design of a wear resistant steel.

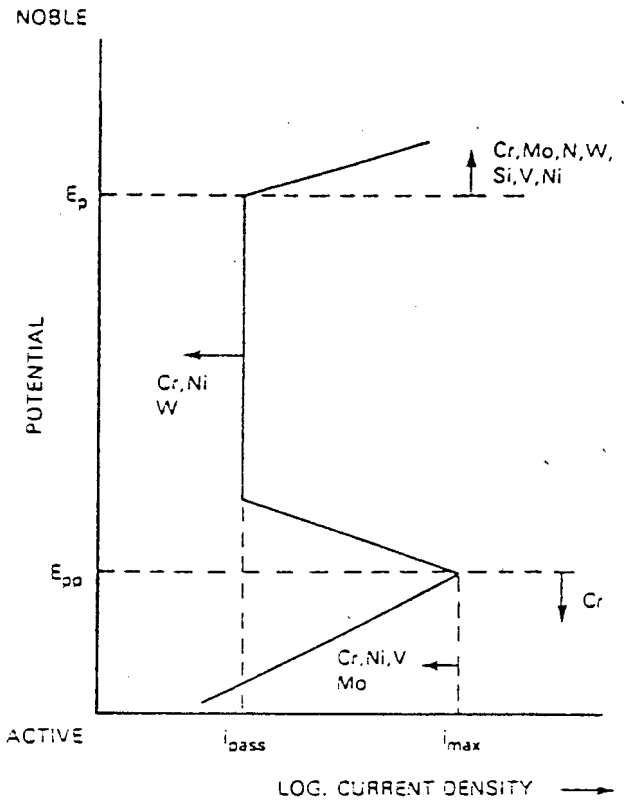

FIGURE 2.10 : Schematic summary of the beneficial effects of the alloying elements in stainless steels on the anodic polarization curve (Sedriks, 1984)

Vanadium, Silicon, and Tungsten alloyed in small amounts assist in the formation of a stable oxide film (Hashimoto et al., 1979; Chen and Stephens, 1979; Floreen, 1982). Copper is beneficial in sulphuric acid environments. Aluminium is deleterious to ambient temperature corrosion resistance (Chen and Stephen, 1979). Nitrogen moves the pitting potential in the noble direction especially in the presence of molybdenum (Sedriks, 1984).

Alloying alone will not produce a corrosion resistant steel as the effect of microstructure is a major factor to be considered (fig. 2.11). A study of pitting potential measurements indicate the importance of the minor constituents in stainless steel alloys.

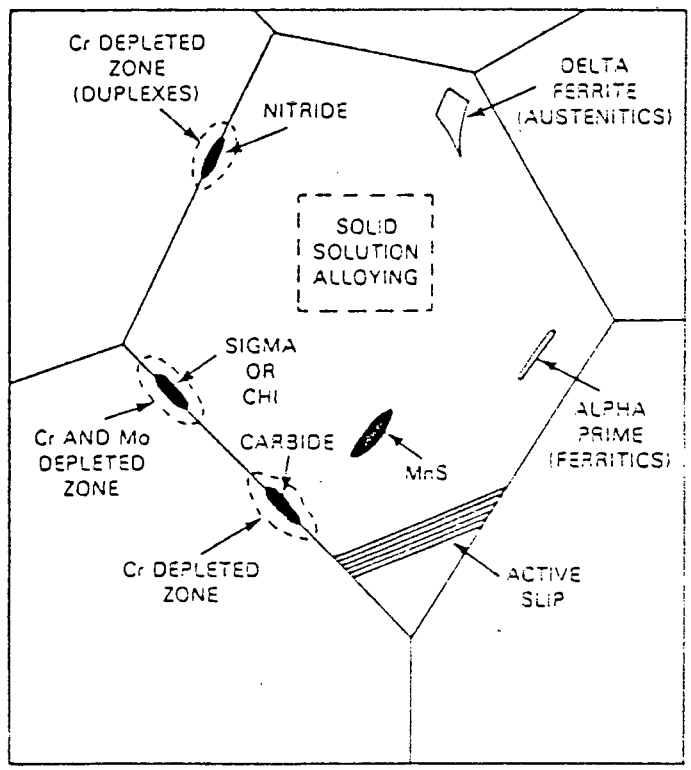

FIGURE 2.11 : Schematic of metallurgical variables affecting the passivation behavior of stainless steels (Sedriks, 1984)

Carbon and nitrogen levels are significant due to the formation of chromium and molybdenum carbides and nitrides (Bond and Lizlovs, 1968). The most susceptible locations for a breakdown in passivity and pit nucleation in quenched steels are the boundaries between the austenite phase and carbide particles (Lunarska et al., 1975). The

precipitation process depletes the matrix immediately surrounding the carbide (or carbonitride) precipitate of those elements (Cr and Mo) required for passivation (Sedriks, 1982). This solution depletion mechanism correllates well with the effect of tempering during which solute-concentration gradients are removed (Truman, 1976; Sedriks, 1982). Titanium is used to tie up carbon and nitrogen and thereby prevent the formation of intergranular chromium carbonitrides, but the correct heat treating procedures must be followed (Devine and Ritter, 1983).

The presence of manganese sulphides is to be avoided as it is well established that manganese sulphides are the most favourable sites for pit initiation in stainless steels due to their active corrosion potential (Sedriks, 1984). Sigma and chi phases (hard, brittle intermetallic crystals) are known to decrease the passive potential range by local depletion of the surrounding matrix. The influence of delta ferrite again depends on whether the surrounding matrix is depleted of chromium (Lunarska et al., 1975).

The role of alloying elements in steels without sufficient chromium for spontaneous passivation is still advantageous in resisting corrosion. A number of mechanisms of self protection have been proposed for low alloy steels, emphasizing either the effect of the alloying elements on certain physical and physical-chemical properties of the oxide scale or their influence on the electro-chemical behaviour of the steel (definitions 1 and 2 of section 2.2.2; Uhlig, 1979). From microprobe examinations of steel surfaces, Bruno, Temba and Bombara (1973) found a considerable concentration of the alloying elements in the rust. They attribute the corrosion generated and enriched interface of the metal/oxide as directly contributing to the self protectiveness of low alloy steels.

When the oxide scale is mechanically disrupted and stripped from the surface under abrasive mining conditions, corrosion would be expected to proceed at an accelerated rate until an oxide scale is again established.

2.2.3 Rate of repassivation

Burstein and co-workers have developed a technique in which they can examine the rate and degree of corrosion which occurs when the passive film on a metal is mechanically ruptured while the metal is immersed in a corrosive environment. Their scratch technique provides a quantitative picture of the corrosion process from which the mechanism and kinetics of the growth of passivating films for a number of materials have been compared.

Burstein and Ashley (1984) showed that freshly generated iron surfaces oxidise randomly (without nucleation) and that the first step is the adsorption of a monolayer of FeOH onto the surface. Thickening of the monolayer towards repassivation occurs by ion migration under high electric field. The film growth law is of the form:

$$\log i(t) = k\, q(t)^{-1} \qquad \ldots.(4)$$

where k is a rate constant, i(t) is the current density and q(t) is the charge density that has flowed in time t after scratching.

Burstein and Marshall (1984) found for type 304L stainless steel that oxide film growth occurs by two consecutive rate laws each governed by ion migration under high electric field (fig. 2.12). The second of these rate laws causes the rapid decay of current density towards the final passive current density. In fig. 2.12, the abscissa A to B is increasing charge density (a measure of the rate of metal cations dissociating into solution), and on the ordinate the active current density of a new scratch is initially at C and decays to D.

The presence of molybdenum in type 316L stainless steel accelerates the onset of the second law of film growth and the earlier onset of iron(Fe) dissolution resulting in passivity being attained earlier than for 304L stainless steel (Marshall and Burstein, 1984). Chloride ions are thought to increase the dissolution rate significantly for both chromium and iron and to be in competition with growth of the passive oxide film (Burstein, Ashley and Marshall, 1983).

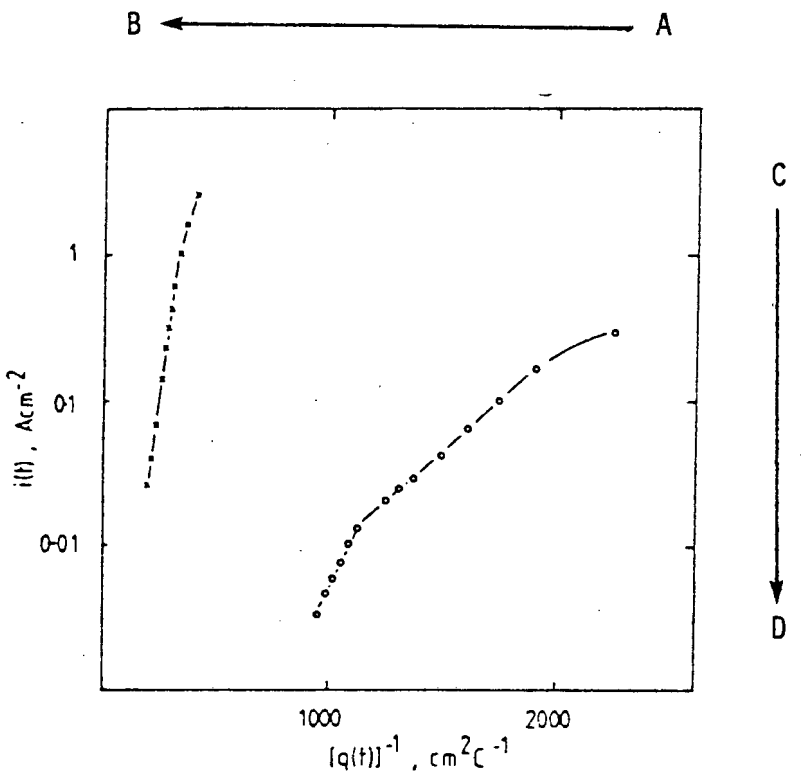

FIGURE 2.12 : Kinetics of oxide film growth on iron (X) and Type 304L stainless steel (O). Note the two consecutive rate laws for the stainless steel (Burstein and Marshall, 1984). Refer to AB CD in text

At a particular electric field (pH dependent), dissolution of the iron(Fe) component begins from the oxide film-electrolyte interface. This type of dissolution is constructive in that the resulting chromium enriched oxide film retards further dissolution thereby producing passivity.

The above mechanism proposed by Burstein and co-workers supports the earlier work of Pessal and Lui (1971). They found that during repassivation there is an abrupt drop in current (adsorption of an oxide film) followed by an exponential decay (net growth of an oxide film coupled with dissolution). Abd El-Kader, et al. have studied the rate of oxide film thickening under open-circuit conditions. They measured the steady state mixed potential, E_{corr}, whilst abrading and monitored the open circuit mixed potential from the moment the abrasive was removed. They found for multiple scratches that the rate of oxide film thickening followed a similar logarithmic growth law.

Cieslak and Duquette (1984) analysed the passive films of ferritic stainless steels by Auger electron spectroscopy. They showed that increased chromium in an alloy leads to increased chromium enrichment and decreased thickness of the passive oxide films as would be predicted by Burstein's kinetic model. They found in addition that the passive film is basically unchanged by the presence of molybdenum except "the highest level of protection is achieved with less metal oxidation". Passivation is thus achieved with less total charge density expended. They also studied the interaction of chloride ions in pit initiation and found no chlorides in the oxide film. They suggested that the inability of a film to grow and develop in the presence of chloride ions is due to a mismatch in the kinetic balance of chloride and oxide ions, such that the film reformation rate is surpassed by the metal dissolution rate in the presence of chloride ions.

Bruno, Tamba and Bombara (1973) looked at the alloying elements at the steel/rust interface of low alloyed steels and found the more corrosion resistant the steel, the higher the rust to steel concentration gradient (higher electric field) and the closer the most enriched layers are to the steel/rust interface. They attribute the enriched interface of the metal/oxide as contributing directly to the self protectiveness of the low alloy steels. The reduction in corrosion current density is either thermodynamically controlled as for copper (ennobling) or kinetically controlled as for chromium (passivating) when alloyed to steel (definitions of passivation section 2.2.2).

The stability of the passive film is strongly dependent on the time to achieve steady state conditions. Covino and Rosen (1984) found that the induction time to passive film breakdown was dependent on whether a steady state condition (final free corrosion potential) had been reached. It was also observed that higher chloride ion concentrations and higher open circuit potentials resulted in shorter induction times to film breakdown and corrosion with one exception. They argued that mechanistically the breakdown of passive films on steels is the same regardless of environment or metal composition. However the composition of the bare metal, the condition of the oxide film and the ionic concentration of the electrolyte effect their qualitative relationship to the induction time

before film breakdown and corrosion. In the case where a scratch is made, the oxide is removed and a new passive film begins to form. The time to achieve steady state conditions is closely related to the induction time for breakdown and the same relationships must hold.

In conclusion, repassivation is seen to be a dynamic process of passivating oxide film growth and active metal oxide dissolution. The kinetics of this dynamic process are dependant upon the composition of the alloy, the level of aeration and the aggressiveness of the environment.

It is easy to see how abrasive particles may affect corrosion rates by destroying the protective films and exposing fresh metal to the environment. The oxide films take time to build up and if they are continually being destroyed by an abrasive action, corrosion rates are expected to increase dramatically. There is another aspect to abrasion that may also influence corrosion rates. In section 2.1.4 abrasion was seen as an energy process dominated by plastic deformation and heat. This will now be considered in greater depth.

2.2.4 The effect of plastic deformation on passivity and the rate of corrosion

Shamseldin, Abd El-Kadar, Abd El-Wahab and Hegazy (1983) found a greater critical anodic dissolution rate and a higher passive current density for a 0.26% carbon steel in a cold worked condition than in the annealed condition. They also noted that excessive cold work appears to improve the corrosion resistance slightly. They found on tempering the cold drawn steel that there was an increase in the dissolution of iron(Fe) in the active region until the critical current density but a reduced passive current density. They concluded that cold work increased the tendency of steel to undergo general corrosion and pitting but the effect depends on the magnitude of the lattice imperfection at the surface. Grassiani (1978) noted that the flow velocity of the electrolyte more strongly influenced the corrosion rate of cold worked steel. Since the oxygen concentration is the rate controlling factor this would suggest an increased tendency for dissolution. Shamseldin et al. (1983) noted that cold work intensified the aggressive action of chloride ions

which is further evidence in support of cold work enhancing the anodic dissolution rate. Thus prior cold work in mild steel will facilitate an increase in the kinetics of both the anodic and cathodic reactions and is detrimental to its corrosion resistance.

Elayaperumal, De and Balachandra (1972) found that cold work shifts the open circuit potential of type 304 in the active direction and increases the critical current density for passivity. They related the increased corrosion rate to the formation of bcc martensite which was measured to have a more active corrosion potential. To test their proposal, they showed that a similarly cold worked sample of type 430 (which undergoes no phase change) saw no change in the active dissolution behaviour. Salvago, Fumagalli and Sinigaglia (1983) found the volume fraction of martensite in cold worked type 304L to influence the steels corrosion behaviour but were unable to explain the phenomenon satisfactorily.

Grassiani (1978) investigated type 304, 304L and 316 stainless steel and found cold work will reduce the rate of corrosion in the active and passive states at neutral pH conditions. He argued against attributing his observations to any partial phase transformation. Instead he proposes that cold work has a kinetic effect on the rate of corrosion due to a higher rate of adsorption of hydroxyl ions and chloride ions onto the emerging dislocations at the metal surface. Subsequently, there is a more rapid build up of the protective oxide film but this also leads to a deleterious effect on pitting and crevice corrosion resistance as was reported. He felt that the increased kinetics theory should also explain why the cold worked stainless steels are more susceptible than annealed material to the initiation of crevices and pits in chloride environments but he was unable to conclude anything.

Chastell, Doig, Flewitt and Ryan (1979) found that for a 12% Cr martensitic stainless steel the tensile stresses increased the susceptibility to pitting. They suggested the effects of brittle surface films and of stress and plastic deformation on hydrogen solubility accounted for their observations (stress corrosion cracking theory).

Heidemeyer (1981) supported the kinetic proposal for the effect of plastic deformation on the corrosion rate of a metal. He found that after friction the rates of both the anodic and cathodic reactions areincreased although there is a net shift in the active direction of the open circuit corrosion potential. The factors contributing to this effect are: heat of friction, the removal of the protective surface layers, an increase in the effective surface area, faster transport of reacting particles and production of lattice defects during plastic deformation. The lattice defects were demonstrated to cause a marked increase in the reactivity of metals. The increase in the free enthalpy of reactions was argued to be much higher than that calculated from the shift in the open circuit corrosion potential after friction. He concluded that the increase in corrosion rate is not a function of the number of dislocation lines at the surface alone, but also depends on the individual dissolution kinetics of each reaction.

In summary it can be said that plastic deformation and lattice disorder at the metal surface increases the kinetics of chemical reactions. The composition of the metal and the activity of the electrolyte at the surface determines whether the metal will passivate and how robust is the passive oxide layer.

2.3 ABRASIVE CORROSIVE WEAR

Metals are continually subjected to oxidation or corrosion during their useful life and this cannot be separated from the abrasive wear process. Although there is discussion as to the dominating influence of these wear mechanisms in mining equipment, there is only indirect evidence available in the literature. Moore (1980) expressed surprise at how little is understood of the phenomena of corrosion and environmental effects on the wear of materials. Reported work that is related to abrasive-corrosive wear is pipe line wear due to the conveyance of slurries and grinding media wear in ore crushing plants.

Postlethwaite, Tinker and Hawrylak (1974) and, Postlethwaite and Hawrylak (1975) used electrochemical techniques to determine the corrosion component of erosion-corrosion of steel pipes carrying a variety of slurries. They showed that the presence of suspended solids substantially increased the chemical corrosion rate in straight pipe lines. The effect of the particles was discussed in terms of the total or partial destruction of rust films, the change in the kinetics of the anodic dissolution of iron(Fe) and "yield assisted" anodic dissolution.

Any added effect of the heat generated during abrasion on the rate of corrosion has not been discussed in the literature but it is known that the rate of corrosion is related to temperature through the Arrenhius Rate Law for chemical reactions. Kim, Bhattacharyya and Agarwala (1981) studied the effect of corrosion in a rubbing situation and found that increasing the load at constant speed (extent of deformation) increased the open-circuit potential significantly in the active direction. Lokhvitskii, Anan'evskii, Krokhmal, Kolesnikov and Stepanenko (1979) considered the system to be in a state of dynamic equilibrium and attributed it to the high energetic state and microstructure of the rubbing surfaces resulting in a unique electrochemical potential with the electrolytic environment.

El-Koussy, El-Raghy and El-Mehairy (1981) studied the wear resistance of four cast chromium steels (1 to 12 %Cr) under wet and dry abrasion conditions. A marked synergistic increase in abrasion and corrosion was noted. Their results showed approximately double the volume is lost in 96 hours of grinding in sand mixed with sea water as opposed to dry grinding followed by a period of corrosion. They found the corrosive-abrasive wear resistance in wet-sand/sea-water to be determined predominantly by the

chemical composition and microstructure of the steel and not by its general corrosion resistance. They suggested the optimum microstructure be composed mainly of martensite with a fine dispertion of carbides and a residual amount of retained austenite. The optimuim wear properties were found on quenching from well within the austenite region followed by a temper at 180°C. Tempering at higher or lower temperatures caused a deterioration in the wear resistance.

Allen, Protheroe and Ball (1981/1982), in recognising the detrimental influence of corrosion, studied the abrasive-corrosive wear of stainless steels. They considered various ferritic, martensitic and austenitic stainless steels and found the stainless steels to show superior conjoint wear properties than the majority of the proprietary abrasion resistant alloys. The metastable austenitic alloys were seen to have the best potential. Their high abrasion resistance was explained in terms of the materials ability to accommodate high strains by the stress induced transformation and the consequent high work hardening rate. Schumacher (1985) also found in laboratory wet ball mill tests that the stainless steels with the highest strain hardening capacity were the most effective in resisting abrasive-corrosive wear.

Moore, Iwasaki, Natarajan, Perez and Adam (1984) studied abrasive-corrosive wear of grinding balls. They found two corrosion mechanisms operating at the abraded surface. A strain induced corrosion of the ridges prevalent in softer materials and pitting corrosion associated with electrically conducting second phase particles in the more wear resistant martensitic materials. The pitting was shown to be largely due to inclusions and segregation in the microstructure of the ball material. In some cases, pitting occured due to embedded ore particles which had fragmented to create narrow crevice sites. An increase in the corrosivity of the ore slurry or in the level of aeration resulted in an increase in corrosive wear. However for an austenitic stainless steel no increase in wear was measured despite the materials low abrasion resistance. Electrochemical measurements were made to supplement these results. They concluded that abrasive-corrosive wear is controlled by the composition of the electrolyte and its electrochemical interaction with the steel, the level of aeration, the physical properties of the abrasive slurry and, the abrasion resistance and complexity of the microstructure of the steel.

Dunn (1985) discussed the wear of grinding balls in a production ball mill operating under wet conditions. He argued that ball wear is a combination of abrasive, corrosive and impact mechanisms acting in concert. He showed that losses due to each wear mechanism vary widely and bear no fixed numerical or ranking relationship to each other. In many wear situations the separate actions of abrasion and corrosion do not account for the total volume of material lost. A synergistic relationship is seen to exist between the "concurrently operating wear mechanisms which increase their net combined effects beyond the additive loss rates attributable to each separately." (Dunn, 1985). He found that due to this synergistic relationship a knowledge of submechanisms through laboratory studies could not be extrapolated to production systems. He pointed out that the mechanical force, stress, kinetic energy and chemical activity of the environments determine the absolute wear rates and must be properly simulated or accounted for in bench scale simulations of ball mills.

Noël (1981) studied the interactive effects of abrasion and corrosion on the abrasive wear of mild steel. He measured a higher corrosion rate for an initially abraded specimen than an initially polished surface of the same steel (fig. 2.13).

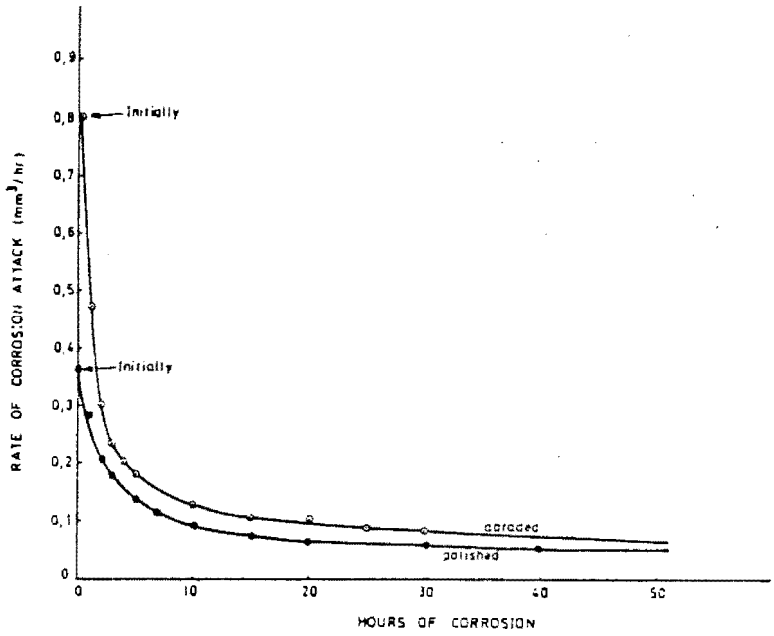

FIGURE 2.13 : Comparison between the rate of corrosive attack on an initially abraded and an initially polished mild steel specimen (Noël, 1981)

Noël showed using single scratches, that it is the nature of the corrosive attack to initially form deep multiple pits at the deformed ridges and grooves while leaving the rest of the undeformed surface cathodic. He determined the relative contributions of abrasion and corrosion and found them to be virtually independent of nominal abrasive load but strongly dependent on the uninterrupted time of corrosion. It is noted in fig. 2.13 that the rate of corrosion decreases with time of corrosion. Noël calculated that the accelerated corrosion rate would occur for the depth of the deformed layer. He proposed that intermittent abrasion which would recreate the highly active surface would increase the total wear loss and the relative contribution of the corrosion portion. The more frequent is the intermittent abrasion for the same total period of corrosion and the same total distance abraded, the greater is the total volume loss. Noël and Ball (1983) discussed the significance of these results in selecting materials to extend the useful life of mining equipment in an abrasive--corrosive environment.

The developement of abrasive-corrosive wear resistant materials encompasses a combined study of abrasive wear and corrosion. Their conjoint action has been observed to synergistically increase wear in many tribological systems but no estimation for the magnitude of the synergism has been proposed.

CHAPTER 3

EXPERIMENTAL METHOD AND MATERIALS

The experimental techniques used and developed in this dissertation are presented in three parts in section 3.1. The materials are thereafter introduced and their particulars detailed in section 3.2.

3.1 EXPERIMENTAL TECHNIQUES

3.1.1 Microstructural Characterisation

Optical Metallography

A microstructural examination was carried out on all the test specimens. Sections were cut from the fractured Charpy specimens for polishing and etching in the normal way. All optical micrographs were taken using oblique angle lighting.

A universal etchant was needed for the experimental alloys. The successful etchant developed was a solution of:

5 g $FeCl_3$
15 ml HCl
60 ml C_2H_5OH
20 ml H_2O
5 drops HNO_3

The general microstructure showed up after swabbing for 3 to 15 seconds with the prior austenite grain boundries and inclusions distinctly revealed. The etch usually deteriorated with time. Nital was used for etching the carbon steels; 3CR12 and the stainless steels were electrolyticaly etched in 10% hot Oxalic acid.

Grain size was determined using the linear intercept method.

Dilatometry

Dilatometry measurements using a Lietz Universal Dilatometer were carried out on those experimental alloys for which there was sufficient material to machine a 50 x 3 x 3 mm specimen. Transformation temperatures were determined from the onset of a discontinuity in a plot of thermal expansion verse temperature for both the heating and cooling cycles.

Transmission Electron Microscopy (TEM)

Conventional transmission electron microscopy was employed to obtain a fine-scale characterization of the microstructure for selected alloys. Using flood cooling, 1 mm thick sections were carefully cut from broken Charpy specimens. The sections were mechanically abraded to 0.2 mm thick, from which 3 mm diameter discs were punched. Further mechanical abrasion using 600 and 1000 grit paper reduced the thickness of the discs to ± 100 micrometres. Final thinning was carried out in a twin jet electropolisher using a solution of 10% perchloric acid, 20% glycerol and 70% ethanol, with an operating current of 120 mA. The electro-polished foils were stored in dry alcohol and subsequently viewed in a JEOL 200 CX transmission electron microscope operating at 200 kV.

Mechanical and Physical Properties

The hardness was measured using a Vickers diamond indentor set at 30 kg load. Results are quoted as Vickers hardness numbers (Abreviation : HV30).

Standard Charpy-V-notch impact tests were conducted at room temperature according to BS 131 : 1972. Toughness values are quoted in Joules.

Microhardness measurements were carried out using a Shimaden microhardness tester. A diamond indentor with a 100 g load was used. Results are quoted in Vickers hardness numbers (MHV 100).

The density of the experimental alloys was determined by weighing the bouyancy of the specimen submerged in mercury.

Heat Treatments

Samples of the experimental alloys were usually received as half of a fractured charpy specimen. These had already been heat treated. The commercial alloys and a few of the experimental alloys were received as bar stock from which specimens were machined and then heat treated.

Heat treatments were done under vacuum (10^{-5} torr) in a Pfeiffer vertical tube vacuum furnace, fitted with an oil quench bath. The furnace was first preheated. The specimens were suspended in the furnace under vacuum for the prescribed 30 or 60 minutes and then released to drop into the oil quenching bath below. Where air cooling was required the specimens were dropped out of the furnace region and cooled by a steady stream of Argon gas.

3.1.2 The laboratory evaluation of wear performance

Laboratory tests are more convenient than conducting lengthy in situ tests. However, it is essential that laboratory experiments be designed to closely simulate the real conditions. It has been suggested that it is only after doing a definitive study of the working conditions and having acquired a knowledge of the in-situ mechanisms of material deterioration that a successful laboratory test can be designed (Ball and Ward, 1985).

The results of any laboratory test need to be verified by a parallel in-situ test. It is only after the ranking of material performance is equivalent for the in-situ and laboratory tests that a program of laboratory material testing can proceed.

The Two-body Dry Abrasion Test

A fundamental appreciation of dry two-body abrasion is important if the added factor in abrasive-corrosive wear is to be understood. An accelerated laboratory dry abrasive wear test facility had previously been established (Noël, 1981; Allen, Protheroe and Ball, 1981/1982). The abrasion rig and test conditions were designed to model the mining situation by producing a surface with a

similar topography to materials worn in-situ. The rig is of the pin-on-abrasive-paper type and incorporates a Rockwell belt sander which has been extensively modified (fig. 3.1).

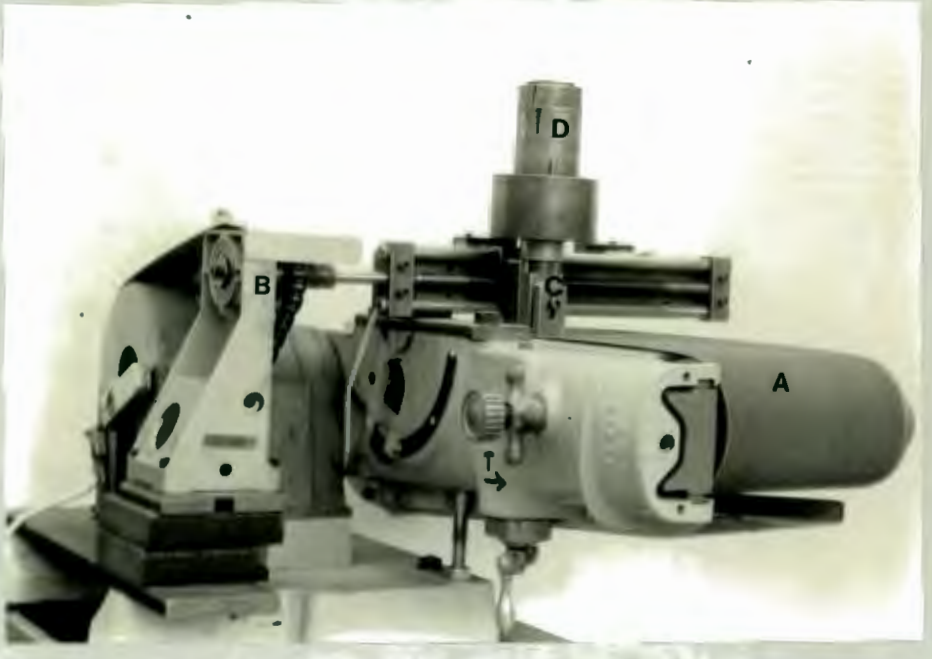

FIGURE 3.1 : Abrasion test rig showing the abrasive belt (A), the traverse mechanism (B) and the specimen in the specimen holder (C) with the load applied by means of weights (D)

The main features of the abrasion test rig are:

a) The belt runs horizontally at a constant velocity while the specimen traverses the belt at a constant velocity. The specimen is thus abraded against unworn particles at all times.
b) The load, speed, abrasive particle size and the abrasion path length can be changed.
c) A cam operated microswitch (to stop the abrasive belt) reduced the human factor when abrading short distances.
d) The square specimens, 10 mm x 10 mm in cross section, are produced from broken charpy impact specimens (fig 3.2).
e) The specimen holder is designed to firmly clamp the specimen and prevent any chattering problems when using short specimens (Rice, Nowotny and Wayne, 1982).

f) The specimen holder fits in a slide which restricts free movement to the vertical direction only (direction in which load is applied).

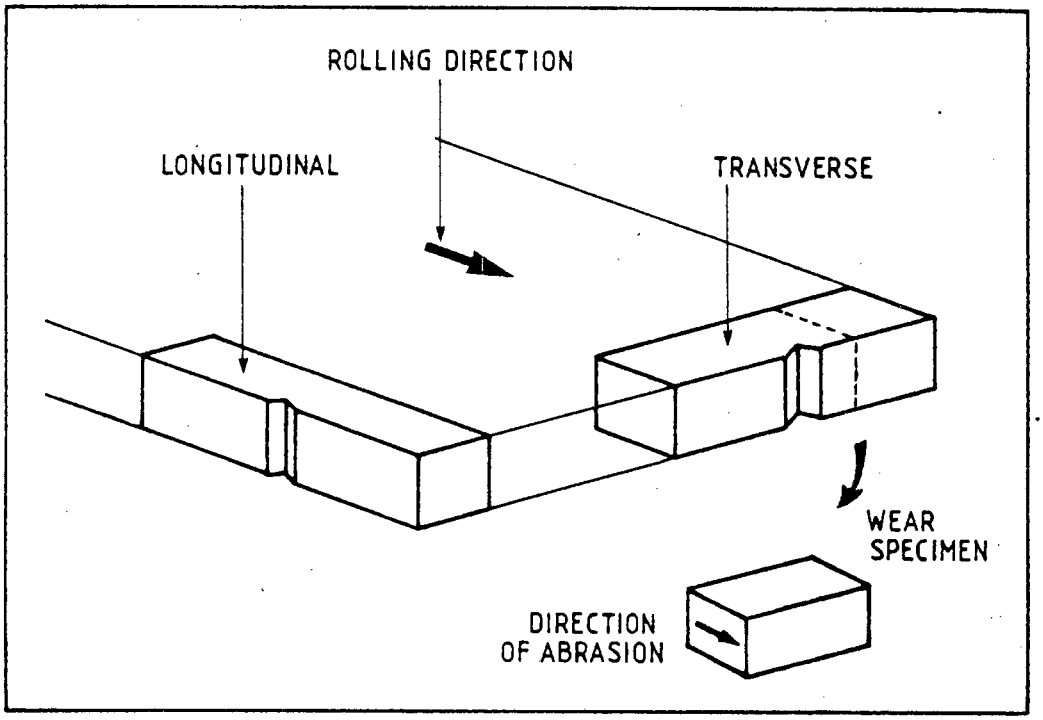

FIGURE 3.2 : A schematic diagram showing the orientation of specimens in the rolled plate material. The direction of abrasion is marked on the face of the wear specimen produced from a broken charpy impact specimen

Relative Abrasion Resistance (R.A.R)

Noël (1981) developed a standard laboratory two-body abrasion test which allowed for a wide range of materials to be tested easily and ranked according to their relative abrasion resistance. The conditions for the standard R.A.R test are given in Table 3.1.

TABLE 3.1 : Characteristics of the abrasion test

Specimen size	10 x 10 mm cross-section
Abrasion speed	260 mm/s
Load	32.1 N
Abrasive particle	80 grit Alumina
Abrasive path length	4 x 3 m

The test procedure involves an initial "running in" of the specimens to achieve a steady state situation. Once a uniform abraded surface is achieved, the specimens are weighed to an accuracy of 0.1 mg, abraded for 3 metres and reweighed. Weight losses are converted to volume loss per metre of abrasion. The relative dry abrasion resistance is defined as:

$$R.A.R = \frac{\text{Volume loss per metre of the standard material}}{\text{Volume loss per metre of material X}} \quad \ldots.(5)$$

Mild steel (070M20) is the standard and assigned on R.A.R value of unity.

The correlation coefficient for linearity between the four points of any one test was better than 0.998 units. The reproducability of the test method was found to be ± 1.5% over a six month period.

The Corrosion Test

Noël (1981) developed a simple laboratory corrosion rig to simulate the corrosive environment in which mining equipment operates (fig 3.3). The characteristics of the corrosion rig are:

a) The test specimens are placed in a corrosion cell through which aerated simulated mine water flows.

b) The composition of the simulated mine water is based on an analysis over a one year period of the mine service water at a particular gold mine situated in the Transvaal.

c) The water is pumped from a reservoir through a filter to a surge tank. The level in the surge tank is kept constant by an overflow which returns the excess water to the reservoir. Thus the water is piped at a constant head of pressure to the corrosion test cell.

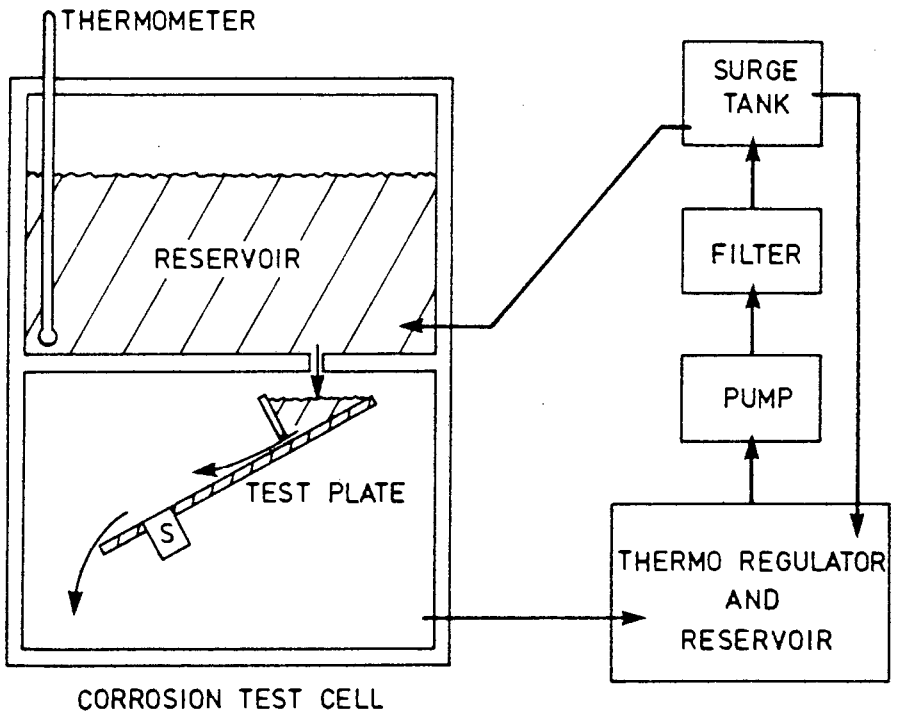

FIGURE 3.3 : Schematic diagram of corrosion test loop incorporating the corrosion test cell with the test plate and specimen (S) in place. The direction of flow is indicated

d) The corrosion test cell consists of a reservoir with a row of 2 mm diameter holes in the bottom. A 'wall' of water drains through these holes and over the test plate. The test plate is mounted at a 30 degree incline to the horizontal.

e) The test plate holds nine square specimens in a staggered arrangement to avoid turbulence over the second row of specimens. The height of the specimens can be adjusted so that the abraded surface is flushed with the test plate. A flow regulator eliminates any turbulance and regulates the flow over the specimen (fig. 3.4).

f) A thermo-regulator is used to keep the temperature constant throughout the test.

A fresh solution of synthetic mine water is made up at the start of each test. Specimens are placed in the Corrosion Test Cell and exposed to a fully aerated, continous flow of water in the same direction as the abrasion. The period of exposure, temperature and chemical activity of the water can be changed.

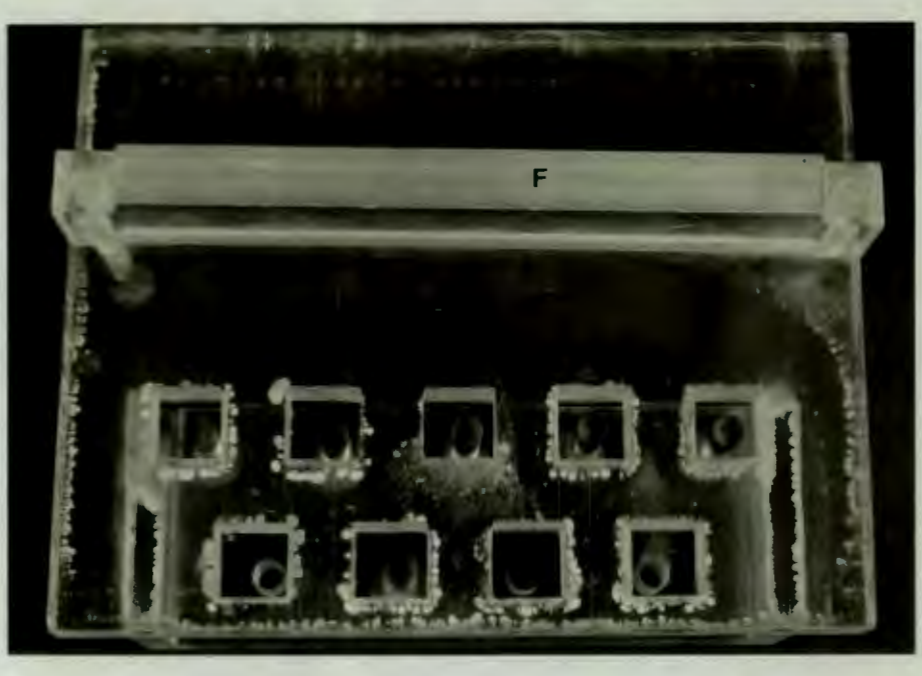

FIGURE 3.4 : The perspex corrosion test plate showing a staggered arrangement of holes and the flow regulator (F). The specimens are electrically isolated from each other

The identical square R.A.R specimens are used in the corrosion test. The 'run-in' specimens where first weighed to an accuracy of 0,01 mg, then coated on the five unabraded sides with a lacquer to prevent unwanted crevice corrosion, before being placed in the test plate. After a predetermined time in the corrosive environment the specimens were taken out, cleaned, the lacquer dissolved off and then reweighed.

The bulk of the corrosion product was cleaned off by ultrasonic agitation in a 10 per cent aqueous solution of di-ammonium hydrogen citrate ($C_6H_{14}N_2O_7$). This proved to be a very mild acid which helped to loosen the oxide product on the surface without etching away the underlying steel matrix. On the specific occasions when a more efficient solvent was desired a solution of 6N HCl with 2g/l of hexamethyltetramine as inhibitor was used (MacMillan and Flewitt, 1975). The high source of chloride ions precluded its general use. The effective removal of the oxide (rust) allowed the volume loss due to corrosion to be determined.

Relative Wear Resistance (RWRL, RWRL #2)

Noël (1981) defined the laboratory relative two-body abrasive corrosive wear resistance (R.W.R.L) as:

$$RWRL = \frac{\text{Volume loss of the standard material}}{\text{Volume loss of material X}} \quad \ldots.(6)$$

The standard is mild steel (070M20) and included each time in the test cell as one of the nine specimens. The RWRL test involves an initial run-in abrasion, then a period of corrosion followed by a short length of dry abrasion. The alternating corrosion and abrasion is repeated four times. Details of the test conditions are given in Table 3.2.

Experience with the RWRL test lead to the following observations:

a) the ratio of corrosion to abrasion in the RWRL test was too high for practical purposes (80 : 20 by volume on mild steel). That is, the superiority of the commercial stainless steels was unrealistically high. In practice the stainless steels do not outrank the abrasion resistant steels to such a great extent (Noël, Allen and Ball, 1984).

b) The test could not discriminate between the better alloys.

Consequently it was decided to revise the two-body abrasive corrosive wear test conditions. After due consideration (the details will be discussed in section 5.1), the period of corrosion was reduced to 22 hours and the abrasion distance increased to 1 metre. This revised test was referred to as RWRL #2. The reasons for the changes were:

a) the ratio of corrosion to abrasion would be reduced. This would be equivalent in mining terms, to a greater and more frequent tonnage of rock passing over the material per day.

b) The longer abrasive path length would remove sufficient material to produce a virgin surface at a level below the penetrated depth of anodic corrosion sites. The rate of corrosion of the surface would not change with time as observed previously for the low alloy steels (fig. 4.4).

The RWRL #2 is defined as:

$$\text{RWRL \#2} = \frac{\text{Volume loss of standard material}}{\text{Volume loss of material X}} \qquad \ldots.(7)$$

The standard material and material X are tested under the conditions tabulated in Table 3.2. Tests are conducted in the same manner as for the RWRL test.

TABLE 3.2 : Parameters for the two corrosive-abrasive wear test conditions

TEST CONDITION	RWRL	RWRL #2
Specimen size	10 x 10 mm	10 x 10 mm
Abrasion speed	260 mm/s	260 mm/s
Load	32.1 N	32.1 N
Abrasive particles Al_2O_3	80 grit	80 grit
Abrasion path length*	4 x 0.250 m	4 x 1 m
Synthetic mine water	518 ppm TDS	518 ppm TDS
pH at start	6.5 to 7.0	6.5 to 7.0
Temperature of water	30°C	30°C
Duration of corrosion*	4 x 46 hrs	4 x 22 hrs

* Test conditions that have changed

Reproducibility of the RWRL and RWRL #2 Tests

Noël (1981) showed that the reproducibility of the RWRL test is within 3,7% using a set of nine mild steel specimens. The present study found that over a three month period of testing the volume loss of the standard steadily increased. This was finally arrested and attributed to the proliferated growth of an algae on the walls of the reservoirs and tubes. Thereafter a stricter control was kept; with the corrosion rig being scrubed regularly and pipes replaced when necessary.

Two materials at opposite ends of the performance range were used to monitor the consistancy of the RWRL #2 results. A breakdown of the results over a 6 week testing period is given in Table 3.3.

TABLE 3.3 : Reproducibility of RWRL #2 laboratory test

WEEK #	070M20				UA 200			
	Abrasion	Corrosion	Total	Correlation coefficient	Abrasion	Corrosion	Total	Correlation coefficient
1	6.25	6.16	12.41	1.000	2.82	0.06	2.88	1.000
2	6.13	7.65	13.78	.997	3.13	0.40	3.53	.999
3	5.95	8.04	13.99	.996	3.17	0.42	3.59	1.000
4	6.12	7.86	13.98	.998	3.15	0.10	3.26	1.000
5	5.47	7.19	12.66	.996	2.72	0.05	2.77	1.000
6	5.06	8.42	13.48	.997	2.51	0.17	2.68	.999
Average	5.83	7.56	13.48 mm^3		2.91	0.21	3.12 mm^3	
Standard deviation			± 0.69 mm^3				± 0.40 mm^3	
Percentage			5.2%				12.7%	

3.1.3 Techniques Used in an Exploritory Investigation into Abrasive--Corrosive Wear

Visual and stereo optical microscopy

The clear perspex corrosion test cell allowed visual observation of the specimens throughout the test. Specimens were regularly examined after abrasion or corrosion under the stereo optical microscope. Colour optical micrographs of the corroded surface were taken in some instances as a visual record of a materials wear performance.

Scanning Electron Microscopy

Specimens were thouroghly cleaned and degreased before being mounted and gold splatter coated. The coated specimens were examined in a Cambridge S200 scanning electron microscope (SEM) to which a Tracor EDAX system was attached for semi-quantitative element analysis.

Tapered sections

Tapered sections were cut through the abraded surface to see the microstructure and measure hardness as a function of depth. Abraded surfaces were first electroplated with a layer of nickel to preserve the edge. The specimens were then mounted in a holder and mechanically abraded and polished at a 2 degree angle. This gave a 29 times magnification of the depth below the surface. Microhardness indents were made to determine the depth of work hardening. The size of the indents were measured off micrographs, and any corresponding change in the microstructure below the worn surface was noted.

Single scratch experiments

Single scratch experiments were carried out to gain an understanding of the process of abrasion and relate this to the microstructural features. This involved dragging a weighted diamond stylus across a polished/etched surface. A description of the rig is given by Glover (1980). A second method was to take a polished

specimen and abrade it for 10 to 15 mm on the abrasion rig under full load. The latter method proved more fruitful because of the much higher stresses imposed. The abrasive attack angle was however, completely random. In another experiment these individual abrasive strikes were exposed to a corrosive environment. The specimens were subsequently examined in the SEM.

Wet abrasion experiment

A series of experiments was conducted to investigate what effect a corrosive environment may have on the abrasion process. These were conducted on the abrasion rig.

The abrasive belts were first washed on the abrasive side to reduce the chance of contamination. Then whilst the specimen was being abraded, a continous jet of synthetic mine water, pre-heated to 30°C, was sprayed ahead of the abrasion path (room temperature 22-23°C). As soon as the abrasion had stopped, the specimen was removed, rinsed in distilled water, and stored under alcohol until the end of a series (20 minutes maximum). They were then ultra-sonically cleaned, dried and weighed. The volume loss due to wet abrasion was compared to a similar test under dry conditions. A range of materials was thus abraded under both wet and dry conditions.

The influence of work hardening on the corrosion of an abraded surface

The extent of corrosion of a freshly abraded surface was compared to a similar surface that had been annealed.

Two identical specimens were initially 'run-in' on the abrasion rig. They were then both annealed in the vacuum furnace by cooling in Argon from 1100°C. A high annealing temperature and medium cooling rate was used to avoid the formation of chromium carbides.

No oxide layer or scale was detected on the specimens because of the inert argon atmosphere present during the heating and cooling cycles. When air did leak in, a multi coloured tint was visible on the polished surfaces and the preparation was repeated.

One of the two specimens was then re-abraded to introduce the internal stresses and workhardening back into the surface. Both specimens then followed the same route. After chemical cleaning and weighing, the specimens were stored overnight in a dessicator so that the metal-oxide interface could come to stochiometric equilibrium. The specimens were then placed in the corrosion rig until the first visual signs of heamatite forming on the surface. Colour photographs were taken on removal from the rig, before cleaning and weighing. Specimens were later examined in the SEM. The extent of work hardening was determined from microhardness measurements.

The influence of time on the rate of corrosion

The rate of corrosion of an abraded surface was measured with respect to time. This involved removing a specimen from the corrosion rig at periodic intervals and determining the volume loss.

UA 200 in a heat-treated condition (1100°-OQ-200°-OQ) was chosen for this investigation because its chemical composition is in the critical region of interest and there was sufficient material available. Nine specimens were polished to 800 grit on five sides and the sixth side was run-in on the abrasion rig. The specimens were ultrasonically cleaned and weighed in the usual way. After 1 metre of wet abrasion the specimens were placed in the corrosion rig and at intervals over the next 72 hours a specimen was removed. Colour photographs were taken. The volume loss due to corrosion was then determined as a function of time. This experiment was repeated three times and showed good reproducability. A similar experiment on mild steel was conducted for comparison.

The frequency of abrasion and corrosion on total wear rates

The "frequency" experiment was designed to shed light on the synergistic effect of abrasive-corrosive wear. For a selected range of materials, a "high" and a "low" frequency RWRL test was conducted.

High freq. RWRL test = 8 cycles x (22 hrs corr. + 1 metre abr.)

Low freq. RWRL test = 4 cycles x (44 hrs corr. + 2 metres abr.)

TOTAL : 176 hrs corrosion + 8 metres abrasion

The "high frequency" test involves double the abrasion-corrosion-abrasion-corrosion cycles for the same total distance abraded and total period of corrosion. The standard RWRL experimental technique was used to monitor this experiment. Thus the influence abrasion has on the corrosion cycle is enhanced but the converse is not strictly true because of the ultrasonic and chemical cleaning off of the oxide scale.

This omittance was investigated since it was thought that the oxide layer that adheres to the metal surface and the crevice or pit sites may have an influence on the volume of material removed and on the slidability during abrasion. Mild steel specimens were exposed to the the corrosive environment for various periods of time. The specimens with oxide layers at different stages of development were then abraded a distance of one metre. Note was taken of the trail of debris, the abraded surface and the total volume loss.

The effect corrosivity has on wear rates

The concentration and activity of dissolved solids in an aqueous solution is known to have a bearing on the rate of corrosion of steels. It was decided to investigate whether the chemical nature of the synthetic mine water had any influence on the abrasive corrosive wear results. Other environmental influences such as temperature and humidity were not considered.

Two solutions of different total dissolved solids (TDS) content were used in the corrosion rig to test a range of the better materials (Table 3.4). The standard RWRL test used solution A based on the service water of a particular gold mine in the Transvaal, while solution B is based on the mine service water of a particular gold mine in the Orange Free State.

TABLE 3.4 : Composition of RWRL test solutions

SOLUBLE SALT	SOLUTION A		SOLUTION B	
	(g/l)	ppm	(g/l)	ppm
$Na_2SO_4 \cdot 10H_2O$	2,400	343	5,762	815
$Ca\ Cl_2$	0,485	175	3,032	1 094
$Ca\ (NO_3)_2 \cdot 4H_2O$			0,5796	98
$Mg\ (NO_3)_2 \cdot 6H_2O$			1,9605	186
Total dissolved solids (ppm)		518		2 193
pH (measured at start)		6.8		6.6

It will be noted in Table 3.4 that the chloride and sulphate content is much higher in solution B. These are the aggressive ions in the context of corrosion and originate from the fissure water and the natural oxidation of pyrite respectively (Higginson and White, 1983). The nitrates are as a result of blasting fumes. In this experiment the standard RWRL test procedure was followed except for the change in TDS of the water. Colour photographs of the specimens were taken on completion of the test.

Electrochemical measurements

The potentiodynamic polarization measurements were recorded for five representitive materials. The free corrosion mixed potential of the abraded surfaces was monitored in a separate experiment.

To measure the free corrosion potential, a square specimen was coated on five polished sides with a layer of lacquer with the sixth side run-in on the abrasion rig. The abraded specimen was then mounted in the open-circuit test cell (fig. 3.5). Aerated synthetic mine water was pumped through the cell for 48 hours at 30°C at a constant rate of flow. The mixed potential of the abraded surface was measured relative to a calomel reference electrode and recorded with respect to time using a high impedance chart recorder.

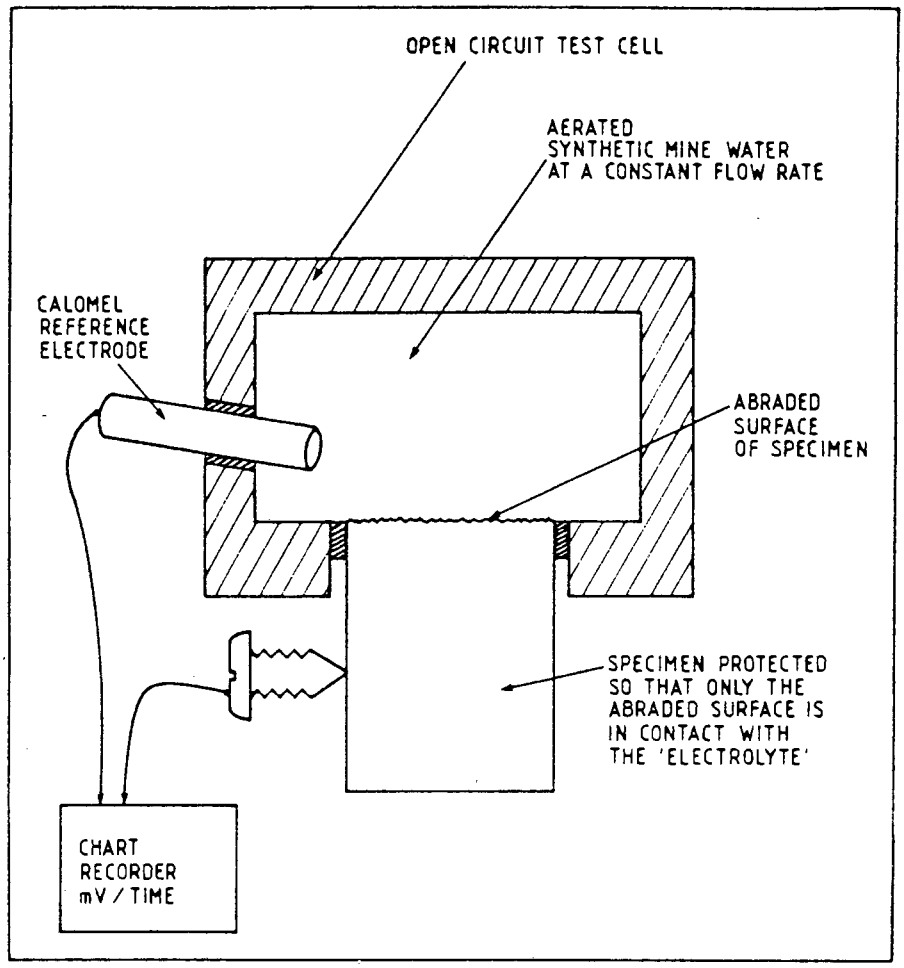

FIGURE 3.5 : A schematic cross-section through the open circuit test cell for monitoring the mixed potential of an abraded surface

In a separate test series, anodic polarization measurements were done using a Princeton Applied Research Poteniostat (Model 173) fitted with a base line advancer and logarithmic current convertor (fig 3.6). The recommended ASTM method (G5-78) was followed. The face of a 19.5 mm diameter disc was polished to 1 micrometre, degreased, and mounted in a specimen holder so that a flat surface of 1 cm^2 in area was exposed to the solution (Capendale, 1985). Specimens were held at the negative starting potential for 3 hours in the case of deareated scans (UHP Nitrogen purge gas) or 30 minutes in the case of areated scans (oxygen bubbling through solution). Scan rate was +0.14 mV/sec. The potentiodynamic traces were done in the synthetic mine water solution (pH 6.7) at 30°C. The solution was made up as for the standard RWRL corrosion test and allowed to stand for 24 hours before using.

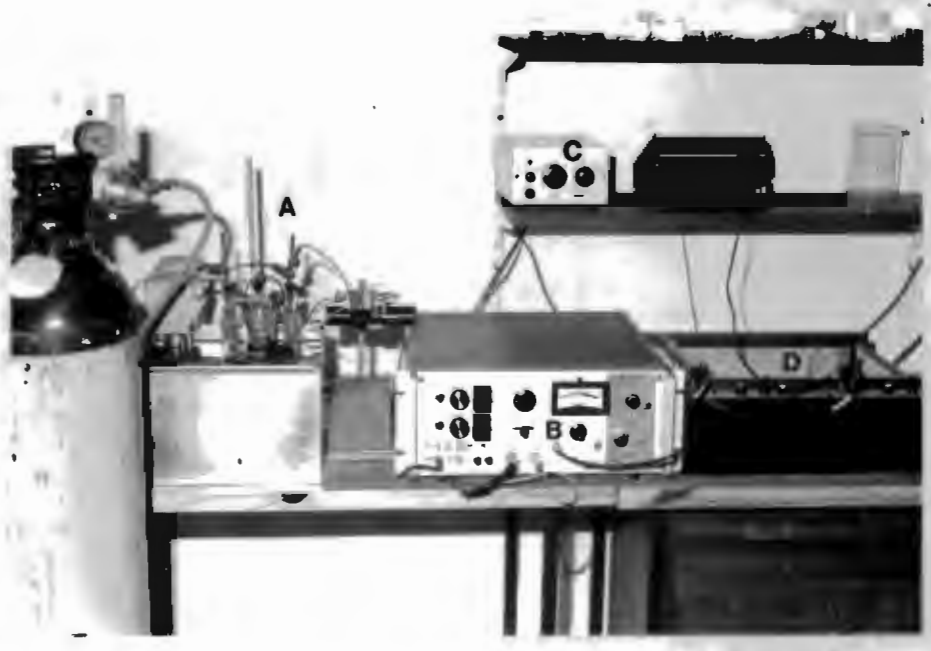

FIGURE 3.6 : The potentiostat equipment used consists of :
A. the corrosion cell in a thermal bath;
B. potentiostat incorporating log current convertor;
C. Ramp generator;
D. X/Y plotter

3.2 CHARACTERISATION OF ALLOYS

3.2.1 Introduction

A primary feature of a good abrasion resistant microstructure is its capacity to accommodate a large amount of strain produced under abrasive wear conditions (Ball, 1983). Other notable microstructural features are a high resistance to particle indentation (high surface hardness) and a high resistance to microfracture.

The development of steels with the desired features have followed a number of routes. Examples are the use of dual phase steels, transformable austenitic stainless steels, tough martensitic steels, introducing fine secondary carbides in a martensitic matrix, high nickel marageing steels and austenitic manganese steels. Many of these steels would not be applicable to general structural applications for underground mining equipment but have proved themselves in specific applications.

Four main requirements for a general purpose abrasive-corrosive wear resistant steel have been identified (Protheroe, Ball and Heathcock, 1982). These are high hardness with good toughness, corrosion resistance and low cost. A microstructure which is considered to fit the above requirements is a corrosion resistant version of an existing dual phase steel, Quatough. A second approach taken was to modify an existing corrosion resistant steel to improve its abrasion resistance. A third approach was to design a microstructure with the desired features introduced above and that meets the requirements identified by Protheroe, Ball and Heathcock (1982).

Experimental alloys have been produced by various collaborators following one of the above mentioned approaches. An assortment of potential commercial and proprietary wear resistant alloys have been included in this study. The materials have been grouped according to the laboratory or steel works at which they were produced. The alloying approach taken in developing a superior abrasive-corrosive wear resistant steel is outlined in each case. The materials are presented in section 3.2.3 together with details of their chemical composition, microstructure, fabrication history, and any other relevant information*.

3.2.2 Nomenclature

A standard system of nomenclature was devised for all the materials handled in this program. The system is outlined below:

1	2	3	4

Example: WSA6 200

(1) The first letter identifies the source of the material (eg. W). There is an added advantage as the suppliers have usually followed different alloying approaches.

(2) The second letter (or numerals) is the suppliers code name or heat number for the material (eg. SA6).

(3) A space separates the material name from the heat treatment code.

(4) The heat treatment code follows a set format described in Table 3.5. (eg. 200°).

* Footnote : The quantity of material made available often precluded the author from conducting investigative tests in support of the wear results and for a more comprehensive characterisation of the materials. Certain information has also been withheld from the author due to the commercial importance of these potential alloy steels and possible infringments of patenting rights.

TABLE 3.5 : Description of heat treatment abbreviations

Code	Description
ar	as received (usually hot rolled and air cooled)
Ann	full anneal from 1050°C
AC	1100°C (1 hr) air cooled
OQ	1100°C (1 hr) oil quenched
200	1100°C (1 hr) OQ; 200°C (½ hr) OQ (tempering temperature 200° - 600°C)
ii	1000°C (½ hr) OQ; 200°C (½ hr) OQ
iii	1020°C (½ hr) OQ; 200°C (½ hr) OQ
iv	1100°C (1 hr) OQ: 200°C (½ hr) OQ; 870°C (½ hr) OQ; 200°C (½ hr) OQ
vi	1100°C (1 hr) OQ; 200°C (½ hr) OQ
viii	1100°C (1 hr) OQ; 200°C (½ hr) OQ; 1100°C (½ hr) OQ; 200°C (½ hr) OQ
AHR (1)	1150°C (3/4 hr); hot roll 30% at 1100°C finnish roll 43% at 1000°C, Oil quench
AHR (2)	Same as AHR (1) except additional finish roll at 950°C, Oil quench
AHR 200	Same as above except tempering after OQ at 200°C

3.2.3 Presentation of Materials

Low carbon and proprietary wear resistant steels

Mild steel (070M20) has been selected as the standard for the abrasion and corrosion tests (Allen, Protheroe and Ball, 1981; Noël, Allen and Ball, 1984); the performance of all the other materials has been recorded relative to 070M20. Specimens were machined from commercial flat bar and tested in the as-received (normalized) condition. The microstructure is equiaxed grains of ferrite with pearlite at the triple point boundries (fig. 3.7).

FIGURE 3.7 : Microstructure of the standard material 070M20 in the normalized condition. Ferrite (light), pearlite (dark)

The steel 835M30 is a low alloyed carbon steel that is presently being used in the heads of rock hammer drills. Specimens were heat treated to full hardness by an oil quench from 830°C followed by a temper at 200°C. The microstructure is tempered martensite.

The steel SS10/200 (also known as Bennox) is marketed as a wear resistant steel. The material was tested in the 860°C oil quenched condition and has a fine martensitic microstructure.

Abrasalloy and Wearalloy 400 are presently being used as abrasive resistant steels in the mines. These steels are not resistant to corrosion so their rate of degradation has become unacceptable. The steels are used in the roller quenched and tempered condition, having a microstructure of tempered martensite. Both materials were found to have stringers of silicate and manganese sulphide inclusions parallel to the rolling direction. Wearalloy 400 also had coarse, angular inclusions characteristic of titanium nitride or possibly zirconium nitride (Peters, 1983).

The chemical compositions for the above mentioned steels are given in Table 3.6 and the determined mechanical properties are tabulated in Table 3.7.

TABLE 3.6 : Chemical composition of the low carbon and proprietary wear resistant steels

MATERIAL	C	Cr	Mn	Ni	Mo	V	Ti	Al	Cu	Si	S	P	Other
070M20	.15	.02	.5	.03	.01	.01	.01			.35	.06	.06	
835M30	.34	1.35	.42	3.88	.22	.01	.005			.25	.013	.011	
SS10/200	.48	.16	.94	.15	.024	.002	.001	.024	.17	.24	.025	.012	
Abrasalloy	.39	.34	.85	.6	.16			.04	.05	.17	.018	.02.	
Wearalloy 400	.21	.02	.97	.03	.01	.01	.03			.24			.001%B

TABLE 3.7 : Mechanical properties of the low carbon and proprietry wear resistant steels

MATERIAL	HARDNESS HV30	TOUGHNESS Joules
070M20	149	119
835M30	530	55
SS10/200	775	2
Abrasalloy	436	25
Wearalloy 400	406	66

Commercial stainless steels

AISI 304L and AISI 316 are austenitic stainless steels and have been included in the program because of their high resistance to corrosion. The austenitic matrix of AISI 304L is metastable and has been used to study the mechanisms of abrasive wear (Allen, Protheroe and Ball, 1981/1982). The materials were tested in the hot rolled and annealed condition.

AISI 431 and AISI 440B are heat treatable, martensitic stainless steels. AISI 431 was heat treated to full hardness by an oil quench from 1100°C and tempered at 200°C. The microstructure consists of islands of austenite in a matrix of martensite. AISI 440B was hardened by an oil quench from 1060°C and tempered at 260°C to achieve maximum toughness (fig. 3.8).

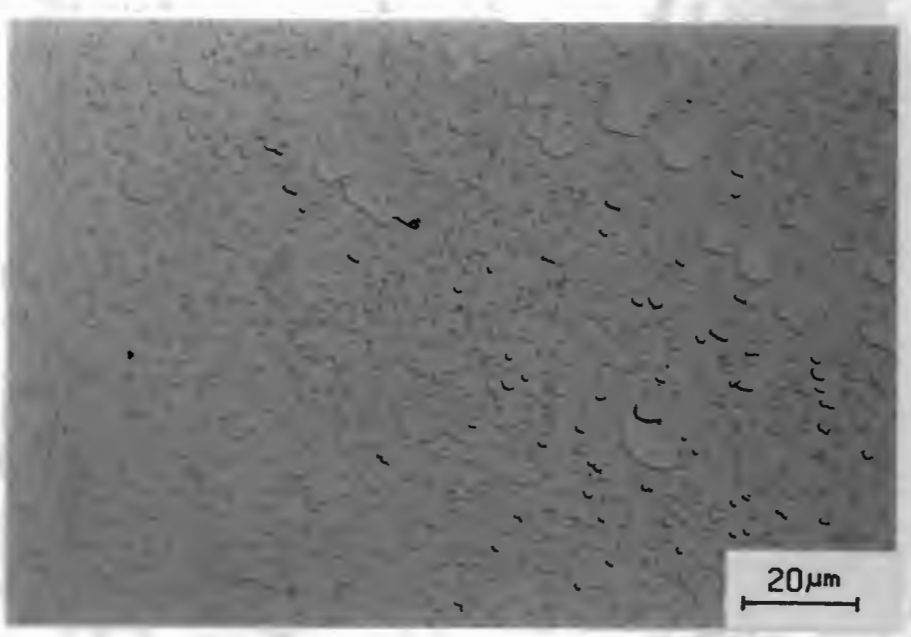

FIGURE 3.8 : Optical micrograph of AISI 440B. The microstructure consists of large primary, and spheroidized secondary carbide particles in a matrix of tempered martensite

The alloy NP599 produced by Armco is a developmental nitrogen strengthened austenitic stainless steel for applications involving wear. It is known to transform to martensite and work harden

rapidly when cold worked. It has been developed to replace AISI 304 where higher strength is needed together with good resistance to abrasive wear under wet sliding conditions. Nitronic 60 produced by Armco is a galling and wear resistant stainless steel for ambient and elavated temperature applications. It has superior oxidation resistance, toughness and yield strength properties to AISI 304. Nitronic 60 is austenitic with chromium- nitrides present as fine dispersed particles (Hsu, Ahn and Rigney, 1980).

The approximate chemical compositions and mechanical properties for the stainless steels are given in Tables 3.8 and 3.9 respectively.

TABLE 3.8 : The chemical composition of the commercial stainless steels

MATERIAL	C	Cr	Mn	Ni	Mo	V	Ti	Si	S	P	N
AISI 304L	.035	18.8	1.38	8.4	.11	.09	.02	.42			
AISI 316	.08	16.6	1.32	10.4	2.2	.08	.02	.55	.030	.045	
AISI 431	.20	16	1.0	2.0				1.0	.030	.040	
AISI 440B	.80	17	1.0		.75			1.0	.03	.04	
NP599	.10	16	8.0	2.3				1.0			.23
Nitronic60	.10	17	8.0	8.5				4.0			.13

TABLE 3.9 : The mechanical properties of the commercial stainless steels

MATERIAL	HARDNESS HV30	TOUGHNESS Joules
AISI 304L	206	178
AISI 316	210	172
AISI 431	496	72
AISI 440B	648	5
NP599	230	107
Nitronic60	231	325

Steels from Source W

Source W produced alloys based on Quatough (fig. 3.9), a high strength, tough, martensitic steel developed in the USA by Thomas and co-workers (Roa and Thomas, 1980; Salesky and Thomas, 1981).

The requirement of improved corrosion resistance suggested an alloy with a higher chromium content. In formulating the chemical compositions of the experimental alloys (WA, WB and WC) Bee, Peters, Atkinson and Garrett (1985) noted the following. Chromium increases the strength of a martensitic matrix but it lowers the M_S* temperature. This in turn drastically reduces the toughness through the formation of an undesirable twinned martensitic sub-structure. Similarly, carbon in solid solution strongly influences the strength and M_S temperature of a martensitic steel, but to a much greater extent than chromium. Nickel is used in preference to manganese as an austenite stabiliser as it provides added corrosion resistance and increases the fracture toughness in chromium containing steels.

The microstructure of alloys WA, WB and WC are predominately lath martensite. The microstructures were similar in all the heat treated conditions but the re-austenitisation treatments generally produced a finer grain size and decreased the volume fraction of coarse carbides. The carbides tended to cluster into bands following the rolling direction and decorate the prior austenite grain boundaries.

Alloy WD had a higher carbon content and was designed as a dual phase martensitic matrix (with up to 15% volume fraction retained austenite), consisting of coarse, well bonded, spheroidal chromium carbides (Peters, 1983). The microstructure achieved had a lath martensitic matrix with a uniform distribution of the coarse carbides.

* Footnote : M_S temperature is the temperature at which the austenite to martesite phase transformation starts on cooling from the austenite phase. M_f is the finish temperature.

WA2 and WB2 are second heats of experimental alloys WA and WB with nominally the same composition. There was a noticable improvement in toughness. The microstructure of alloys WA2 and WB2 were tested in a range of heat treated conditions and are detailed in Section 4.1.3 (fig. 4.13).

The steel designated WSA6 is a laboratory air melted alloy, the composition of which is based on a specification as being typical of an air melt using selected scrap as the base material. This material was developed from alloys WA and WB as the forerunner to a full scale commercial melt. The general microstructure was lath martensite within the equi-axed, prior austenite grains. There was a degree of banding which suggests a segregation of nickel but this could not be confirmed. In the re-austenitisation heat treatment, the banding was not evident, but some grain growth had occured (fig. 3.10).

Table 3.10 lists the chemical composition of the Source W alloys together with Quatough. The dilatometry results are given in Table 3.11 and the mechanical properties in all the heat treated conditions are given in Table 3.12.

TABLE 3.10 : Chemical composition of the Source W alloys

MATERIAL	C	Cr	Mn	Ni	Mo	V	Al	Si	S	P
WA	.24	7.08	.02	3.2	.01			.027	.010	.007
WB	.24	10.3	.07	3.25	.02			.020	.011	.008
WC	.25	12.3	.02	1.0	.02			.026	.009	.007
WD	.43	12.2	.05	2.01	1.50	.26		.053	.014	.013
WA2	.26	7.18	.01	3.21	.01	.01		.04	.007	.005
WB2	.27	10.4	.01	3.19	.01	.02		.04	.01	.01
WSA6	.25	8.0	.5	3.0	.06		.05	.5	.008	.02
Quatough	.3	4.0	2.0	.03				.04	.003	.012

NOTE : Alloy WV69 has been included with the Source M alloys on which it is based.

TABLE 3.11 : Equilibrium transformation temperatures of the source W alloys. KB - own work; JP - cited in Peters (1983)

MATERIAL	A_1	A_3	M_s	M_f	Source
Quatough	769	795	338	135	KB
WA	697	870	288	106	JP
WB	684	839	220	20	JP
WC	666	850	234	118	JP
WD	765	890	179	41	JP

TABLE 3.12 : Mechanical properties of the Source W alloys

MATERIAL	HARDNESS HV30	TOUGHNESS Joules	GRAIN SIZE (μm)
Quatough ar	285	31.1	
200	546	47.6	
WA ar	527	22.8	
iv	470	48.8	
vi	540	67.5	30.5
viii	537	62.5	29.7
WB ar	614	11.3	
vi	573	26.0	30.4
viii	594	26.0	32.8
WC ar	606	7.0	
vi	614	16.0	60.0
viii	610	15.5	40.0
WD ar	705	8.0	
i	462	11.0	
WA2 ar	554	18	
AC	435	27	
200	546	56	28.8
300	503	61	
400	484	50	
500	456	35	
600	268	141	
WB2 ar	604	15	21.8
AC	412	10	22.1
200	509	47	46.4
300	491	52	
400	472	66	
500	425	24	
600	299	126	
WSA6 ar	550	12	40.8
200	532	34	40.2

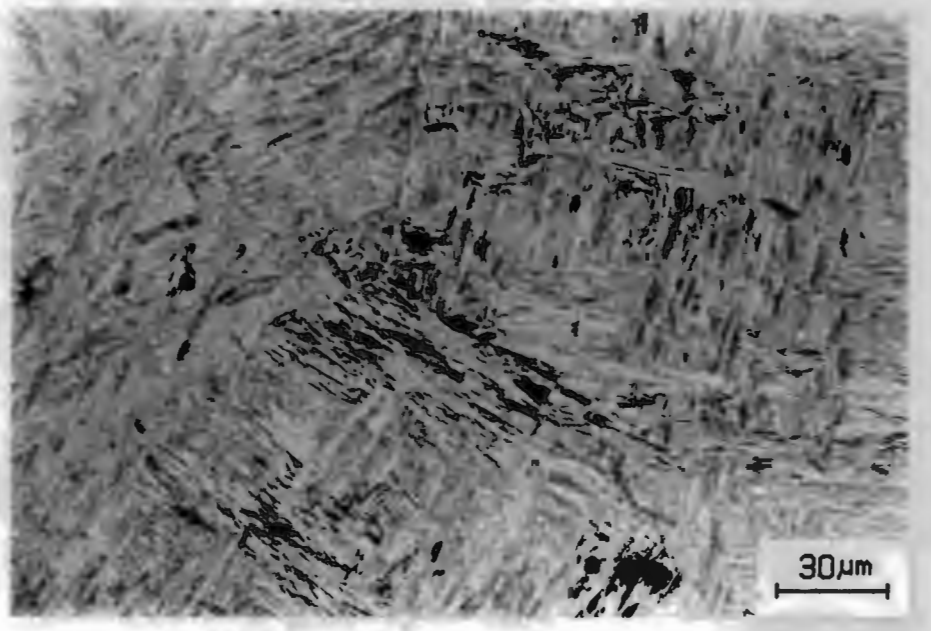

FIGURE 3.9 : Microstructure of Quatough in the quenched and tempered condition (1100°-OQ-200°-OQ) comprising lath martensite with large prior austenite grains and a dispersed carbide precipitate throughout the matrix

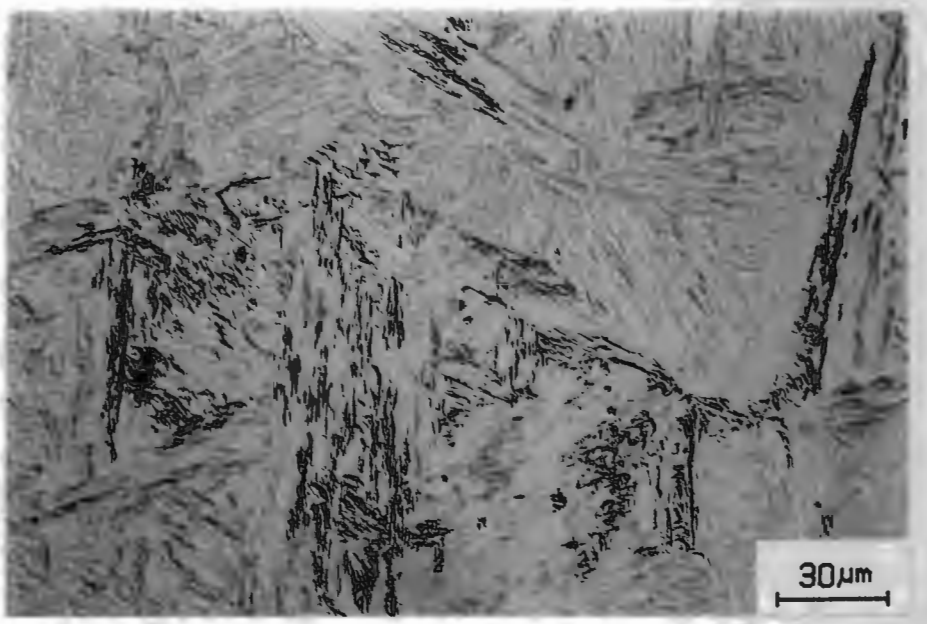

FIGURE 3.10 : Microstructure of WSA6 200 reveals a clean lath martensitic structure. Optical metallography has shown no evidence of carbides dispersed through the matrix or decorating the grain boundries.

Steels from Source I

A range of alloys, with from 6 to 11% chromium, was produced by Source I. The other major elements considered, in addition to chromium, were carbon, nickel and manganese.

Alloy IA has only 6% chromium. However, in an attempt to improve the corrosion resistance, aluminium (1.2%) and silicon (1.6%) were included. The carbon level was kept low at 0.12%. This produced a dual phase steel (ferrite factor = 12.0) consisting of grains of ferrite (45 volume %) and martensite. There were secondary islands of ferrite within the martensite grains (fig. 3.11).

To determine the effect of carbon, nickel and manganese, on the abrasive-corrosive wear properties, alloys IB, IC and ID were produced. These materials have approximately the same amount of chromium present. Similarly, alloys IE and IF were produced with approximately the same chemical composition except for a controlled variation in nickel.

The Source I alloys have been stabilized with niobium and vanadium to control the grain size during rolling. A selection of these alloys have been tempered at various temperatures. The microstructure of these alloys is a tempered martensite with a scattering of coarse spherical carbon-rich inclusions in the matrix. Alloy IF is the only material showing evidence of chromium carbides present in clusters about the inclusions and along the prior austenite grain boundaries (fig. 3.12).

The chemical compositions and mechanical properties for the Source I material are given in Tables 3.13 and 3.14 respectively. No dilatometry results are available for these materials.

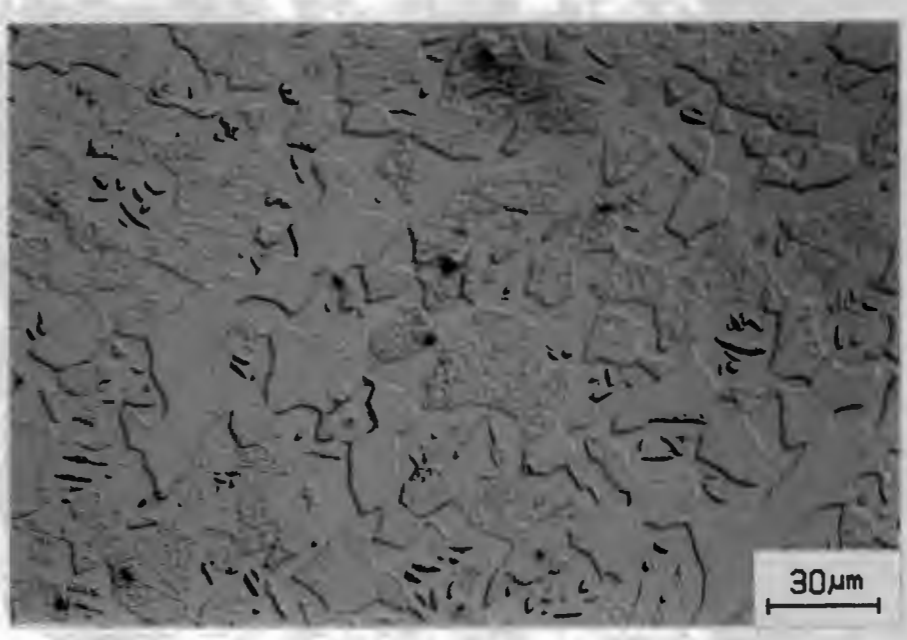

FIGURE 3.11 : Microstructure of IA 200. The white areas are ferrite (MHV=241), matt grey areas are martensite (MHV=584)

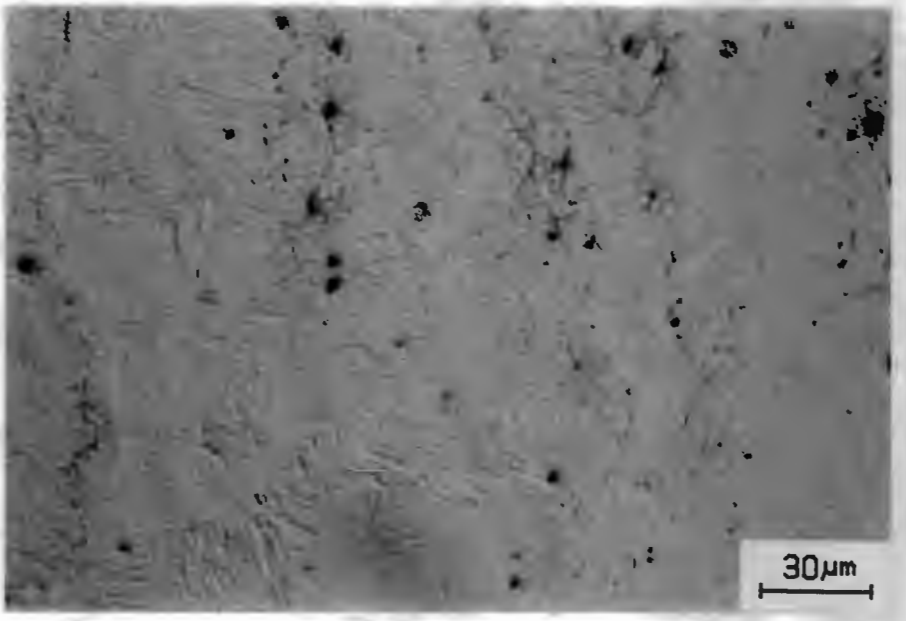

FIGURE 3.12 : Microstructure of IF OQ is a quenched martensite with alloy segregation and carbides in clusters following the rolling direction

TABLE 3.13 : Chemical composition of the Source I alloys

MATERIAL	C	Cr	Mn	Ni	Mo	V	Al	Nb	Si	S	P	F.F.
IA	.12	6.0	.64	.02	.01	.04	1.2	.02	1.6	.014	.009	12.0
IB[c]	.14	8.71	.7	1.93	1.4	-		.044				-
IC[c]	.18	9.0	-	-	.8	.2						5.0
ID[a]	.23	9.06	.60	3.85	.71	.5	.10	.02	.5	.014	.011	-
IE	.20	10.4	.83	.03	.62	.5	.02	.02	.5	.014	.011	6.2
IF[a]	.22	10.8	.65	4.21	.8	.5	.03	.02	.5	.021	.011	-

TABLE 3.14 : Mechanical properties of the Source I alloys

MATERIAL	HARDNESS HV30	TOUGHNESS Joules	GRAIN SIZE (μm)
IA OQ	350	5	11.6
200	320	10	14.6
300	354	10[d]	b.
600	300	22	15.4
IB[c]	478	52	b.
IC[c]	502	59	b.
ID OQ	620	6[d]	30.3
200	562	27	46.3
300	503	36	55.8
600	525	4[d]	50
IE 300	520	36	b.
IF OQ	570	5	20.0
200	524	25	25.3
300	483	36	27.1

a - aimed for 2% Nickel
b - undetermined, grain boundries not resolved
c - the imformation on these alloys is incomplete due to pending patent rights
d - specimen cracked due to forging defects
F - ferrite factor = Cr+6Si+8Ti+4Mo+2Al+2Nb-2Mn-2Ni-40(C+N)
(Kaltenhuaser, cited in Ball and Hoffman, 1981) ....(8)

Steels from Source T

As mentioned previously, the poor corrosion resistance of Quatough can be overcome by increasing the chromium content of the steel. Numerous people have reported that the elements copper and aluminium improve the long term atmospheric corrosion resistance of carbon steels. It was thought that the addition of these elements together with chromium could also provide the necessary corrosion resistance (Protheroe, Ball and Heathcock, 1982). The addition of aluminium and silicon to AISI 4340 (an UHS steel) is found to increase the strength and toughness properties of this material and was used to advantage in improving the abrasion resistance of this type of steel (Bhat, Zackay and Parker, 1979).

Alloys T820 and T102 are based on Quatough with increased amounts of chromium. To investigate the influence of aluminium, alloy T820A was produced with aluminium and T820B without aluminium. Similarly for alloys T102A and T102B, except that the amount of aluminium added was not as much due to the higher level of chromium. In all cases a low level of copper and silicon was maintained.

The first alloys produced at the start of this project did not meet the toughness requirements. Alloy T122 is a 12 percent chromium steel based on the chemical composition of alloy WC and was designed with the aim of improving the toughness of a WC type alloy. Alloy T122 has a clean, lath martensitic microstructure with no evidence of carbides. There are a few manganese sulphide inclusions (3 to 5 micrometres in diameter) scattered throughout the matrix (fig. 3.13).

Controlled rolling is another way of improving the toughness of a steel and has the added attraction of relatively low production costs and good fatigue strength (Honeycombe, 1981). Controlled rolling has eliminated quenched and tempered steels in many applications. The Source T alloys were produced both in the air quenched and tempered condition, and subjected to a controlled rolling treatment. The influence of tempering after a roller quench was also considered.

The microstructure of these alloys is lath martensite with large prior austenite grains. There were no carbides found using optical metallurgraphy. The samples that were tempered after controlled rolling have a lightly tempered martensitic structure. The grain size of the air quenched samples are massive (± 300 μm for T820A and T102A) compared to the control rolled material (± 70 μm for T820A and ± 30 μm for T102A). T820A has a scattering of spherical manganese sulphide inclusions (2-3 μm in size) throughout the matrix.

T820B has islands of a second phase, possibly delta ferrite, at the grain boundries which occupies 3% of the volume. This second phase prevented grain growth during air cooling and may be instrumental in the high M_s and M_f temperatures (Table 3.15). The microhardness of the air quenched sample of alloy T820B is 524HV for the martensitic phase and 262HV for the secondary phase. The prior austenite grain size is ± 80 μm for the air quenched material and ± 35 μm for the controlled rolled material. After the rolling treatment the second phase was found as elongated stringers within equi-axed grains of lath martensite (fig. 3.14). This suggests that the second phase is stable at 1100°C. EDAX analysis could not detect any chemical difference between the two phases.

TABLE 3.15 : Phase transformation temperatures (°C) for the Source T alloys

MATERIAL	A_1	A_3	M_s	M_f	Source
T820A	800	821	357	183	KB
T820B	903	940	768	703	KB
T102A	844	927	392	20	KB
T102B	832	894	346	159	KB
T122	810	901	361	159	KB

The calculated M_s temperatures are in the Appendix

The chemical composition of the Source T alloys is given in Table 3.16. Note the difference in aluminium content between the A and B alloys (Table 3.10 for the composition of Quatough). Despite the low nickel content the carbon level is to high for ferrite to be present. The mechanical properties are given in Table 3.17. The impact toughness values are higher than any of the Source W or Source I alloys.

TABLE 3.16 : Chemical composition of the Source T alloys

Material	C	Cr	Mn	Ni	Ti	Al	Cu	Si	F.F
820A	.20	7.66	1.01	.01	.002	1.46	.01	.019	0.65
820B	.20	7.61	1.02	.01	.002	.002	.01	.020	-2.33
102A	.20	9.85	1.01	.007	.002	.50	.01	.018	0.93
102B	.21	9.86	1.01	.012	.002	.002	.01	.016	-0.49
122	.21	12.0	1.00	.008	.003	.002	.01	.018	1.70

TABLE 3.17 : Mechanical properties of the Source T alloys

MATERIAL	HARDNESS HV30	TOUGHNESS Joules
T820A AQ 200	465	57.5
AHR1	465	50.3
AHR1 200	459	67.9
AHR2	476	53.0
T820B AQ 200	457	62.0
AHR1	441	48.7
AHR1 200	444	69.0
AHR2	465	52.0
AHR2 200	467	70.2
T102A AQ 200	520	64.3
AHR1	517	34.5
AHR1 200	451	92.5
T102B AHR1	481	38.5
AHR1 200	505	91.1
T122 AQ 200	470	57.5
AHR1	504	25.7
AHR1 200	499	64.3

FIGURE 3.13 : Microstructure of T122 AHR 200 a 12%Cr steel showing a tempered lath martensitic structure

FIGURE 3.14 : Microstructure of T820B AHR2 200. The microhardness of the martensitic matrix is 524MHV and the second phase is 263MHV. EDAX analysis found no difference in composition between the two phases

Steels from Source F

One school of thought (Protheroe, Ball and Heathcock, 1982) in providing an abrasion resistant material is to produce a microstructure that is metastable. The high strains associated with abrasion can then be accommodated without local fracture by the strain induced phase transformation. This process provides a high work hardening capacity and the steel would respond plastically to abrasion. Such a material would have a very large work hardening capacity resulting in the required high strength, surface hardness and toughness (section 2.1.3).

Based on the work of Zackay and co-workers (1967), a range of transformation induced plasticity (TRIP) steels have been produced by Source F. The chemical compositions of these alloys have been adjusted to accommodate the requirements of corrosion resistance and low cost. The four materials produced cover an area that falls within the 'austenite plus martensite' region of the Schaeffler diagram (Honeycombe, 1981). It is predicted from the Schaeffler diagram that alloy F351 has the highest volume fraction austenite and that alloy F353 is fully martensitic (fig. 5.5 of section 5.2). Through control of the chemical composition and fabrication route it was anticipated that the M_s temperature would be below room temperature while the M_d (transformation of martensite on deformation) temperature remains above room temperature. It can be seen in Table 3.18 that nitrogen has replaced carbon as the solid solution strengthener of the martensite phase. Nitrogen, like carbon, is a very strong austenite former but has less tendency to cause intergranular corrosion. In this way the mechanical properties of these austenitic steels are improved without impairing their corrosion resistance. It is hoped that an optimum TRIP steel for gold mining applications can be selected from this range.

The information available on these steels is given in Table 3.18. Alloys F350 to F352 are only slightly magnetic. These alloys are austenitic but mechanical polishing has transformed some of the polished surface to martensite (fig. 3.15). Alloy F353 has a martensitic microstructure and is magnetic. It is anticipated that the M_s of F353 is above room temperature (Appendix A1).

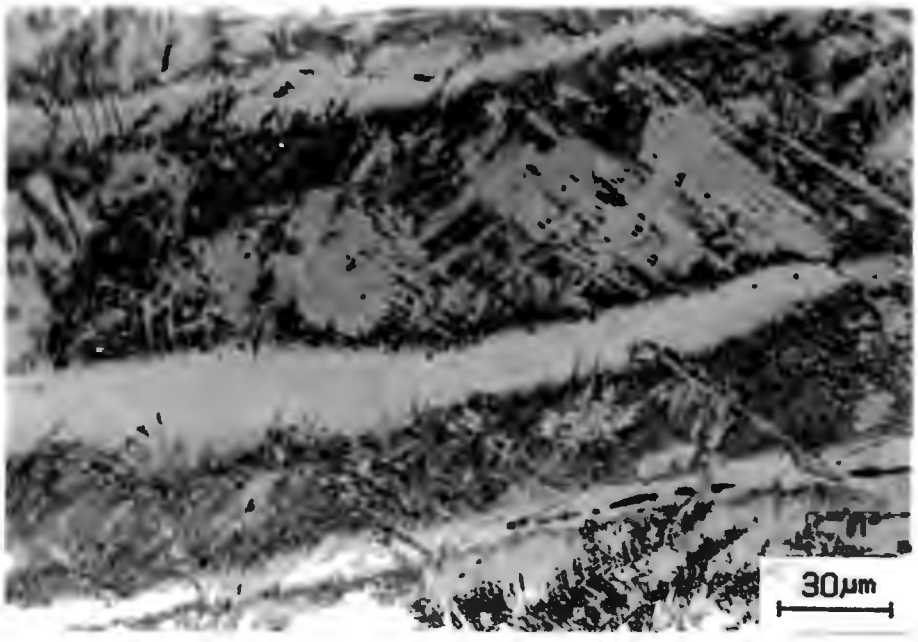

FIGURE 3.15 : Optical micrograph of F350 showing a twinned austenitic microstructure with preferential etching of slip lines. There are some areas of martensite which are a result of the mechanical polishing

TABLE 3.18 : The approximate composition of the Source F alloys

MATERIAL	HEAT TREATMENT	% C	% N	% Cr	% Mn	BULK HARDNESS HV30
F350	1050° Air cooled	.05	.2	10	10	223
F351	1050° Air cooled	.05	.2	12	10	225
F352	1050° AC; 200 (1 hr)	.05	.2	12	8	230
F353	1050° Air cooled	.05	.2	12	5	465

Steels from Source M

It has been shown that 3CR12 (a dual phase, ferritic-martensitic corrosion resistant steel) has the potential to be an abrasive-corrosive wear resistant steel (Allen, Protheroe and Ball, 1981/1982; Allen, Ball and Noël, 1984) and was found to be an economical alternative structural steel in certain applications.

To improve its dry abrasion resistance 3CR12 was heat treated to produce a harder structure without impairing its toughness greatly. 3CR12Ni is a high strength version of 3CR12 and differs mainly in its nickel content. WV69 is a 'high carbon' version of 3CR12 where the carbon level was increased to increase the bulk hardness of 3CR12. The increase in carbon resulted in the microstructure changing from a duplex structure, of martensite with islands of ferrite, to a fully martensitic structure (figs. 3.16 and 3.17). The chemical composition phase transformation temperature and mechanical properties of these materials are given in Tables 3.19, 3.20 and 3.21. respectivly.

TABLE 3.19 : Chemical composition of the 3CR12 type alloys

MATERIAL	C	Cr	Mn	Ni	Ti	N	Si	S	P	F.F
3CR12	.022	11.3	1.14	.62	.20	.02	.37	.015	.016	8.7
3CR12Ni	.027	11.71	.90	1.21	.23	.019	.47	.011	.022	7.9
WV69	.07	12.0	.05	1.55			.05	.01	.003	3.1

FIGURE 3.16 : Microstructure of 3CR12Ni ii consists of a matrix of low carbon quenched martensite with islands of ferrite. Manganese sulphide inclusions are also visible

FIGURE 3.17 : Microstructure of WV69 200 is fully martensitic

TABLE 3.20 : Transformation temperatures of the 3CR12 type alloys

MATERIAL	A_1	A_3	M_s	M_f	Source
3CR12	792	856	456	RT	YC
3CR12Ni	745	842	389	RT	YC
WV69	765	861	420	195	KB

TABLE 3.21 : Mechanical properties of the 3CR12 type alloys

MATERIAL	HARDNESS HV30	TOUGHNESS Joules
3CR12 ar	153	75.5
3CR12 iii	250	80.0
3CR12Ni ii	308	55.9
WV69 ar	413	90.0*
WV69 200	379	175.0*

* Longitudinal not transverse section

Steels from Source U

The early results emerging from the alloy development programme were informative and most encouraging. The decision was then made to produce an alloy on a small commercial scale.

Source U produced 4 tonnes of steel from selected scrap. The advantages were threefold. (i) More material was available so that specific components for in-situ testing could be made. (ii) Sufficient material was now available for an indepth study of corrosive-abrasive wear. (iii) The results would have the added significance of coming from a commercially viable steel produced with conventional fabricating techniques.

According to Source U, Alloy UA was made in a 5 tonne basic furnace using selected scrap. The steel was tapped and teemed into four ingots. The ingots were forged into a suitable shape for electroslag remelting. The refined ingots were then precision forged into 150 mm diameter bars. The resulting bars were initially too hard to machine but after a workable annealing cycle was found, the bars were supplied with a hardness of 40 HRC. The chemical composition is given in Table 3.22.

The sample received was first tempered at 650°C in the laboratory (to achieve a hardness of 27 HRC) before test specimens were machined. With reference to the dilatometry trace (fig. 3.18) and from experience (section 4.1.3), the selected heat treatment of UA was 1100°C (1 hour) under vacuum, oil quench and temper at 200°C. The resulting mechanical properties are given in Table 3.23.

Alloy UA has a clean, tempered martensitic microstructure with no inclusions or precipitates visual under optical examination (fig. 3.19). TEM examination shows the martensitic laths to be highly dislocated (fig. 3.20). No retained austenite was detected in UA 200 using the TEM or Xray defraction tequniques thus it must be less than 5 volume per cent if present. Examination of a fractured surface under the SEM showed the presence of minute spheroidal particles (less than 1 micrometre in diameter) which are thought to be precipitates of manganese sulphide (figs. 3.21 and 3.22).

TABLE 3.22 : The chemical composition of UA

MATERIAL	C	Cr	Mn	Ni	Mo	V	Sn	Al	Cu	Si	S	P
UA	.23	8.65	.35	3.33	.02	.04	.01	.01	.08	.32	.008	.012

TABLE 3.23 : The mechanical properties of UA

MATERIAL	HARDNESS HV30	TOUGHNESS Joules
UA	559	78.5

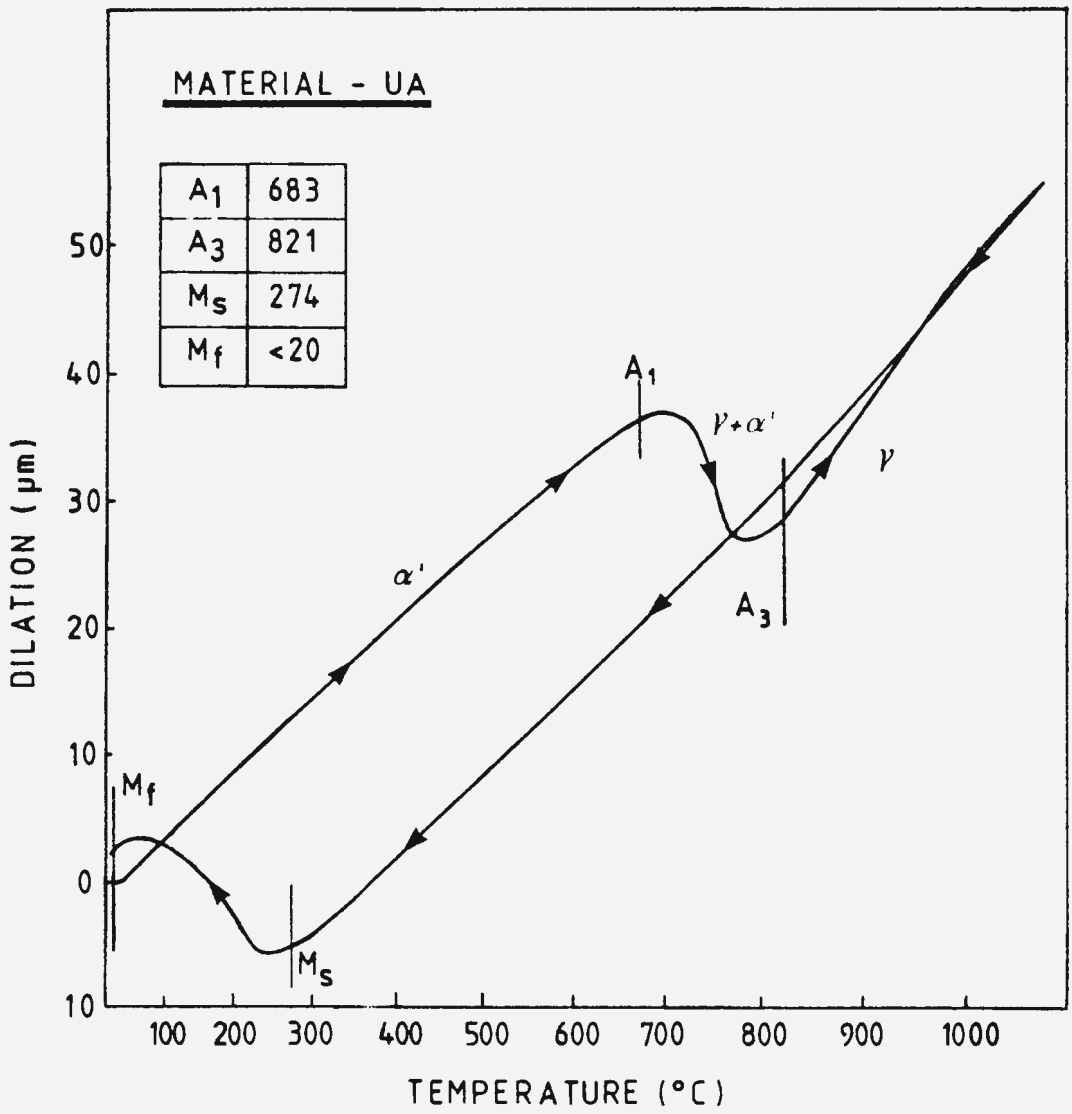

FIGURE 3.18 : Dilatometry trace of UA showing the start and finish temperatures for the transformation between the austenite and martensite phases under controlled heating and cooling conditions

FIGURE 3.19 : Optical micrograph of UA 200 showing a tempered martensite with large prior austenite grains and a matrix free of coarce precipitates or inclusions

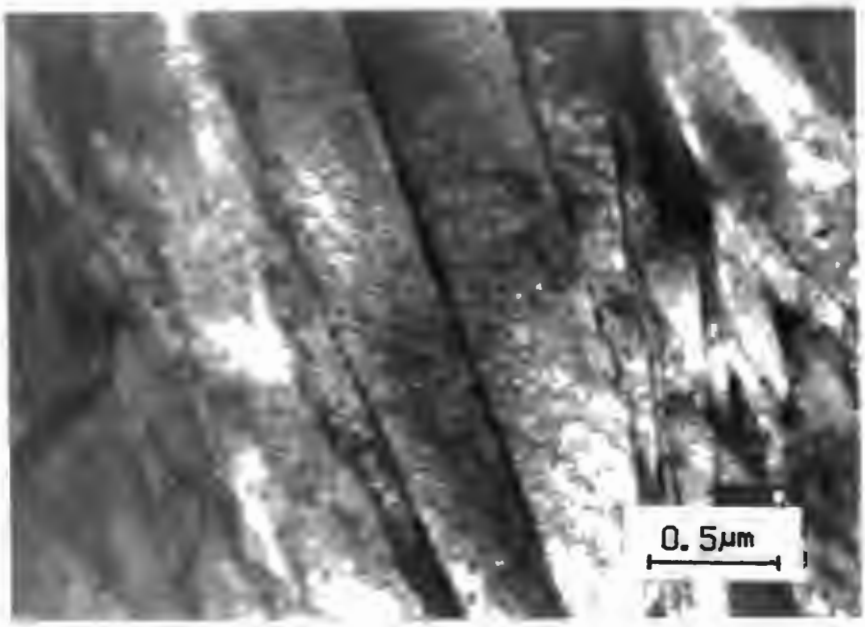

FIGURE 3.20 : TEM micrograph of UA 200 reveals a structure of dislocated lath martensite free of interlath secondary carbide precipitates

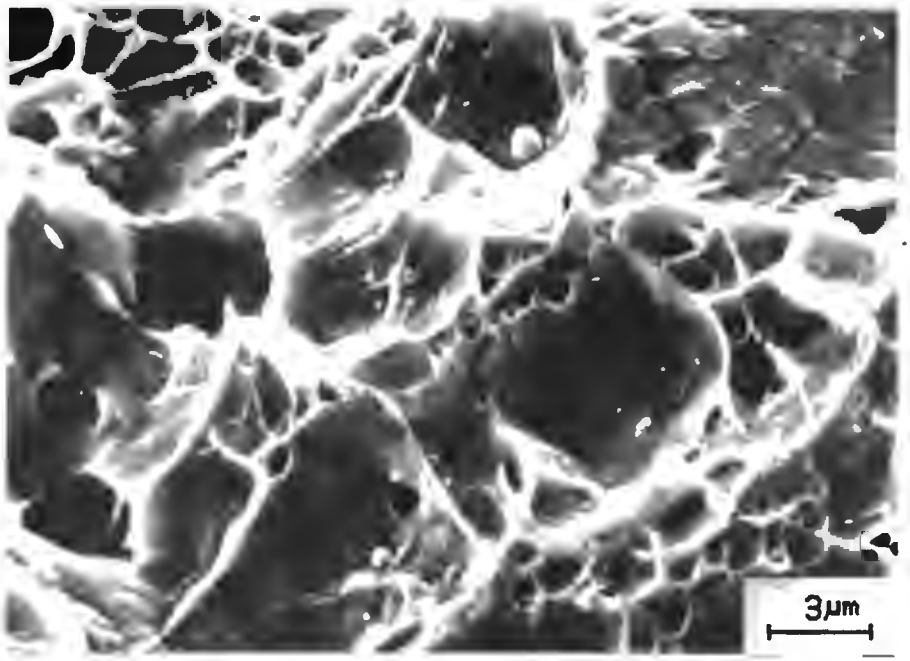

FIGURE 3.21 : SEM micrograph of the Charpy fractured surface of UA 200. The spheroidal particles are associated with the initiation of voids in ductile fracture

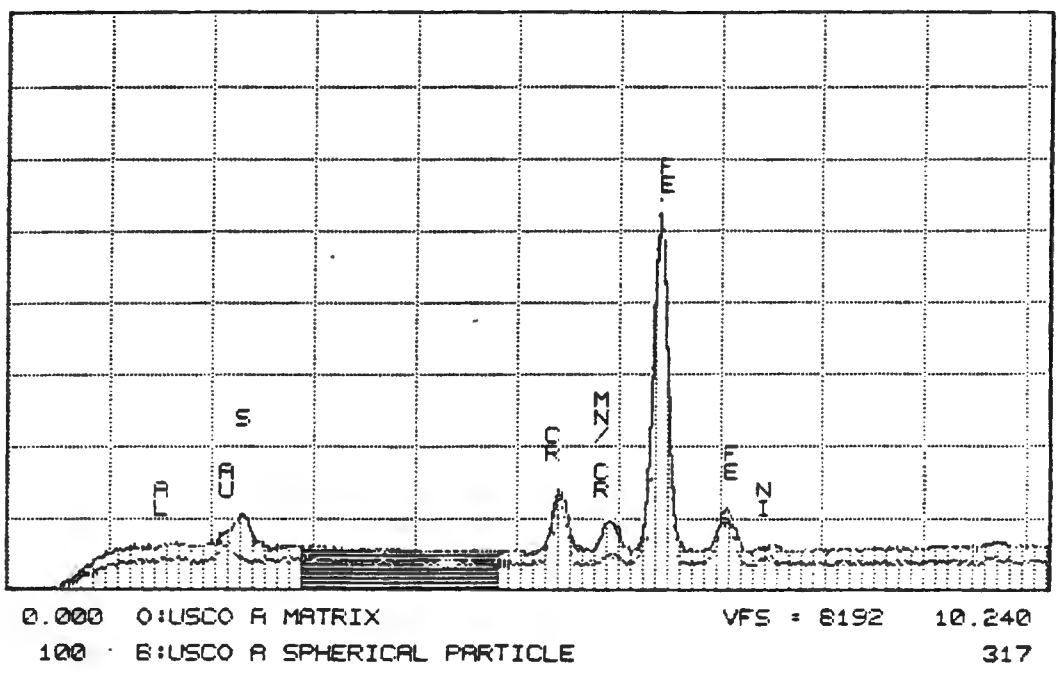

FIGURE 3.22 : Superimposed EDAX analysis of the matrix (outline) and the spherical particle (background) showing a high predominance of manganese and sulphur

CHAPTER 4

RESULTS

An evaluation of the abrasion-corrosion wear results for the standard tests and the general trends and relationships will be presented in section 4.1. A comprehensive table of the results for all the materials introduced in section 3.2 will be found in Appendix A3. A detailed study of more specific aspects is covered in section 4.2.

4.1 ABRASIVE-CORROSIVE WEAR PERFORMANCE OF MATERIALS

4.1.1 Interpretation of the Wear Results

Wear resistance is not a straight forward material property, but the property of a system. Thus the amount of wear determined for a material cannot be separated from the wear test method.

A good understanding of the conditions under which the results were obtained is necessary in their analysis. It is therefore important that the reader is familiar with the various test methods and conditions of testing as described in section 3.1.2.

Relative dry Abrasion Resistance (RAR)

The volume of material removed during abrasion is linearly dependent on the length of the abrasive path (fig. 4.1). RAR is calculated from the slopes of the lines (section 3.1.2) with respect to the standard material, mild steel (070M20). The distribution in dry abrasion results (fig. 4.2) shows what progress has been made in the alloy development program. The majority of experimental materials have an RAR that is at least 50% better than mild steel which is presently being used in many applications and 20% better than the commecially available proprietry abrasion resistant alloys like Abrasalloy and Wearalloy 400. There are a few alloys with more than twice the abrasion resistance of mild steel.

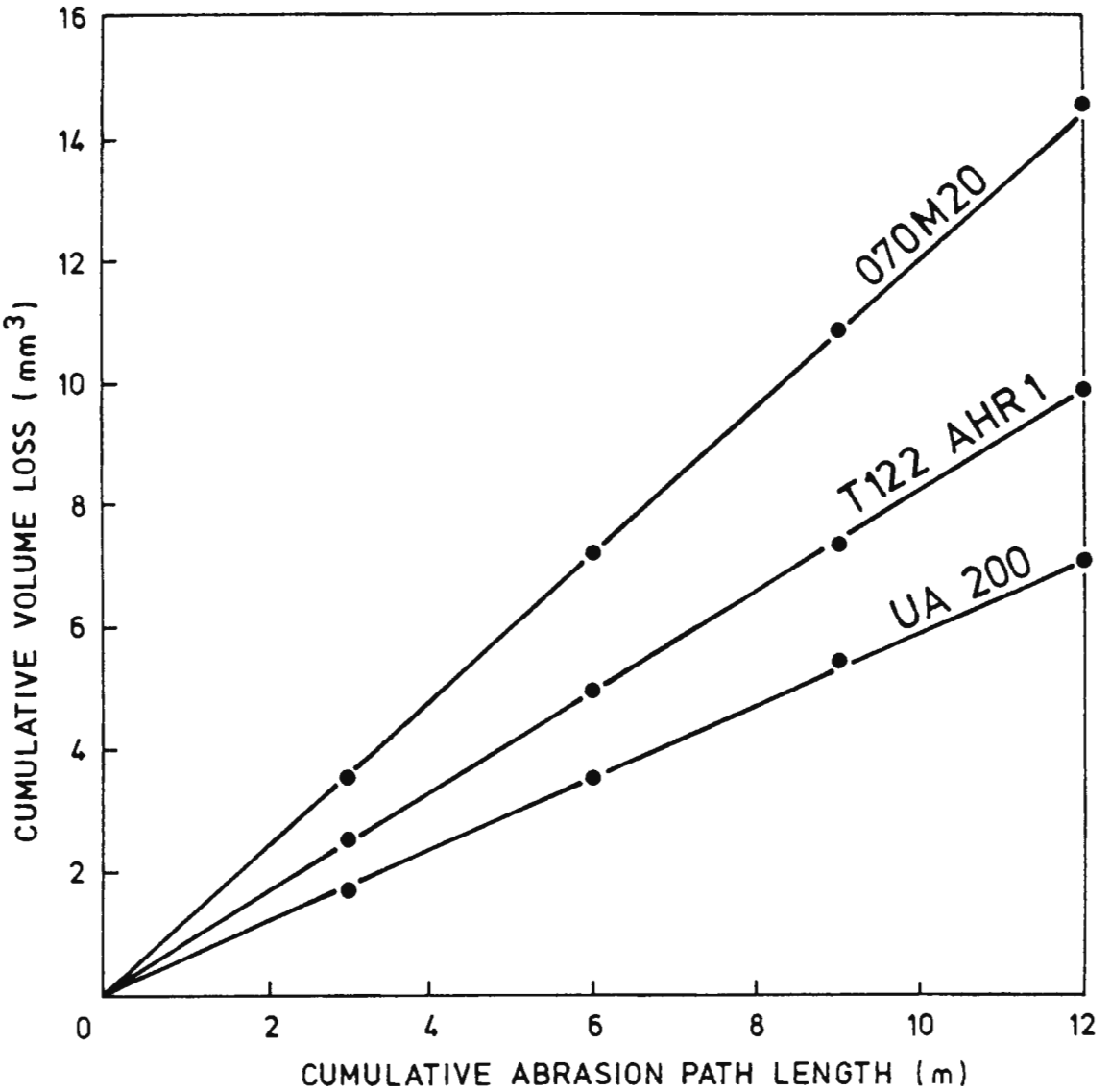

FIGURE 4.1 : Typical results for the RAR test from which the abrasion performance ratios are calculated. Material 070M20 (the standard) has an inferior RAR of 1.00; T122 AHR1 has a good RAR of 1.5 while UA 200 has an excellent RAR of 2.10

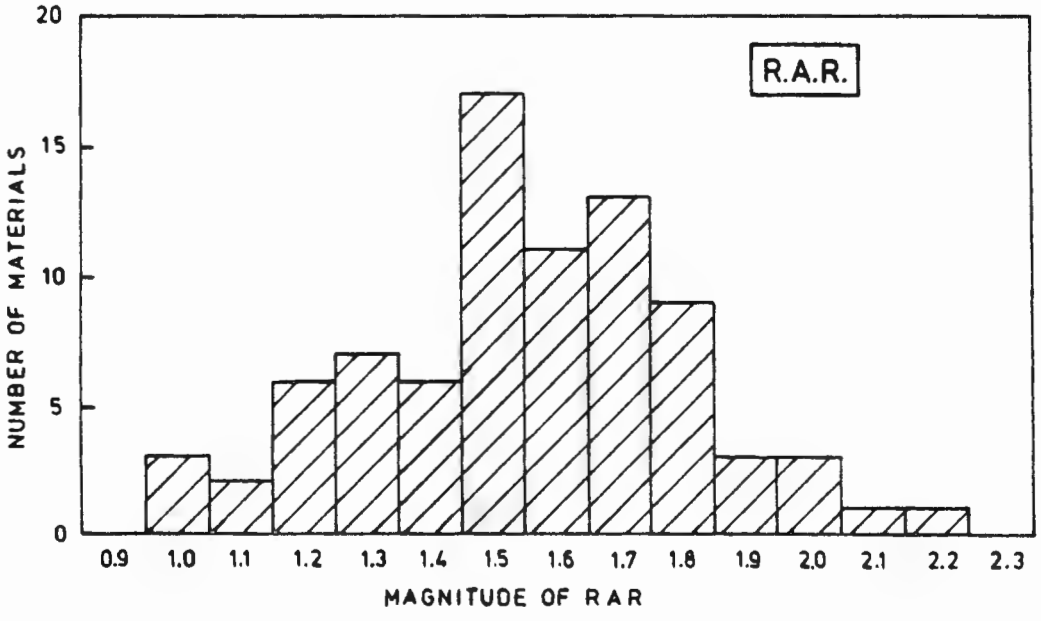

FIGURE 4.2 : A histogram showing the distribution of RAR results for all the steels and experimental alloys tested

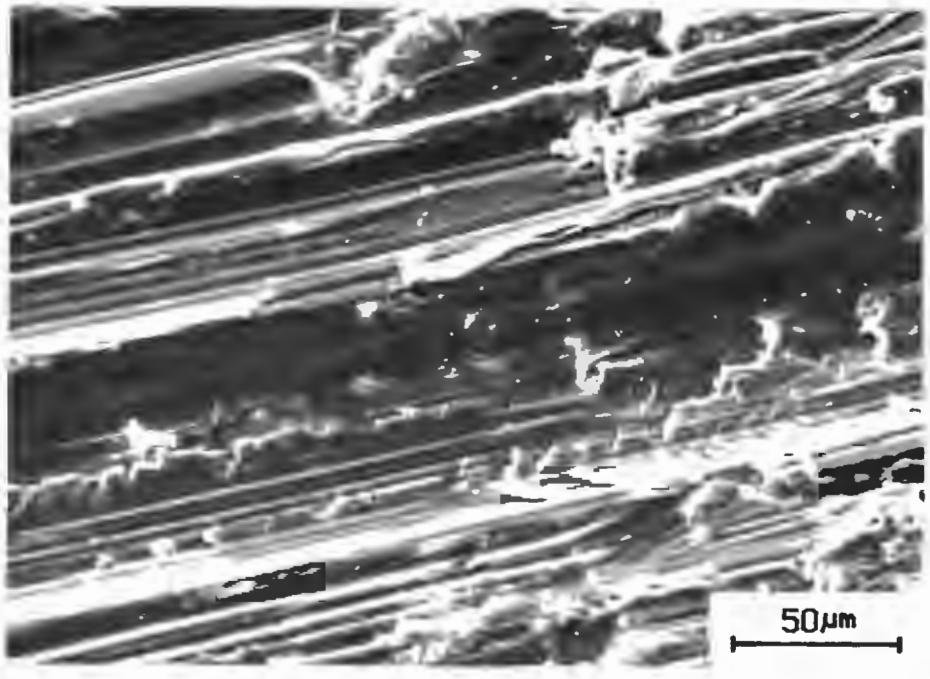

FIGURE 4.3 : SEM micrograph of the abraded surface of the experimental steel alloy T102A AHR 200 after 12 metres of dry abrasion under laboratory conditions. Abrasive moved left to right.
Microstructure : fine tempered lath martensite
Bulk Hardness : 451 HV30
Charpy Toughness : 93 Joules

Laboratory Relative abrasive-corrosive Wear Resistance (RWRL) and the alternate version (RWRL #2)

There are two facets to the RWRL and RWRL #2 tests (section 3.1.2) namely the influence of abrasion and the influence of corrosion. Figures 4.4 to 4.7 are examples of test results from which the RWRL or RWRL #2 values are determined. In both these tests the contributions of abrasion and corrosion have been separated.

It is found that the total volume of material lost or removed is a property of the material, as are the relative fractions of material lost due to corrosion and due to abrasion. A characteristic of the RWRL test (for the materials with little or no corrosion resistance) is a non-linear increase in accumulative volume loss. It is non-linear because of a decrease in the rate of volume loss due to corrosion with each cycle. That is, the volume loss due to corrosion is not linearly dependent on time (figs. 4.4a, 4.5a, 4.6a), but is related to the length of abrasion and frequency of the cycles. It should be noted that the scale of the ordinates in figs. 4.4, 4.5 and 4.6 differ. The RWRL and RWRL #2 values determined from figs. 4.4 to 4.7 inclusive are tabulated in Table 4.1. together their RAR and with an interpretation of the results.

TABLE 4.1 : RWRL results determined from figs. 4.4 to 4.7

MATERIAL	RAR	RWRL #2	RWRL	COMMENTS
070M20	1.00	1.0	1.0	poor; the standard as presently used in the mines
IA 200	1.39	1.8	2.2	both abrasion and corrosion resistance is poor
UA 200	2.10	4.3	4.6	excellent abrasion resistance but the corrosion resistance is doubtful
AISI 431	1.56	3.8	13.5	excellent corrosion resistance but the abrasion resistance is mediocre

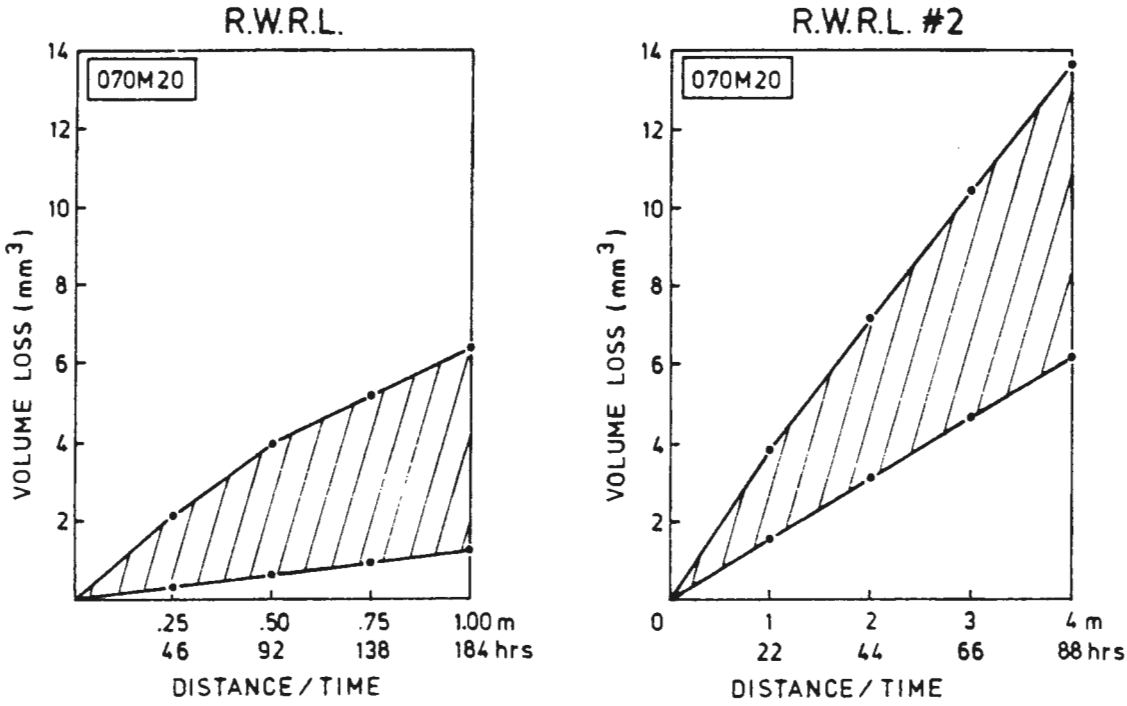

FIGURE 4.4 : The RWRL and RWRL #2 results of 070M20. The lower line is abrasion only, the upper line includes the contribution by corrosion to the total volume loss

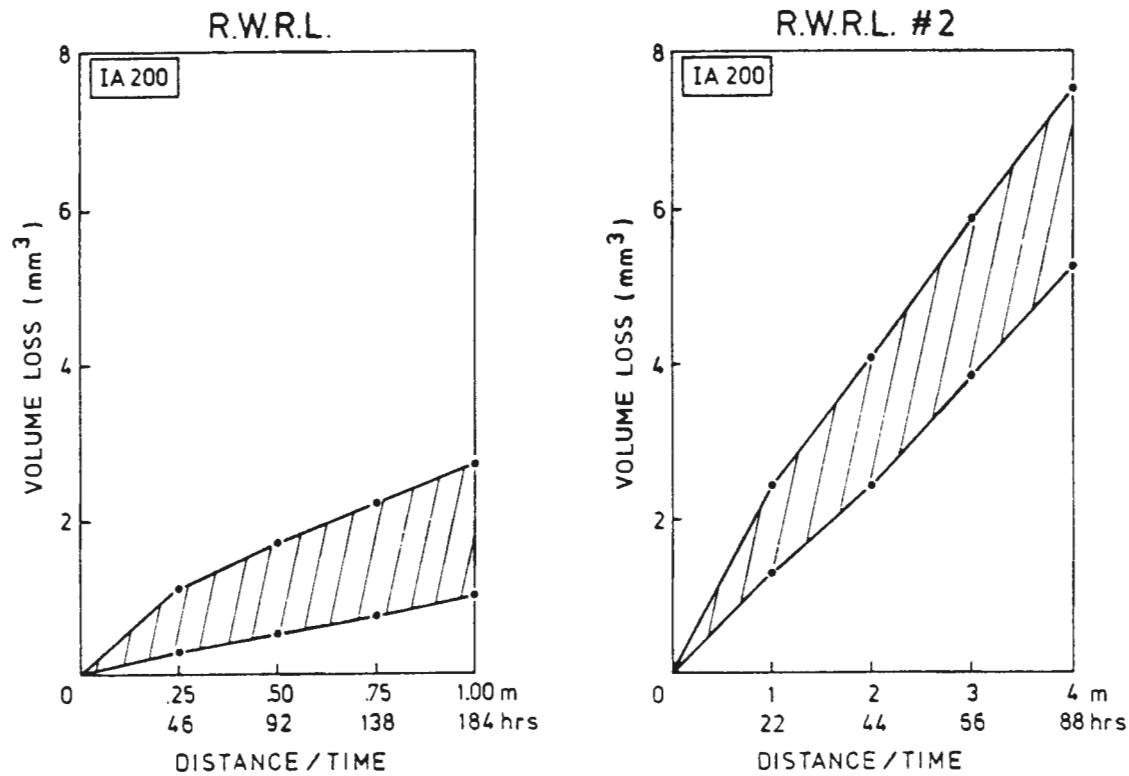

FIGURE 4.5 : The RWRL and RWRL #2 results of IA 200. The shaded portion is the contribution by corrosion to the total volume loss with respect to time of corrosion and interspersed with a short distance of abrasion. The ordinate scale is double that of 070M20 above

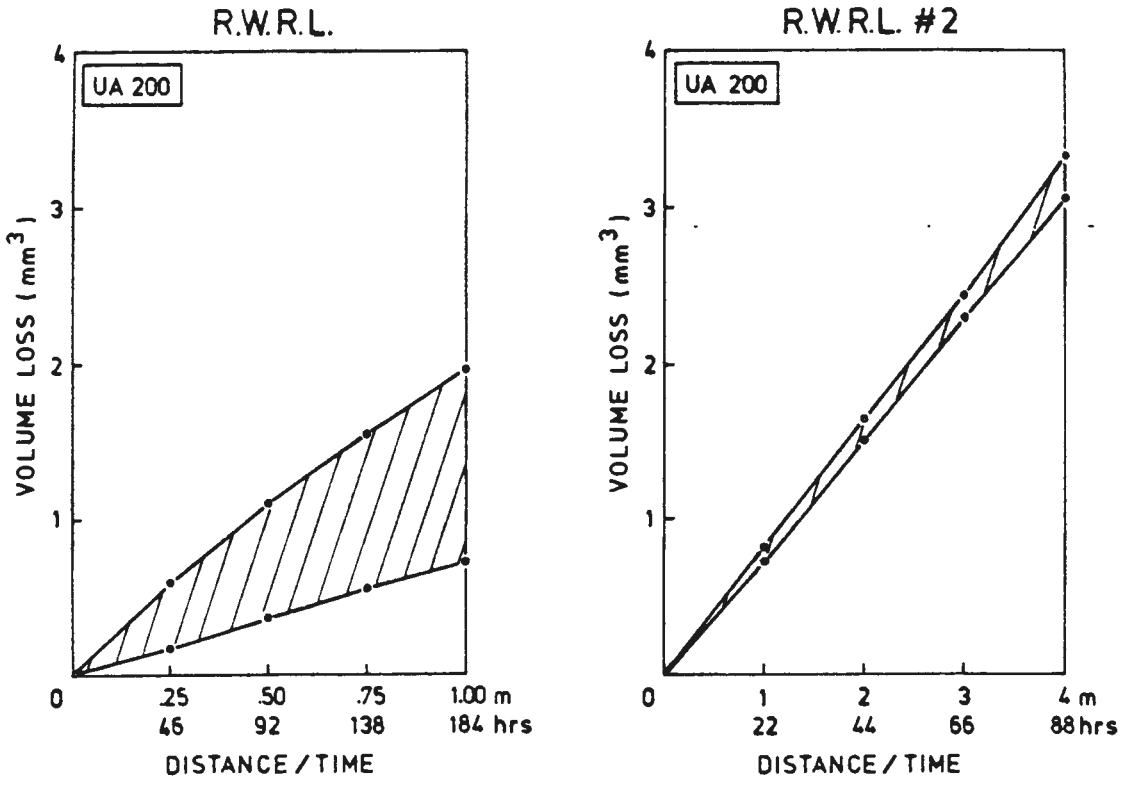

FIGURE 4.6 : The RWRL and RWRL #2 results of UA 200. The corrosion portion (shaded) is strongly influenced by the difference in the period of corrosion between the two tests. The ordinate is double that of IA 200

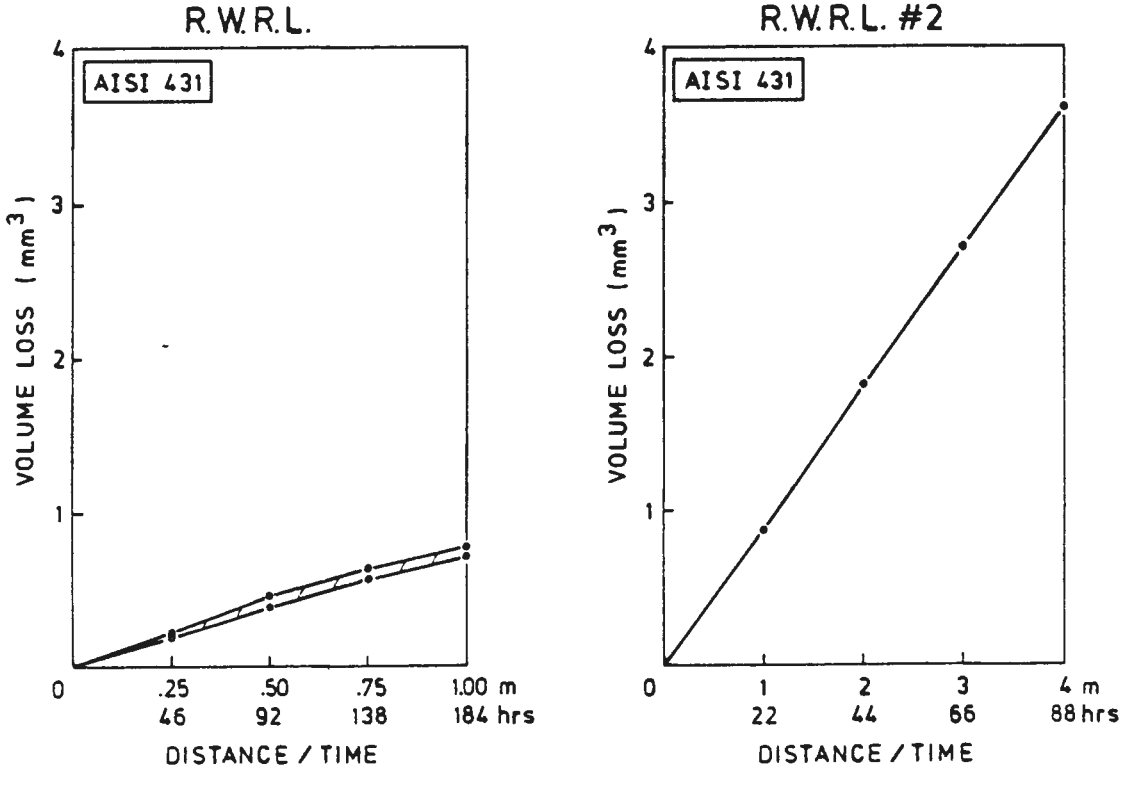

FIGURE 4.7 : The RWRL and RWRL #2 results of AISI 431. Stainless steels show little or no corrosion contribution thus total volume loss is a linear function of abrasion distance and can be interpolated from either test

The distribution in the results for the eighty two materials subjected to the RWRL test is shown in fig. 4.8. The wide spread in results highlights the potential of some of the materials under discussion, with some materials performing fifteen times better than the proprietary wear resistant steels.

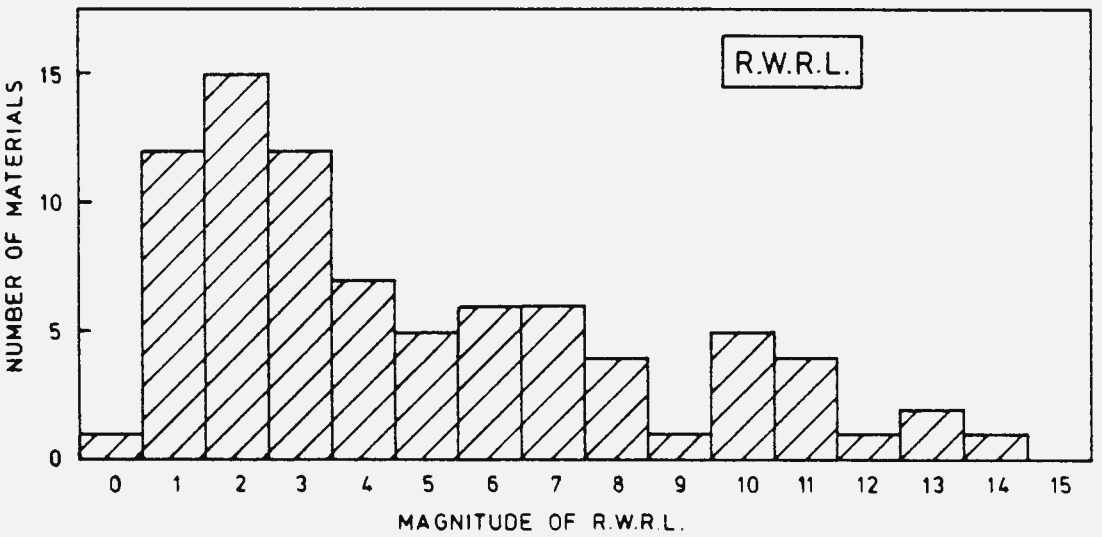

FIGURE 4.8 : A histogram showing the distribution of RWRL results for all the steels and experimental alloys tested. The significance of the shape is discussed in the text below

The concentration of materials at the lower end of the abscissa of fig. 4.8 is attributed to two factors. Firstly, an objective of this research is to develop a commercially viable material, so a compromise was reached between the potential performance and cost of the material. Only materials with a minimum amount of alloying but with potentially good wear resistance characteristics were considered. Secondly, it should be noted that, from the mathematical definition of RWRL, an ideal material would have an RWRL value of infinity. In this way the vast differences in the volumes of the material lost between the standard and the superior experimental alloys, results in the accuracy of the RWRL value being dependant on its magnitude. That is, the magnitude of the error increases exponentially as the detectable amount of material lost approaches the degree of error in the experimental technique. Therefore the reproducibility in the results of the

superior materials is less and little emphasis should be placed on the absolute value of an RWRL result when it is greater than 10. The second maxima at 10 (fig. 4.8) is due to the austenitic and abrasion resistant stainless steels.

4.1.2 The Influence of Hardness and Microstructure on a Materials Resistance to Abrasion

The relationship between the bulk hardness of a material and its RAR is illustrated in fig. 4.9. The graph includes all the results for all the materials in all their various heat treated conditions. It can be seen that bulk hardness is not a good indication of abrasion resistance. This fact is illustrated best by the transformable alloys which would appear to have a different abrasion mechanism to the martensitic and other alloys. The one austenitic steel, NP599 that has deviated from the general rule was cold worked prior to testing (as indicated in fig. 4.9).

It can also be seen in fig. 4.9 that the dual phase steels, of ferrite plus martensite or ferrite plus pearlite, show relatively poor dry abrasion resistance irrespective of the bulk hardness. The martensitic stainless steel containing coarse precipitates of chromium carbides, namely AISI 440B, was found to have an abrasion resistance 2.3 times better than mild steel (or 1.7 times better than the proprietry wear resistant materials). The martensitic developmental alloys with a hardness between 450 and 650 HV range in their resistance to dry abrasion between 1.3 and 2.1 (i.e. mediocre to excellent). A broadly positive trend is found between hardness and RAR for this latter group of steels.

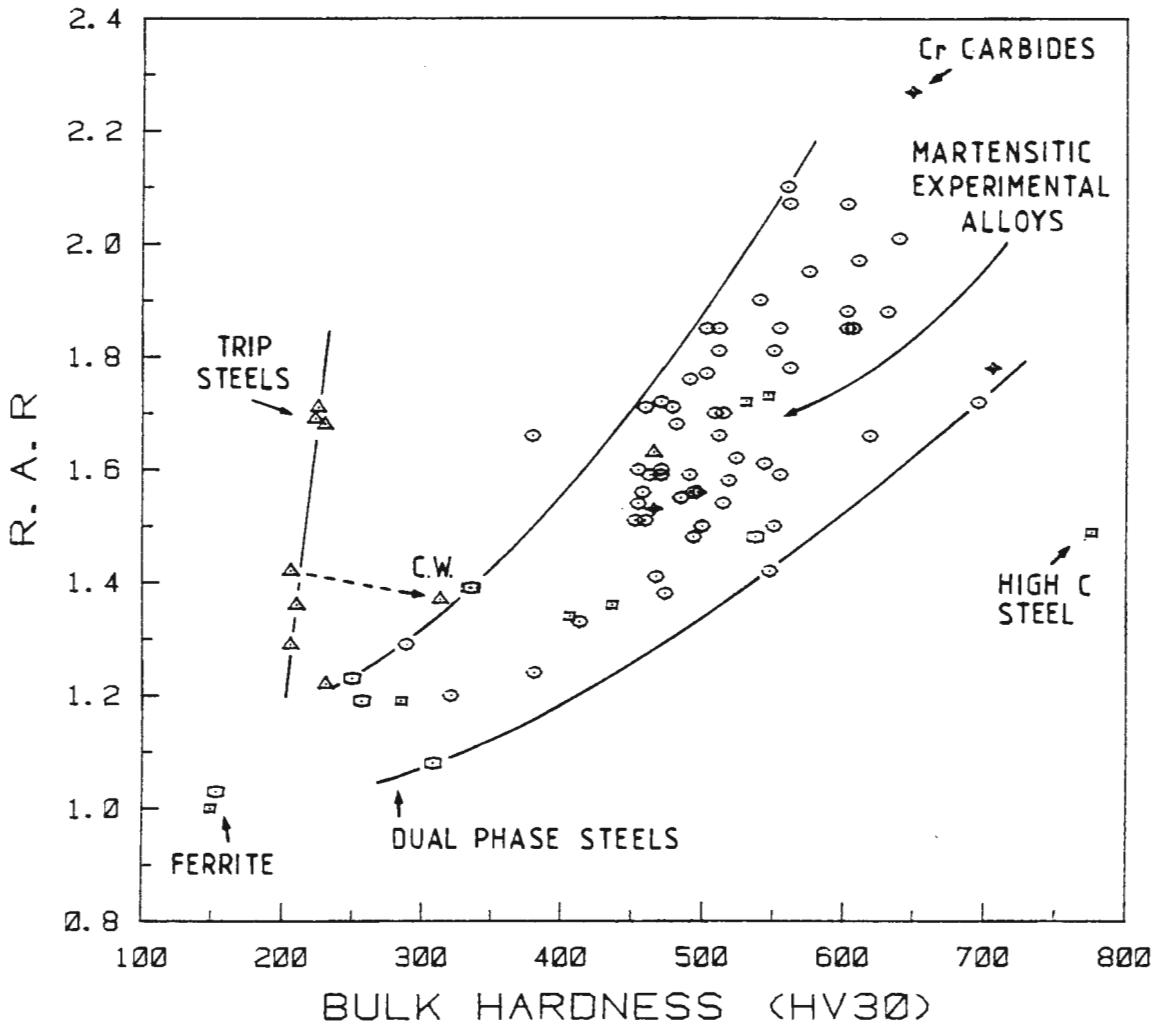

FIGURE 4.9 : The relationship between bulk hardness and RAR. The materials within the same microstructural category have been assigned a common plotting symbol.
⊡ carbon steel; ⊙ martensitic experimental alloys;
⊙ ferritic dual phase; * precipitation hardened;
△ austenitic & TRIP steels; ▽ other steels

A simple relationship between RWRL and bulk hardness is not expected (fig. 4.10), but the influence of microstructure and chemical composition on RWRL is demonstrated. Materials have been roughly separated into two classes by the RWRL test. Alloys with at least 11% chromium generally have an RWRL value greater than 5.5 subject to microstructure. Conversely, those materials with less than 11% chromium do not attain an RWRL value greater than 5.5 irrespective of the heat treatment and microstructure.

The metastable austenitic stainless steels perform very well and are on par with the best of the hard martensitic stainless steels. AISI 431 and AISI 440B outperform the other martensitic steels of lower percentage chromium. The dual phase steels (ferrite plus martensite) are found to lie below the austenitic steels of comparable hardness. The carbon and low alloy steels lie in a line across the bottom, having RWRL's approaching unity. The low and high carbon martensitic stainless steels have similar RWRL values.

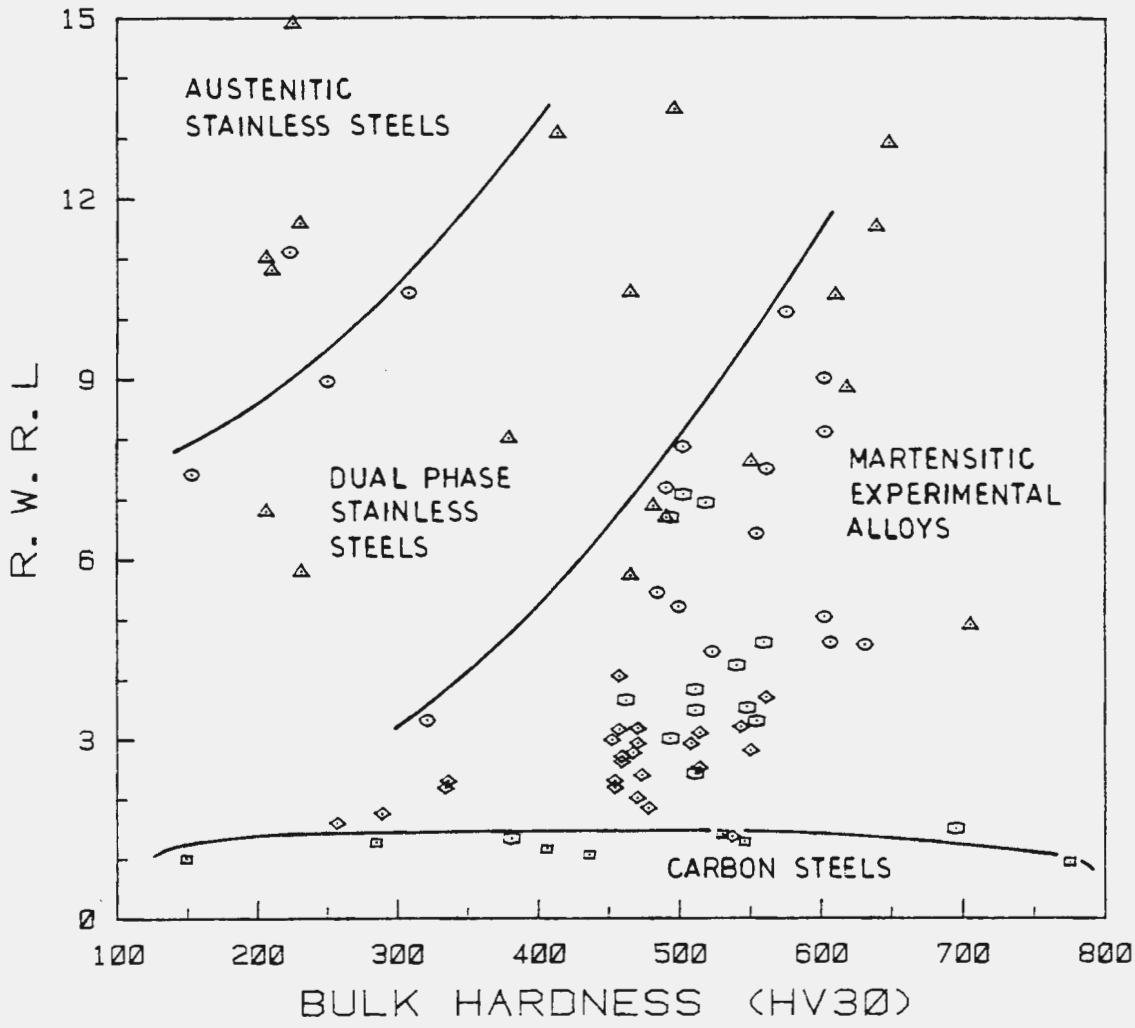

FIGURE 4.10 : The abrasive-corrosive wear performance of the materials is influenced by the microstructure and chemical composition. Materials have been classified with respect to chromium content and have fallen into groups having similar microstructures (⊡ 0-5.99%; ◇ 6-8%; ⬡ 8-10%; ⊙ 10-12%; △ 12-18% Cr)

A graph of RWRL #2 versus bulk hardness (fig. 4.11) has characteristics of both figs. 4.9 and 4.10. Only selected steels were included in the RWRL #2 test programme. It is interesting to note that the austenitic stainless steels lie along a straight line which diverges away from the martensitic and other steels. This is characteristic of the dry abrasion results (fig. 4.9). On the other hand the carbon and low alloy steels lie in a line across the bottom as seen in fig. 4.10 (abrasive-corrosive wear). It is also noted that the low chromium dual phase steels are found to lie below the high chromium dual phase steels. The hard martensitic steels and martensitic stainless steels fall within a band ranging from a RWRL #2 value of 2.8 to 5.1.

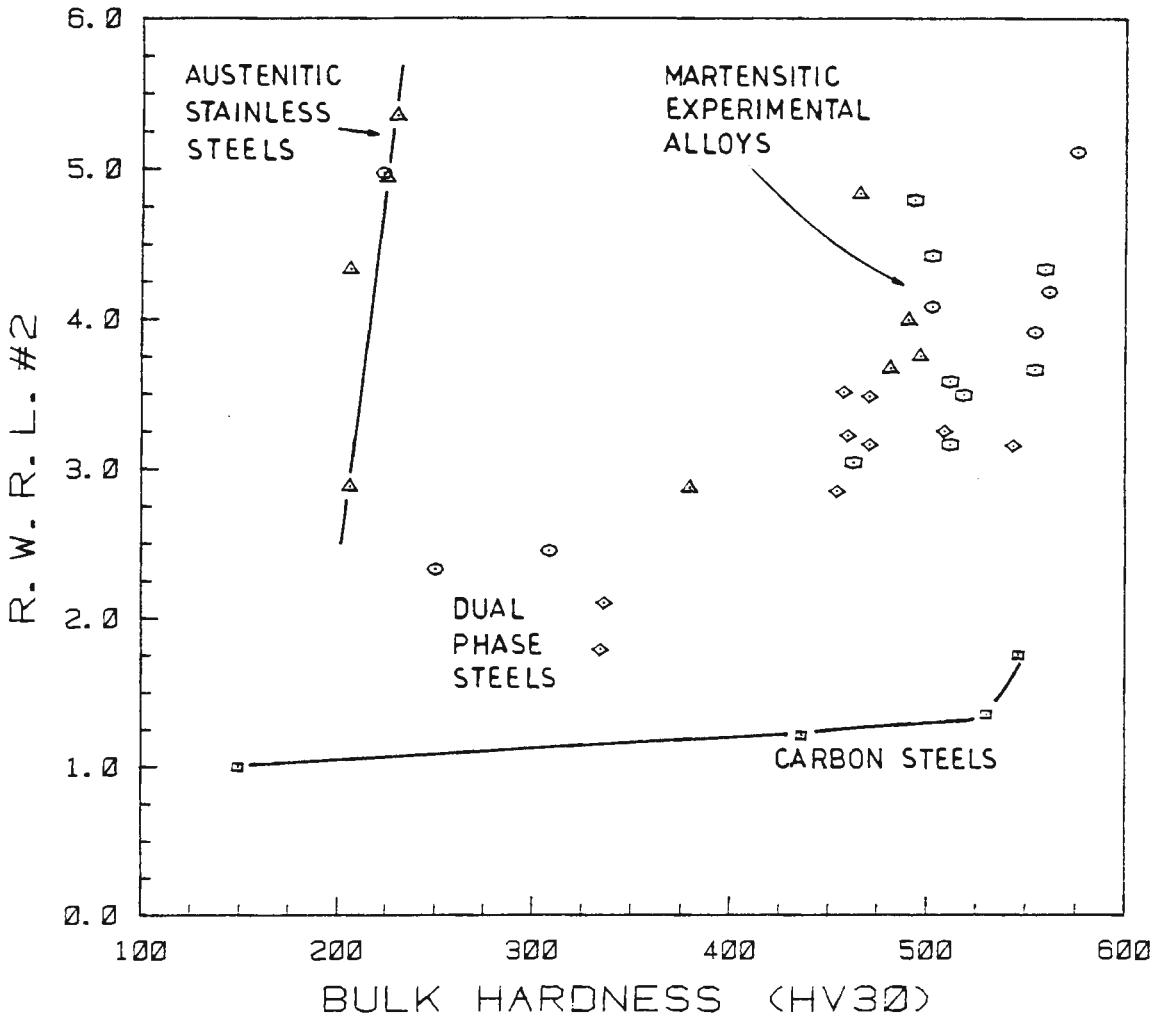

FIGURE 4.11 : The RWRL #2 test results have characteristics of both the RAR and RWRL test results. Materials have been plotted with respect to chromium content. (⊡ 0-5.99%; ◇ 6-8%; ⊙ 8-10%; ⊙ 10-12%; △ 12-18% Cr)

4.1.3 The Optimum Heat Treatment for Wear Performance

The first batch of alloys from Source W were tested in a variety of heat treated conditions. All the materials had been hot rolled with starting temperatures of 1100°C and allowed to air cool after the final pass (Peters, 1983). The subsequent heat treatments are described in Table 3.5 of section 3.2.2. Tabulated in Table 4.2 is the percentage increase in RAR as determined for each material and heat treatment. It should be noted that a post-rolling heat treatment is necessary to improve the toughness of these materials. After examination of Table 4.2 and Table 3.12, it was decided that there is no economical advantage in the double heat treatment (viii). All the materials showed an improvement in abrasion resistance after heat treatment except alloy WD.

TABLE 4.2 : The influence of heat treatment on RAR

Percentage change in RAR

MATERIAL	HEAT TREATMENT				
	i	iv	vi	viii	200°
WA		-10	5	16	
WB			5	12	
WC			21	19	
WD	-14				
WSA6					30
WV69					25
Quatough					45
3CR12					19

As the hardness and toughness combination can be controlled through the heat treatment, it is necessary to know the effect tempering temperature has on a materials abrasion and corrosion resistance. To this end two Source W alloys, WA2 and WB2, were tested in a range of tempered conditions. From the results in fig. 4.12 it can be seen that RAR is influenced by both the hardness and toughness of a material. An anomaly exists with the air cooled specimen which has an RAR higher than what might be expected from its hardness and toughness values. The drop at 500°C is due to temper embrittlement (fig. 4.12).

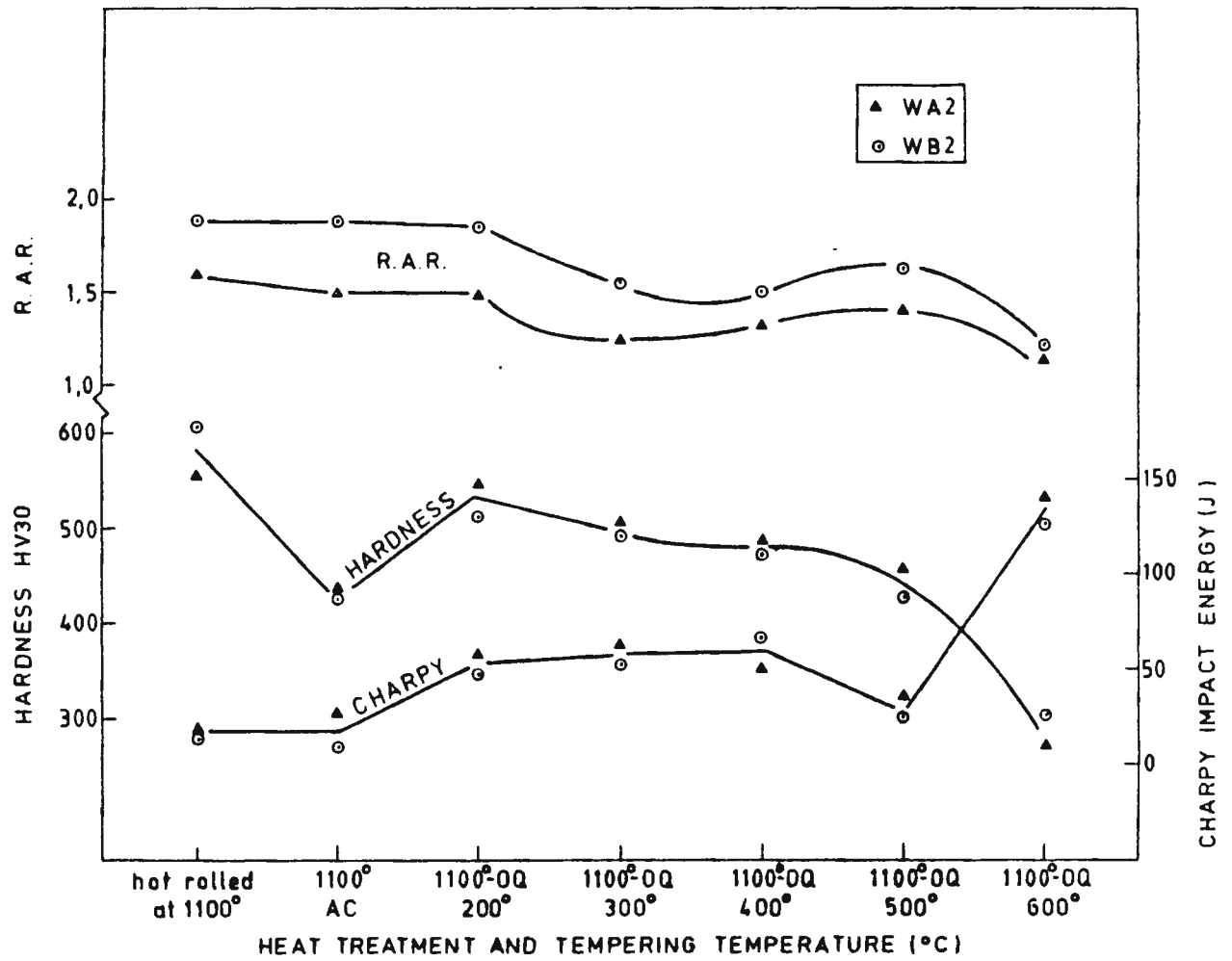

FIGURE 4.12 : The effect on RAR of heat treatment and tempering temperature for the alloys WA2 and WB2. It can not be related to the hardness and toughness without a knowledge of the microstructure (fig. 4.13)

It can be deduced from fig. 4.14 that corrosion resistance is inversely dependent on tempering temperature above 200°C. The volume loss due to corrosion is highest for the material tempered at 600°C and lowest at between 200° and 300°C. The higher abrasion resistance of WA2 200 and WB2 200 make a heat treatment of 1100°(1 hr)OQ; 200°(½ hr)OQ the optimum heat treatment for abrasive-corrosive wear resistance for this type of alloy (fig. 4.13). The Source I alloys support this (Table 4.3) although the oil quenched and untempered condition is equally favourable if toughness were not a consideration in its general usage.

FIGURE 4.13 : Optical micrographs depicting the change in microstructure with heat treatment and tempering temperature for steels WA2 and WB2.
(next page)

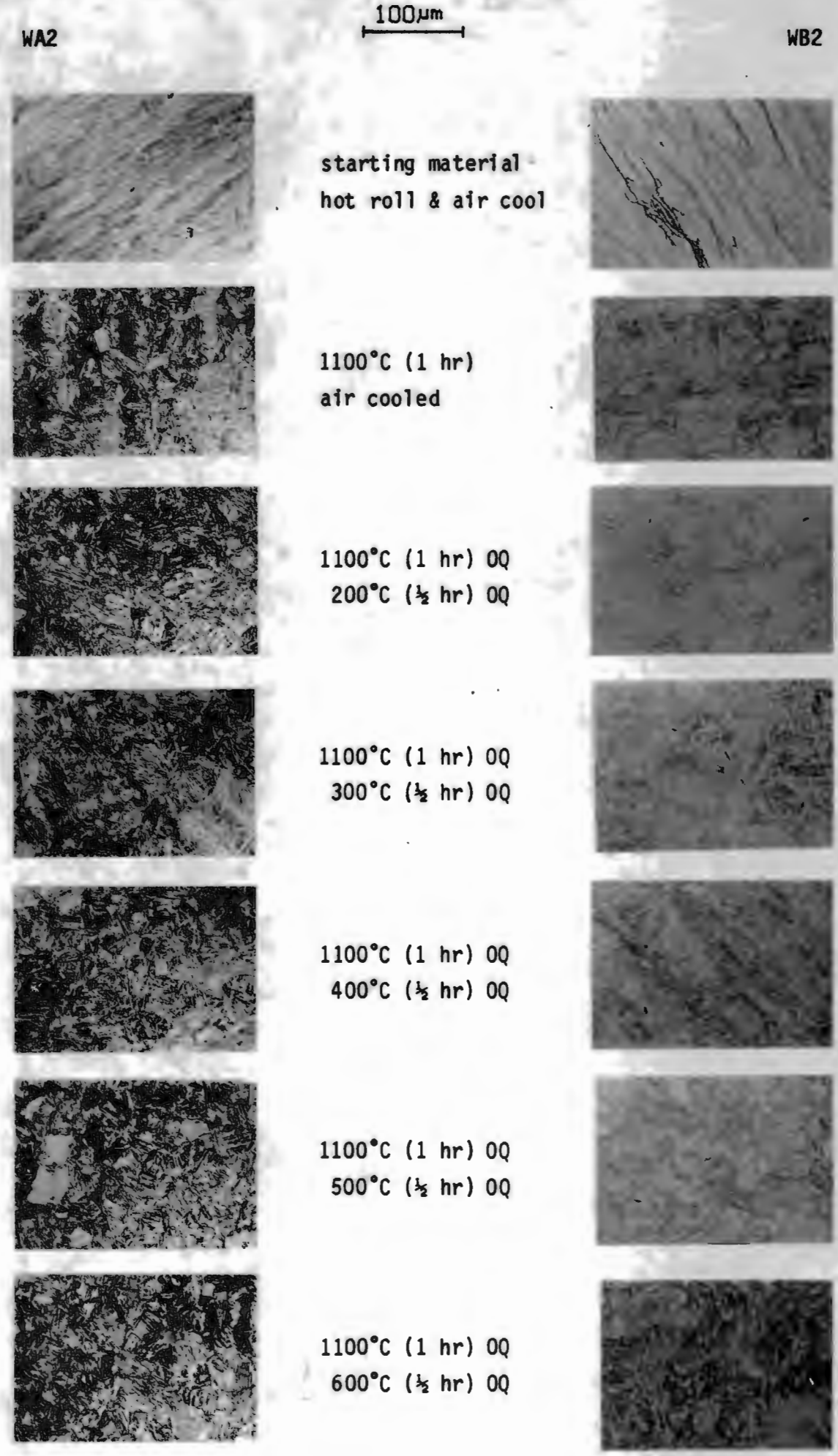
100μm
WA2
WB2
starting material
hot roll & air cool
1100°C (1 hr)
air cooled
1100°C (1 hr) OQ
200°C (½ hr) OQ
1100°C (1 hr) OQ
300°C (½ hr) OQ
1100°C (1 hr) OQ
400°C (½ hr) OQ
1100°C (1 hr) OQ
500°C (½ hr) OQ
1100°C (1 hr) OQ
600°C (½ hr) OQ

FIGURE 4.13 :

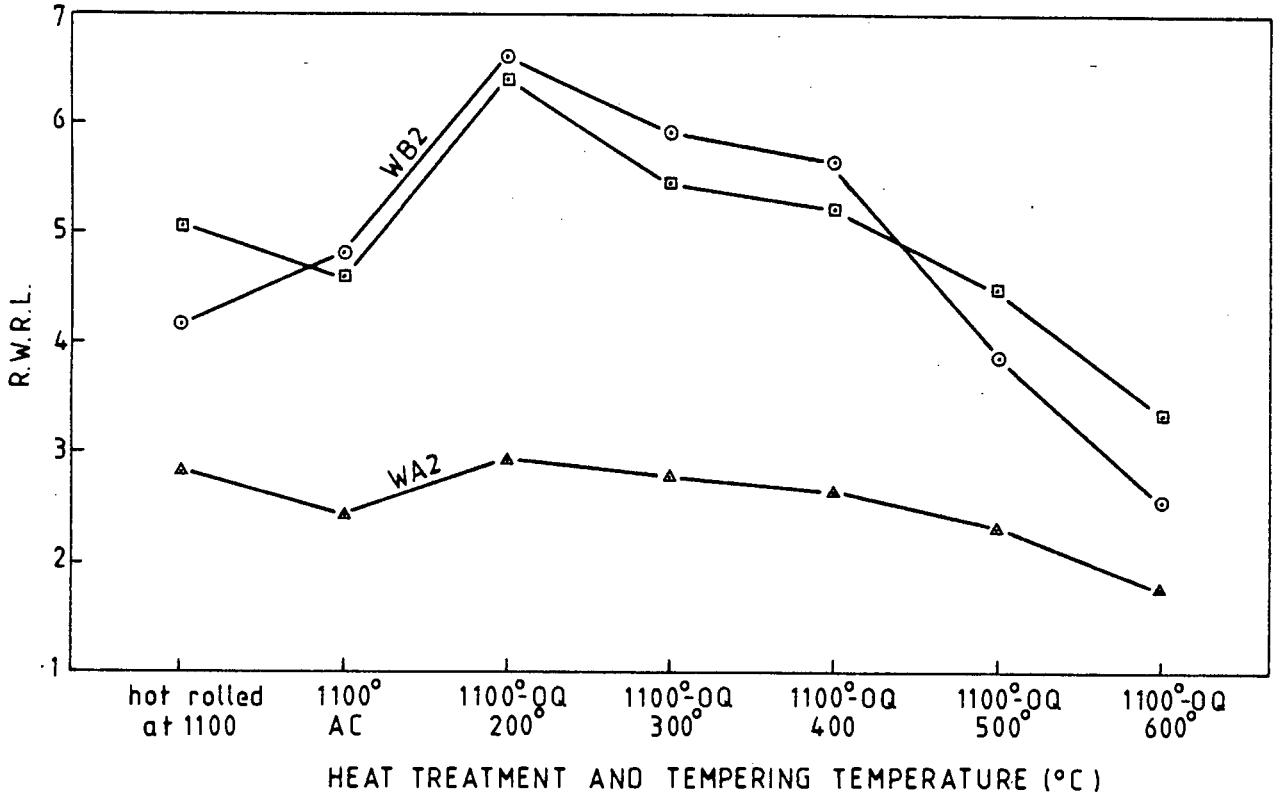

FIGURE 4.14 : The influence of heat treatment and tempering temperature on the abrasive corrosive wear resistance of alloys WA2 and WB2 (7.2 and 10.4% Cr)

TABLE 4.3 : The influence of tempering temperature on RWRL for the Source I alloys

MATERIAL	TEMPERING TEMPERATURE			
	OQ*	200°	300°	600°
IA	2.3	2.2	1.4	1.6
ID	1.5	3.3	3.0	1.3
IF	8.1	7.5	7.2	-

* 1100° (1 hr) OQ; untempered

4.1.4 An Alternative Fabrication Technique

The results of using a controlled rolling treatment to produce a tough, abrasion resistant material is given in Table 4.4. Comparison was made between a material that has been air quenched from 1100°C and one which has undergone a controlled rolling treatment (as detailed in Table 3.5).

A small decrease in RAR is noted for the hot rolled and tempered materials as compared to the air quenched and tempered material. Tempering after hot rolling has increased the toughness 150% for materials T102A, T102B and T122 (Table 3.17) and by 35% for materials T820A and T820B. The hardness in each case has remained unchanged. However, the RAR of the tempered material is lower than the RAR of the untempered material (Table 4.4). The additional pass at 950°C (AHR2) improves the RAR of T820A and T820B but this improvement is again lost on tempering.

TABLE 4.4 : The influence of hot rolling on RAR for the Source T alloys. The rolling schedule is given in Table 3.5

MATERIAL	AQ 200	AHR1	AHR1 200°	AHR 2	AHR2 200°
T102A	1.77	1.81	1.59	-	-
T102B	-	1.90	1.66	-	-
T820A	1.72	1.60	1.51	1.71	-
T820B	1.56	1.59	1.54	1.71	1.56
T122	1.76	1.50	1.68	-	-

4.1.5 The Influence of the Major Alloying Elements

Alloys are added during the steel making process for their controlling influence on the microstructure which in turn imparts specific properties to the steel. Only the source F and source T alloys were specifically prepared with this intention. However, some conclusions can be drawn from the behaviour of the other materials with similar chemical composition and heat treatment.

Table 4.5 is a list of materials that have closely related chemical compositions. The base chemical composition varies between pairs or groups of materials but any major element that differs within a group has been identified.

TABLE 4.5 : Materials grouped with respect to chemical composition

MATERIALS WITH SIMILAR CHEMICAL COMPOSITIONS	MAJOR ALLOYING ELEMENTS THAT DIFFER
WB, WB2	C
F353, F352, F351	Mn
F350, F351	Cr
Wearalloy 400, T820B, T102A,IE, AISI 431	Cr
T102A, T102B	Al
T820A, T802B	Al
WV69, T122	C, Ni
3CR12Ni, WV69	C, Mn
3CR12, 3CR12Ni	Ni, Mn
WA, WSA6, UA, ID, WB, WC	Cr, Mn
IE, WB2	C, Mn, Ni
IC, ID	C, Mn, Ni
WC, WD	C, Ni, Mo
IB, UA	C, Mn, Ni, Mo

Carbon

The effect carbon has on a materials wear performance is found to depend on the materials heat treatment. A study of Table 4.6 reveals that the influence carbon has on a materials wear resistance is dependent on the microstructure.

The material couple in row A (steels WB ar and WB2 ar) are in the hot rolled and air cooled condition and have approximately the same hardness and toughness. The microstructure of these alloys is similar except that WB2 has smaller more elongated grains, with well defined grain boundries. The RAR and RWRL of these alloys is approximately equal. The situation changes for the heat treated condition (same material couple, row B). The microstructures have recrystallized to equi-axed grains of martensite with most of the carbon now in a supersaturated solid solution. The greater hardness of WB vi has resulted in a higher RAR. This together with the lower carbon level has resulted in WB vi also having a higher RWRL and RWRL #2 ratio than WB2 200 (Table 4.6, row B).

TABLE 4.6 : Effect of carbon on wear resistance for a selection of alloys having similar chemical composition

	MATERIAL	% CARBON	OTHER ELEMENTS TO CONSIDER	HARDNESS HV30	TOUGHNESS Joules	RAR	RWRL	RWRL#2
A	WB ar	.24	None	610	11	1.85	4.6	-
	WB2 ar	.27		603	15	1.88	5.1	-
B	WB vi	.24	None	574	27	1.95	10.1	5.1
	WB2 200	.27		532	47	1.85	6.4	3.9
C	WC ar	.25		612	7	1.66	8.9	-
	WD ar	.43	Ni, Mo, V	692	8	1.78	4.9	-
D	IB	.14	Mn, Ni	513	52	1.56	6.7	4.8
	UA 200	.23	Mo	559	79	2.10	4.6	4.3
E	IC	.18	Mn, Ni	510	59	1.58	6.9	3.5
	ID 200	.23		558	27	1.59	3.3	3.7
F	3CR12Ni HT	.027	Mn, Ni	308	215	1.08	10.4	2.5
	WV69 200	.070		379	175	1.66	8.0	2.9
	T122 AQ200	.210		480	58	1.76	6.7	4.0
G	IE 300	.20	Mn, Ni	511	36	1.85	7.9	4.1
	WB2 300	.27		488	52	1.55	5.4	-

Similarly for each material couple in rows C through F of Table 4.6, an increase in carbon content has resulted in an increase in hardness but not necessary a corresponding increase in RAR. The higher levels of carbon however have an adverse effect on corrosion resistance. Thus there is expected to be an inverse relationship between carbon content and RWRL. This is generally true despite the counter influence of RAR and irrespective of Mn and Ni content (Table 4.6, rows B to G).

There is not a strong relationship between percentage carbon and RAR or hardness for the alloyed martensitic steels. The RAR is greatly improved when sufficient carbon or equivalent alloying elements are present to produce a fully martensitic steel. The three materials of row F (3CR12Ni, WV69 and T122) indicate that a martensitic microstructure is more favourable for RAR than a dual phase ferrite plus martensite steel. Generally there has not been a significant drop in RWRL with this change in matrix structure.

Chromium

The alloying element chromium above 11 weight percent is known to passivate a steel but still higher quantities together with other alloying elements are needed in more aggresive environments (Sedriks, 1982). The relationship between the chromium content and corrosion resistance for the simulated mining environment of the RWRL test follows an S-shaped curve similar to fig. 4.15.

Two groups of materials, each having a range of chromium contents and closely related martensitic microstructures, are listed in Table 4.7. The first group all contain approximately 0,20% carbon while the second group has a carbon level of 0,26% (± 0.01). This second group which encompasses a narrower range of chromium levels, shows that for a constant percentage carbon and other alloying elements and for the same heat treatment, an increase in chromium increases the hardness of the material proportionally. Subsequently the RAR improves. The corrosion resistance and RWRL also improves especially above 10% chromium. No clear trend is seen for the RWRL #2 test results but this will be discussed in Chapter 5.

TABLE 4.7 : Effect of Chromium content on wear resistance

MATERIAL AND HEAT TREATMENT	% CHROMIUM	OTHER ELEMENTS TO CONSIDER	HARDNESS HV30	TOUGHNESS Joules	RAR	RWRL	RWRL #2
Wearalloy 400	0.02	None	433	66	1.34	1.2	-
T820B AQ200	7.61		457	62	1.56	4.1	3.5
T102A AQ200	9.85		511	64	1.77	7.1	4.4
IE 300	10.4		511	36	1.85	7.9	4.1
AISI 431	16.3		496	72	1.56	13.5	3.8
WA vi	7.08	.02% Mn	472	49	1.38	2.4	-
WSA6 200	8.00	.50% Mn	521	34	1.85	3.5	3.6
UA 200	8.65	.35% Mn	559	79	2.10	4.6	4.3
ID 200	9.06	.60% Mn	558	27	1.59	3.3	3.7
WB vi	10.3	.07% Mn	574	27	1.95	10.1	5.1
WC vi	12.3	.02% Mn	626	16	2.01	11.5	-

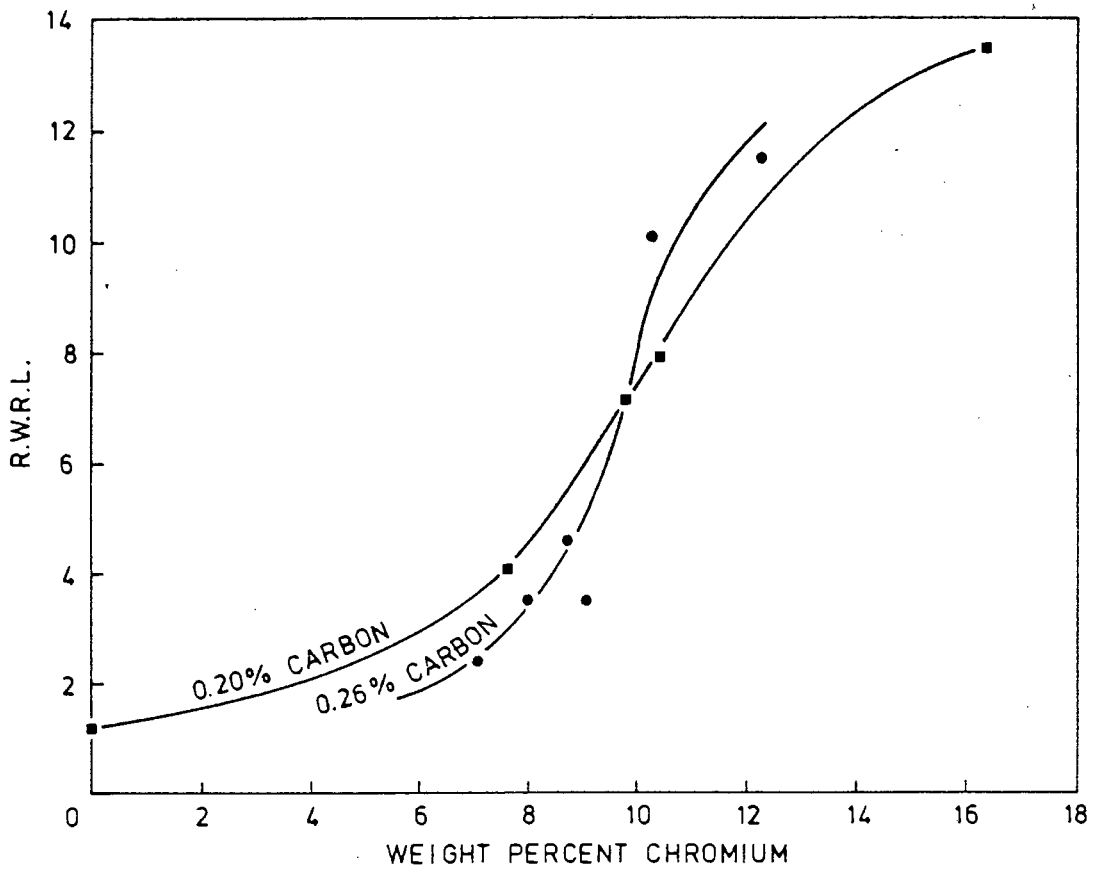

FIGURE 4.15 : Effect of Chromium content on wear resistance for the two groups of alloys tabulated in Table 4.7. All have similar martensitic microstructures

Not withstanding the obvious passivating effect of chromium, its effectiveness in improved wear resistance is dependent upon the microstructure. This can be demonstrated in a comparison of RAR and RWRL (fig. 4.16). The martensitic steels with up to 6% chromium can have a wide range of RAR values but all have the same low RWRL values. The abrasive-corrosive wear resistance of a martensitic steel with 10% chromium shows a noticable improvement within certain limits. The upper limit is around 4.6 for these martensitic steels. The microstructure and heat treatment is also critical (section 4.1.3). Note that those steels with around 10% Cr which have good RWRL's all have RAR's in excess of 1.8.

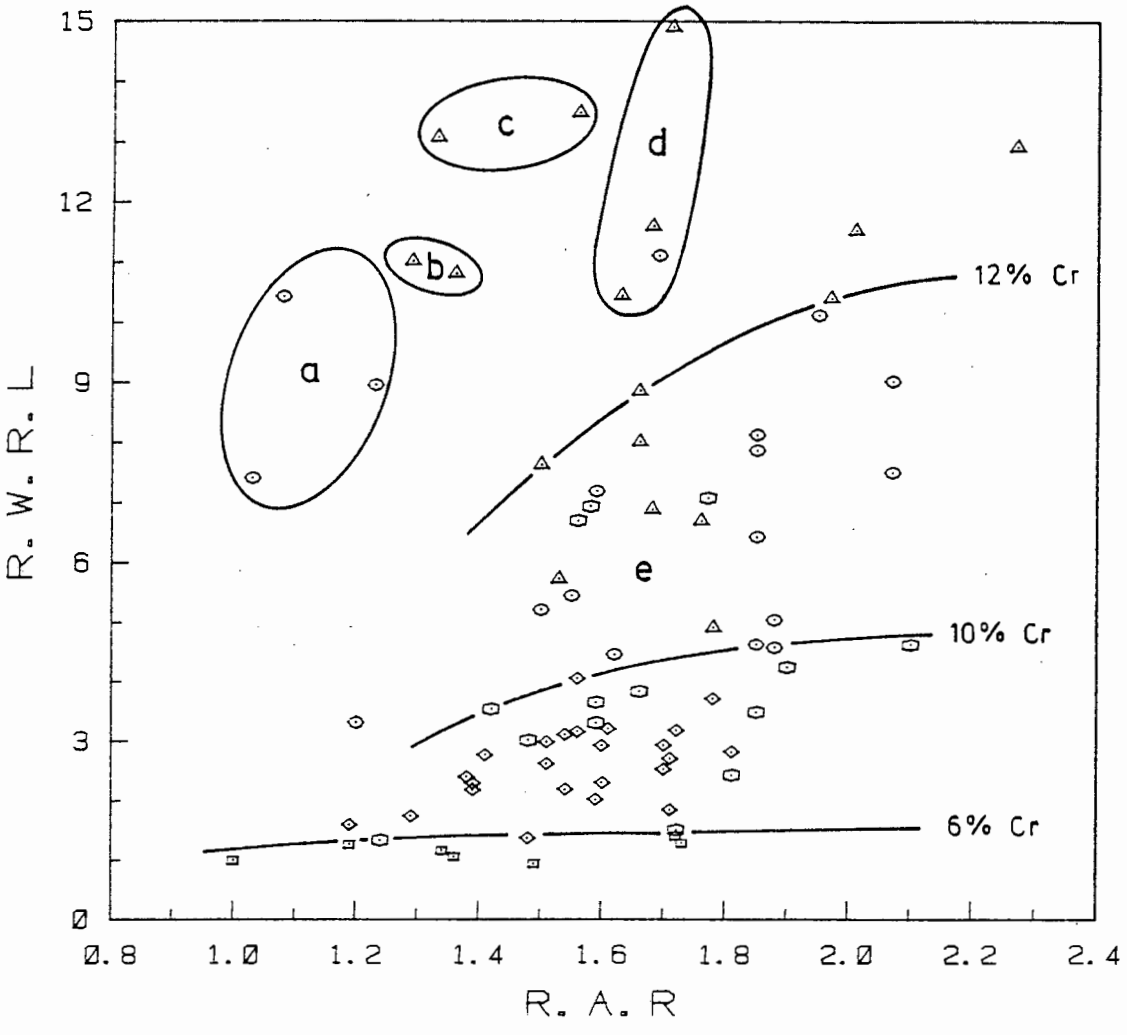

FIGURE 4.16 : A comparison of RAR and RWRL with respect to chromium content highlights the importance of microstructure. (a) ferritic dual phase SS; (b) austenitic SS; (c) martensitic SS; (d) metastable austenitic steels; (e) martensitic develop. steels
(⊡ ,0-6%; ◇ 6-8%; ⊙ 8-10%; ⊙ 10-12%; △ 12-18% Cr)

The martensitic steels with between 10% and 12% chromium have a RWRL which is related to both its RAR and chromium content but this is still sensitive to details in the microstructure (fig. 4.16). For example, the ferrite dual phase source M alloys with between 10% and 12% chromium have RWRL values on par with their martensitic counterparts despite their poor dry abrasion resistance. The high RWRL values of the austenitic and martensitic stainless steels are due to their inherent corrosion resistance irrespective of their RAR. The effect of chromium content on RAR and RWRL remains indeterminate for the metastable austenitic source F alloys (10% or 12% Cr plus 5-10% manganese).

Aluminium

The source T alloys, T102 and T820, were produced with and without the element aluminium (Table 3.16). There is no clear advantage in including aluminium as a corrosion inhibitor or any effect it may have as a deoxidiser in improving the corrosion resistance (Table 4.8). The tabulated volume losses due to corrosion were documented after 46 hours uninterrupted corrosion of a previously abraded surface.

TABLE 4.8 : Aluminium as a corrosion inhibitor

MATERIAL	% Al	VOLUME LOSS CORROSION (mm^3)
T102A AHR1	0.50	1.73
T102B AHR1	0.002	.62
T102A AHR1 200	0.50	.67
T102B AHR1 200	0.002	.67
T820A AQ 200	1.46	.96
T820B AQ 200	0.002	.83
T820A AHR1	1.46	1.35
T820B AHR1	0.002	2.03
T820A AHR1 200	1.46	1.41
T820B AHR1 200	0.002	1.63
T820A AHR2	1.46	2.42
T820B AHR2	0.002	1.37

Nickel and Manganese

No direct influence of the elements nickel or manganese could be detected for the martensitic experimental alloys on their dry abrasion resistance. However for the dual phase steels two facts were noted. A decrease in manganese in the source F alloys results in a decrease in RAR and similarly for RWRL to a lesser extent. The result is associated with a change in the metastable austenitic microstructure. An increase in the nickel content of the alloy 3CR12 results in a higher tensile strength (Brink, 1983) together with an increase in hardness. This has the effect of increasing the RAR for this type of material (3CR12Ni). Possibly the pitting resistance was improved as lower corrosion weight losses were recorded in the RWRL test.

4.1.6 An Engineering Classification of the Materials

A design engineer works within certain guidelines when making a material selection. In a gold mining application, consideration needs to be given to the type of environment in which it will operate, the severity of abrasion it will undergo, the extent of impact load, in addition to other factors such as strength, ease of fabrication, ease of welding and cost. Tables have been drawn up as an aid with all the materials classified according to the materials transverse impact energy. Within each class the materials have been ranked according to their resistance to wear.

The complete tables are to be found in the Appendices A4, A5 and A6. Abridged versions which present only the most important features and alloy steels are presented below. A guide to the interpretation of Tables 4.9, 4.10 and 4.11 is outlined in fig. 4.17.

Let us suppose that a material is required having excellent abrasion resistance properties for a structural application that will involve impact. Consideration should be given to materials in the left hand upper corner (quadrant 1A) of Table 4.9. Alloy UA 200 shows potential (quadrant 1B). Alternatively, if toughness is not so important Alloys IF 200 and WB viii could be considered (quadrant 1D of Table 4.9).

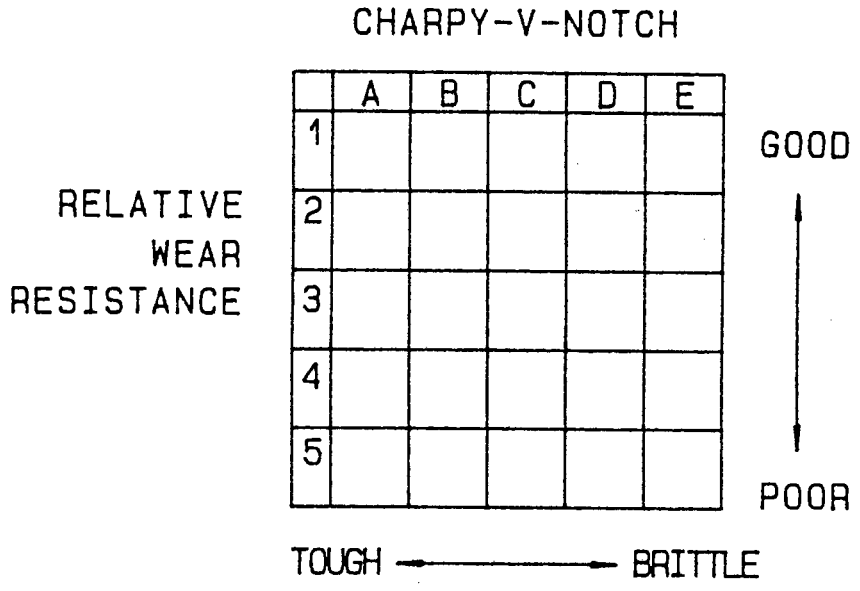

FIGURE 4.17 : Schematic interpretation for Tables 4.9 to 4.11. Down a column is decending order of wear resistance and across a row is decreasing toughness (Joules)

In another application where corrosion resistance is most important, the materials listed in the left hand upper corner of Table 4.10 need to be examined. The commercial stainless steels will be found in this region. The proprietary wear resistant steels are to be found in row 5 which reflects the fact that they have very poor corrosion resistance.

Many of these steels are destined for application in a situation that is both highly abrasive and corrosive. The materials in Table 4.11 have been ranked with respect to RWRL #2. Potential materials are NP 599, T102A AQ200 and UA 200. Cross reference to Tables 4.9 and 4.10 shows that T102A AQ200 is the more corrosion resistant material and UA 200 is the more abrasion resistant material. The source F alloys have very attractive abrasive-corrosive wear resistant properties. As the toughness values for these alloys were not made available to the author they have been assigned a toughness value of 40 Joules, so as to be classified, but are expected to have higher values.

TABLE 4.9 : Materials classified with respect to toughness and ranked according to their dry Relative Abrasion Resistance (RAR)

RAR \ TOUGHNESS	A	B	C	D	E
1		UA 200		IF 200 WB viii	AISI 440B
2			WB2 200	WB vi IE 300 WSA6 200	WB2 AC WB2 ar WB ar
3	WV69 200 T102B AHR1T	T102A AQ200 T122 AHR1T	QUATOUGH T F351	WB2 500	
4	NP599 ann	AISI 431 WB2 400	IC WB2 300	ID 200	SS10/200 WSA6 ar
5	NP599 cw WV69 ar WB2 600 3CR12Ni HT 3CR12 ar 070M20	WEARALLOY4 3CR12 iii		ABRASALLOY IA 600	

TABLE 4.10 : Materials classified with respect to toughness and ranked according to their Corrosive-Abrasive Wear Resistance (RWRL) where the emphasis is on corrosion of an abraded surface

RWRL \ TOUGHNESS	A	B	C	D	E
1	WV69 ar AISI 304L	AISI 431	F351		AISI 440B
2	AISI 316	3CR12 iii T102A AQ200			
3	NP599 ann	WB2 400 UA 200	WB2 200 WB2 300	WB2 500	WB2 ar WB2 AC
4	WB2 600				
5	070M20	WEARALLOY4	835M30 QUATOUGH T	QUATOUGHar ABRASALLOY	SS10/200

TABLE 4.11 : Materials classified with respect to toughness and ranked according to their Resistance to Abrasive-Corrosive Wear (RWRL #2). The emphasis is on abrasion resistance coupled with a resistance to corrosion

TOUGHNESS

RWRL#2		A	B	C	D	E
	1	NP599 ann	T102A AQ200 UA 200	F352 F350 F351 F353		
	2		AISI 431	WB2 200		
	3	T102B AHR1T				
	4	AISI 304L	3CR12 iii			
	5	070M20		QUATOUGH T	ABRASALLOY	

Similar tables could be drawn up for other engineering properties such as tensile strength, machinability and weldability. A compromise will have to reached between outstanding wear properties and practical engineering properties in the final selection of a material.

A selected few of these materials are destined for wide scale application in the mining industry and the economics of any proposal is a central issue in the final material selection. A cost factor has been calculated for each material based on a knowledge of its chemical composition (Appendix A2). This can only serve as a very crude guide as other factors to be included in any price structure are: the method of fabrication; the tolerances in the product specification, be it composition, mechanical properties or dimension; the tonnage of the steel to be produced; distribution; and the economics of the market.

A comparison of the local prices for the commercial steels with the calculated cost factor (Table 4.12) shows that the cost of alloying content takes second place to the other factors just mentioned. However it is reasonable to assume that there is no difference in the relative manufacturing costs for the developmental alloys and thus alloying content would be the major contributor in determining their price differential.

TABLE 4.12 : Comparison of the calculated cost factor with local steel prices in Rand per tonne of steel

MATERIAL	LOCAL (R/t)	CALCULATED (R/t)	RATIO
AISI 316	7120	2359	3.0
AISI 304	5530	1694	3.3
AISI 431	7300	914	8.0
070M20	1820	198	9.2
835M30	3520	689	5.1
SS10/200	3750	235	16.0

Rands 3.5 = £1 Rands 2 = $1 as at Jan. 1988

The cost factor of the materials has roughly divided them into carbon and low alloy steels, the low chromium steels and chromium-/manganese steels, the carbon/chromium/nickel steels and the high chromium austenitic stainless steels. The additional cost of heat treatment has not been included. Materials have been ranked according to RAR (Table 4.13) and RWRL (Table 4.14) within each price category. Detailed tables that include all the materials are given in Appendices A7 and A8. A guide to the interpretation of Tables 4.13 and 4.14 is outlined in fig. 4.18.

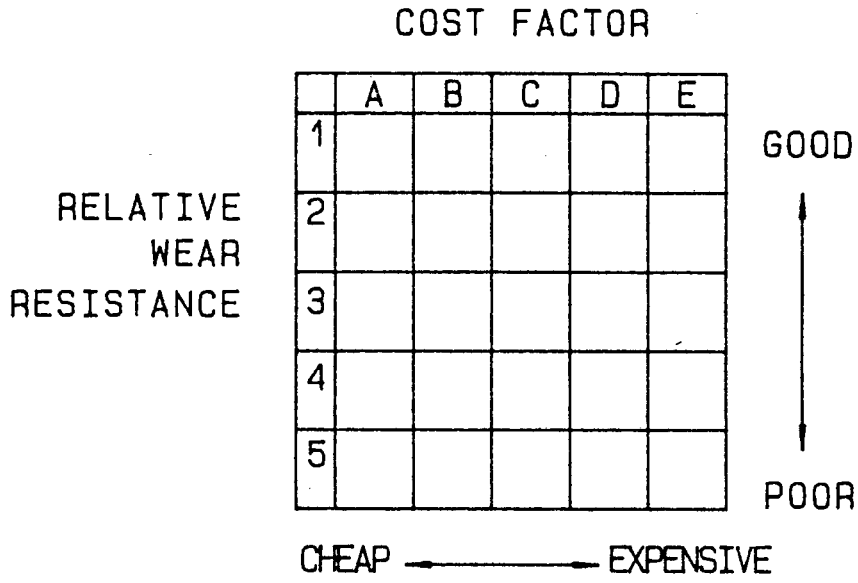

FIGURE 4.18 : Schematic interpretation for Tables 4.13 and 4.14. Materials in Column A are the cheapest alloys and those in Column E are the most expensive alloys (in terms of alloying content). Materials are ranked in decending order of wear resistance down a column

As outlined in fig. 4.18, materials found in the left hand upper corner are to be considered for wear applications. Thus Quatough (quadrant 2A, Table 4.13) would be the first choice in a dry abrasive wear application. It is cheap, has good dry abrasion resistance and is known to have good mechanical properties. If a longer in-service life is important then maybe T102B AHR1 (quadrant 1B, Table 4.13) would be a better choice. T102B AHR1 is also seen to have a moderate resistance to corrosion (quadrant 3B, Table 4.14) so that it would work equally well in an abrasive-corrosive environment where corrosion is slight or inhibited.

It can be seen from Table 4.14 that the stainless steels AISI 304L and AISI 316 are costly choices in any application involving corrosion and abrasion. The Source F alloys (quadrants 1C and 2C) may prove to be cheaper and more effective alternatives. The carbon and low alloy steels are inexpensive but they show poor abrasive-corrosive wear resistance (quadrant 5A).

TABLE 4.13 : Classification with respect to the cost factor of the materials and ranked according to dry abrasion resistance, RAR

COST FACTOR

RAR	A	B	C	D	E
1		T102B AHR1		UA 200 WB viii	AISI 440B IF 200
2	QUATOUGH T	T122 AQ200	WSA6 200 F351	WB2 200	
3		T102B AHR1T	F350 WV69 200	AISI 431	
4	ABRASALLOY				NP599 ann
5	070M20		3CR12		AISI 304L

TABLE 4.14 : Classification with respect to the cost factor of the materials and ranked according to the corrosive-abrasive wear resistance, RWRL

COST FACTOR

RWRL	A	B	C	D	E
1			F351 F352 F350	AISI 431	AISI 440B AISI 304L
2		T102A AQ200	F353 3CR12		AISI 316
3		T102B AHR1		WB2 200 UA 200	NP599 ann
4			WSA6 200		
5	QUATOUGH T WEARALLOY4 ABRASALLOY		835M30		

4.2 MECHANISTIC ASPECTS OF ABRASION AND CORROSION ON THE WEAR OF STEELS

A study of dry and wet abrasion, corrosion of an abraded surface and their interrelationship with microstructure was undertaken. The following section serves as an aid in understanding the quantitative results of the previous section and to assist in their interpretation. It is necessary in the 'design' and selection of an optimum alloy steel that the abrasive and abrasive-corrosive wear mechanisms be established.

4.2.1 Characteristics of an Abraded Surface

A range of materials was selected to study how the microstructure and mechanical properties of a material influences the process of dry abrasion. A mechanistic understanding of the process of abrasion with respect to microstructure would assist in this study. A description of the materials is given in Table 4.15. They have been divided into three broad groups, namely: materials with low initial hardness; those with very low toughness; and a group of materials which are hard and cover a range of toughness values. The descriptive terminology used in this section is defined in fig 4.19.

TABLE 4.15 : Description of the materials selected for a study of the dry abrasion process

MATERIAL	HARDNESS (HV30)	TOUGHNESS (Joules)	RAR	MICROSTRUCTURE
3CR12 iii	228	75	1.23	Dual phase, Martensite plus islands of ferrite
F351	225	40	1.71	Austenite (metastable)
AISI 440B	684	5	2.27	Martensite plus massive chrome carbides
SS10/200	775	2	1.49	Quenched martensitic medium carbon steel
T102A AHRT	450	92	1.59	Tempered lath martensite. No coarse carbide precipitates
WV69 200	380	175	1.66	Low carbon large grain lath martensite
WA2 AC	435	27	1.70	Lath martensite with carbide ppt along grain boundries
UA 200	560	78	2.10	Martensite with interlath film of retained austenite

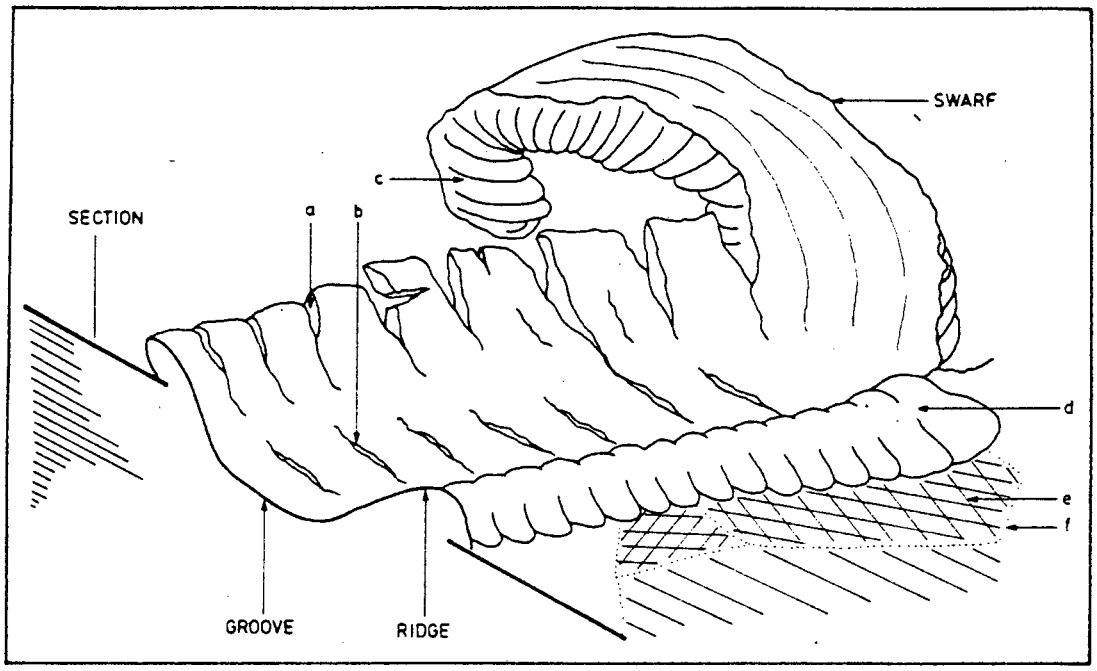

FIGURE 4.19 : Sketch of the dominant features seen during SEM studies of the abraded surfaces. Material is moved to the sides and accumulates ahead of the point of an abrasive (analogous to a knife scraping butter)

a) fracture of strain hardened material
b) ductile tearing (and smearing) in soft metals alternatively cracking and the occasional delamination in the hardest surface material
c) localized zones of shear
d) high ductility results in a rounded ridge shape if zero work hardening
e) crystallographic lines of slip
f) grain boundary

Comparison of the abraded surfaces of 3CR12 iii and F351 showed some important differences in the material response to abrasion (figs.4.20 and 4.21). Both materials have the same bulk hardness but the different microstructures resulted in a large difference in RAR. The presence of debris is abundant on the surface of 3CR12 but uncommon on F351. The debris is in the form of extruded (machined) swarfs or as friable sections from a ridge formed after multiple passage of abrasives.

The depth of the grooves of materials AISI 440B and SS10/200 would not appear to be as deep as for 3CR12 and F351 (figs 4.22 and 4.23). This is to be expected from their measured bulk hardness. It has been noted that 3CR12 (and 070M20) tend to pluck whole abrasive particles out of the abrasive belt whilst AISI 440B causes a cleavage fracture of the asperities of the abrasive particle resulting in a decrease in the average effective grit diameter.

The third group of materials which represent the bulk of the experimental alloys all have single phase martensitic structures. Within this group there is very little difference in the surface morphology between materials with a good or bad resistance to abrasion. It is noticed, in comparison with the surface morphology of the other groups, that there is an absence of microfracture to the bottom and sides of the abrasive grooves, (fig. 4.24) with the exception of T102A which showed it to a small degree. The material WV69 has the highest incidence of deep grooves (within the 3rd group) and the lowest measured hardness. Material WA2 AC, which has a lower toughness than the others, has a 'more tidy' appearance in that there is less debris attached to the surface and the abrasive grooves have a longer path length before disruption.

A study of the debris produced after abrasion revealed one clear association with the known properties of the material. It was noted that for example the debris of 3CR12 tended to be short, broken up fragments of swarfs in comparison to the long helical swarfs of UA 200. Material AISI 440B had shorter, thinner helical swarfs with very little of the fine non-descript fragments usually found in a sample of debris. The debris collected from F351 was made up of long helical swarfs and a large number of smaller fragments. It was concluded from the study that the helical swarfs originate from materials with a high surface hardness and a predominantly cutting mode of abrasion. The debris consisting of fragments of ploughed material and other particles of a more ragged, friable form, originate from materials with a high toughness or exhibiting a predominantly ploughing mechanism of material removal.

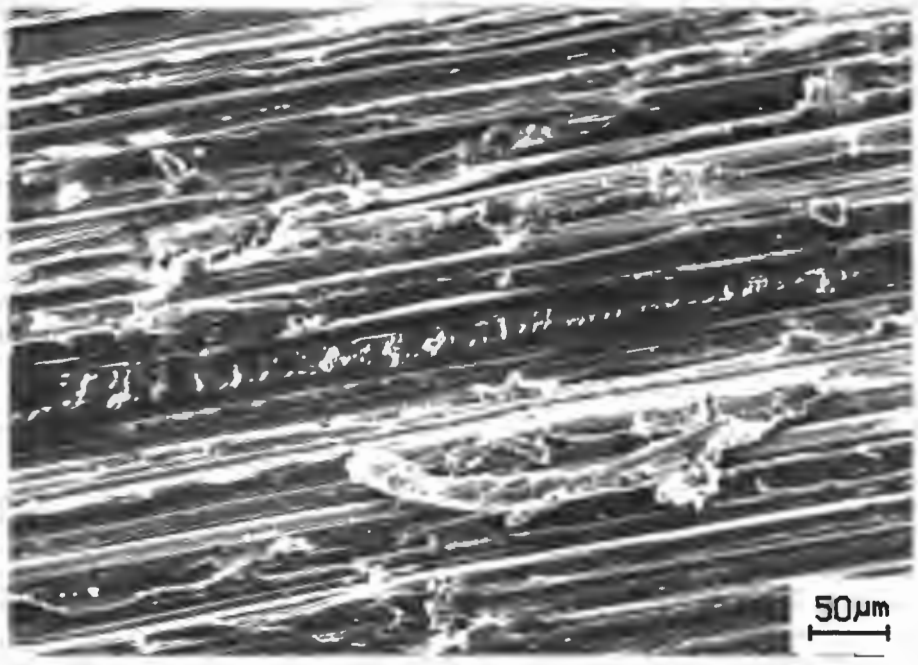

FIGURE 4.20 : Abraded surface of 3CR12 iii. This material is found to have a high predominace of microfracture along the bottom and sides of the abrasion groove. The ridges are ragged with swarfs still attached. Ductile tearing of the friable ridge material is a common feature

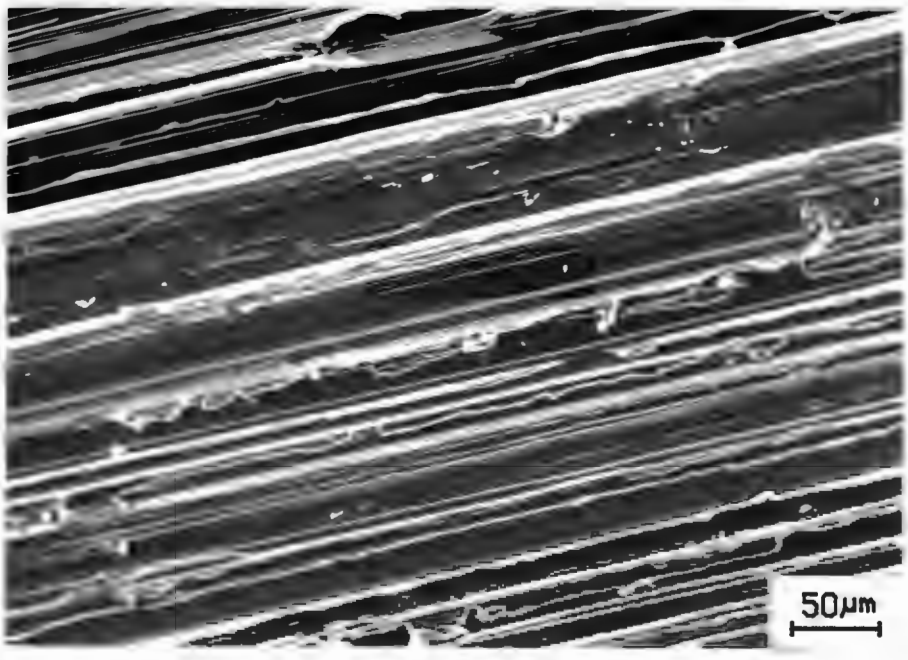

FIGURE 4.21 : Abraded surface of F351. Here there is less evidence of microfracture. The grooves are shallow with material displaced plastically to the sides. This material is known to work harden by 300 per cent and is removed in a predominantly cutting mechanism

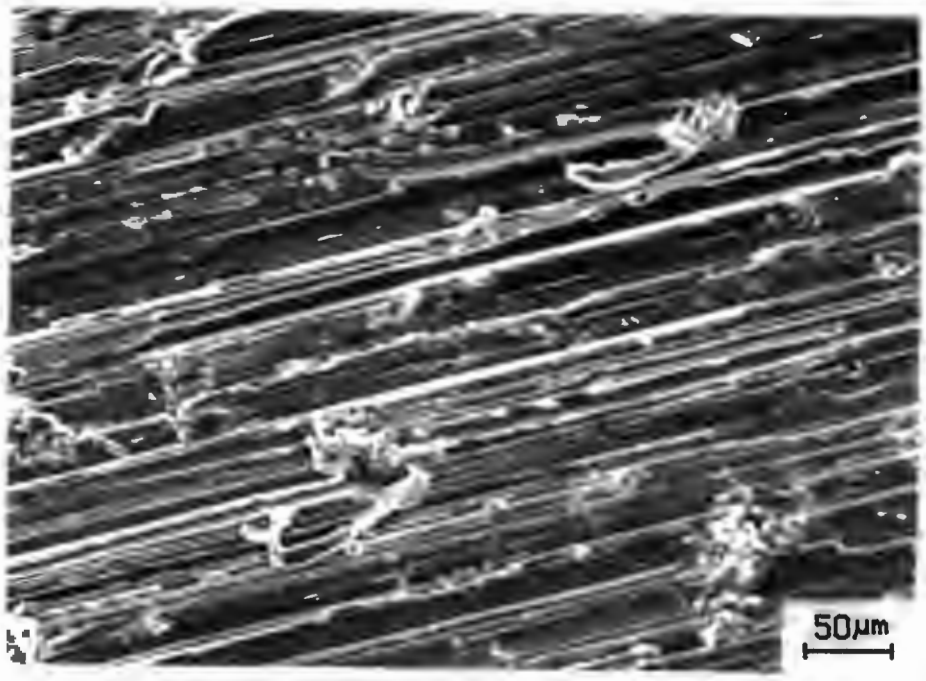

FIGURE 4.22 : Abraded surface of AISI 440B. The abrasive tracks are short and end abruptly, typically when the abrasive fragments. Microfracture of the surface is uncommon with little evidence of ductile tearing. Possibly microcracks sighted at the carbide/matrix interface. No evidence of whole carbides being plucked out of the surface

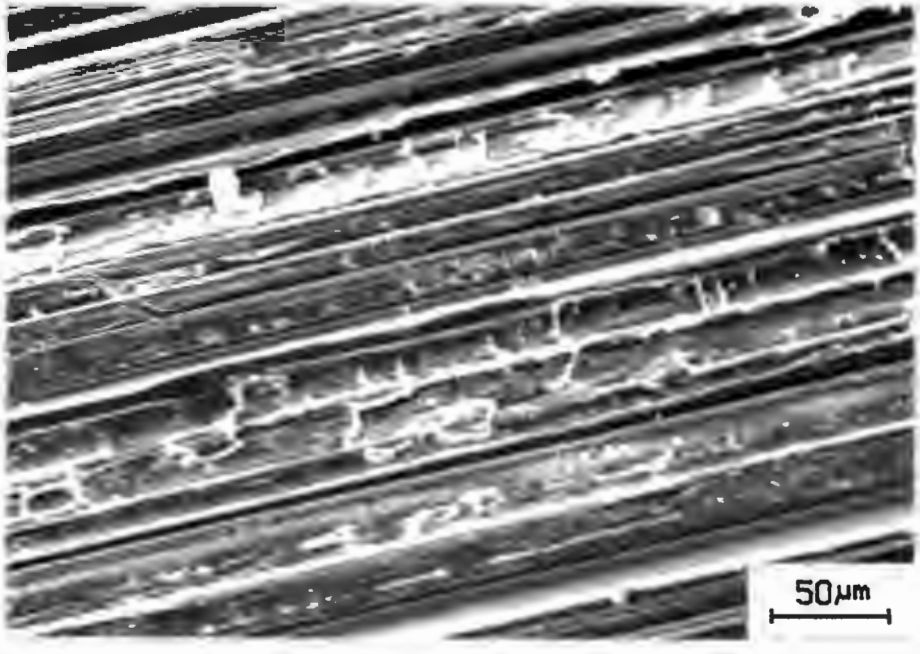

FIGURE 4.23 : Abraded surface of SS 10/200. Abrasive grooves appear very shallow. The high incidence of microfracture is dissimilar to 3CR12, being in the material adjacent to the abrasive track. Friable surface appearance with many microcracks

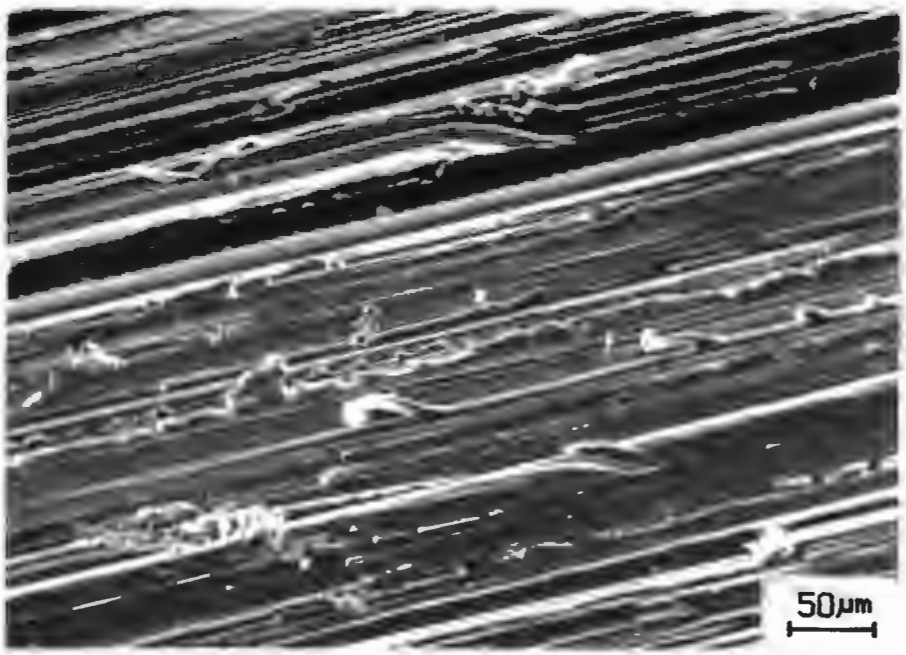

FIGURE 4.24 : Abraded surface of UA 200. Material is plastically deformed to the front and sides during passage of an abrasive particle. An absence of microfracture on the face of the abrasive groove (as noted for F351). The rended material has features more akin to 3CR12 than SS10/200

4.2.2 The extent of permanent deformation at an abraded surface

Microhardness measurements of the surface after abrasion, and of the bulk material, are compared to dry abrasion resistance (Table 4.16). Since the experimental conditions remain constant, the differences in results between materials must be attributed to differences in their microstructure.

An isolated abrasive track on a polished surface of the austenitic material NP599, showed slip lines in the fcc grains adjacent to the scratch (fig. 4.25). The material of the scratch was found to be ferromagnetic while the unscratched, polished areas remained non-magnetic. This indicates a crystallographic change in the scratched material, probably to martensite which is the product phase when this alloy is cold worked (material data sheet).

A tapered 2° section through the abraded surface of the metastable austenitic steel, F350 showed three zones with small differences in microstructure (fig. 4.26). The material at a depth greater than 100 micrometres from the abraded surface has a microstructure identical to the bulk structure (fig. 3.15). The material etches dark in the surface region to a depth of 20 micrometres except at selected areas to the sides and bottom of the tapered groove where the material etches white. There is evidence on the right of fig. 4.26 that an abrasive had penetrated deep into the material and was abruptly stopped. Possibly the tip of an abrasive broke off at this site. The white etched area about this site corresponds to the material that would have plastically deformed to accommodate the embedded point.

Similar "white etched" areas are noted on tapered sections of the martensitic developmental alloys (fig. 4.27) and on sections through the debris (fig. 4.28). These regions are an ultra-fine grained martensite that developed during frictional heating under high strains and rapid cooling. A microhardness trace indicates that strain leading to work hardening of an abraded surface penetrates to a depth of 25 micrometres for F350 (fig. 4.29). The depth and extent of work hardening for the martensitic alloys was too small for a microhardness trace to be meaningful.

TABLE 4.16 : The measured extent of work hardening for a range of steels with different microstructures

Material	Surface	Bulk	H_s-H_b	RAR	Microstructure
3CR12	226	168	58	1.03	ferrite & martensite
WV69 200	441	421	20	1.66	martensite (0.07% C)
T122 AHRT	548	525	23	1.68	martensite (0.21% C)
Quatough T	539	500	39	1.73	martensite & retained austenite (4% Cr)
WA vi	558	500	58	1.61	martensite & retained austenite (7% Cr)
WC vi	566	528	38	2.01	martensite & retained austenite (12% Cr)
UA 200	644	568	76	2.10	martensite
AISI 304L	363	243	120	1.29	austenite
F350	531	302	229	1.69	austenite & martensite
F351	506	310	196	1.71	austenite & martensite

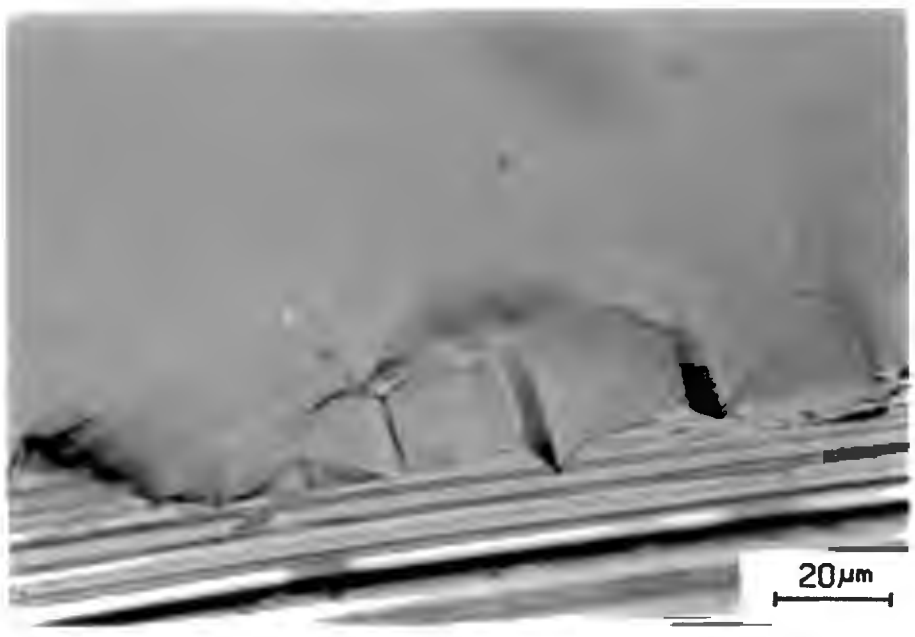

FIGURE 4.25 : Plastic deformation due to the ploughing action of an abrasive has caused parallel sets of slip lines to occur within the austenite grains of NP599

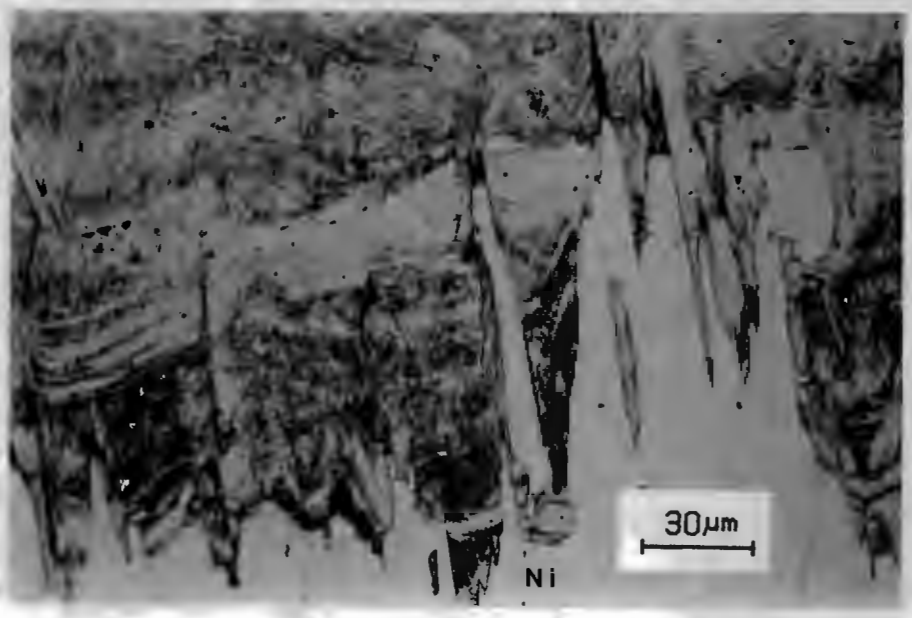

FIGURE 4.26 : Tapered section through the abraded surface of the metastable austenitic alloy, F350. The 2° taper results in a 29 times magnification of depth. The smooth white area across the bottom is electroplated nickel. Note the white etched areas alongside some of the tapered grooves and about the square shaped hole on the right

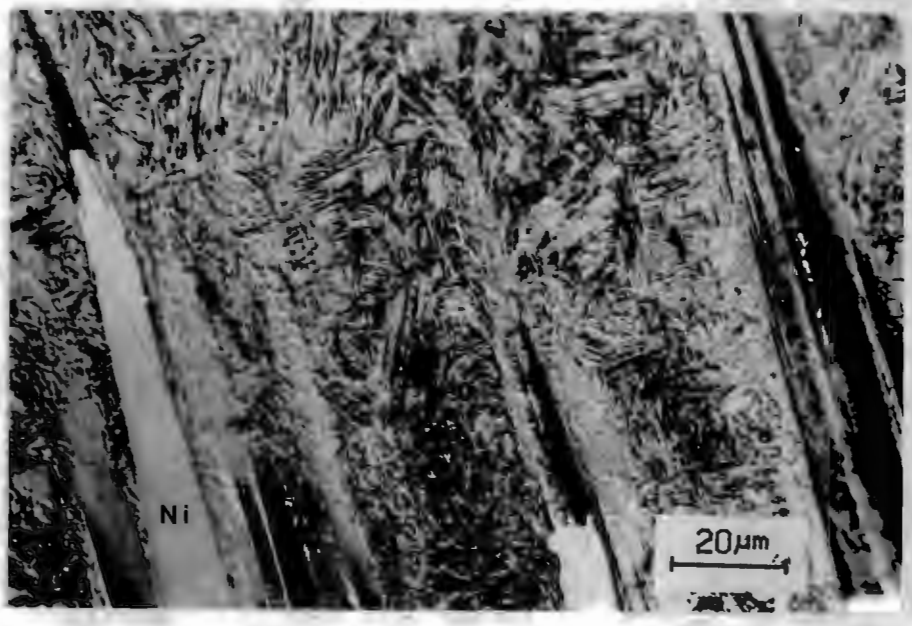

FIGURE 4.27 : Tapered section through the abraded surface of a martensitic alloy, WA vi. Many of the martensitic alloys exhibited areas alongside the tapered grooves that etch white. There is no evidence of the microstructure being disrupted between the grooves as is seen for the austenitic material.

FIGURE 4.28 : A section through a swarf of steel WA vi. The microstructure has a virtually homogenous morphology due to multiple lines of slip. The lightest etched region is along the 'shear' edge.

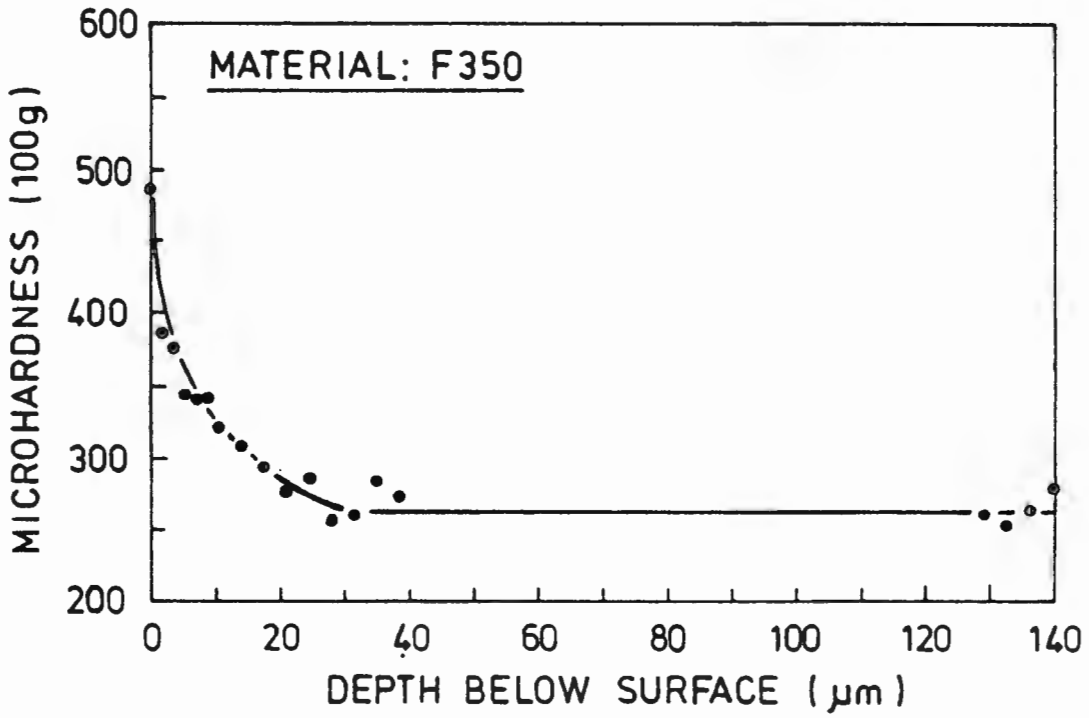

FIGURE 4.29 : Microhardness profile showing the change in microhardness with depth below the abraded surface of alloy F350. Strain hardening reached a depth of 25 micrometres. The indents were too big to detect a zone of recovery at the surface.

4.2.3 Material Response to a Change in the Velocity of Abrasion

Materials selected for this investigation can be separated into two groups. The first group consists of those materials having an M_s at or below room temperature (start of martensitic phase transformation) and an M_d above room temperature (temperature below which an applied stress can induce an austenite to martensite transformation). The second group consists of materials with an M_s temperture above and an M_f at or above room temperture. Materials in the first group fall under the collective title of metastable austenitic steels. Materials in the second group are martensitic steels.

The abrasion performance (inverse of volume loss per metre) of the metastable austentic stainless steels is ranked third through to seventh at low abrasion velocities (fig. 4.30). However, at the higher velocity of 600 mm/sec they are ranked sixth to eleventh. This suggests that the response of a material to a change in the velocity of abrasion is dependant on its microstructure.

The rate of change of volume loss with velocity is 0.9 mm^3 sec m^{-2} for the metastable austenitic stainless steels and 0.3 mm^3 sec m^{-2} for the martensitic steels (fig. 4.30). The martensitic steels are found to have a weak relationship between volume loss and the velocity of abrasion in the range 60 mm sec^{-1} and 260 mm sec^{-1} and virtually no relationship above this range. On the other hand, the volume loss of the metastable austenitic stainless steels is strongly related to velocity over the whole range (fig. 4.30).

SEM studies of the abraded surfaces provided little visual evidence of a change in the material response. There was no evidence to suggest a change in the mechanism of fracture or removal of material from the abraded surfaces. However, UA 200 showed an increase in the predominance of those features associated with a cutting mechanism. AISI 440B had a greater incidence of microcracks and other features associated with the wear of composite materials at the higher velocity. No change in microstructure was detected optically that could be associated with the velocity dependence. There was also no measurable change in work hardening for these materials.

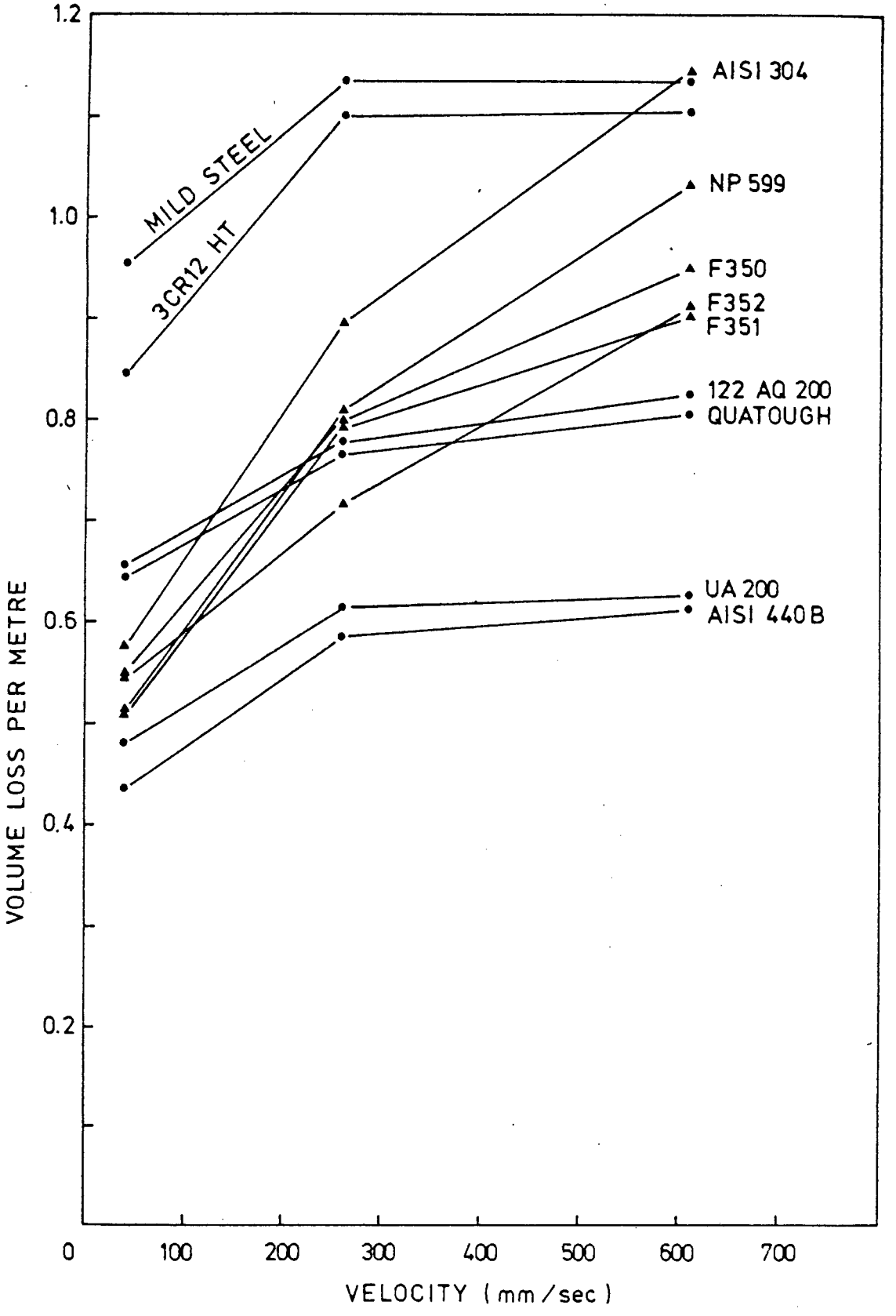

FIGURE 4.30 : The volume of material removed per metre of abrasive path length is dependant on both the velocity of the abrasive and the microstructure of the material.
● martensite steels; ▲ metastable austenitic steels

4.2.4 Corrosion of an abraded surface

It is the nature of metals to corrode on being exposed to a corrosive environment. A SEM study of abraded metal surfaces revealed that corrosion initiates at certain specific sites. These are (for steels that do not exhibit passivity) in decreasing order of occurrence:

a) along the tops of ridges
b) at cracks and holes in the groove face
c) randomly scattered along the sides and base of the groove
d) at disruptions in the path of the abrasive where it has changed direction, stopped or become embedded
e) at grain boundaries (for certain steels only).

The active sites are anodic and can develop into pits or crevices with ferric oxide being precipitated about the edge. Such oxide deposits can be seen in fig. 4.31 and consist mainly of haematite (red-brown rust) with magnetite (black) underneath.

The plastically deformed regions about a wear track are the preferred sites for corrosive attack as demonstrated by the pitting of a single scratch on a polished metal surface (fig. 4.32). The rate of corrosion of an abraded surface is found to be greater than a surface of similar roughness but without the high internal energy and atomic disorder of the abraded material (fig. 4.33). Figure 4.34 vividly shows the outcome of this difference in corrosion rate. The difference is greatest for steels of minimal chromium content and decreases with an increase in chromium content. At 12 weight per cent chromium the abraded, and thus work hardened, surface has a slightly lower rate of volume loss than the annealed material of similar roughness (fig. 4.33). Microhardness measurements confirmed that the abraded surface was in a higher state of work hardening than the same surface of the annealed specimen for all the materials (Table 4.17).

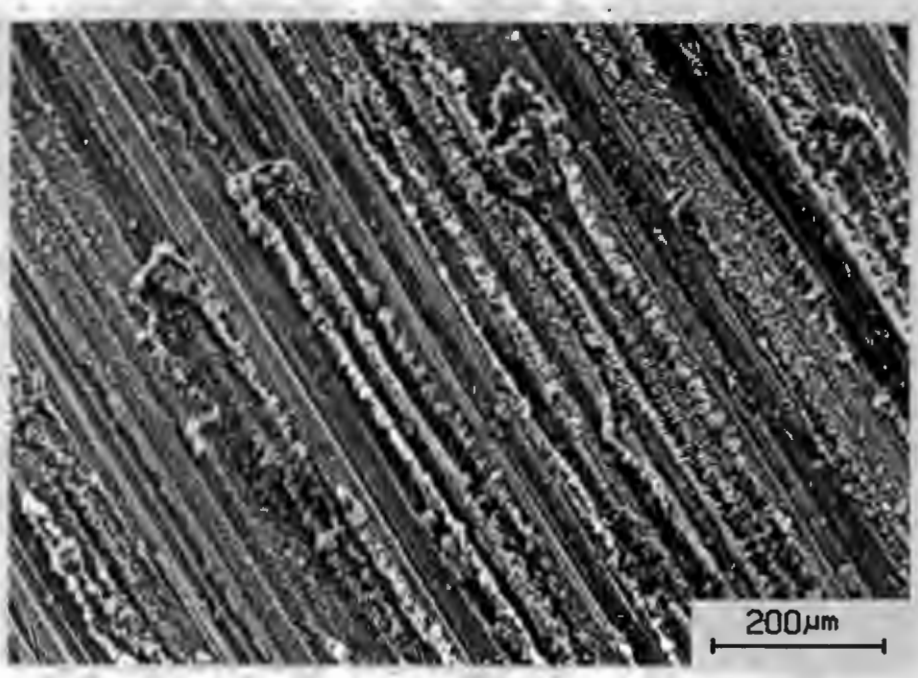

FIGURE 4.31 : Corrosion products on the ridges of an IA 200 specimen after 46 hours corrosion (SEM)

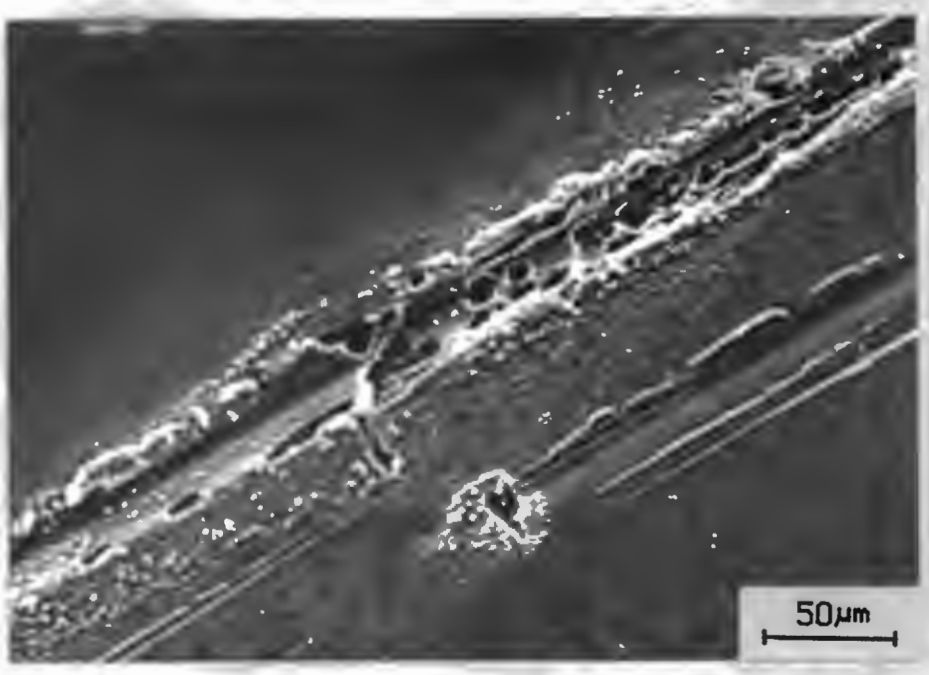

FIGURE 4.32 : Corrosion pits in the plastically deformed regions of an isolated wear track in 070M20. Corrosion products have been deposited in the area adjacent to the active sites (SEM)

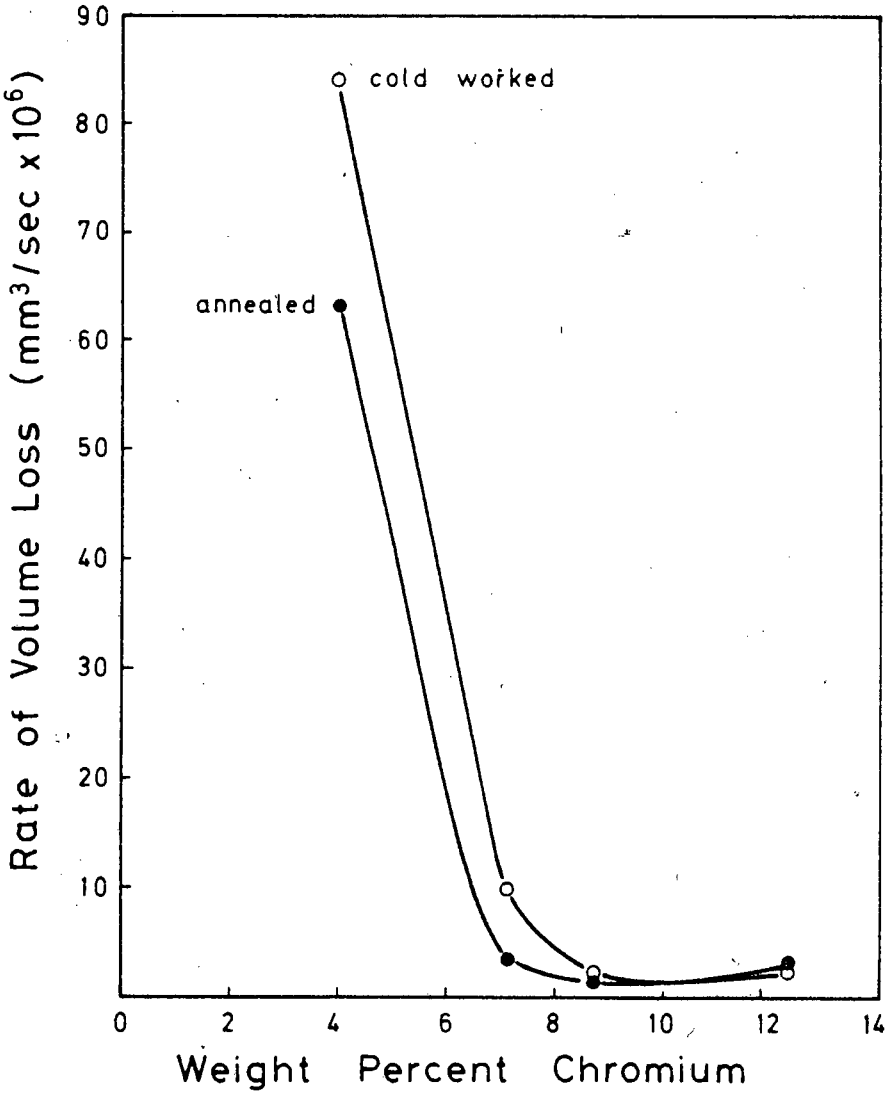

FIGURE 4.33 : The influence of abrasion with its associated work hardening on the rate of corrosion of a rough surface. The difference in the rate of volume loss between a rough abraded surface and a similarly rough annealed surface is proportional to the rate of corrosion. This is dependant on the chromium content of the material

TABLE 4.17 : The extent of work hardening at the rough surface of the annealed and abraded material prior to corrosion.

Material	% Cr (wt%)	Annealed (MHV_{100})	Abraded (MHV_{100})
Quatough	4	14	39
WA	7	-5	58
UA	9	-15	71
WC	12	18	38

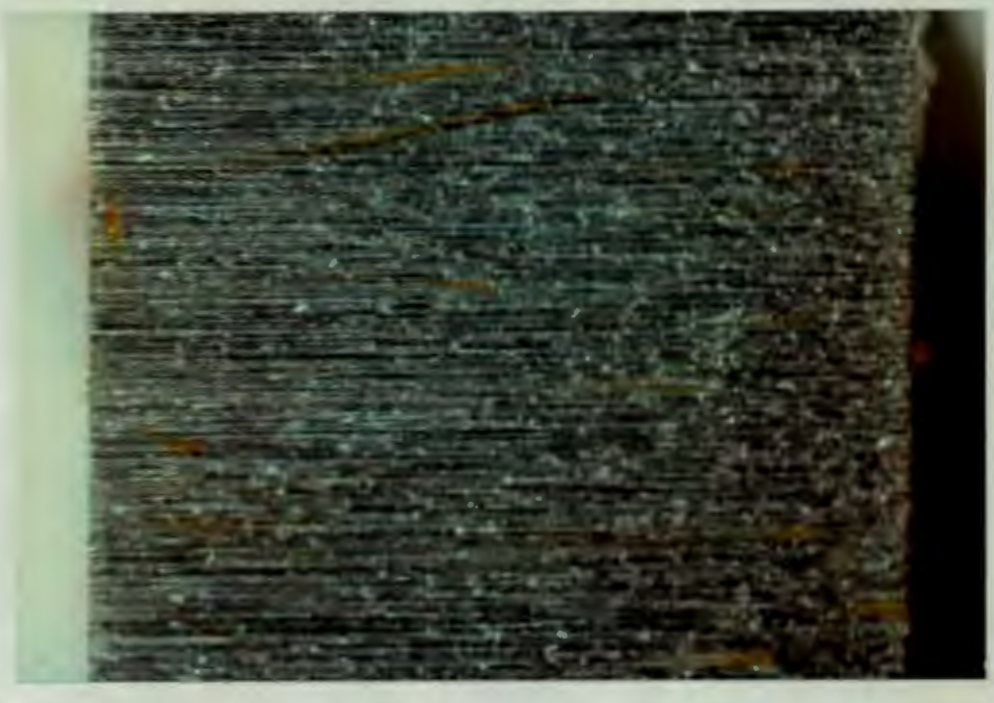

ANNEALED STATE

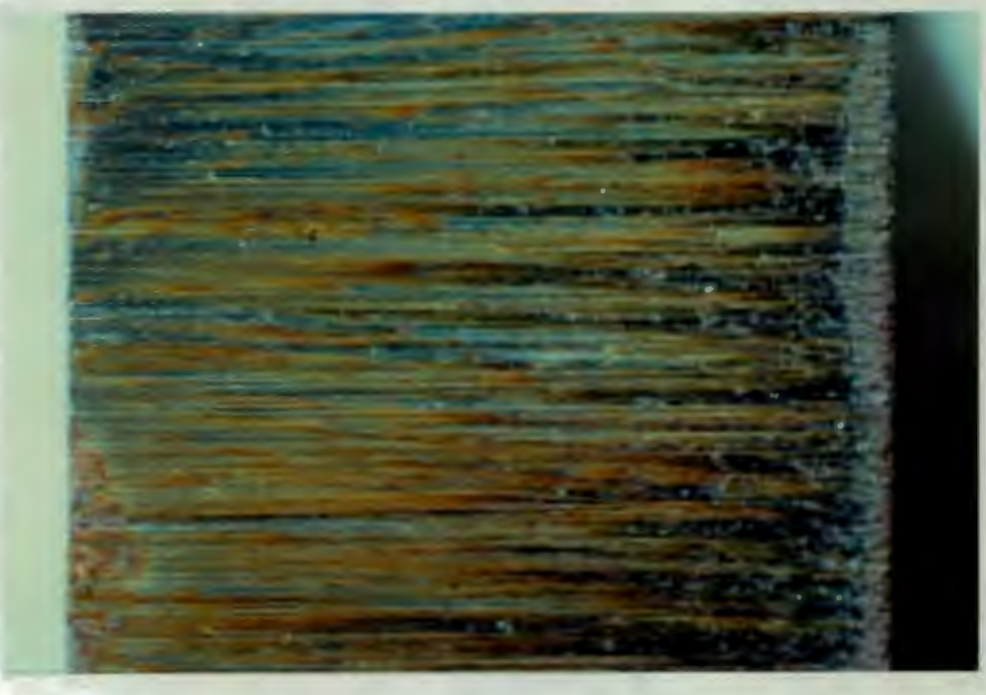

WORK HARDENED STATE

FIGURE 4.34 : The abraded surfaces of WA (7% Cr) after exposure to a corrosive environment for 80 minutes. The specimen in the work hardened state has corroded at a faster rate than the specimen in the annealed state

4.2.5 Passivity of Abrasion Resistant Steels

Corrosion Index

A crevice corrosion index (also known as "wirksumme") was devised by steel suppliers based on parametric observations of pitting and crevice corrosion resistance (Sedriks, 1984). This has not met with wide acceptance as it was derived from the compositional parameters of chromium, molybdenum and nitrogen content only and totally ignored any microstructural factors which could contribute to the breakdown of passivity. The development of a similar corrosion index for the martensitic developmental alloys would not have been successful due to the complex and interactive nature of the alloying elements. It was therefore decided to correlate the corrosion results with chromium content only and be aware of the presence of other major alloying elements and the microstructure in the interpretation of the results.

Weight loss measurements

Stainless steels passivate due to the presence of chromium in solid solution. For those abrasion resistant steels with less than 4 weight per cent chromium, more than 80% of the total volume loss is due to corrosion in the RWRL test (abrasion plus corrosion). This contribution drops to less than 10% for those steels with greater than 12 weight per cent chromium.

An increase in chromium content (up to 10% Cr) will reduce the volume of material lost due to corrosion (fig. 4.35). Above 10% chromium there is a dramatic decrease in the volume of material lost. This is observed for both the RWRL and RWRL #2 test although the decrease is not as dramatic in the latter. Materials with above 12 weight per cent chromium in solid solution have a consistantly low corrosion rate in both the RWRL tests.

Electrochemical measurments

Potentiodynamic polarization measurements for five abrasion resistant martensitic steels with increasing chromium content are shown in figures 4.36 and 4.37. The same synthetic mine water

composition as for the RWRL corrosion test was used (Table 3.4). The steels included in this investigation are given in Table 4.18.

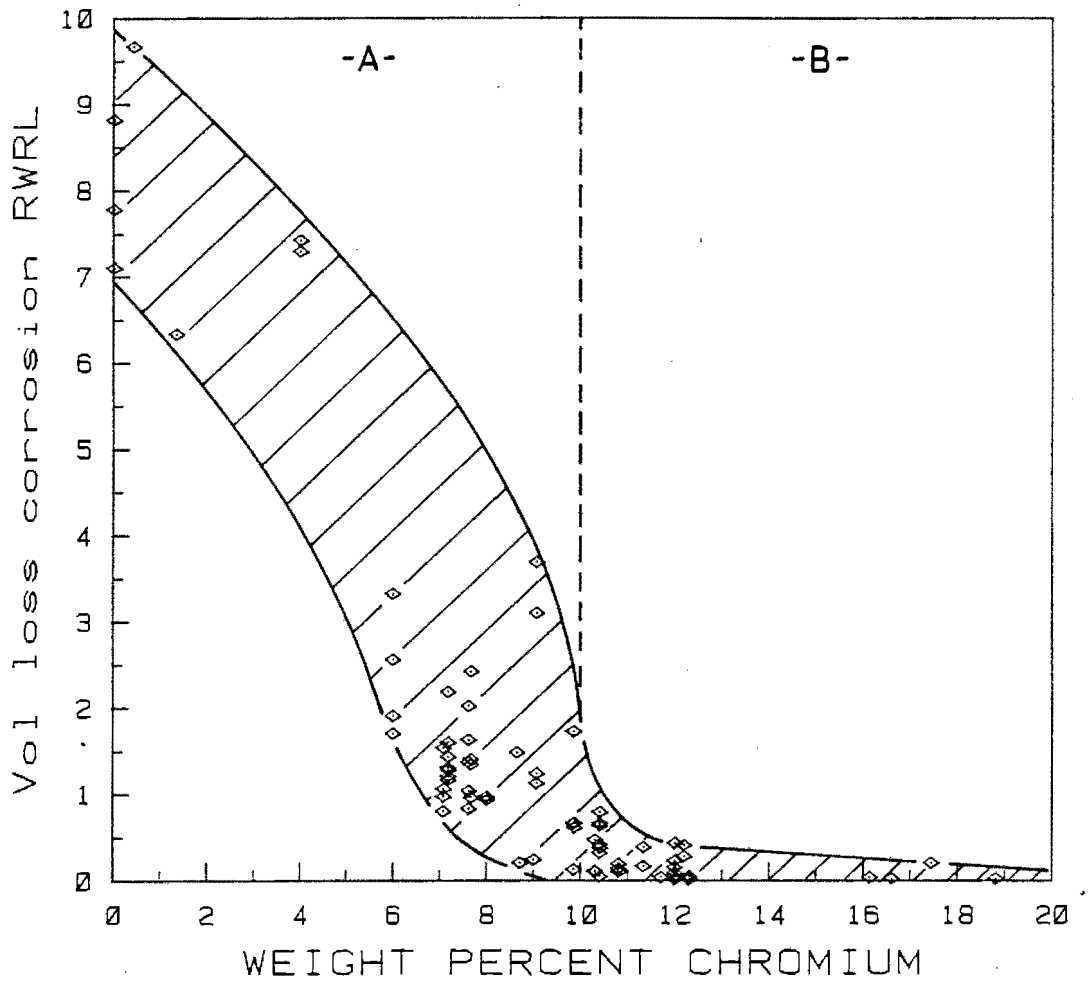

FIGURE 4.35 : The volume of material lost due to corrosion is dependant on the chromium content. There is a significant decrease in corrosion for materials with above 10% Cr. Materials in region -A- do not exhibit passivity while those in region -B- generally do

TABLE 4.18 : The corrosion potentials for a selected range of alloyed steels with increasing chromium content

	Material	%C	%Cr	%Mn	%Ni	E_{corr}^{d}	E_{corr}^{a}
1	070M20	.15	0.02	0.5	0.03	-1085*	-595*
2	Quatough	.30	4.0	2.0	0.03	-1064	-507
3	UA 200	.23	8.6	0.35	3.33	-1080	-580
4	WV69 200	.07	12.0	0.05	1.55	-1079	-560
5	AISI 431	.20	16.0	1.0	2.0	-1095	-501

a - aerated ; d - deaerated conditions ; * - mV (S.H.E.)

The alloying of iron with chromium has not changed the corrosion potential, E_{corr}, in the deaerated synthetic mine water solution (Table 4.18). Steel 070M20 remains active and has no passive range (fig. 4.36). The passive range of the steels containing increasing chromium has expanded to noble potentials before breakdown and pitting occurs. On the reverse scan from a noble potential, the repassivation or protection potential, E_x, is also related to chromium content. 070M20 and Quatough have no E_x and cross the cathodic line at E_{corr}. AISI 431 is the only steel that shows an active to passive transition (fig. 4.36).

The E_{corr} in oxygen saturated conditions (fig 4.37) is influenced by alloying content. There is a small shift to a more active potential with increasing chromium content. The exception is Quatough which has 2% Mn. The corrosion current density, I_{corr}, is 0.5×10^{-1} Am^{-2} for 070M20 and approximately 8×10^{-3} Am^{-2} for the four chromium containing steels.

The size of the passive potential range is influenced by the chromium content and microstructure under aerated conditions (fig. 4.37). 070M20 has no passive range. Quatough has a passive range of 50 mV while UA 200 has a passive range greater than 150 mV. This latter material was very susceptable to crevice attack under the gasket and would breakdown at any potential between -430 mV SHE and the transpassive potential. Optical examination afterwards usually showed crevicing at the gasket edge and pitting of the surface. The instance where breakdown occured at the noble potential of +400 mV SHE the specimen showed a partly transpassive surface with many pits but no attack at the gasket edge. AISI 431 pits at +75 mV and WV69 200 pits at +360 mV SHE. (fig. 4.37).

The pitting potential was found to be influenced by the scan rate and all scans were at 0.14 mV per second. The repassivation potential, E_x, was difficult to reproduce. All the steels showed hysteresis on reversing the scan direction after pitting commenced (fig. 4.37). WV69 200 and AISI 431 have E_x above E_{corr}. UA 200 repassivates at or below E_{corr} in aerated solutions. Quatough and 070M20 repassivate at the deaerated corrosion potential.

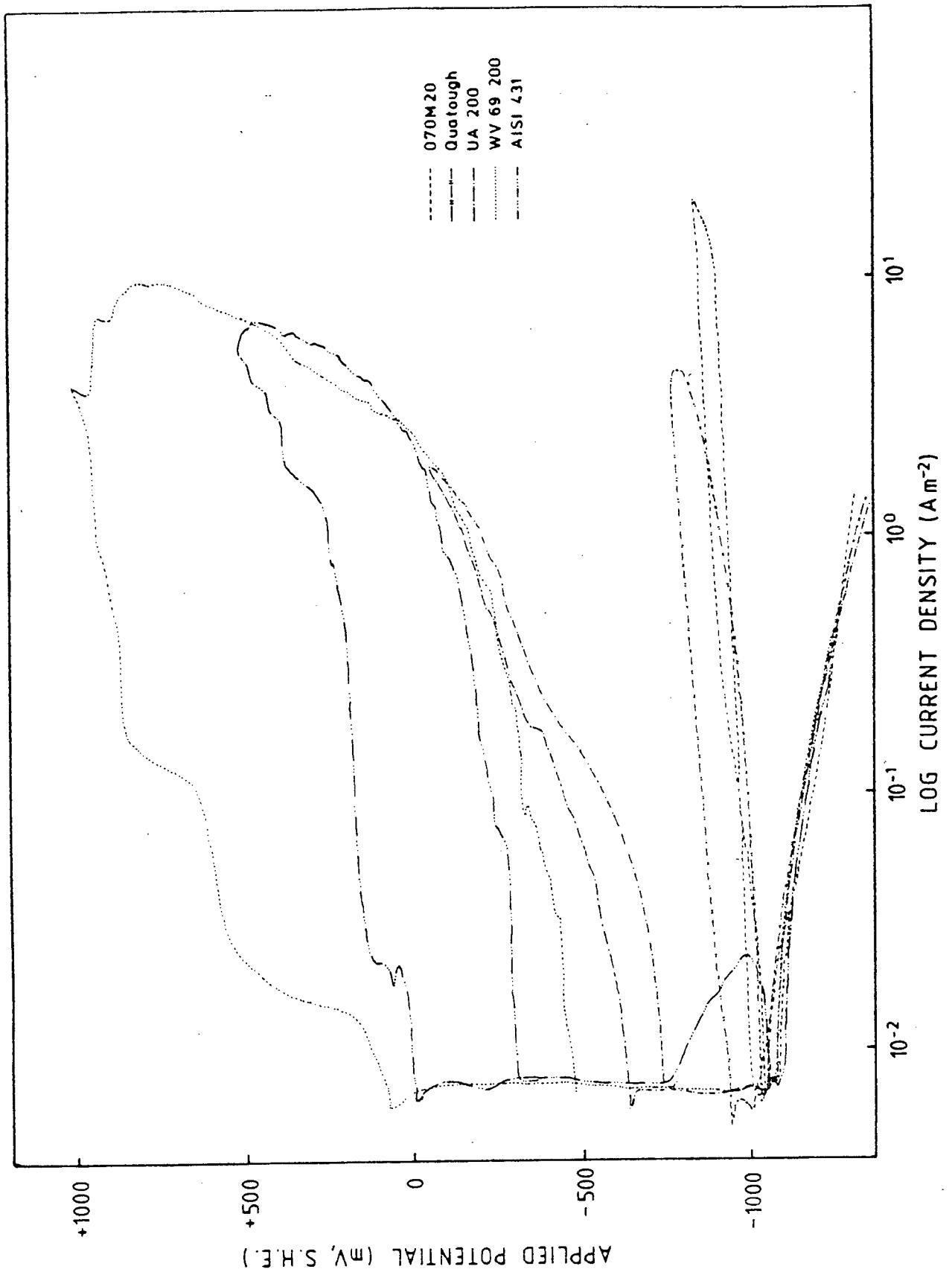

FIGURE 4.36 : Effect of chromium content in steels on their anodic polarization behaviour in synthetic mine water at 30°C. Deaerated conditions

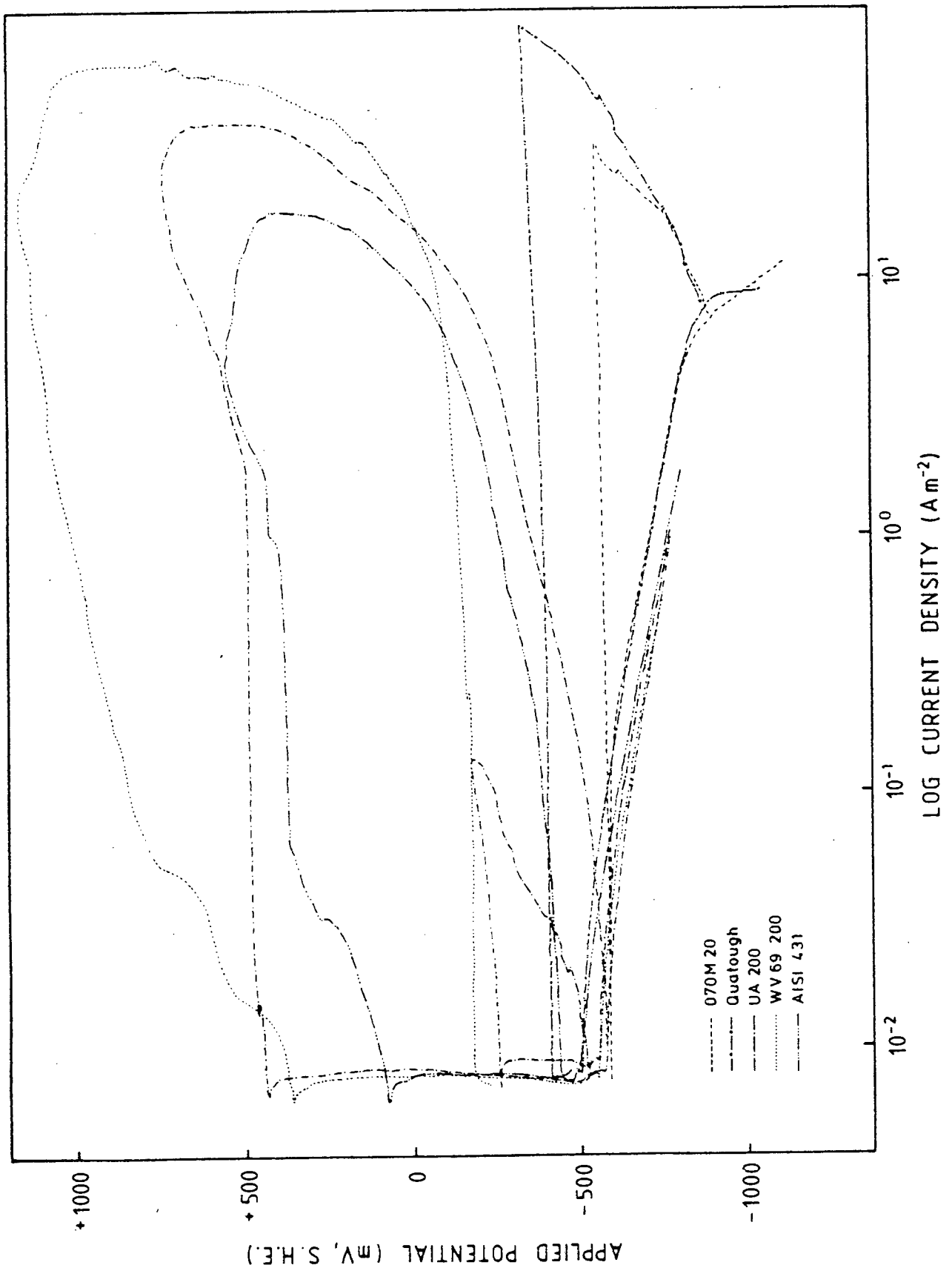

FIGURE 4.37 : Effect of chromium content in steels on their anodic polarization behaviour in synthetic mine water at 30°C. Aerated conditions

4.2.6 Passivity and the Time Factor

To a first approximation the minimum chromium content for corrosion resistance is 10 weight per cent chromium (fig. 4.35) but the time factor in corrosion resistance needs to be studied in more detail.

Let us first consider two materials at the two limits of region -A- of figure 4.35. The volume of material lost from the abraded surface of 070M20 (mild steel) is a strong function of time (fig. 4.38). The rate of material loss is initially very high so that the volume of material corroded in the first hour and a half is equivalent to the material lost in 47 hours for UA 200 (8.6% Cr). The rate of volume loss for UA 200 is initially slow for the first 10 hours but thereafter increases to a steady rate of material loss (figure 4.38). The volume loss for the standard RWRL tests of these materials have been included in figure 4.38 for comparison.

Figure 4.39 depicts the visual progress of corrosion for UA 200. Isolated anodic sites are active after 4 hours but the majority of the abraded surface is passive. At 12 hours the active sites continue to corrode and deposit corrosion products on the surface. The oxide layer for the rest of the surface has thickened and begun to take on a red-brown tint. This continues until at 40 hours the whole of the surface is uniformly discoloured to the naked eye. The activity of the isolated pits now decreases and general corrosion of the entire surface follows. The strady state general corrosion rate (67 hours, figure 4.39) is slower for UA 200 than for 070M20 (fig. 4.38).

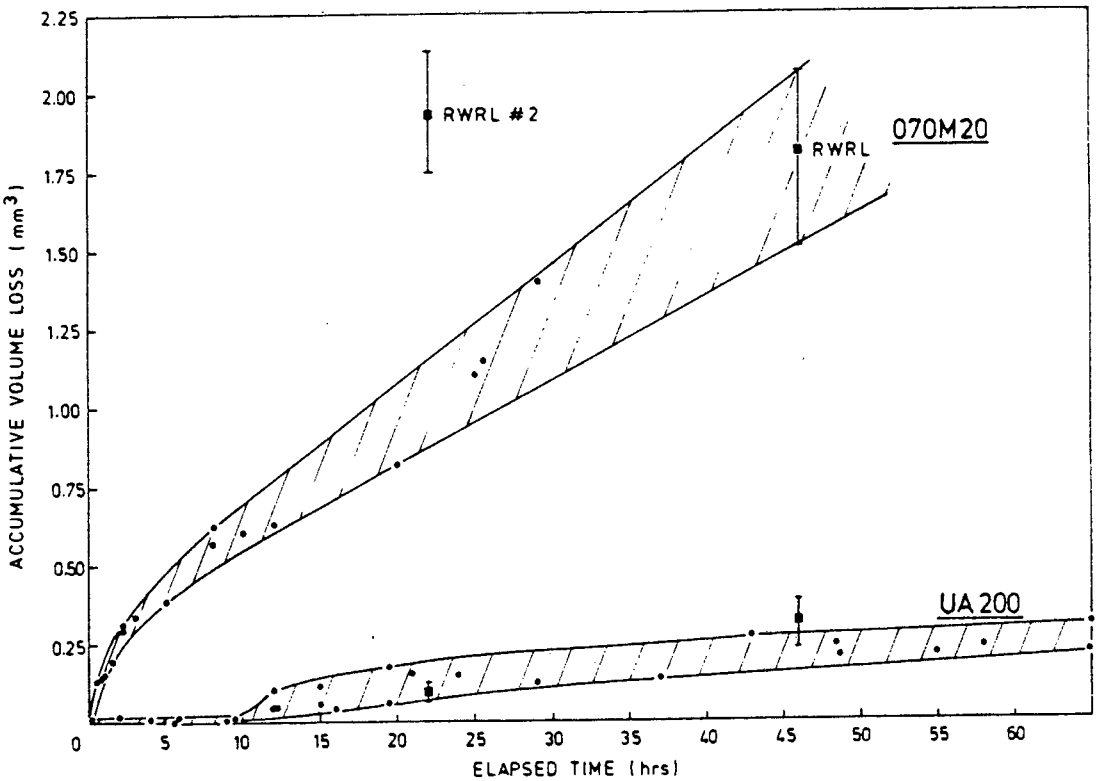

FIGURE 4.38 : The accumulative volume loss of material due to corrosion as a function of time for materals 070M20 and UA 200. The results for the RWRL and RWRL#2 corrosion tests are included for comparison at 46hrs and 22hrs respectively

FIGURE 4.39 (next page) : Colour micrographs showing the state of oxide film growth with time. The flow of the synthetic mine water (from right to left) results in a trail of oxide products behind an active pitting site.

Material : UA 200
Heat treatment : 1100°OQ; 200°OQ
Chromium content : 8.6%
RAR : 2.10
RWRL : 4.6

4 hours corrosion

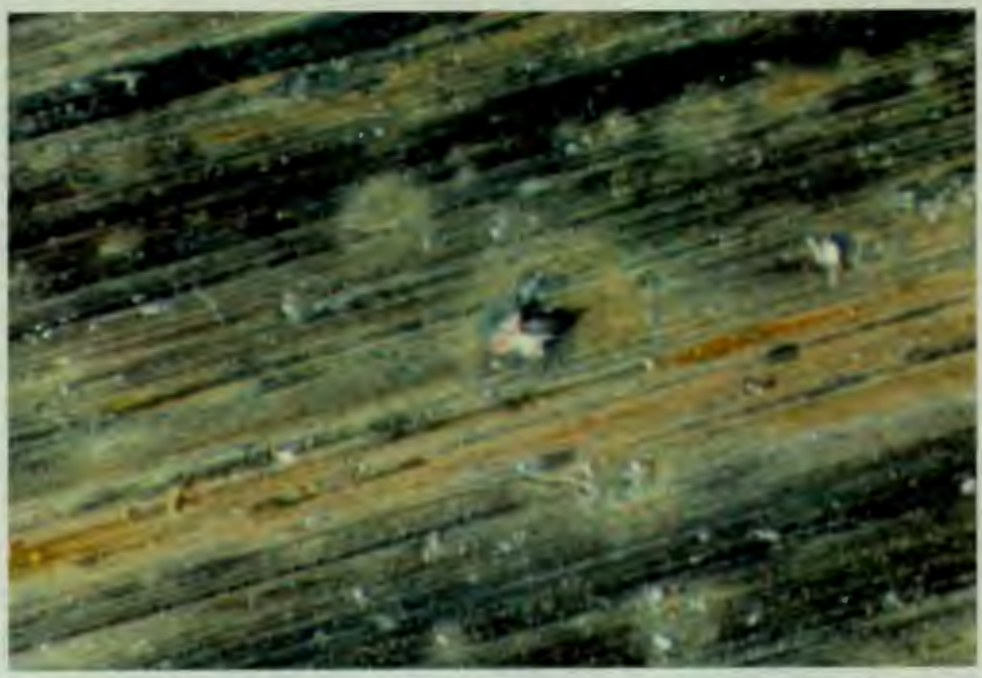

12 hours corrosion

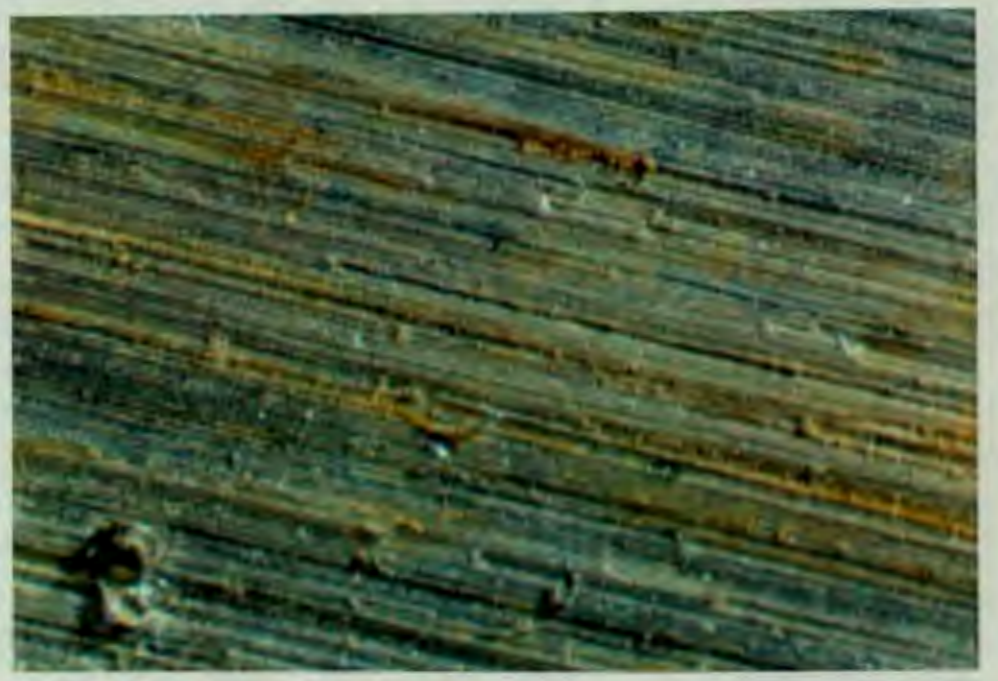

67 hours corrosion

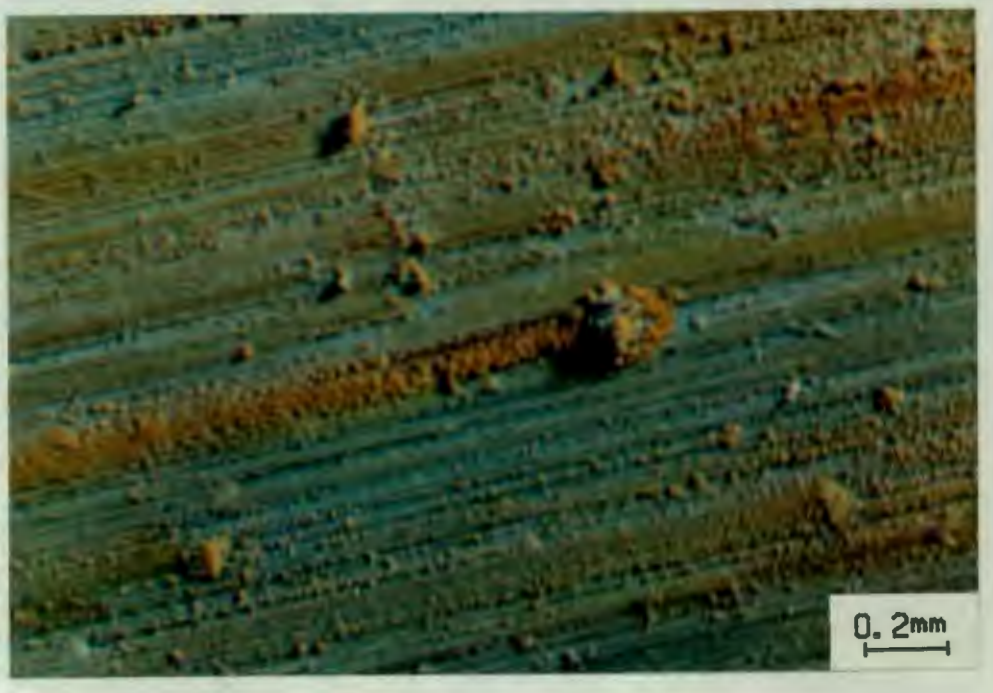

FIGURE 4.39 :

The free corrosion mixed potential of the abraded surfaces was monitored for the same materials as in Table 4.18. The traces for the first 10 hours are reproduced in fig. 4.40. The corrosion behaviour can be broadly grouped into three classes. (i) Quatough and 070M20 shift to a more active potential with time. (ii) UA 200 becomes noble at first but within 43 hours has dropped to a potential close to the corrosion potential of mild steel. Similiarly WV69 is at first noble but slowly drops to the corrosion potential for the chroimium steels. (iii) AISI 431 is seen to rapidly become passive and remain noble. The trace over a 2 day period for this latter martensitic stainless steel recorded a rapid drop of 40 mV and then a slow rise to the previously noble potential.

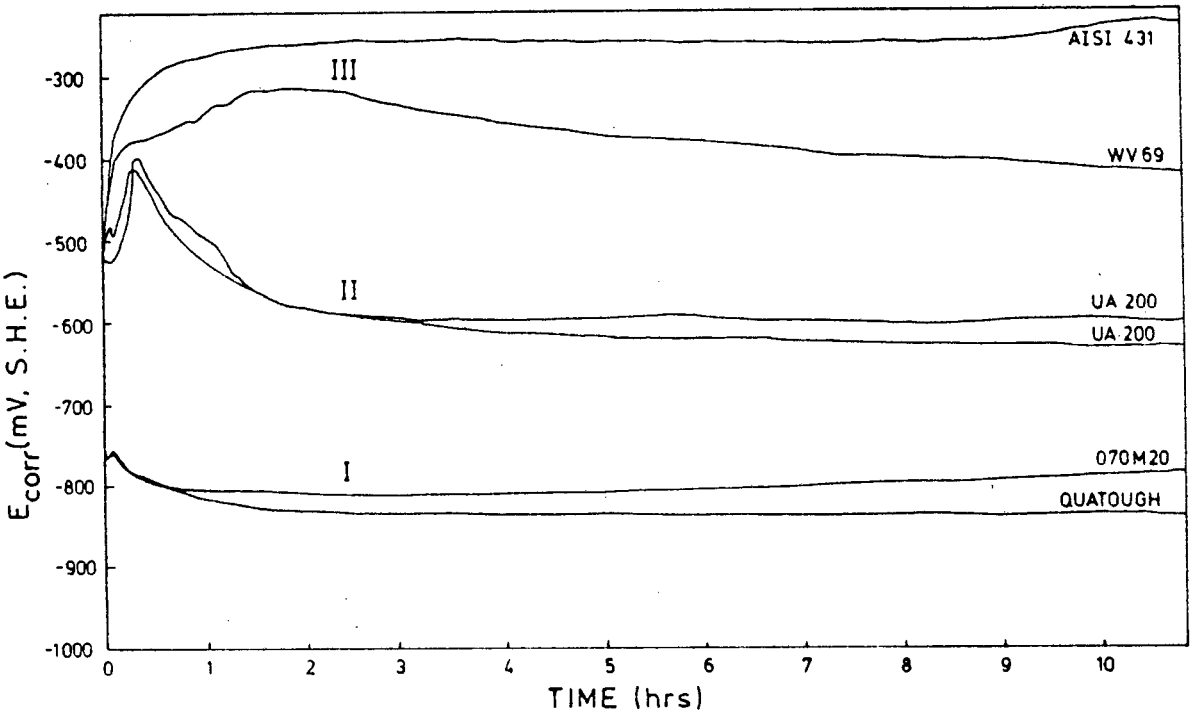

FIGURE 4.40 : The free corrosion mixed potential of four abrasion resistant martensitic steels and mild steel. Abrasion stopped at time, t=0 thereafter a steady flow of aerated synthetic mine water passed across the freshly abraded surface without further mechanical disruption. Three types of corrosion behaviour are identified

4.2.7 The Frequency of Abrasion and Corrosion

If the rate of corrosion and the subsequent volume of material removed is a function of time, then the frequency with which abrasion interrupts the corrosion process will have an influence on the total volume of material lost in an abrasive-corrosive wear situation. This can be readily seen in the RWRL and RWRL #2 results of figures 4.4, 4.5, 4.6 and 4.7 in section 4.1.1 and in the wear test results included in fig. 4.38.

The experimental conditions for the frequency experiment are detailed in section 3.1.3. The "high frequency" relative to the "low frequency" test series subjects the specimen to double the cycles of abrasion and corrosion for the same total distance abraded and total period of corrosion. The greatest difference in the rate of material loss between a high and low frequency of alternating abrasion-corrosion was recorded for 070M20. The volume of material lost due to corrosion in the high frequency RWRL test was double that for the low frequency RWRL test (fig. 4.41). The abrasion contribution for 070M20 remains the same for both tests. Material with increasing amounts of chromium show smaller differences in total material lost (shown as a delta wear rate in fig. 4.41) between high and low frequency (group I). The materials with 10 and 12 weight per cent chromium (group III) show approximately no change in total volume loss with a change in frequency of the RWRL test . It should be noted that the materials around 8 per cent chromium (group II) show higher corrosion contributions to the total volume loss for the low frequency RWRL test where there is a longer un-interrupted period of corrosion (contrary to the other groups).

The highest frequency of abrasion-corrosion would be the instantaneous situation where abrasion and corrosion are occurring concurrently. A comparison of abrasion under wet and dry conditions would reveal the effect a corrosive environment has on the rate of material removal from a metal surface. The results for a range of steels of different microstructure and chemical composition showed a slight but reproducible shift (fig. 4.42). At an abrasion

velocity of 260 mm/sec there is an average increase of 0.040 mm^3/m in material lost during wet abrasion as compared to dry abrasion (the exception being 3CR12).

At the slower speed of 42 mm/sec there was an average decrease of 0.046 mm^3/m in the amount of material removed during wet abrasion. These apparently conflicting results are just inside the limits of experimental error (0.045 mm^3/m) and could suggest that a corrosive environment may have an influence on the rate at which material is removed during abrasion. This possible influence may be associated with the velocity of abrasion.

A second influence corrosion may have on the volume of material removed during abrasion is to do with the presence of the oxide layer. Figure 4.43 shows the volume loss due to one metre of abrasion followed by a period of corrosion as a function of the period of corrosion (taken from fig. 4.38). Superimposed upon this is the result of a period of corrosion followed by one metre of abrasion. A comparison reveals that a short period of corrosion (up to 10 hours) produces a surface that is more resistant to the process of abrasion. It can be seen in fig. 4.44 that the oxide layer formed over a longer period of time is very quickly removed during abrasion and has less influence on the abrasion resistance, while the oxide layer formed in the first few hours is robust and not as readily removed.

The mild steel specimens were examined after 1 metre of abrasion. The bottoms of the corrosion sites were first visible on the 5 hour specimen. It has been calculated that the average thickness of the layer of material that is removed per metre of abrasion is 12.3 micrometres for 070M20. Thus the first anodic sites must have reached a depth greater than 12 micrometres after 5 hours corrosion. The anodic sites will grow with longer periods of corrosion, so that after 45 hours almost seventy per cent of the surface consists of holes that remain largely untouched by the abrasive. The change in the nature of the surface is observed to retard the rate of further corrosion as manifested in the non-linearity of fig. 4.4a (section 4.1.1).

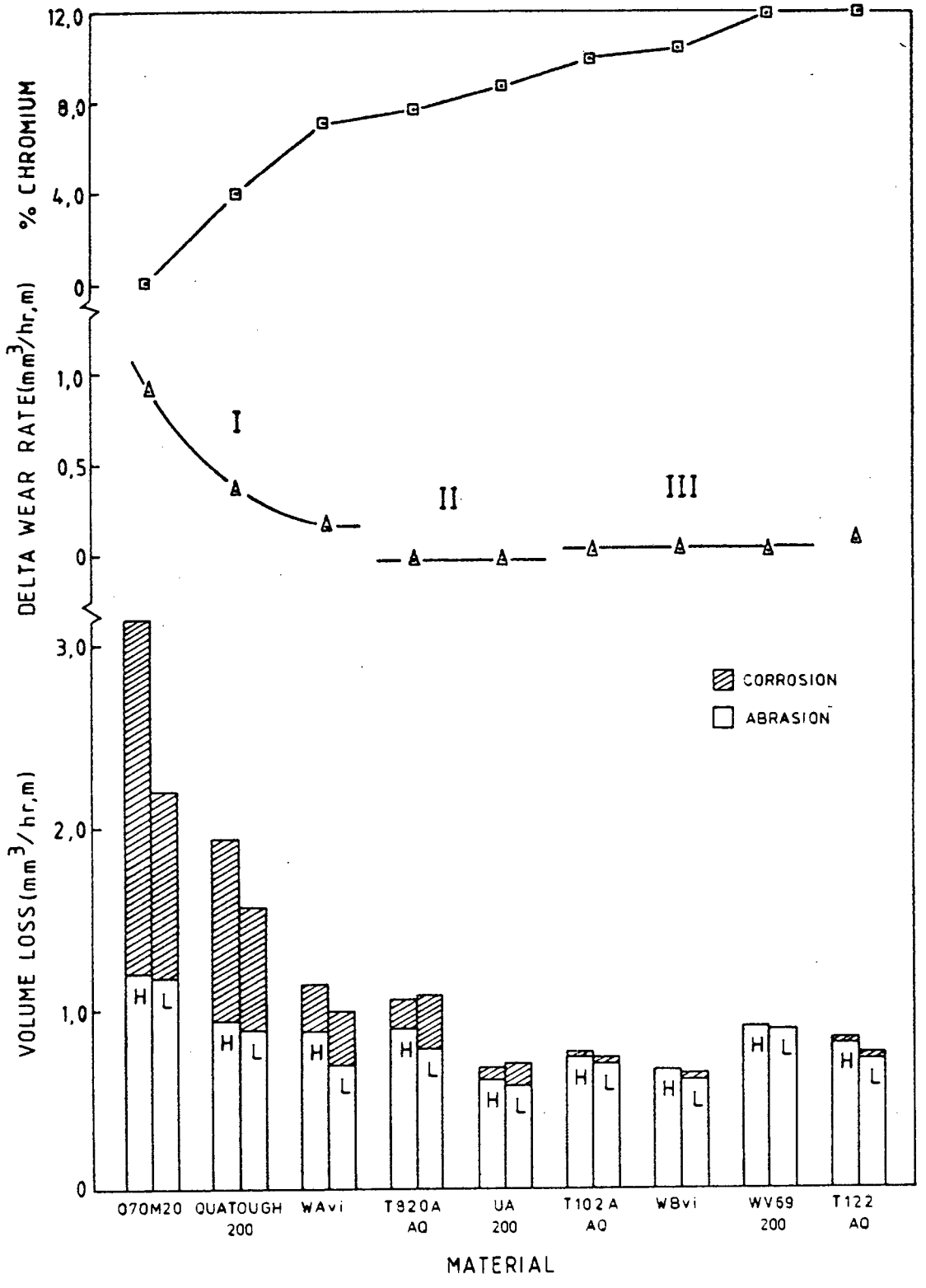

FIGURE 4.41 : The total volume of material lost for a high (H) and low (L) frequency RWRL test. The separate contributions of abrasion and corrosion are shown for each material. The difference in total volume loss between the two tests (delta wear rate) and the chromium content of each material is shown. Three types of material response; I, II and III are identified

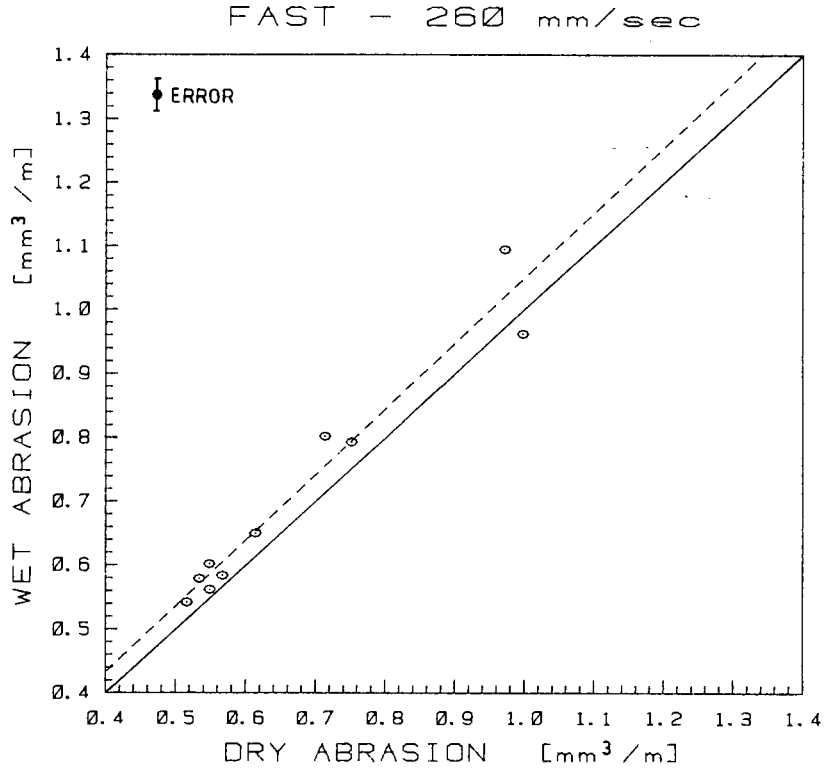

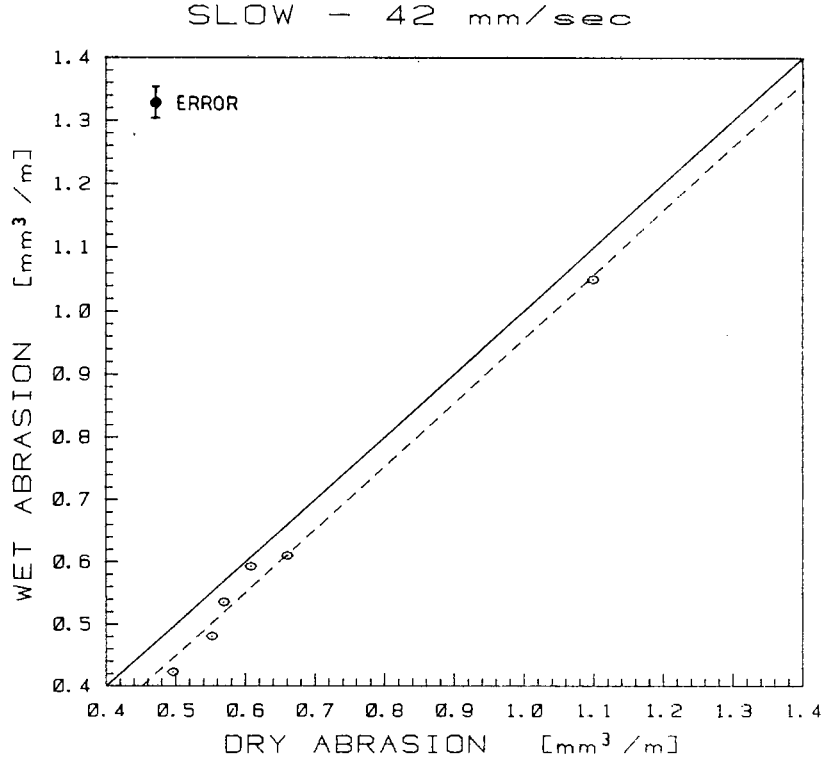

FIGURE 4.42 : Comparison of abrasion resistance for a range of steels in synthetic mine water (wet) and in air (dry) at two abrasion velocities. The solid line marks equal volume losses (wet and dry) and the dashed line is fitted through the points

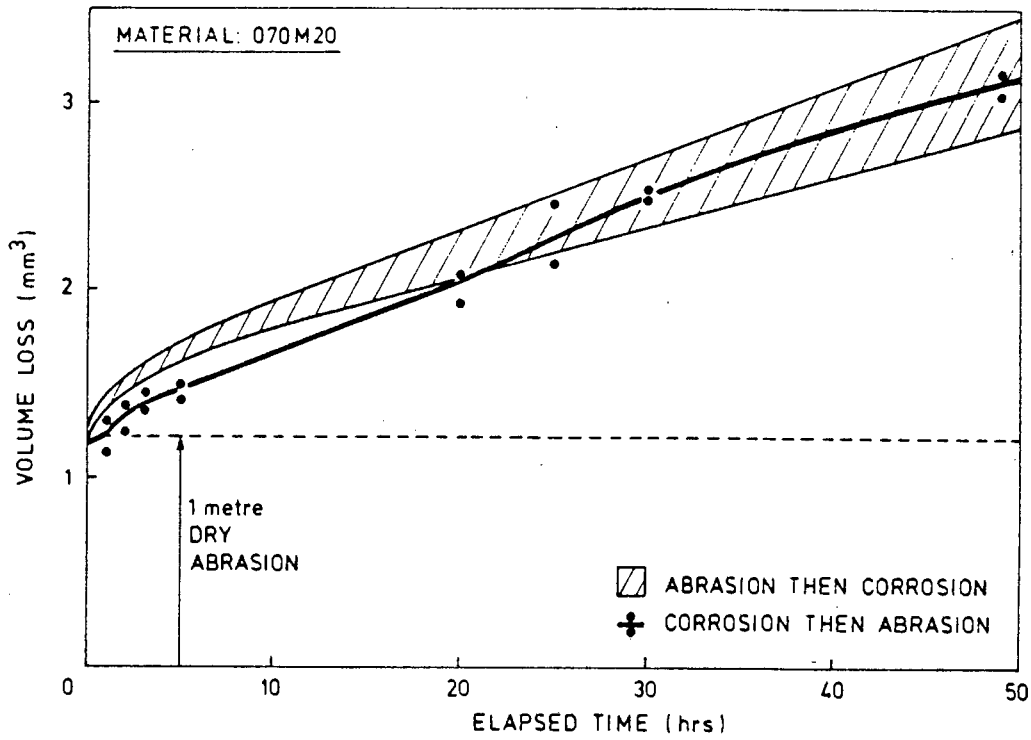

FIGURE 4.43 : The presence of an oxide layer adhering to its metal surface can inhibit the abrasion process at $t < 20$ hours. The total volume loss is less than predicted from the summation of the two separate processes

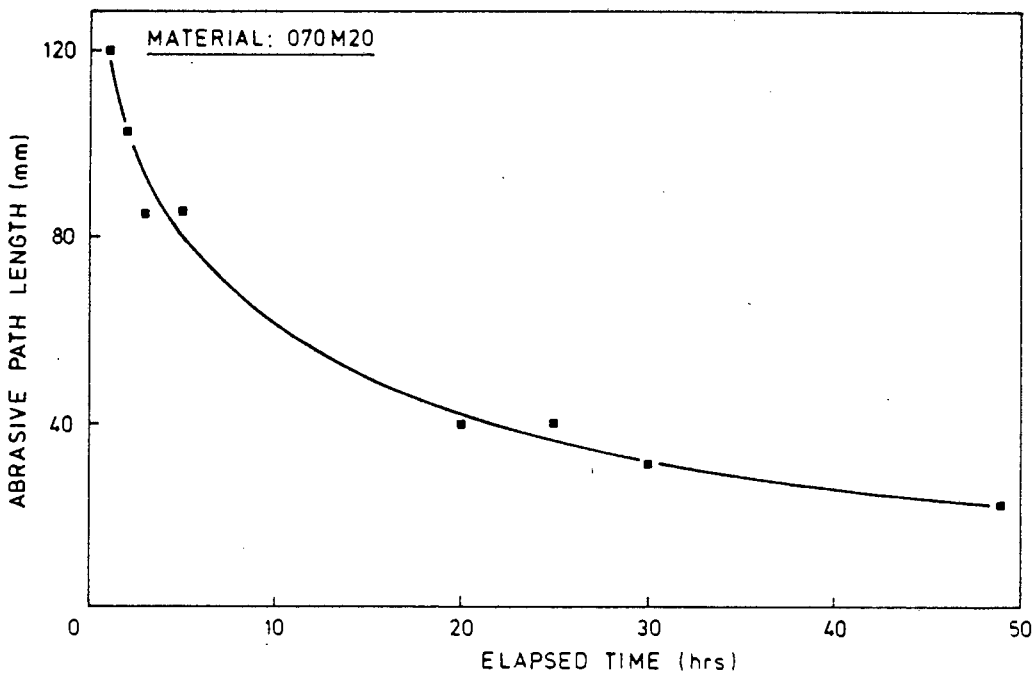

FIGURE 4.44 : The abrasive path length, necessary to remove all the oxide that has been deposited with time, is an indication of the adhesiveness and robustness of the oxide layer to mechanical damage

4.2.8 An Environmental Influence on Wear

Chloride and sulphate ions, amongst others, are known to disrupt passivity in stainless steels. The results show that an increase in total dissolved solids (TDS) of the synthetic mine water has led to higher weight losses (fig. 4.45). The materials are presented in fig. 4.45 in increasing chromium content from left to right and are separated into groups by their mode of corrosion.

The materials with less than 6% chromium exhibit general corrosion over the entire surface. The rate of corrosion is not influenced significantly by the increase in TDS over the 46 hour period of the test. The materials with between 7% and 9% chromium initially corrode by localised anodic activity which develops into open crevices capped by oxide product. General breakdown and corrosion of the entire surface then follows. The introduction of increased TDS to the environment accelerates the inital anodic activity so that general corrosion is reached sooner. For materials with greater than 10% chromium, the localised anodic activity is more restricted. Corrosion proceeds in the form of small isolated crevices and pits. An increase in TDS is observed to increase the size and number of these active sites over the 46 hour period. The total volume loss for the latter group of materials is the most significantly affected by the change in total dissolved solids.

An examination of the response of individual materials identifies that the mode of corrosion is not solely related to the chromium content of the material. AISI 316, which contains 2.2% molybdenum in solid solution, shows no change in wear resistance with an increase in TDS. Alloy ID in the 200°C tempered condition is recorded in fig. 4.45 and shows a crevice type corrosive activity. The same material tempered at 600°C is found to lose 3.2 times more material during abrasive-corrosive wear in the respective solutions of synthetic mine water. Furthermore the result for ID 600 falls within the group exhibiting general corrosion, characteristic of the alloys with a lower chromium content.

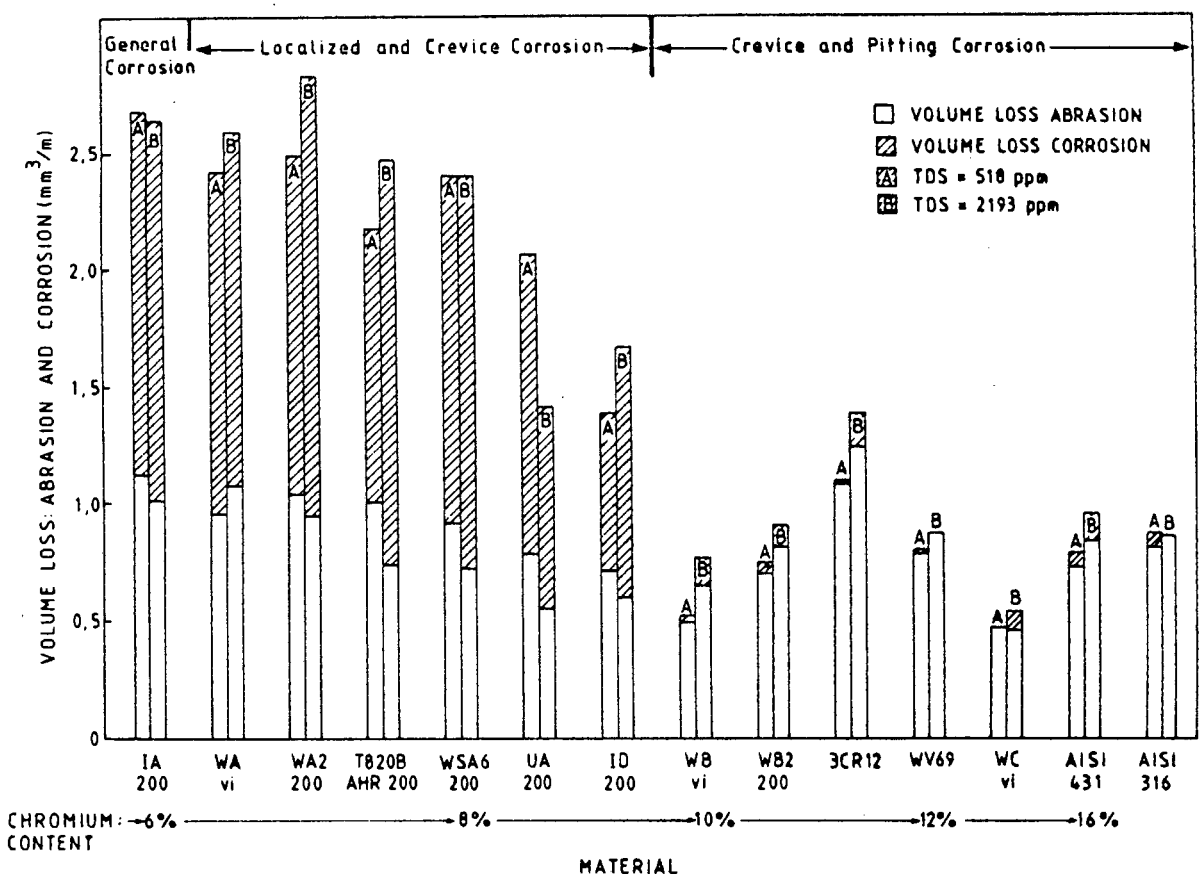

FIGURE 4.45 : The material losses during abrasive-corrosive wear for two different synthetic mine water solutions. The total dissolved solids of solution B is 4 times that of solution A and is characteristic of mines from separate geographic regions. The chromium content of the materials increases from left to right and their mode of corrosion is indicated.

CHAPTER 5

DISCUSSION

5.1 THE RELEVANCE OF THE LABORATORY WEAR TESTS IN MATERIAL SELECTION

Many reviewers have commented on the proliferation of test methods being used in the field of abrasive wear. It is widely recognised that service conditions differ enough to require laboratory tests which provide valid comparisons with in-service performance.

Ball and Ward (1985) outlined the philosophy that has been developed in recent years by the combined research effort of the University of Cape Town and the Chamber of Mines Research Organisation of South Africa whereby a limited number of in-situ tests can establish the validity of a laboratory test. Once it is verified that the laboratory test accurately simulates the real in-situ situation, a programme of materials evaluation can proceed. The primary objective remains to test candidate materials and provide a complete ranking list of conventional and non-conventional materials which can be supplied to the design engineer with confidence.

Noël, Allen and Ball (1984) developed the two test methods described in section 3.1.2 to assist in the selection of materials for the construction of underground mining and transport equipment. The dry abrasion laboratory test (RAR) was developed from the classical pin-on-disc method (Allen, Protheroe and Ball, 1981). The laboratory abrasive-corrosive wear test (RWRL) was developed to simulate the mining conditions and showed good correlation with the in-situ results (Noël, Allen and Ball, 1984). Let us consider this latter test in more detail.

Protheroe (1979) observed severe wear in the U-shaped mild steel pans of a shaker conveyor after one year and 6000 tonnes of rock had been conveyed. He found that the mild steel pans had lost an average 1.35 mm (± 0,08) in thickness at the bottom, while pans made of the stainless steels, AISI 430 and AISI 304 had lost only 0.24 mm and 0.18 mm in thickness respectively. He argued that the presence of corrosive mine water was a major factor in the accelerated wear.

Noël (1981) determined the corrosion contribution to be two thirds of the total volume loss for mild steel. The shaker conveyor on which Noël based his calculations, conveyed on average 9.3 tonnes of quartz rock per day over a three week period. This is half the daily tonnage reported by Protheroe for a similar shaker conveyor and possibly an order of magnitude less than the tonnage conveyed at full production. The shaker conveyor commonly operates at a rate of 60 tonnes of rock per running hour. The equivalent idle time is calculated as 163 hours (6.8 days) in the case of Noël's conveyor. This is not a typical situation. The shaker conveyor, in reality, would have been in operation more frequently than once a week. However, with the total tonnage being so low, the material wear due to abrasion was lower and the idle times longer than for a conveyor operating at full production capacity.

Fig. 4.4 shows that the contribution of corrosion is closer to four fifths of the total volume loss for mild steel using the RWRL test. The deviation from linearity in figs. 4.4 to 4.6 was found to be common for all the materials showing little or no corrosion resistance and is attributed to the short abrasion path length of the test. During the 46 hour period of corrosion the pits are observed to grow to a greater depth than can be removed during 250 mm of abrasion (section 4.2.7). Thus subsequent to the first abrasion-corrosion cycle the bottom of the corrosion pits are exposed, any oxide layer present within the pit has not been removed mechanically and the entire surface no longer consists of newly abraded material. The oxide covered areas are protected and do not immediately actively corrode when reintroduced into the corrosion cell. The net drop in active surface area leads to a decrease in the rate of corrosion with the number of test cycles for the carbon and low alloy steels.

Together with the problem of non-linearity, the dissatisfaction in the RWRL test was further aggravated by the emphasis the test results placed on the stainless steels (fig. 4.8). It was felt that the test conditions should be changed to highlight a more abrasion resistant steel which would also show some resistance to corrosion. It must be remembered that the highest material costs are in the conveying and crushing equipment which handle large tonnages of rock material and operate semi-continuously. After consultation calculations were based on a figure of 75 tonnes per day of rock conveyed down a shaker conveyor operating at 60 tonnes per hour capacity. An increase in the operating period and a

decrease in the idle period between operations is equivalent to an increase in the path length of abrasion and a decrease in the period of corrosion for the laboratory test (Noël, 1981). The load remains unchanged (fig. 2.2). These changes resulted in the RWRL #2 laboratory test (Table 3.2, Section 3.1.2). The conditions of the modified test (RWRL #2) were considered to be of more relevance to a design engineer.

Although the RWRL test would seem to be based on an abnormal situation it still has great relevance to the mining industry. It will be shown after further discussion that the greatest material losses are recorded after unscheduled stoppages, and when equipment is operating outside its designed production capacity. There are also innumerable situations where equipment such as pumps and power packs are dragged to a location and then left to operate intermittently.

It should be apparent that a single standard laboratory wear test cannot adequately cover the range of conditions under which mining equipment will operate. Let us consider two practical examples in the selection of a suitable material. The mine lift cages are at present fabricated from a corrosion resistant aluminium alloy primarily because the materials strength to weight ratio permits greater payloads. The abrasion resistance of aluminium is 0.3 relative to mild steel (Noël, 1981) and to include it in the floors of the cages (regions of highest wear) would necessitate developing an abrasion resistant aluminium alloy. On the other hand, rock crusher jaws experience high-stress abrasive wear. The corrosion contribution to total material loss is judged to be virtually zero. Thus despite the corrosive environment underground, steels like Hadfield's manganese steels will continue to be used in crusher jaws.

The degradation of material due to abrasive-corrosive wear is seen to range from the limiting situations of virtually zero abrasion to virtually zero corrosion. A material ranking list is specific to a previously established set of conditions and can only serve as a guide in anticipating the relative performance of a material in-situ. In the selection of a suitable material for an application outside the conditions modelled by the laboratory test, a proper judgement must be made of the operating conditions and the properties of the material under these conditions. Therefore, parallel to any materials evaluation programme, it is important to establish the fundamental mechanisms which make up the wear process and attempt to quantify their relative contributions.

5.2 MICROSTRUCTURE AND ABRASION RESISTANCE

Microstructure controls the physical and mechanical properties of a material and thus can be accountable for a materials resistance to dry abrasion. The following discussion is centred around the response of the microstructures to abrasion, the capacity for structural changes, plastic deformation and its resistance to micro-fracture. The observed wear behaviour of a material will be explained in terms of its microstructure and the mechanism of material removal. The relative performance of the steels and experimental alloys in a dry abrasive wear situation will be discussed as an aid to furthering the design of a wear resistant microstructure.

The mechanisms of abrasive wear

The results of fig. 4.9 correspond well to the relationships outlined by Murray, Mutton and Watson (1979) in their study of abrasive wear mechanisms in steels (fig. 2.4). A comparison between the abraded surface and debris of the dual phase steel, 3CR12 (fig. 4.20) with that of the harder martensitic steel, UA 200 (fig. 4.24) illustrates the differences between a predominantly ploughing mechanism and a predominantly cutting mechanism of groove formation respectively as categorized by Murray, et al. (1979).

The conclusion of the SEM study (section 4.2.1) is that the abrasion mechanisms of ploughing and cutting use the same localized zone of shear in material displacement (fig. 2.6).

> Ploughing is synonymous with deep penetration and extensive plastic flow of material laterally to the sides of the abrasive groove. Fracture is by ductile tearing and fatigue of the ridge material (fig. 5.1).
>
> Cutting has a shallow groove with no ridges. It involves only the shearing off of material immediately ahead of the abrasive. Fracture is by the growth of shear cracks through the most strain-hardened material (fig. 2.6).

A mixture of these two mechanisms was in evidence at the worn surfaces of all the metals examined, roughly in proportion to the maximum surface hardness attained.

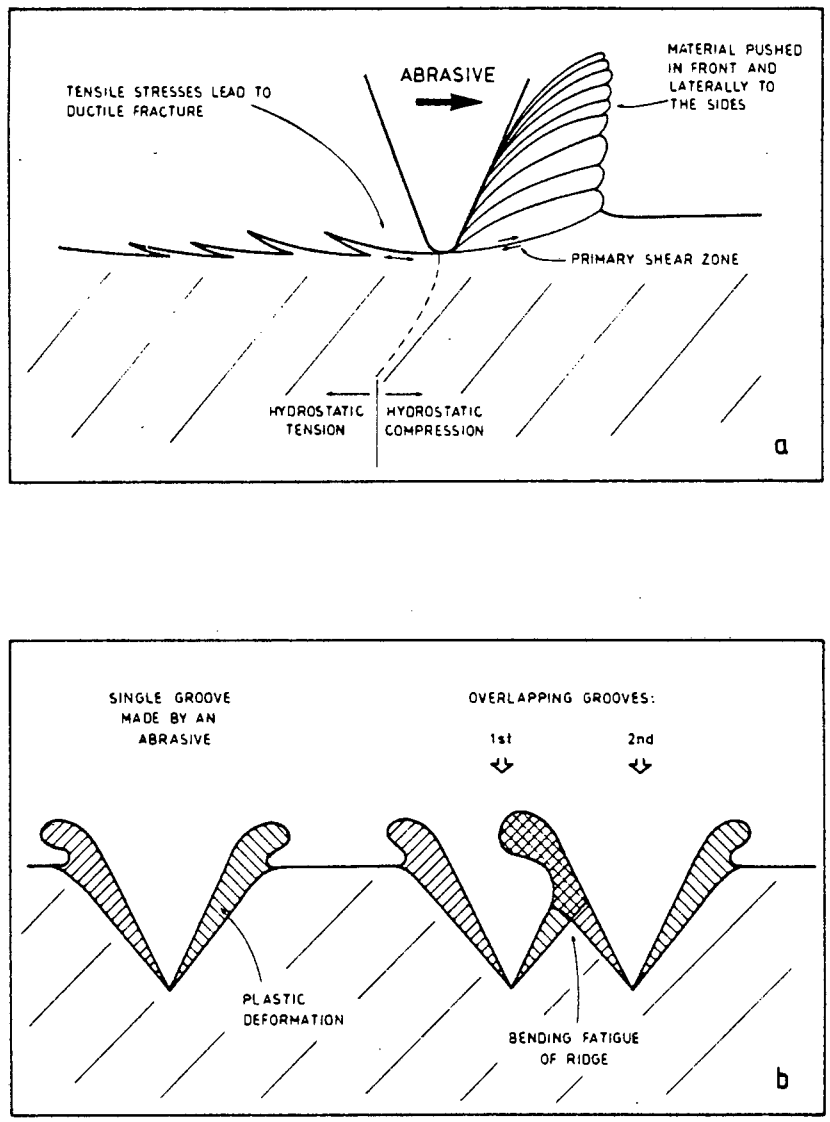

FIGURE 5.1 : a) A predominantly ploughing mechanism is associated with a low material strength and the ductile fracture of the highly strained metal. b) Overlapping grooves result in fatigue of the plastically deformed material that make up the ridges

Work hardening and ductility

Murray, Mutton and Watson (1979) have suggested that the transition from ploughing to cutting is not the result of the increase in hardness but rather the loss of ductility associated with an increase in hardness. The microstructure of tapered sections reveal the regions of greatest strain (figs 4.26, 4.27 and 4.28). The shape of the debris indicates that fracture of the ridge material and of the swarfs are the primary cause of material loss (fig. 5.2a). The shape of the stress-strain curve can help to explain this (fig. 5.2b).

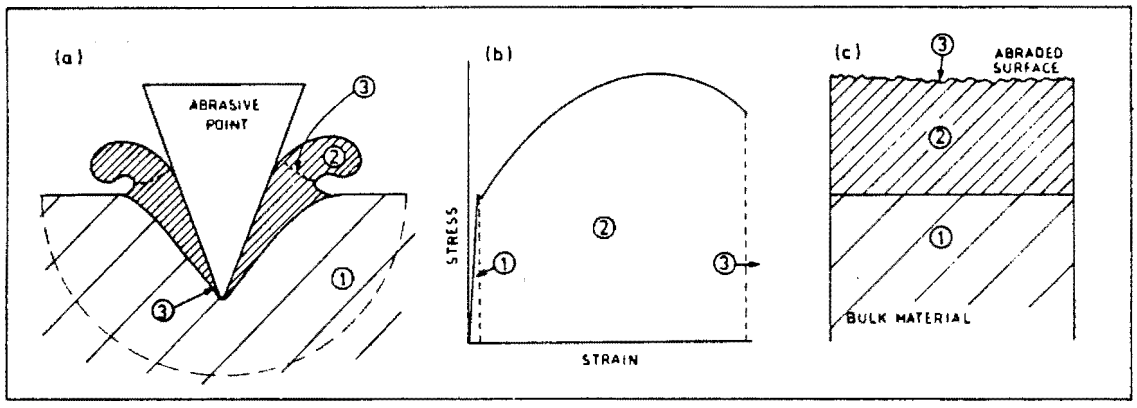

FIGURE 5.2 : (a) A section through the wear groove has three distinct regions determined by the extent of imposed strain.
(b) These can be identified on an engineering stress/strain curve if plastic constraint is to be ignored.
(c) The degree of strain diminishes with depth below an abraded surface and the situation is dynamically maintained during abrasion

It should be borne in mind that abrasion is a dynamic process. That is, as the surface material is removed on attainment of the critical strain for fracture, so material well below the surface is at the point of yielding (fig. 5.2c). Consider a strain in excess of the yield point (regions 2 and 3 of fig. 5.2b). A metal wih a very low ductility would fracture and as there is no means of arresting the propagation of a crack, wear is accelerated. This is the case for hard martensitic steels like SS10/200 (Type I of fig. 5.3). On the other hand, materials having high ductility can deform plastically. The amount of strain imposed during abrasion is however considerable, and those materials with zero work hardening have no inherent property to prevent ductile fracture once the metal has yielded (Type II of fig. 5.3). Material losses are again expected to be high. The over tempered martensites and materials like Abrasalloy and Wearalloy 400 which show a predominantly ploughing wear morphology tend towards this category. Ball (1983) identified these two cases in his discussion on the importance of work hardening in abrasive wear. He outlined how a material with a high work hardening capacity would attain its ultimate strength while plastically accommodating the imposed stresses of an abrasive (Type III of fig 5.3).

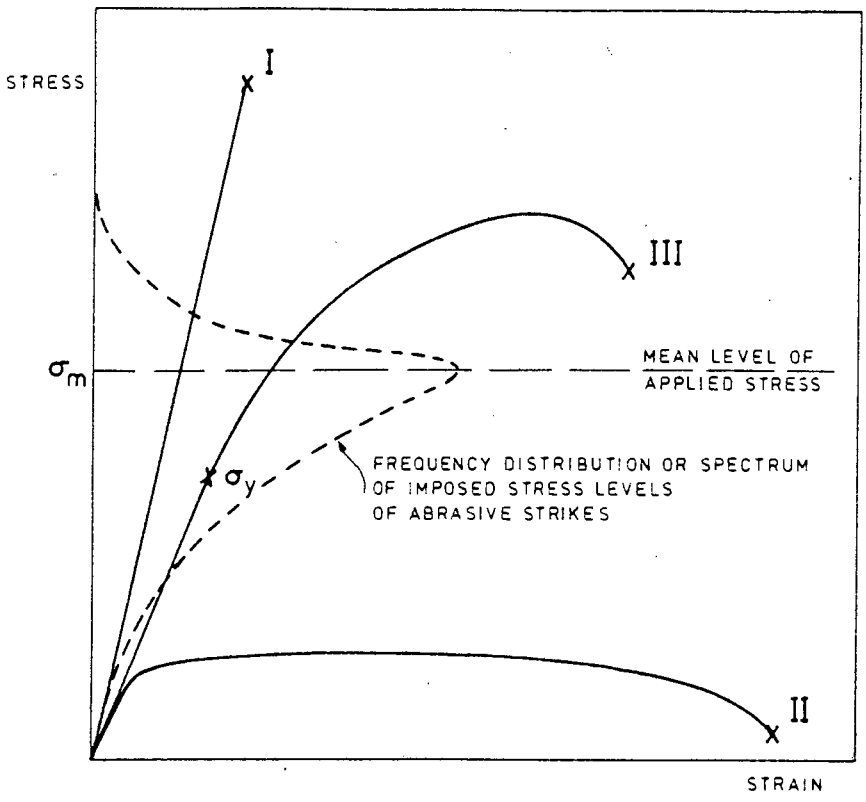

FIGURE 5.3 : The hypothetical stress-strain curves of three classes of material superimposed upon the frequency distribution of abrasive strikes of given stress magnitude (Ball, 1983)

The rationale presented by Ball (1983) is essentially correct but there is one aspect that should be addressed. Ball has assumed for simplicity that the three classes of materials will see the same imposed stress distribution about a common mean stress level for a unique abrasive wear situation. Fundamentally, wear is the result of an energy transformative process and the stress levels should be established from this basis.

The initial or input energy, in impact and impinging type wear, is simply dependent on the initial kinetic energy of the striking abrasive particle. The energy transformed is that necessary to stop, deflect, rotate or fracture the abrasive. In sliding-type hard-abrasive wear under constant load, the system will "draw as much energy as is necessary to maintain the sliding motion." (Uetz and Föhl, 1979).

The input energy is distributed during abrasion into energy for elastic and plastic deformation, fracture and new surface energy and energy for secondary processes like noise and microstructural transformations. The

plastic deformation energy is by far the largest term for the type of abrasive wear system under examination.

Vingsbo and Hogmark (1984) have measured the instantaneous grooving energy during the formation of a groove. They found that the energy oscillated about a mean value. The frequency, amplitude and magnitude were dependent primarily on the depth and severity of the groove but this varied with material. The input energy is then not a simple term but a distribution of energies depending upon the continually varying kinetic frictional energy, plastic deformation and fracture events at the abraded surface. This is determined by the physical and mechanical properties of the wear couple and will thus vary between materials for a unique abrasive wear situation.

The energy dissipation during abrasive wear, under nominally constant velocity, is then a system variable dependent upon both the abrasive conditions and the mechanical properties of the base material. The magnitude of the stress experienced by the material is a function of the energy input. Thus the stress levels experienced by the different classes of materials will not be the same for a unique abrasive wear situation.

Materials of type I (fig. 5.3) would respond elastically to an abrasive strike. The stiffness of the material results in a high mean stress level. Any flaw in the surface material like a crack will concentrate the stress. The low micro-fracture toughness of this type of material will result in brittle spalling and the rapid removal of material.

Materials of types II and III (fig. 5.3) respond plastically to an abrasive strike. The plastic deformation increases the contact area with the abrasive tip so that the mean stress level experienced is less than what would have been experienced under an elastic contact. For the soft and ductile materials (type II of fig. 5.3), the shear strength is easily exceeded and because the energy to reach critical strain for fracture is small, plastic deformation and ductile chip formation leads to the rapid removal of material from the abraded surface.

Materials that have a rising stress-strain curve in the post yield period (type III of fig. 5.3) have the capacity to work harden. This type of material can plastically accommodate the abrasive strikes thus moderating

the mean applied stress level while simultaneously increasing its strength to balance the applied stress. The good micro-fracture toughness inherent with this type of material prevents the loss of material until work hardening and strain are exhausted.

Since abrasion is a dynamic process (fig. 5.2), under steady state conditions the material in the highest state of work hardening is at the extreme surface. This results in the abrasive particles making only a shallow indent as they slide across the surface. Abrasive strikes of greater energy which cannot be deflected are plastically accommodated until there are enough contact areas to deflect the load. The high material strengths then force a shallow cutting mechanism and a small quantity of material is removed.

In conclusion, a material with a combination of good strength, ductility and a high work hardening capacity (a large area under the stress-strain curve) will have an advantage in resisting abrasive wear.

An assortment of uniaxial tensile stress-strain curves are presented in fig. 5.4. Steel A corresponds to type I of fig 5.3, steels B, C and D correspond to type II, and steels E, F, G, H and I correspond to type III. In light of the above argument, steels A to D are not expected to have good abrasion resistance while steels G and I will have a distinct advantage. A description of these steels is given in Table 5.1.

TABLE 5.1 : Description of the engineering steels presented in fig. 5.4

Steel	Material	Ref	Description of microstructure
A	AISI 440B	a	60 vol.% massive carbides in martensitic matrix
B	3CR12	b	dual phase low carbon martensite plus ferrite
C	070M20 cw	c	cold rolled, ferrite plus pearlite
D	AISI 304 an	a	annealed, austenite
E	AISI 304 cw	a	45% cold work, 50% martensite balance austenite
F	AISI 630	a	precipitation hardened martensite (ARMCO 17-4 PH)
G	AISI 431	c	martensite plus islands of austenite
H	825*	c	martensite plus interlath retained austenite
I	122*	c	martensite plus interlath retained austenite
J	1210*	c	meta-stable austenite with 10% martensite

Notes: a) various engineering hand books, b) Brink (1983), c) Harty (1988)
* Developmental alloyed steels (Appendix A9)

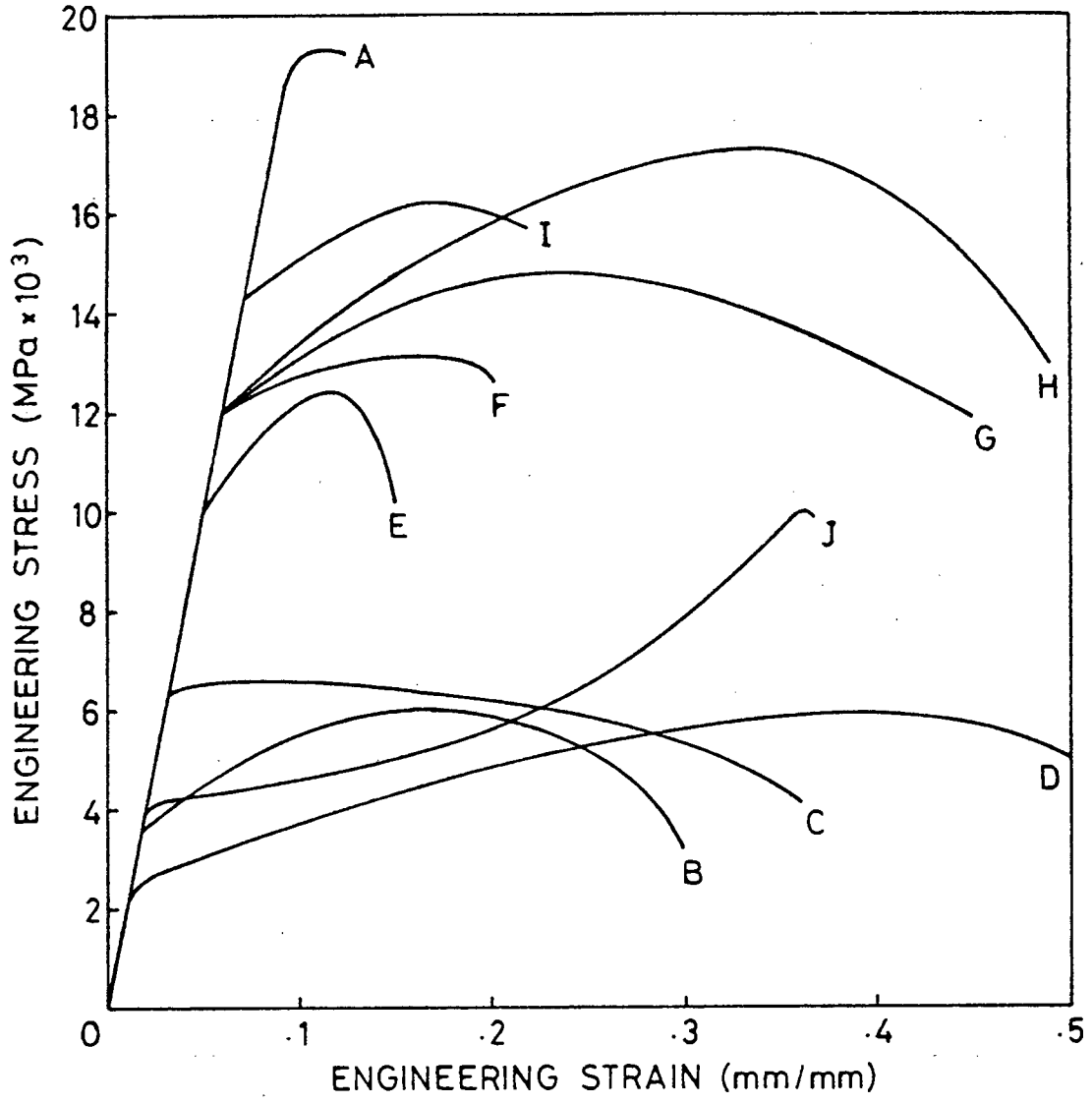

FIGURE 5.4 : The stress-strain curves for an assortment of engineering steels that will see service in an abrasive environment. A description of these steels is given in Table 5.1

It will be noted that steel C has no capacity to work harden because it is in a cold rolled condition. Once this material yields to the stress of an abrasive strike, it has no means of further restraint and fracture will occur because of the high strains inherent in the abrasion process. Increasing the hardness and yield stress by cold work is not seen to be an advantage in resisting abrasive wear. Steel B which reaches a comparable strength after work hardening is anticipated to have a better relative abrasion resistance.

Steel D is a meta-stable austenitic steel that transforms to martensite during plastic deformation. Under the triaxial conditions of plastic constraint at the abraded surface, this material can reach the strength levels of steel E and still retain its high ductility. Thus TRIP type steels are seen to have an advantage in abrasive wear resistance. Steel J was designed to maximize this feature (Lenel and Knott, 1986) and is presently under consideration as an abrasion resistant steel (Appendix A9).

Steel H and I are representative of the martensitic experimental alloyed steels developed to have high work hardening rates and anticipated to show excellent abrasive wear resistant properties. These two steels in particular are also presently under consideration.

The relative performance of these assorted materials will now be examined in turn.

Ferritic and dual phase ferritic-martensitic steels

The abrasion of materials of low hardness (120HV) such as 070M20 (ferrite plus pearlite) or 3CR12 (ferrite plus martensite) involves extensive plastic flow laterally to the sides of the deep grooves. The debris is formed by shearing and ductile fracture of the most highly strained material (fig 5.1; Bryggman, 1983).

Cold rolled plate of these steels have a higher bulk hardness than normalised or annealed plate. Harris (1983) found that a 30% increase in hardness by cold work resulted in a 10% decrease in RAR for mild steel. He explained that this was due to a loss of ductility and a reduction in the energy expended for tensile fracture. Since the abraded surface will work harden regardless of prior cold work, by cold rolling the yield stress is raised relative to the tensile strength and the extent of work hardening and the energy to fracture is reduced. This was predicted earlier in the discussion of fig. 5.4.

Moore, Richardson and Attwood (1972) maintain that ductile fracture occurs when the limit in the "strength" of the worn surface material is reached. The microhardness of the highly strained surface material, a measure of the maximum "strength" (Moore et al., 1972), is relatively low

for 3CR12 (Table 4.16). The small degree of work hardening which did occur can be attributed to the dislocation mobility in the bcc ferrite phase. Quenching 3CR12 from inside its austenite loop for maximum tensile strength coupled with good fracture toughness (Protopappas, 1983) did improve the dry abrasion resistance (5B of Table 4.9). The improvement is due to an increase in the proportion of the hard martensite phase but it still falls far short of what is required.

Substitution solid solution strengthening by increasing the nickel alloying content would reduce the ferrite factor (Table 3.19) and increase the volume fraction of martensite in the quenched structure (fig. 3.16). Despite the improvement in strength and hardness, (Table 3.21) with a corresponding fall in elongation, (Brink, 1983) the RAR of 3CR12Ni showed only a marginal increase (Table 4.9). Allen, Ball and Noël (1984) studied this dual phase material over a wide range of nickel contents and found no significant change in RAR. They observed that an improvement in yield strength is "offset during abrasion by the reduced ability of the material to accommodate the strain to fracture." They suggested increasing the hardness of the martensite phase while maintaining a ferrite factor of 11.5 necessary for good forming and welding characteristics. This would best be achieved by increasing the carbon and chromium content in strict proportion.

Martensitic steels

An increase in carbon to 0.07 weight per cent without adjustments to the chromium or nickel contents resulted in the alloy WV69 having a fully martensitic structure (fig. 3.17) with a ferrite factor of 3. There is a notable improvement in dry abrasion resistance (from quad 5A to 3A of Table 4.9). A change in the mechanism of material removal towards a cutting mechanism (Section 4.2.1) accompanied the increase in the limiting strength of the matrix. The carbon content is however very low for a martensitic steel so the maximum attainable hardness and "strength" is expected to remain low (Table 4.16). The increase in limiting strength (100 to 200 MHV greater surface hardness) of the martensitic steels with further increases in carbon content is offset by a noticeable drop in toughness (row F of Table 4.6).

The martensitic steels cover the widest range of hardness and RAR, (fig. 4.9) and include more than one abrasive wear mechanism. Variations in the abraded surface morphology and debris are related to differences in the microstructure and chemical content of the alloys (Zum-Gahr, 1981/ 1982). The martensitic steels, with low carbon and correspondingly a low hardness, have a mixture of ploughing and cutting wear mechanisms (Section 4.2.1). The higher carbon and alloyed martensitic steels with a hardness around 500 HV (which constitute the majority of the experimental alloys) exhibit a predominantly cutting mechanism of material removal (fig. 4.24). These will be discussed in detail later. Martensitic steels with still higher carbon contents tend to be very hard and brittle (type I of fig. 5.3) and exhibit cracking and spalling around the abrasive groove (fig. 4.23). The RAR for SS10/200 of fig. 4.23 is below average (fig. 4.9 and Table 4.9) as was predicted in the discussion of a type I steel (fig. 5.3).

Steels containing a hard carbide phase

The excellent abrasion resistance observed for AISI 440B (Table 4.9) which is typical for this type of material (Diesburg and Borik, 1974) will serve to highlight the wear performance of steels containing a hard carbide phase.

The material AISI 440B is alloyed with large amounts of carbon and chromium (0.8%C, 17%Cr) which results in a profusion of massive chromium--carbide particles (60-65% volume fraction) in a matrix of martensite (fig. 3.8). These hard carbides effectively resist the penetration of an abrasive particle and are observed to obstruct its passage across the surface, often resulting in fragmentation of the abrasive (fig. 4.22). Carbides that are smaller than the wear grooves can be dug out while the larger ones which cannot be pulled out will terminate an abrasive groove or be fractured. Microcracks may be produced during abrasion where the carbide-matrix coherency is low and separation has occurred, or at a fractured carbide (fig. 4.22). Shetty, Kosel and Fiore (1983) identified interface separation, erosion of the matrix and the plucking out of whole carbides as the adverse effects which lead to gross material losses in composite materials. Thus the carbide size relative to groove width, shape of the carbide (for mechanical bond strength and its elongated cross section) and the mean free path length between carbides, all need

to be considered in relation to the abrasive wear situation. The size, shape and close packing of the carbides together with the "dynamic fracture toughness" of the martensite matrix phase (Zum-Gahr and Doane, 1980) resist the propagation of cracks and the loss of material. The impact toughness and workability of this type of material however makes it impractical as a constructural steel.

The presence of coarse interlath carbides as found in WD ar (0.4%C, 12%Cr) are also thought to provide an obstruction to the indenting abrasive particle (Peters, 1983). The high level of carbon which remains in solid solution gives the martensitic matrix of this alloy its strength and stabilizes the large volume fraction (15%) of interlath retained austenite necessary for crack resistance. The hard incoherent precipitates cannot be sheared by dislocations and provide a second means of improved hardness and yield strength. They also result in the material having high work hardening rates and a higher capacity for deformation during abrasion than the massive carbides. The good RAR is due to the superior indentation hardness afforded by the 30% volume fraction of coarse carbides and the dynamic toughness of the martensitic plus retained austenite matrix. However like AISI 440B, this material also has poor mechanical and fabrication properties.

The martensitic alloys developed

The source W alloys are one attempt towards achieving high strength together with ductility (type III of fig. 5.3) and are seen to be fairly successful (Table 4.9; Bee, Peters, Atkinson and Garrett, 1985). Alloy WB and more importantly the second heat, WB2 with improved toughness shows good abrasion resistance. The source I alloys, IE and IF, can show good abrasion resistance but their RAR is very sensitive to the microstructure achieved after heat treating. The toughness of these alloys tends to be too low for engineering purposes and while 1C and 1D have adequate toughness, it was gained at the expense of hardness and RAR. An examination of the source T alloys identifies T102 (A and B) to have potential as an abrasive wear resistant alloy. Alloy T122 also shows promise.

It is of interest to note the similarities in the above alloys. The carbon content ranges between 0.20% and 0.27% but tends towards the lower

end of the range. The chromium content falls within a narrow range between 9.8% and 10.8% Cr while nickel is between 0% and 4% Ni and manganese below 1% Mn. All the alloys have small amounts of other trace elements, some of which have been deliberately added to control the microstructure. For example, molybdenum (up to 1.5%) serves as a grain refiner and vanadium (0.5% max.) will assist in this task.

The alloys of this composition have a predominantly martensitic microstructure (figs. 3.12, 3.13 and 4.13). This has been the preferred structure when considering improved abrasion resistance and toughness properties (Diesburg and Borik, 1974). The strength of lath martensite is due to a combination of dislocation density hardening and precipitation hardening (Verhoeven, 1975). As these strengthening mechanisms impart a high initial strength to the martensite matrix, the degree of work hardening during abrasion is expected to be limited (Moore, Richardson and Attwood, 1972). A quenched martensite has the highest dislocation density and finest precipitation (fig. 4.13) and thus the highest work hardening potential. Tempering causes growth of the iron carbides precipitates, although, with the alloying element levels present, growth is restrained until higher tempering temperatures are reached (Honeycombe, 1981). The work hardening potential falls on tempering at higher temperatures due to the coarsening of these precipitates (Moore, Richardson and Attwood, 1972). This has an adverse effect on RAR (fig 4.12). In short, the best strength and highest work hardening potential is found in the as-quenched martensitic structure but toughness and resistance to crack propogation is improved on tempering. Tailoring of the microstructure through heat treatment to provide the optimum properties for abrasion resistance is presented in section 4.1.3 and discussed further in section 5.4.

The advantages of retained austenite

The presence of a continuous, inter-lath film of retained austenite is known to improve the toughness to strength ratio in the quenched martensitic steels (Roa and Thomas, 1980). It has been suggested that the presence of this phase along the martensitic lath boundary serves to interrupt the crystallographic alignment of laths within a packet, thus preventing transpacket cleavage (Thomas, Sarikaya, Smith and Barnard, 1981; cited Bee et al., 1984). An empirical relationship between retained austenite, toughness and sliding wear resistance of a Quatough

type steel has been demonstrated by Salesky (1980). Thus it seems reasonable to suggest that the presence of retained austenite is advantageous in the abrasive wear resistance of martensitic steels.

The alloys Quatough, WA, WB, and WC which are known to have retained austenite (Peters, 1983) are seen to exhibit above average abrasive wear resistance within their class of material. It is anticipated that the second heats (WA2 and WB2) with improved toughness will also have retained austenite in the quenched material and these too are observed to have performed well (Appendix A4). Tempering at 300°C resulted in a sharp decrease in RAR (fig 4.12) which may be a reflection of the decomposition of retained austenite to inter-lath iron carbides. The closely related alloy WSA6 has an M_S temperature calculated to be 10°C lower than that of WA2 (280°C, Appendix A1). This alloy in the as-rolled condition showed alloy segregation and a poor RAR. However, a re-austenitisation heat treatment aimed to homogenise the matrix and produce a small volume fraction of retained austenite in solid solution improved the dry abrasion resistance substantially (from quad 4E to 2D of Table 4.9).

The M_S and M_f temperatures of the source T alloys (except T820B) suggest the possibility of retained austenite in the quenched condition (Table 3.15). The Source I alloys, ID and IF, are calculated to have M_S temperatures of 240°C and 215°C respectively and the constitution diagram (fig. 5.5) predicts some austenite to be stable at room temperature. Alloy IF 200, which potentially has the larger volume fraction of retained austenite, is observed to have an excellent RAR (quad 1D of Table 4.9). Alloy UA is noted for having both an excellent RAR and good toughness properties (quad 1B of Table 4.9). The measured M_S and M_f temperatures (fig. 3.18), the calculated stability of the austenite phase (fig. 5.5) and the measured impact toughness for the alloy UA suggests a strong possibility of retained austenite present in the quenched condition.

A higher degree of work hardening is shown by those martensitic steels which have (or are most likely to have) retained austenite (Table 4.16). As we have already established, work hardening increases the limiting "strength" of the abraded surface material while plastically accommodating the strain without micro-fracture. The excellent abrasion resistance of martensitic steels like UA 200 is found to be due to an initial bulk

hardness being in excess of 500 HV coupled with the ability to work harden to a measurable degree (Table 4.16; steel H of fig. 5.4). The resultant hardness is greater than half (Richardson, 1967) the hardness of quartzite (900-1300 HV).

A high initial hardness is needed because there is a limit to the degree of work hardening that is possible in martensitic steels. This precludes the surface material being strengthened to any large degree during the abrasion process. Thus a bulk hardness of 500 HV is prescribed for good RAR properties of martensitic steels in this wear system. A measurable degree of work hardening is still necessary if the metal is to respond plastically to deformation and accommodate the high stresses without fracture, because, the ability to accommodate the high shear strains without fracture is related to the resistance to unstable ductile fracture which in turn is related to the work hardening characteristics of the metal.

This argument would suggest that the initial bulk hardness may be proportionately lower for metals with higher work hardening capacities. Any lowering of the bulk hardness below 500 HV would be subject to an increase in the extent of work hardening being achieved at the abraded surface. The advantage comes in the higher strains which can be accommodated by this energy absorbing mechanism. It is observed in fig. 4.9 (which relates bulk hardness to RAR) that the materials of highest work hardening capacity deviate noticeably from the majority. The transformable austenitic steels make up this group and will now be discussed.

The meta-stable austenitic steels

The austenitic alloyed steels may have similar bulk hardness to the ferritic alloys but their abrasion resistance is superior (fig. 4.9). The RAR of the metastable austenitic stainless steels are on par with all but the best of the martensitic alloys. The large number of slip systems operating in fcc metals accounts for their high work hardening rates (Verhoeven, 1975). This is quantified in the measured work hardening exponents quoted in Table 2.1. The metastable austenitic steels have a distinct advantage over their stable fcc counterparts by the stress induced martensitic transformation and the higher work hardening capacity of the transformation product (Zackay, Parker, Fahr and Busch, 1967). It

is well documented that the metastable austenitic matrix in the alloys AISI 304L and NP599 can undergo a stress induced transformation to bct martensite. Allen, Protheroe and Ball (1981/1982) showed that AISI 316L can also transform to a bct martensite during abrasive wear albeit to a lesser extent than for 304L and only at slow velocities.

Hsu, Ahn and Rigney (1980) and Allen et al.(1981/1982) showed that the wear behaviour of austenitic steels depends upon the stability of the austenite microstructure. That is, the instability of the fcc matrix to stress would influence the wear process through its readiness to transform. Thus a relationship between M_d temperature and RAR is to be expected (Table 5.2).

TABLE 5.2 : The calculated transformation temperatures of the metastable and austenitic steels (Appendix A1)

MATERIAL	M_s	M_d	%C+%N[a]	RAR
Nitronic 60	-425[b]	-114[c]	.23	1.22
AISI 316	-199	- 31	.08	1.36
NP599 ann	-131	5	.33	1.42
AISI 304ann[d]	-53	24	.08	1.55
AISI 304L	-34	38	.035	1.29
F351	-16[e]	f	.25	1.71
F350	8		.25	1.69
F352	45		.25	1.68
F353	136		.25	1.63

Notes: a) wt% carbon plus nitrogen b) °C, Pickering c) °C, 30% strain Pickering d) cited Fogel, 1981 e) °C, Andrews f) no M_d formulae

Nitronic 60 is an 18Cr/8Ni stainless steel designed to operate at elevated temperatures in a galling situation (Alloy data sheet). Consequently, the additional alloying elements needed to improve the toughness, yield strength and oxidation resistance have supressed the M_d temperature. It is anticipated that the austenitic fcc matrix remains stable to all but the severest triaxial stresses. This limits the degree of work hardening which could have been possible by a transformation to martensite.

The alloys AISI 316, NP599, AISI 304L and F351 have respectively higher M_d temperatures and will transform during abrasion with increasing readiness. The low RAR result of AISI 304L may be as a result of the very low carbon and nitrogen content because the absence of interstitial atoms to stabilize the martensite would limit the degree to which the transformed structure can work harden (Table 4.16) (Zackay, Parker, Fahr and Busch, 1969). A more likely explanation is that the material was received for testing in a cold worked state and was not fully annealed. The RAR result for annealed AISI 304 (180 HV) was reported by Fogel (1981) and is included in Table 5.2 for comparison.

The calculated M_s temperature of F531 (Appendix A1) is just below room temperature so that a fully austenitic microstructure is expected on cooling. The M_d temperature is estimated to be between 160° and 200°C higher and indicates that the microstructure may transform and work harden under the smallest strains. The increasingly higher M_s temperatures of the alloys F350, F352 and F353 (Table 5.2) shows that an increasing volume fraction of martensite is expected to form on quenching and before abrasion (fig. 5.5). This is supported by optical microscopy (fig 3.15) and the increasing ferromagenetic susceptibilty of the three alloys (Section 3.2.3). Bulk hardness measurements suggest that only F353 is dual phase prior to abrasion (Table 3.18).

The introduction of the martensite phase prior to abrasion will raise the yield strength of the metal relative to the work hardening rate without affecting the ultimate strength of the material. This effectively decreases the capacity of the material to accommodate the high strains, and reduces the volume of transformable material. The loss of an energy absorbing mechanism in the dual phase austenitic-martensitic microstructure is reflected in the slight drop in RAR (fig. 5.6).

The same argument holds for materials subjected to prior cold work. In a steady state abrasion situation the surface material is work hardened martensite but underneath remains the tough, energy absorbing austenite phase. If the steel is cold worked prior to abrasion, the underlying austenite phase has then already been work hardened. The energy absorbing capacity of this underlying material has been reduced and it is no longer available during the abrasion process. This results in a slight drop in RAR as observed for NP599 (cold worked) despite the significant

increase in hardness over the annealed material (fig. 4.9). Allen, Protheroe and Ball (1981/1982) found prior cold working of AISI grades 304L, 301 and 201 to reduce their abrasion resistance. They argued that the presence of martensite prior to abrasion raised the flow stress of the material relative to the work hardening rate and thus decreased the capacity of the material to accommodate high strains. They also found that AISI 316L did not contain any martensite after 24% cold work and that in this case prior cold work did not reduce the abrasion resistance.

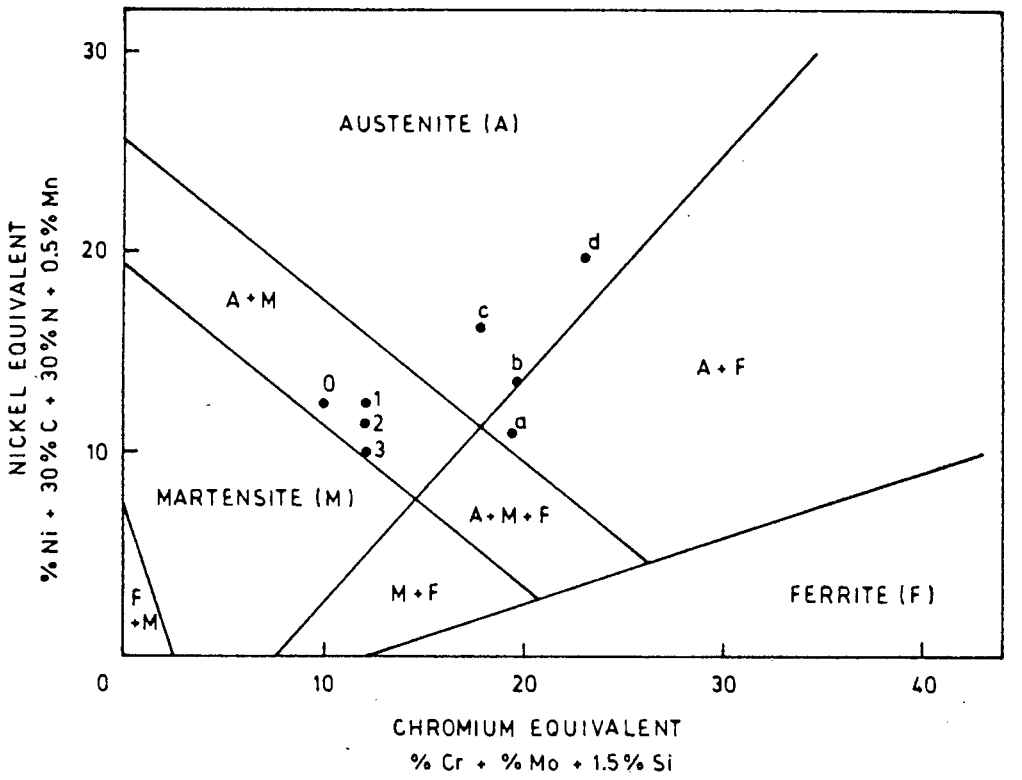

FIGURE 5.5 : Constitutional diagram of stainless steels showing the effect of composition on structure. The alloys F350 (0), F351 (1), F352 (2) and F353 (3) fall within the austenite plus martensite region. Alloys 304L (a), 316 (b), NP599 (c) and NITRONIC 60 (d) are increasingly further from the A + M phase boundary (ASM steels handbook)

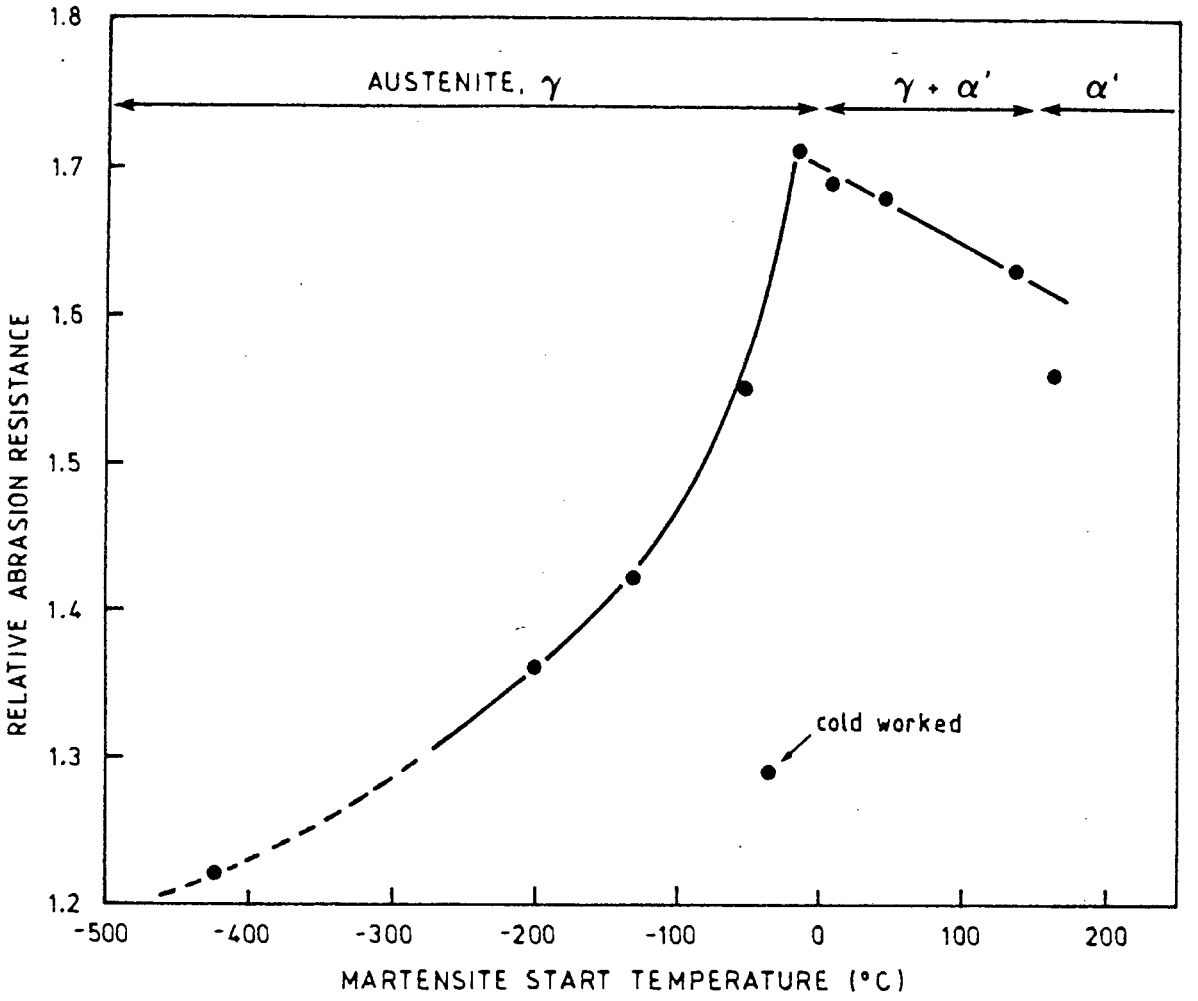

FIGURE 5.6 : The instability of austenite phase (represented by its M_S temperature) is a major influence in the improved RAR of the metastable austenitic steels. The contribution is proportional to the volume fraction of austenite (γ) in the dual phase steels and is absent in the fully martensitic steels (α')

A difference in the response to abrasion

Work hardening of alloys like F350 and F351 occurs to a depth approximately double the mean height between the peaks and valleys of the abraded surface (fig. 4.29). A section through this region (fig. 4.26) bears witness to the microstructural changes discussed earlier. If this is compared with a similar section through a martensitic steel (fig. 4.27) a difference in their response to abrasion is to be anticipated for these two types of microstructure.

Mechanistically the low bulk hardness of the austenitic structure favours a ploughing mechanism but its rapid work hardening ability forces a transition to a predominantly cutting mechanism. This approximates to an ideal wear situation as the most severe strikes are plastically accommodated with no direct loss of material (fig. 5.1). The strained material has undergone a structural transformation increasing its strength so that lesser strikes are thereafter ineffective. (This ploughing mechanism and its energy absorbing ability is absent in the harder quenched martensitic steels.) As has previously been discussed, further work hardening of the TRIP martensitic structure will occur until the strain from imposing strikes can no longer be accommodated. The strength of this now highly strained material resists penetration and forces a shallow cutting mechanism to operate at the extreme surface. This is also the case for the hard experimental martensitic steels. The cutting mechanism involves a zone of shear as detailed in fig. 2.6 (Bryggman, 1983; Vingsbo and Hogmark, 1984) and is synonymous with the homogeneous "white etched" (friction martensite) regions seen in figs. 4.26, 4.27 and 4.28. Thus it is only the process of debris formation that is the same for both types of microstructure. This would account for the similarity in their surface morphology (fig. 4.21 (F351) and fig. 4.24 (UA 200)).

The advantage of a high work hardening capacity (comparison of steels H and J of fig. 5.4) in improved dry abrasion resistance has been demonstrated by the transformable alloys. The RAR for some of these alloys has still fallen short of requirements and can be accounted for in the low surface hardness attained by these alloys. As stated previously, a surface hardness in excess of 550 HV (measure of limiting strength) is needed for the tribological system under examination. Alloys F350 and F351 manage to meet this requirement which is reflected in their RAR (Table 4.16).

The velocity dependence

A second difference in the response of the two microstructures is evident in the velocity dependence of their abrasion performance (fig. 4.30). At very low velocities the abrasion resistance of the metastable austenitic steels is superior.

An increase in the velocity of abrasion would result in an adiabatic rise in temperature within the volume of yielding material (Moore, 1980). The rise in temperature is related to the M_d temperature (and can exceed it) thus there is an increase in the stability of the austenite over the martensite phase. It will also facilitate easier slip, dislocation motion and deformation of the abraded material. A counter influence resulting from an increase in the velocity of abrasion is the strain rate effect which increases the flow stress at faster rates of strain (Larsen-Basse and Tanouye, 1978) and thus making deformation more difficult.

For the martensitic steels, these two effects are balanced out especially at the higher velocities (fig. 4.30) and RAR is virtually independent of the velocity of abrasion. The temperature term dominates in the austenitic steels because RAR is dependent on the instability of the austenite phase. A reduction in the ability to transform to martensite is reflected in a loss of strength, ductility and work hardening. This in turn adversely affects the abrasion resistance. Allen, Protheroe and Ball (1981/1982) found an increase in velocity leads to a decrease in the amount of transformed martensite phase in AISI grades 304L, 301 and 201. Thus the best RAR for the meta-stable austenitic steels is at the slowest velocities of abrasion. Under wet abrasion conditions as in the mines, water may act as a coolant and lubricant and reduce the frictional heating effect at higher velocities.

5.3 CORROSION RESISTANCE AND WEAR

The advantage in the alloying elements especially chromium for imparting corrosion resistance is already well understood. It is important to apply this knowledge to the discussion of corrosion of an abraded metal surface. It will be necessary to restrict the discussion to corrosion in a specific mine water environment and to the materials which are most likely to see service in such an environment. The emphasis is placed on the added influence abrasion has on the rate of corrosion and material loss.

Corrosion of steels in synthetic mine water

The synthetic mine water in which the corrosion tests were conducted contained sulphate and chloride ions (Table 3.4). The typical corrosion behaviour of an unabraded steel in this environment is shown in the polarization curves of figs. 4.36 and 4.37. These indicate the passive nature of the chromium containing experimental alloys in this environment. The ten fold decrease in current density and the more noble corrosion potential of the chromium containing steels is due to the resistance polarization of the oxide layer that is found on the surface (Fontana and Greene, 1982).

A conclusive study of the polarized corrosion behaviour of the experimental alloys in the mine water environment and the effect of alloying content was not possible. Figs 4.36 and 4.37 can only serve as an indication of material behaviour in support of the main objectives.

Idealized anodic polarization curves for the system can be inferred from the main features of figs 4.36 and 4.37. Let us assume that the production of hydroxyl ions and of protons are the two major cathodic reactions under aerated and deaerated conditions respectively. Let us then take 070M20 to represent the iron(Fe) anodic reaction and the steels containing chromium(Cr) to be replaced by a common resistance polarized anodic reaction. We then arrive at the simplified polarization curves of fig. 5.7. In practice, the free corrosion potential of an alloyed steel will range between the hydrogen and oxygen lines in the active state but the chromium steels can move above the oxygen line in the passive state. The exchange current density (a measure of the rate of corrosion) is low

for the chromium containing steels in the passive state while in the active state it will increase and move towards the iron(Fe) line. Note that in the active state a smaller exchange current density is expected under deaerated conditions.

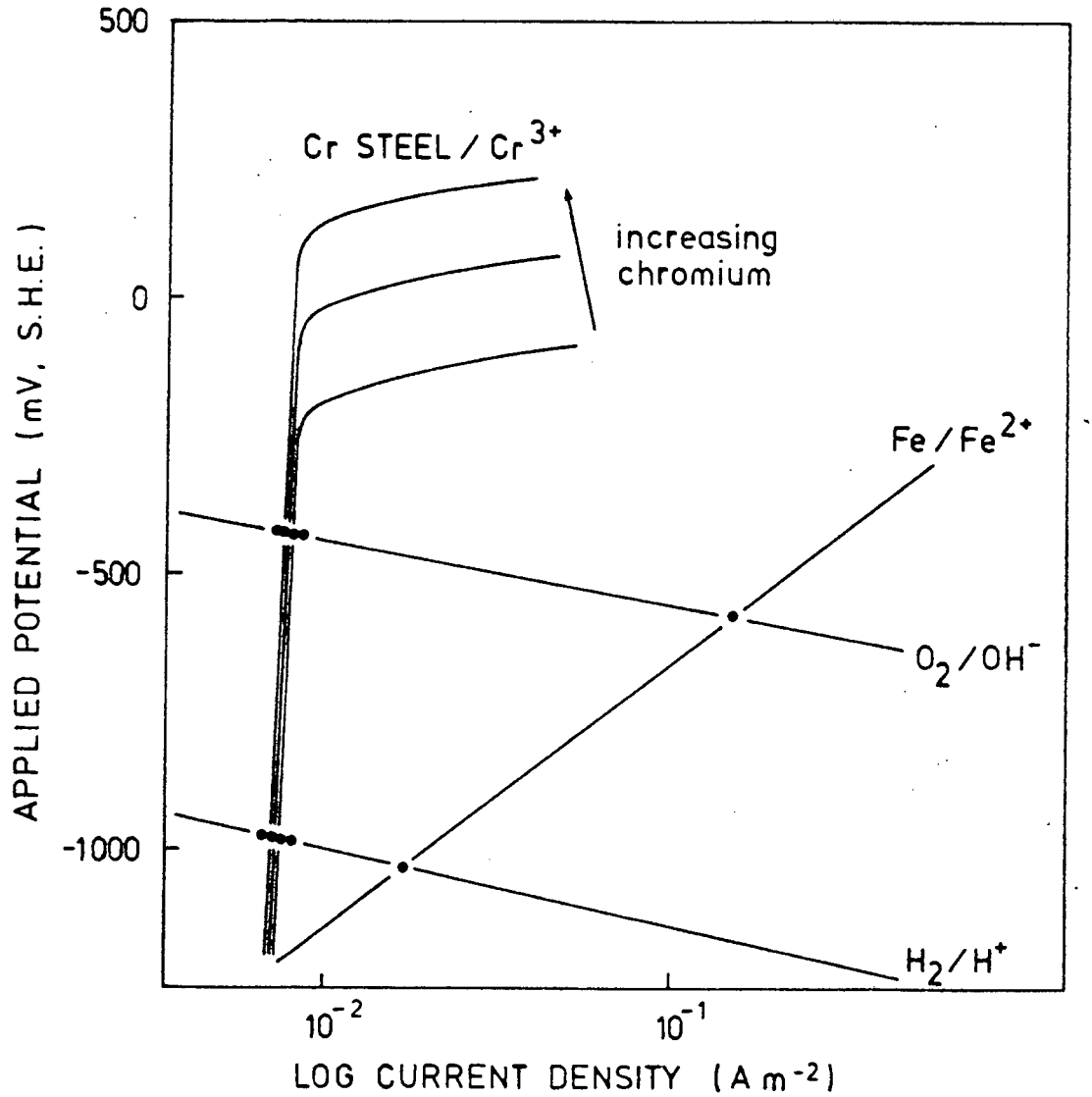

FIGURE 5.7 : Anodic polarization curves for iron(Fe) and chromium(Cr) steels intersected by the oxygen (O_2) and hydrogen (H_2) cathodic reactions in synthetic mine water

The relative stability of the passive state for each material in the synthetic mine water can be determined from figs 4.36 and 4.37. The increase in breakdown potential, E_p, and protection potential, E_x, with increasing chromium content is in agreement with Sedriks (1984). The maximum breakdown potential (noblest pitting potential) and the repassivation or protection potential for the materials of figs 4.36 and 4.37 are plotted relative to chromium content in fig. 5.8.

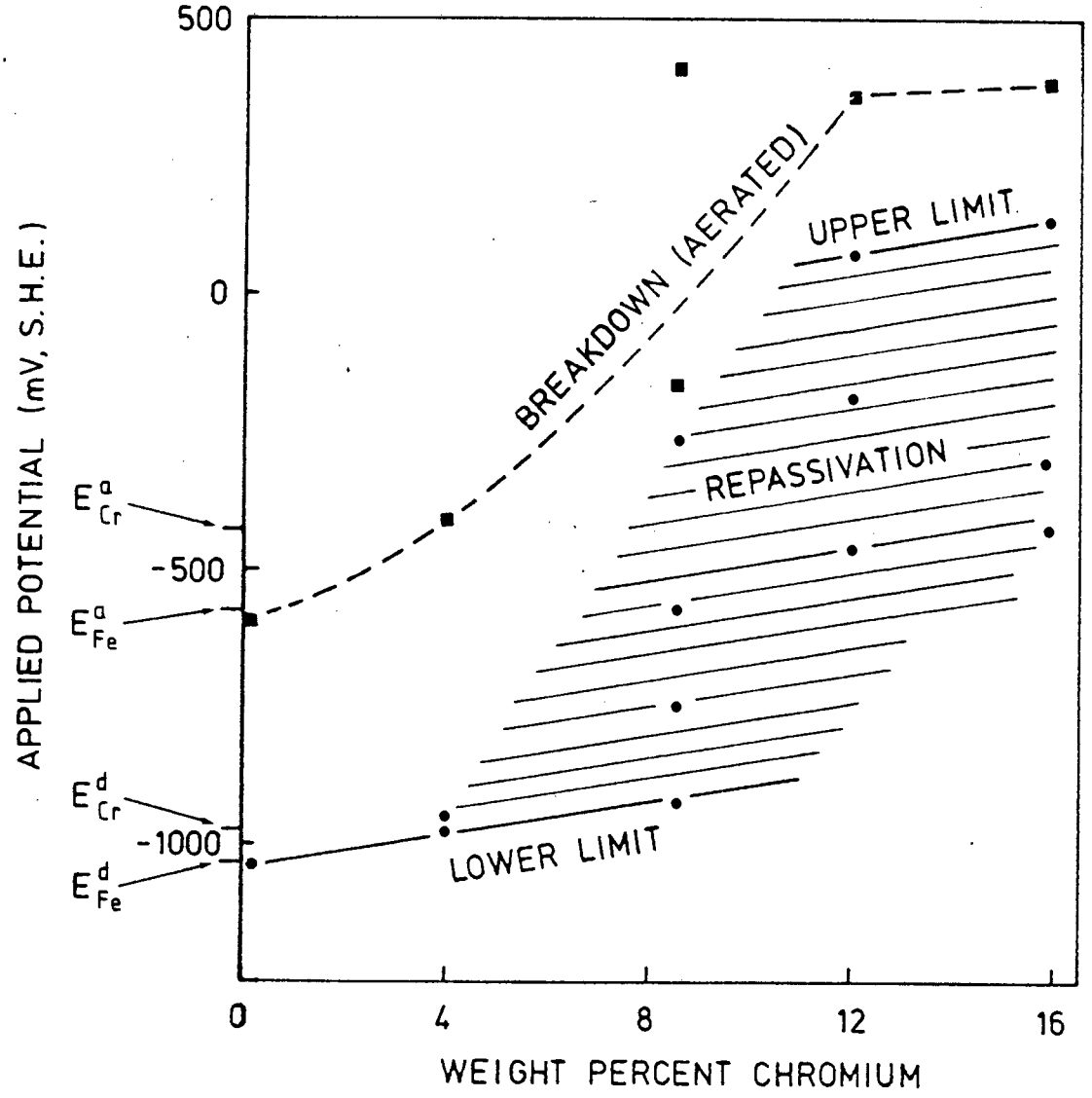

FIGURE 5.8 : The maximum breakdown potential and the limits to the repassivation potential as a function of chromium content

The effectiveness of an alloy in resisting on going corrosive attack is dependent on its chromium content, impurity content and microstructure. For example, alloy WV69 200 is unlike the other steels of Table 4.18 and fig. 4.37 in that it is a laboratory melt sample and has very low impurity levels (especially carbon, manganese and sulphur)(Table 3.19). It has a very fine homogeneous microstructure (fig. 3.17). The corrosion resistance, as a consequence, is better than what may be expected of an industrially produced steel. This would account for WV69 200 showing a generally better corrosion resistance than AISI 431 despite having only 12% chromium. The corrosion behavior of AISI 431 is in close agreement with the results of Capendale (1985), who predicted pitting at these chloride plus sulphate concentrations.

The steel UA 200 which contains 8.6 weight per cent chromium behaves like a stainless steel in the oxygen saturated synthetic mine water solution. This passive state is however unstable and an increase in exchange current density occurs with time. Once anodic sites are established, UA 200 behaves like the carbon steels, Quatough and 070M20, since it is unable to repassivate ($E_x = E_{corr}$, fig. 4.37). UA 200 is in the transition region between carbon steels which corrode unrestrained and passive stainless steels.

Figs 5.7 and 5.8 are representative of the expected corrosion behaviour of the chromium containing experimental alloys in synthetic mine water. (This is without considering the added factors of abrasion and the abraded metal surface.) The steels will in practice begin to show anodic activity at a potential below the maximum pitting potential of fig. 5.8. The chances of repassivation decreases with decreasing chromium content. It is also affected by the localized corrosion potential, local pH and electrolyte concentration, local oxygen concentration, and microstructure (Fontana and Greene, 1982). Since the polarization curves are typical of steels and stainless steels showing passivity in chloride and sulphate solutions (fig. 2.9), the reported effect of the alloying elements on corrosion resistance (fig. 2.10) is expected to apply to the experimental alloys (fig. 5.7). Similiarly the metallurgical principles that determine the passivity of stainless steels (fig. 2.11) will apply equally well to the experimental alloys.

Corrosion of abraded steels in synthetic mine water

Polarization measurements are an instantaneous measure of corrosion rate. Immersion tests over a period of time take into account the factors mentioned above and give an averaged measure of the corrosion rate. The level of agreement between these two test methods can be good if the system is well defined and conditions are strictly controlled. The practicalities of applying polarization techniques to an abraded surface make this method difficult and, since our objective is material selection by simulating the mining conditions, the immersion test is preferred.

The resistance to corrosion of the abraded surface of the experimental alloys is dependent on chromium content as predicted (fig. 4.35). The distinct cut off clearly indicates two corrosion mechanisms are in operation and a change in the means of self protection (Regions A and B of

fig. 4.35). The corrosion resistance of materials in Region A are in direct proportion to their chromium content. Typically the surfaces become discoloured within a short period of time by the corrosion products (fig. 4.39) which is then reflected as a measurable quantity of lost material. The abraded surfaces of material from Region B do not build up a thick oxide film and show significantly smaller volume losses.

Fig. 4.35 illustrates the progressive decrease in volume loss with increasing chromium. A second examination of this figure will reveal that there are three types of response of an abraded metal surface to corrosion at the end of a 46 hour period. This is shown in fig. 5.9.

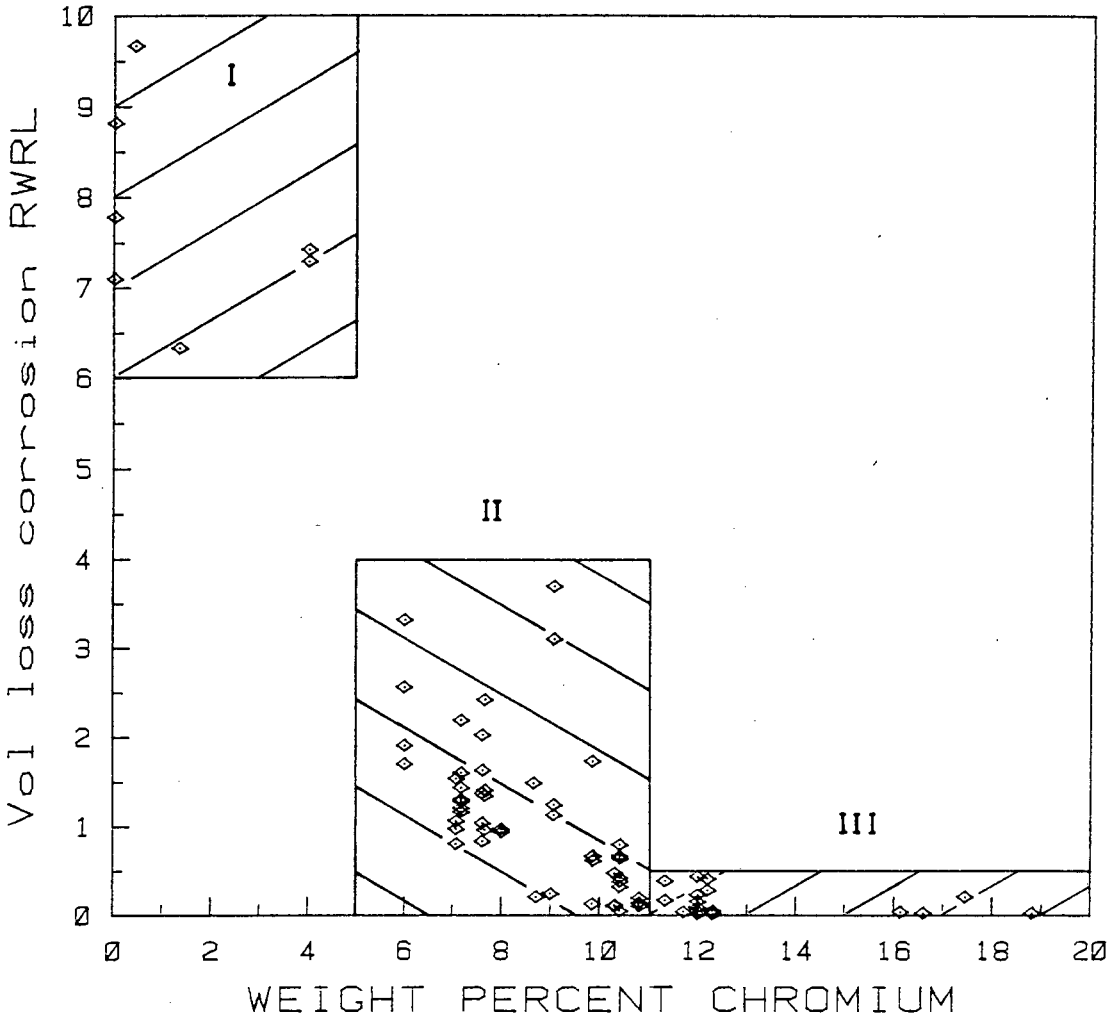

FIGURE 5.9 : The volume of material lost due to corrosion is dependent on the chromium content. Three types of material response are identified for the corrosion of an abraded surface at the end of an uninterupted period of 46 hours. The data is a duplicate of fig. 4.35

The resistance of steels to abrasive-corrosive wear

An analysis of the RWRL results identifies three categories of material response to abrasive-corrosive wear. The group of materials on which the analysis was based encompasses a wide variety of chemical compositions, microstructures and heat treated conditions. The materials have been sorted according to their chromium content and a histogram of the number of samples is given in fig. 5.10. Superimposed upon the histogram is a curve representing the difference between the minimum and maximum RWRL values as a function of chromium content.

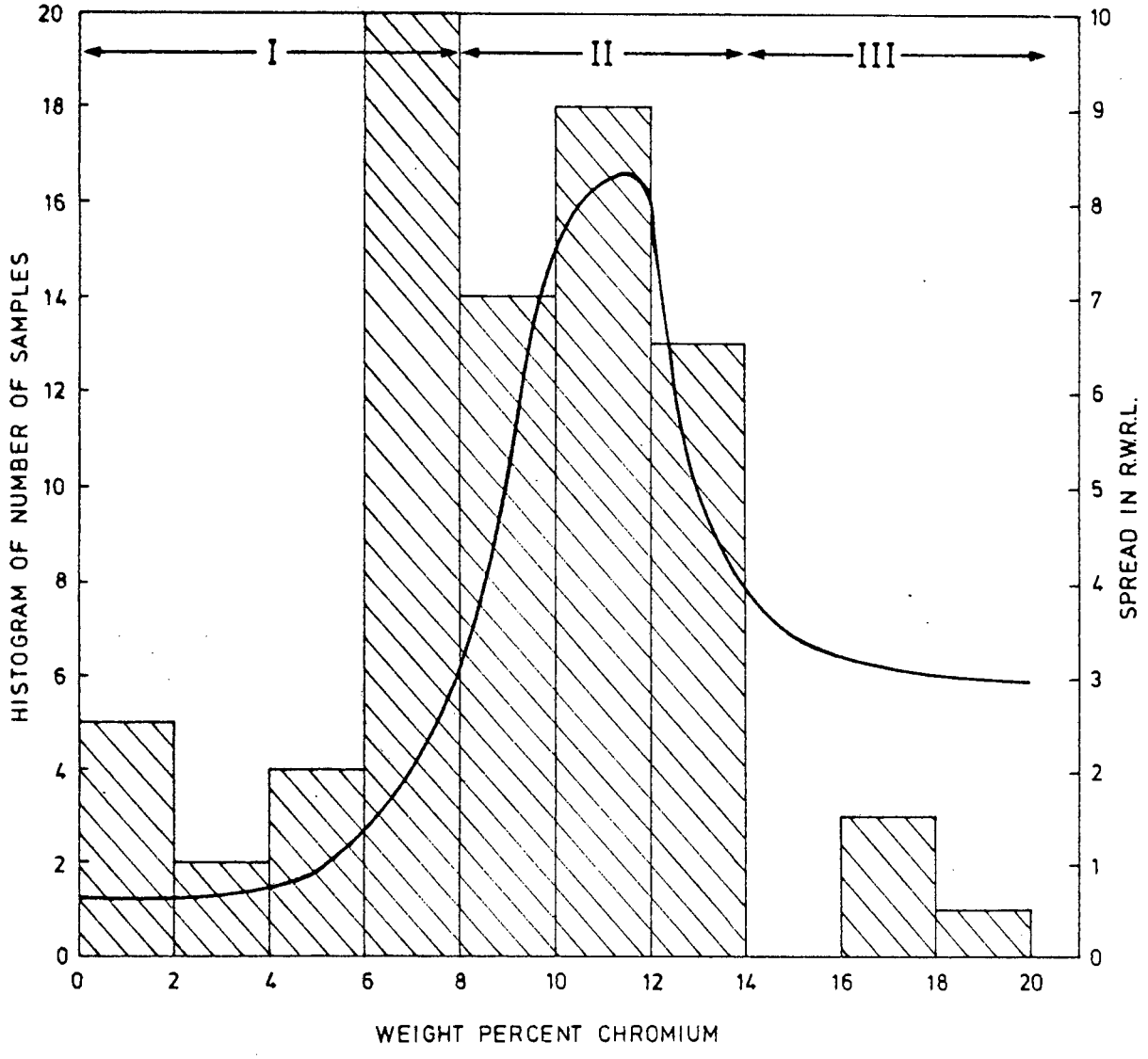

FIGURE 5.10 : Histogram of the sample distribution as a function of chromium content. The superimposed line is the range over which the RWRL values are spread. The level of dependence the RWRL of a material has on chromium content is different for the three regions

The RWRL of materials in region I is independent of the number of samples and thus wear resistance is not influenced by a change in the chromium content. Similarly for the materials in region III but to a lesser extent. The RWRL of materials in region II is a function of the number of samples and thus a function of chromium content. Within region II, the corrosion contribution is accountable for from zero to 80 per cent of the total wear volume loss and covers the transition from general corrosion to spontaneous repassivation.

The position of region II is specific to a unique set of experimental conditions and is influenced by microstructure (Section 4.1.3), the period of uninterrupted corrosion (Sections 4.2.6 and 4.2.7) and by the aggressiveness of the environment (Section 4.2.8).

The transition region (region II) where possibly both the corrosion mechanisms operate is of particular interest to the alloy development programme. We shall first consider what determines the rate of corrosion, and how chemical composition and microstructure influence the rate of corrosion for the experimental alloyed steels, before we examine the interactive nature of abrasion and corrosion and how this contributes to the overall rate of wear.

The creation of a protective oxide film

The mechanical disruption of the metal-oxide surface by an abrasive particle creates a new metallic surface with a high affinity for oxygen. Oxidation occurs randomly and the first monolayer is formed within tens of milliseconds (Barbosa and Scully, 1982; Burstein, Ashley and Marshall, 1983). Thickening of the oxide film in aqueous environments involves two competing processes (Burstein et al., 1983). The initial growth is a function of the total charge density passed and is kinetically controlled by classical ion conduction under a high electric field. The electric field across an oxide decreases as it thickens and an exponential decrease in the rate of film growth occurs with increasing thickness. A decay process is set up in competition to the growth. This can involve mechanical degradation due to the friability of the oxide film or dissolution by the aqueous environment. The kinetics of the dissolution process are accelerated when ions like chloride or sulphate are present in solution (Burstein et al.,1983).

A selective dissolution process operates at the oxide layer of alloyed steels. The selection is under galvanic control (Hashimoto, Asami, Naka and Masumoto, 1979). The alloying elements more noble than iron (eg. Ni) or less noble than iron but passive in their oxide state (eg. Mo) are concentrated in the oxide film of alloyed steels.

The contribution of the alloying elements in resisting corrosion

Chromium in particular is less noble than iron, kinetically more reactive and has a greater affinity for oxygen (Pourbaix, 1966). The stable passive state of chromium oxide at pH 6 to 7 coupled with the high rate of active dissolution of iron results in the enrichment of chromium in the oxide film (Burstein and Marshall, 1984). This acts as a diffusion barrier to further dissolution and improves the protective quality of the product oxide film (Definition 2 of Section 2.2.2).

The improvement in corrosion resistance with increasing chromium content manifests itself in a change from general corrosion of the entire surface to localized or crevice type corrosion (Secion 4.2.8, also Regions I and II of fig. 5.9). If the chromium content is above 11% then the dissolution process is transient and spontaneous passivation takes place in neutral aqueous environments (Region III of fig. 5.9). The thin chromium-rich oxide film makes the surface chemically inert and physically resistant to light mechanical disruption.

Other alloying elements can assist in reducing the rate of corrosion either by forming a rapid but temporary passive film (Mo, V, W, Nb) or by ennobling the metal and decreasing the anodic activity (Cu, Ni) (Hashimoto, et al., 1979). Their contributions are small in comparison to the passive chromium oxide effect and are difficult to detect using weight loss techniques on chromium containing alloys. Thus the contribition, if any, of aluminium and silicon to corrosion resistance goes undetected in the source T alloys (Table 4.8). Chen and Stephens (1979) found alloy substitutes of aluminium-molybdenum or silicon to be effective in improving the passive behaviour of a 12Cr/10Ni steel. The influence of nickel or manganese in solid solution remains unresolved in this study because of the dominating influences of carbon (Table 4.6) and chromium (Table 4.7). Nickel in sufficient quantities is expected to ennoble the alloy (Hashimoto et al., 1979; Sedriks, 1984) while manganese diminishes an alloys ability to passivate and its resistance to pitting (Lunarska,

Szklarska and Janik, 1975). Carbon is detrimental to the passivating influence of chromium because of their mutual affinity and the formation of chromium carbides (fig. 2.11). An increase in carbon can result in a decrease in chromium in solid solution and a decrease in corrosion resistance (Table 4.6, fig. 4.15). Microstructural control by delicate heat treatment can reduce the trend (fig. 4.14).

The direct contribution of the alloying elements in resisting corrosion is masked by the passivating properties of the element chromium but the indirect influence in stabilizing a microstructure and preventing the formation of unfavourable microstructural features is of significant importance.

Defining a corrosion index

The complex and interactive nature of the alloying elements and the diversity of the product microstructure precludes the development of a corrosion index using only compositional parameters (Secton 4.2.5). Where the element chromium is alloyed in quantities greater than 6 per cent, the direct contribution of the other alloying elements to corrosion resistance is negligible and the presence of undesirable microstructural features like chromium carbides and manganese sulphides has increasing importance. It is the chromium present in solid solution and not that which is tied up as precipitates, which is the primary source for passivity. This introduces the concept of an "effective chromium content" as a loose guide to predicting corrosion resistance. The effective chromium content would be less than the total chromium content when chemical inhomogeneities are present in the microstructure.

Corrosion kinetics at a rough abraded surface

The action of abrasion is anticipated to influence the rate of corrosion in a number of ways. For example, the removal of the previously passive film will increase corrosion until the build up of a new impermeable oxide film is complete. The rate of film thickening is a function of surface roughness (Abd El-Kader et al., 1984). Pitting is known to occur preferentially at scratches (fig. 4.32 ;Nöel, 1981; Barbosa and Scully, 1982; Burstein, Ashley, Marshall and Misra, 1983). In acids, cold work increases the corrosion rate (Grassiana, 1978; Uhlig and Revie, 1985). Other factors to consider are the heat of friction, an increase in the

effective surface area, the formation of lattice defects, mechanical agitation of the electrolyte and increased transport rates of reaction partners.

The corrosion of metal is a chemical reaction and can be described by the laws governing the rates of chemical reactions. The difference in free energy, ΔF, between the metal and its corresponding oxide is the thermo-dynamic driving force for corrosion. The increase in internal energy produced by cold work (as during abrasion) is relatively small and insufficient to account for an appreciable change in free energy (Hintermann and Trümpler, 1967; Heidemeyer, 1981). Thus it can be stated that abrasion does not significantly change the thermo-dynamics of corrosion. The observed increase in rate is caused through a change in the kinetics of the chemical reactions taking place at the surface.

As we are concerned with the effect a rough abraded surface has on the corrosion kinetics, we must assume at this stage that the availability of oxygen and the other reactants is constant and in excess. That is, to simplify the discussion, the concentration of the reactants are not a rate limiting factor in the kinetics of the forward reaction.

The rate of chemical reactions is determined by the free energy of activation, Q, according to the Arrhenius rate law,

$$\text{Rate} = A \exp\left(\frac{-Q}{RT}\right) \qquad \ldots.(9)$$

where A is the reaction constant , R is the gas constant and T is the absolute temperature. Q is the energy barrier that the metal atoms and the other reactants must overcome to produce the oxide phase (fig. 5.11). This activation energy is a combination of the energies necessary for metal atoms to break away from the surface, for the migration and diffusion of the reactants, and the probability of the reactants colliding. Let us consider the energies of this process in more detail.

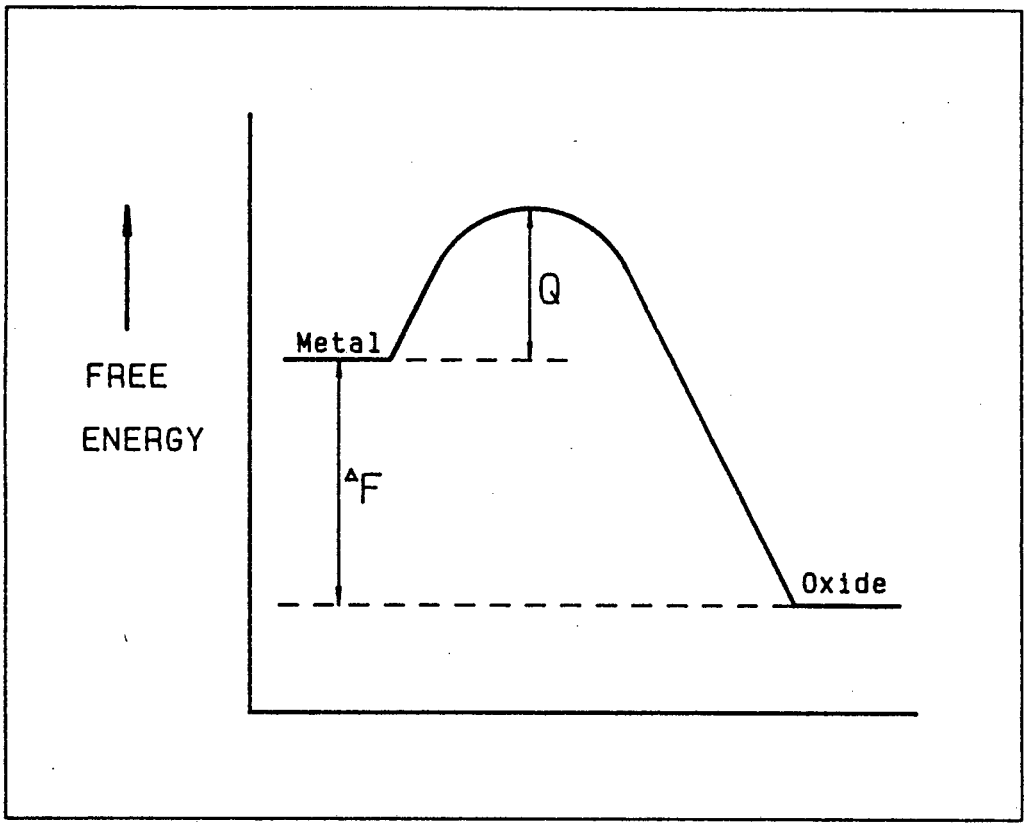

FIGURE 5.11 : Schematic of the activation energy barrier (Q) that metals most overcome to convert to the lower free energy state ($^{\Delta}F$) of the oxide

The energy for the dissolution of an atom from the surface involves the breaking of metallic bonds. An iron or chromium atom has eight nearest neighbours (co-ordination number 8) in a bcc unit cell. The most likely site for dissolution of an atom is a corner or kink site on the surface where the least metallic bonds need be broken (fig. 5.12). Therefore the rate of dissolution will be a function of the number of atoms of lowest co-ordination number. An increase in roughness will decrease the average co-ordination number of the surface atoms and increase the number of active sites for dissolution. Furthermore, the change in microstructure of the most highly strained material (figs 4.26 and 4.27), the presence of strain lines (fig. 4.25) and work hardening (fig. 4.29 and Table 4.16) are indicative of an increase in dislocation density and lattice defects at the surface. This too constitutes a decrease in the average co-ordination number of atoms at or near the abraded surface and a decrease in the activation energy for dissolution (Q_{dsln}) with respect to a polished annealed surface.

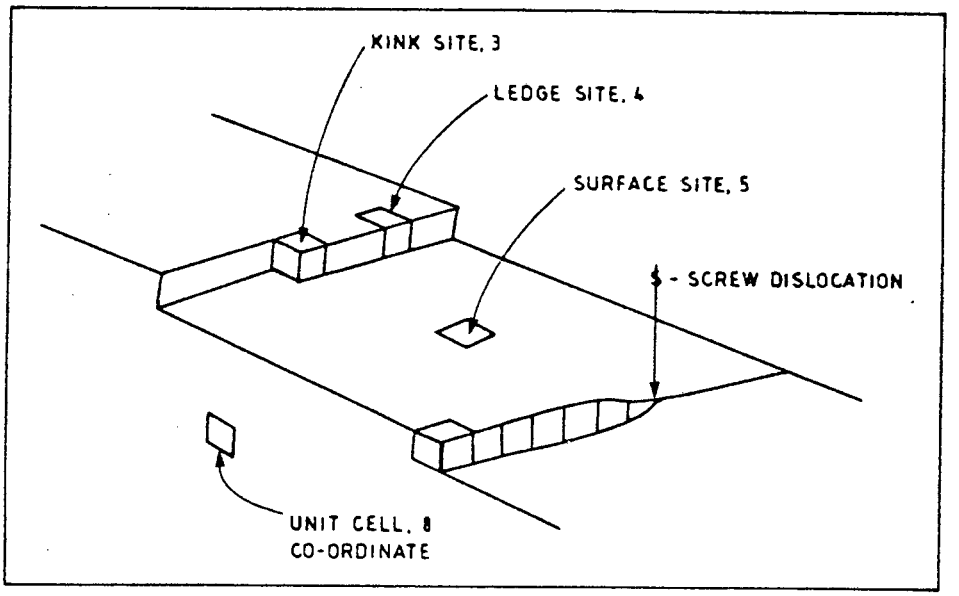

FIGURE 5.12 : The co-ordination number of bcc atoms at a surface, ledge and kink site. Dislocations form new sites where they meet the surface

An increase in roughness increases the actual effective surface area over the nominal surface area. This serves to concentrate the active dissolution sites per unit nominal area and thus increase the concentration of dissociated metal atoms immediatly above the surface which in turn results in an increase in the number of atoms with the energy for diffusion (Q_{dif}) away from the surface. There are also more sites suitable for the metal atoms to redeposit back on the surface. Heidemeyer (1981) does not think these processes are entirely reversible and the net dissolution and migration is reflected in a negative potential shift in the free corrosion potential of iron. Heidemeyer (1981) argues that the free enthalpy of reaction of an abraded surface is higher than what can be calculated from the measured potential shift.

The charge density about an asperity is highest and has the greatest surface to volume ratio (fig. 5.13). Thus dissolution is expected to be faster at the apex than in the valley of an abrasive groove and the lowest Q_{dif} is at the high spots on the surface.

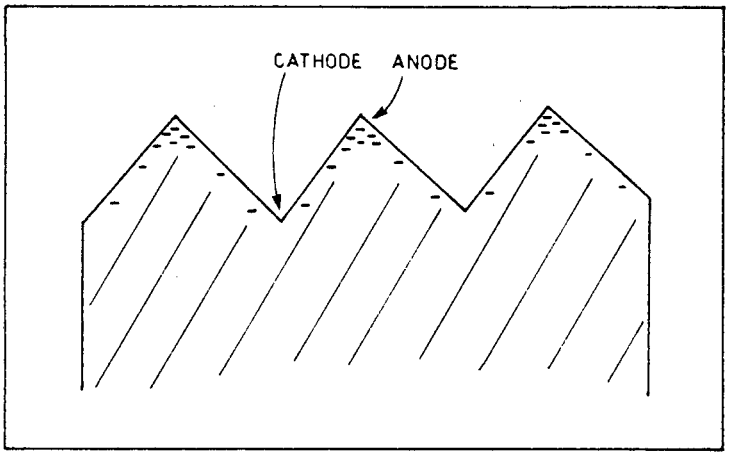

FIGURE 5.13 : The charge density is concentrated about the apex

In studying the effect of cold work in carbon steels, Uhlig and Revie (1985) attribute the rate of dissolution to the segregation of carbon and nitrogen atoms at the sites of lattice imperfection produced by plastic deformation and not to the presence of the lattice imperfections themselves. A lower hydrogen overpotential* is measured at these dislocation sites than elsewhere on the surface (the reason for the etch pitting phenomenon). Uhlig and Revie (1985) consider these sites to act as catalysts in the adsorption and convertion of protons to gaseous bubbles of hydrogen. These catalyitic sites would increase the probibility of the reactants going to products and the entropy of the reaction sequence and thus decrease the activation energy by Q_s.

The total effect of abrasion and an abraded surface is then a summation of the individual effect identified so that:

$$Q = Q_{dsln} + Q_{dif} + Q_s \qquad \ldots.(10)$$

Thus the activation energy at a rough new abraded surface is less than at a polished annealed surface and a faster rate of corrosion is expected.

Abrasion has been considered as an energy dissipating process and frictional heating effects need to be included in the kinetics equation. The rate of energy input at the abraded surface can be controlled by the

*Footnote : The overpotential is the potential shift that occurs in slow electrode reactions for the reaction to proceed and is associated with the activation energy of the slow reaction.

velocity of abrasion. A high abrasion velocity is associated with an adiabatical temperature rise in the yielding surface material. Corrosion rates are related to temperature by the Arrhenius rate law (eqn 9). Thus the heat-energy generated during abrasion is available to increase the rate of corrosion. This would be an additional term to include in the corrosion kinetics of a newly generated metal surface.

The effect of abrasion and atomic disorder on Q_{dsln} is evident in the increase in corrosion rate of the abraded surface over an annealed surface (figs 4.33 and 4.34). The decrease in Q_{dif} would account for the increased rate of corrosion of a rough surface in comparison to a polished surface of the same material (fig. 2.13). The heat-energy effect on the rate of abrasive-corrosive wear may have been detected in "wet abrasion" at 260 mm/sec (fig. 4.42). There are however other factors, such as the increase in heat transfer and the change in kinetic friction, which have also contributed to the result for "wet abrasion". The heat--energy for increasing the corrosion kinetics is expected to be less at the slower abrasion velocity (42 mm/sec) but the frictional effects and the materials ability to accommodate the strains without fracture (fig. 4.30) will also change with velocity. Thus the abrasion resistance may have decreased under "wet conditions" at the fast rates of strain but measuring weight losses is too crude a technique to resolve this question. However an increase in the temperature of the system (for example, abrasive-corrosive wear in a hotter environment) will increase the rate of corrosion at the abraded surface according to equation (9).

The consequences of accelerated corrosion kinetics

The action of abrasion increases the kinetics of oxide film growth by a decrease in the activation energy for oxidation of the metal. The state of lattice disorder and the increased rate of adsorption of oxygen must affect the structure of the oxide film. The diffusion of oxygen atoms below the surface monolayer and the diffusion of metal atoms into the oxide layers is facilitated by the greater degree of disorder. Thus the growth of the monolayer to a non-stoichiometric oxide is expected to be faster because of the ease of migration of metal atoms necessary to stabalize the polarity of charge. Abd El-Kader, El-Raghy and El-Hassen (1984) found an increase in the rate of film thickening with increased surface roughness on an 18Cr/10Ni stainless steel. With greater

stability of charge, a thicker oxide film is possible. The atomic surface roughness would also mechanically stabilize a thicker oxide film.

The kinetics of oxide film dissolution and decay is affected by the increase in growth rate and consequently the structure of the film is affected. After abrasion the passivation of stainless steels may be reached sooner, but the increase in roughness and surface area of the oxide film increases the number of sites suitable for pitting and local breakdown of the film. Thus the period the surface can remain passive is less and an increase in the rate of material loss is expected. The kinetics of oxide dissolution, for the carbon steels, is proportional to the thickness of the oxide film. Thus with the kinetics of oxide film decay keeping abreast of the kinetics for oxide film growth, an accelerated rate of material loss is expected from an abraded surface. However with time, the high spots, sites of greatest lattice disorder and the material of highest strain and work hardening are removed. The activation energy for corrosion to proceed then increases and the rate of corrosion must decrease. It is anticipated that a stainless steel, which would rapidly form an impermeable oxide film, will still have the highly disordered surface layers while a carbon steel would lose more material in establishing its oxide layer.

The corrosion potential is established by the relative rates of the anodic and cathodic reactions. The change in free corrosion potential at an abraded surface with time (fig. 4.40) should be considered a net rate, a difference between a forward rate that is the formation of an oxide film (towards a more noble potential) and a reverse rate that is the disruption and decay of the film (towards an active potential). Moore, Iwasaki, Natarajan, Perez and Adam (1984) published similar results to fig. 4.40 showing the change in potential with time for three abraded steels (austenitic stainless, HCLA and mild steel). They noted that increasing the degree of aeration (and thus turbulence across the surface) moved the potentials to more negative (anodic) values and that oxygen flushing reduced the exchange current density. Each of the martensitic abrasion resistant alloys of fig. 4.40 is uniquely different as it seeks to attain a steady state potential following the establishment of a protective oxide layer. A scenario of their corrosion behaviours will demonstrate the interaction of the kinetic reactions and help towards explaining the outcome.

The free corrosion potential immediately after abrasion (at time t=0 hrs) for 070M20 and Quatough is 150 mV more active than that of annealed, unabraded iron(Fe) in the same aerated, synthetic mine water (figs 4.40 and 5.7). An increase in the net rate of metal dissolution (the anodic reaction) would account for this large negative polarisation. The steady flow rate of electrolyte through the open circiut test cell (fig. 3.5) should minimize the concentration polarisation (cathodic reaction) brought on by the increased reaction kinetics. Material is removed at an accelerated rate (fig. 5.14) and occurs preferentially at the ridges and other high spots (figs. 4.31 and 5.13).

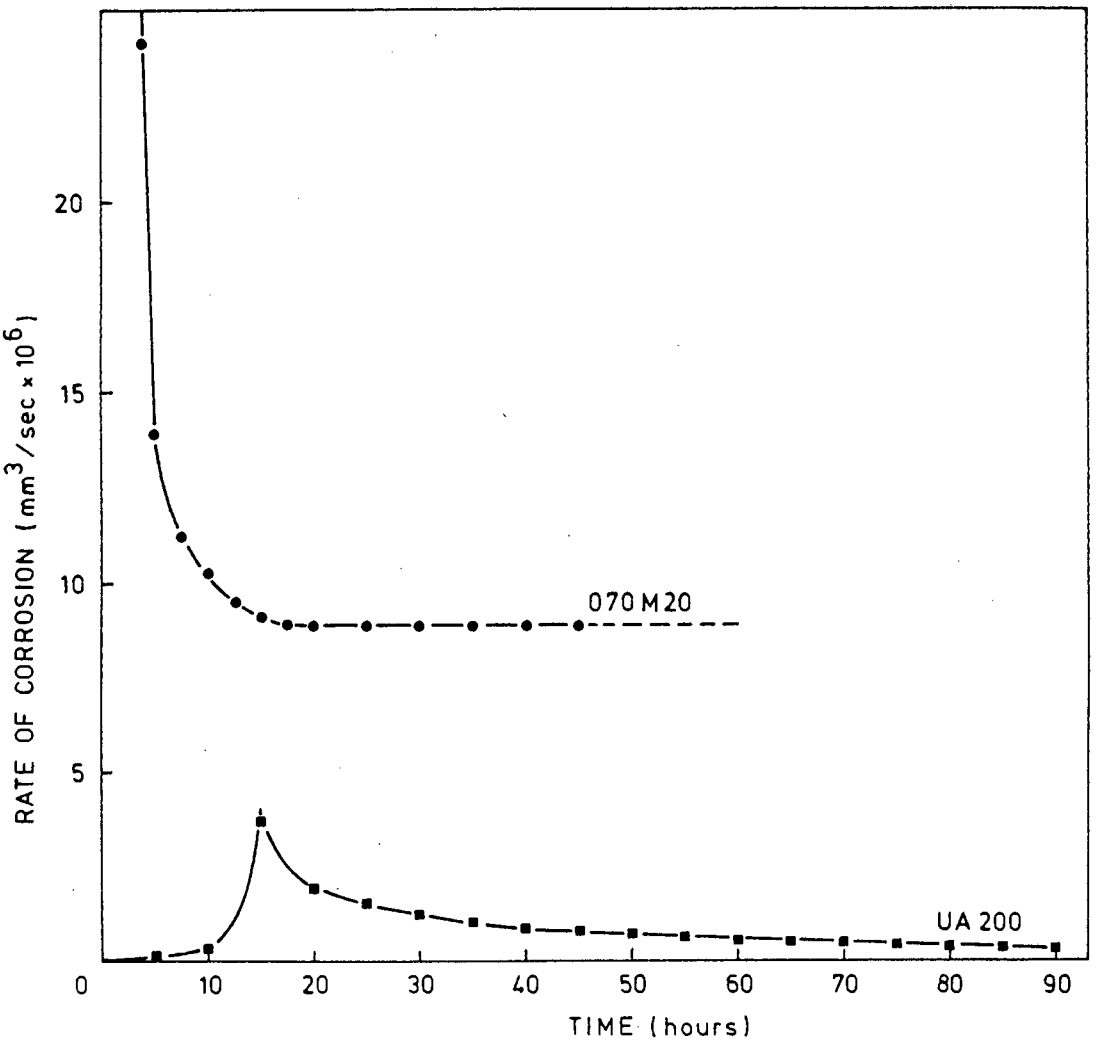

FIGURE 5.14 : The instantaneous rate of material loss due to corrosion of an abraded surface as a function of the period of exposure (Derived from fig. 4.38). General corrosion for 070M20, localised corrosion for UA 200

The steel 070M20 reaches its most active potential after five uninterrupted hours of corrosion (t=5 hrs, fig. 4.40). The rate of material

loss has decreased as thickening of the oxide film occurs (fig. 5.14). The evidence of magnatite (section 4.2.4) at the interface indicates insufficient oxygen for complete oxidation. Thus, the oxidation--reduction reaction at the metal-oxide interface is the rate controllng step and it is dependent on the diffusion of oxygen through the oxide. The anodic sites have reached a depth of 12 micrometres (Section 4.2.7) so the surface roughness effect (apex to valley is ± 7 micrometres) is no longer of importance. The cohesive strength of the oxide is good (fig. 4.44). The more active potential of Quatough may be due to the oxide layer being more impermeable which will result in a greater diffusion polarisation.

A constant rate of corrosion (steady state) is reached after 20 hours for an abraded surface of 070M20 (fig. 5.14). Constant corrosion rates were only established after 100 hours for unabraded coupons in a similar environment (Higginson, 1984). He measured the steady state corrosion rate to be between 0.7 and 1.4 mm per year depending on the flow rate and degree of aeration. The growth of the oxide at steady state is in dynamic equilibrium with the rate of decay. The free corrosion potential of the abraded material remains below the iron(Fe) corrosion potential (fig. 5.7) due to diffusion rates through the thick oxide film. The compactness and cohesive strength of the oxide has decreased (figs. 4.43 and 4.44). The rate of material loss from the abraded surface at steady state is 2.8 mm per year for 070M20 and 2.3 mm per year for Quatough. The corrosion of both is general and occurs over the entire surface.

The slower rate of decay and a more active potential indicates that Quatough formed a more compact and impermeable oxide film. The oxide was noted to be less prone to flaking than was the oxide of 070M20. Quatough is also expected to reach steady state sooner (fig. 4.40). Thus the presence of small amounts of alloying elements is an advantage in reducing the rate of corrosion (Bruno, Temba and Bombara, 1973). It is possible for the more robust oxide to create a stagnant zone by "capping" the active anodic sites so that a crevice corrosion situation may develop. The local change in conditions at the active sites would account for the large polarisation of Quatough to a most active potential. Therefore it would be expedient in the absence of chromium to alloy with elements more noble than iron and those that do not create strongly acidic or basic salts.

The materials UA 200, WV69 and AISI 431 contain chromium in increasing amounts (8, 12 and 16%) and their initial free corrosion potential for a newly abraded surface is approximately 70 to 80 mV below the potential of a smooth annealed surface (figs 4.40 and 5.7). Again an increase in reaction kinetics would account for the active starting potential.

The low ratio of chromium(Cr) to iron(Fe) in UA 200 is reflected in the slightly more active starting potential and the slower rise to a passive potential (fig. 4.40). The selective leaching out of the iron oxide (oxide film decay) results in an enrichment of chromium oxide which imparts a characteristic white tint to the passive oxide film (fig. 4.39). The free corrosion mixed potential at t = 0.3 hrs (fig. 4.40) indicates that stainless steel - chromium oxide is the dominant reaction but this condition is unstable since there is insufficient chromium available in the substrate to maintain it. Breakdown of the passive film then occurs at the weakest spots. The increased anodic activity developes into isolated crevice or pitting sites (fig. 4.39) and the free corrosion potential drifts towards the more active iron(Fe) corrosion potential (fig. 4.40). The localised anodic activity galvanically protects the rest of the surface so that material losses are still negligible at t = 2,5 hrs (fig. 4.38). As new and existing corrosion sites develop, the rate of material loss increases and reaches a maximum at t = 15 hrs (fig. 5.14). Polished coupons of UA 200 in the same electrolyte showed no increase in material loss after 120 hrs except in a deliberate crevice situation (Capendale, 1985). The repassivation potential for this material is indeterminate (fig. 5.8). Further corrosion of the once abraded material thickens the oxide film which then decreases the rate of material loss (fig. 5.14). Complete passivity and a halt to material loss is not possible for this type of material. However, controlling the environment by the introduction of inhibitors orkeeping a positive Langlier index may economically extend the service life of this material (Driver and Meakin, 1977; Higginson and White, 1983).

The abraded surface of steels with above 12 weight per cent chromium passivate before there is a significant loss of material. They are better able to maintain passivity because of their large passive potential range. The free corrosion mixed potential is then a measure of the degree of passivity and of the pitting potential. The cold work and internal stresses introduced during abrasion will remain in the uncor-

roded surface layers. This may influence the structure and make up of the oxide film and lead to stress assisted corrosion in cracks and at other flaws in the oxide film. Micropitting begins after 2 hours on WV69 and as these develop and coalesce the corrosion potential steadily drops towards the chromium corrosion potential (figs 4.40 and 5.7). Almost the entire surface remains passive since current densities and material losses remain low. Closed "capped" pits remain active and can develop whereas open sites exposed to the flowing electrolyte can repassivate. The service life of articles made from this material would depend on the design and avoidance of stagnant conditions. The breakdown and repassivation potentials for AISI 431 is high (figs 4.36 and 4.37) and the material is ostensibly passive with little material lost (figs 4.40 and 5.9).

Defining the induction period

The feature of greatest interest in the application of the experimental alloys is to be able to identify the point at which material begins to be lost at an accelerated rate. The induction period is then defined as the time elapsed between the creation of a new metallic surface by abrasion and the maxima in the rate of material loss due to corrosion of the abraded surface.

Three types of corrosion behaviour at an abraded surface have been identified. Steels like 070M20 lose material immediately after abrasion (fig. 5.14). Steels like UA 200 have a short induction period before they begin to lose material (fig. 5.14) while a stainless steel may have an infinitely long induction period and never lose a measurable quantity of material due to corrosion. In descriptive terms, these are loosely referred to as respectively : general corrosion, localized corrosion and pitting corrosion. A synopsis of the the three types of corrosion behaviour of an abraded metal is outlined in fig. 5.15.

Abrasion accelerates the forward reaction (the rate of oxide film growth) while the rate of dissolution and oxide decay increases in proportion to the thickness of the oxide film (Burstein, Ashley and Marshall, 1983). Steels with little or no alloying elements lose material at an accelerated rate which is restricted only by the thickness of the oxide layer (Type I, fig. 5.16). Their induction period is zero. Steels containing chromium resist corrosive attack because of the chromium-rich passive

oxide layer that is created through selective dissolution. The induction time before breakdown of the passive film is a function of the effective chromium content of the underlying material (Type II, fig. 5.16). Materials with chromium in excess of 12 per cent will passivate in tens of milliseconds and have long induction times (Type III).

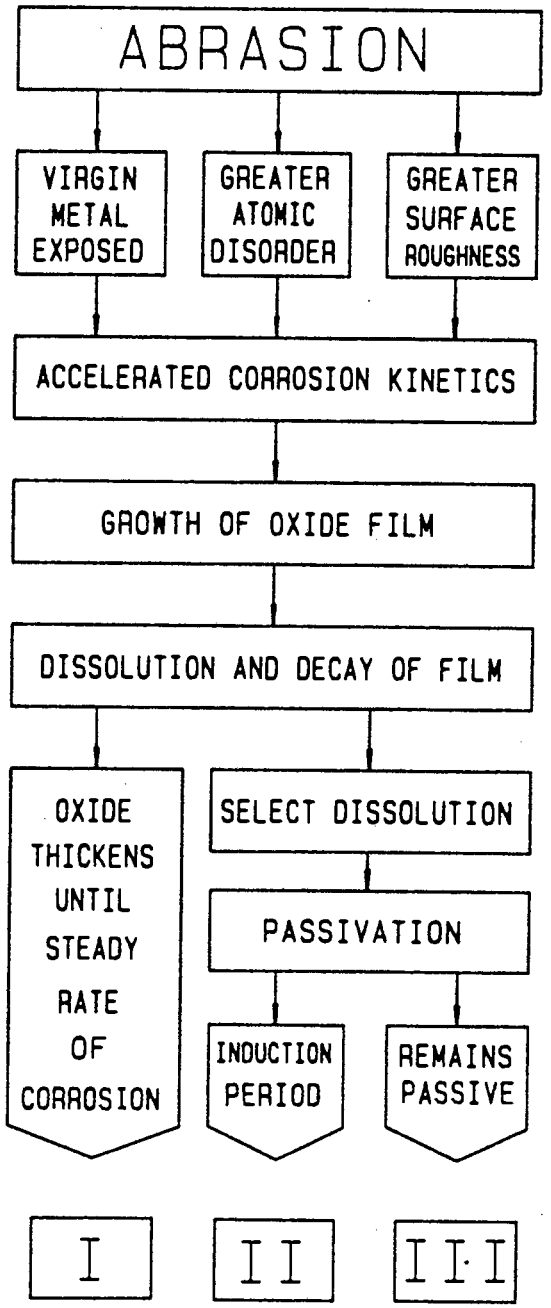

FIGURE 5.15 : The corrosion behaviour of a material after abrasion can follow a number of routes. The resultant material loss within a specific time period falls into material types I, II or III of fig. 5.9

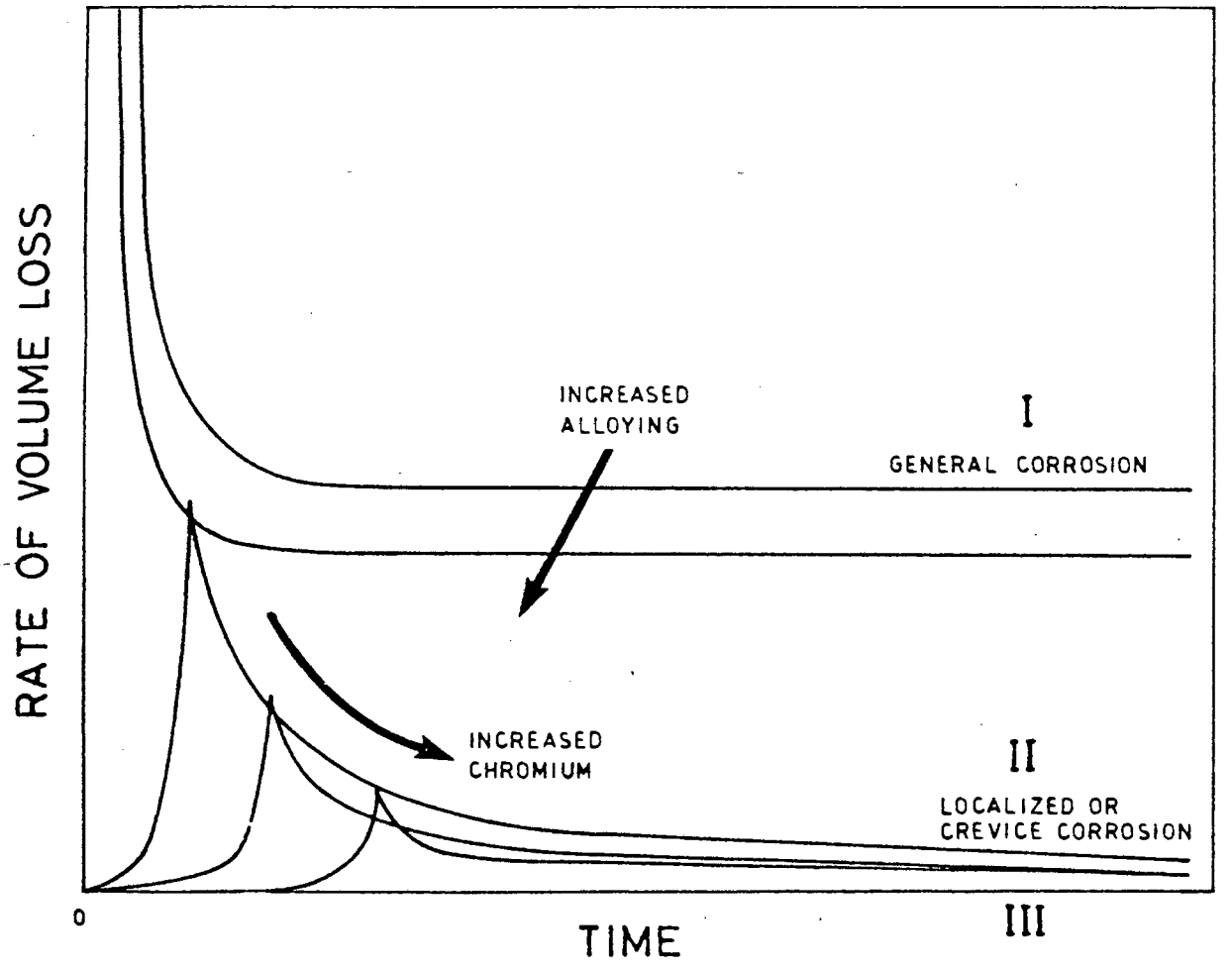

FIGURE 5.16 : Schematic summary of the effect of increasing the alloying content of steels on the rate of material loss from an abraded surface. The line for type III is a virtually straight line at zero

Mining equipment is in the continual presence of an aggressively corrosive environment. With the introduction of abrasion the situation between a steel and its environment is in a constant state of flux. Two extreme examples are: (i) a semi-continuous abrasive action which is periodically halted for a space of time; and (ii) a long idle time which is periodically interrupted by intense abrasive action. The induction period is thus an important concept when considering abrasive-corrosive wear as a cyclic phenomenon.

The significance of the induction period in repeated abrasive action

The three types of corrosion behaviour for an abraded material are described in fig. 5.17. The three cases A, B and C of fig. 5.17 are representative of the three types of corrosion behavior I, II and III respectively outlined in fig. 5.15.

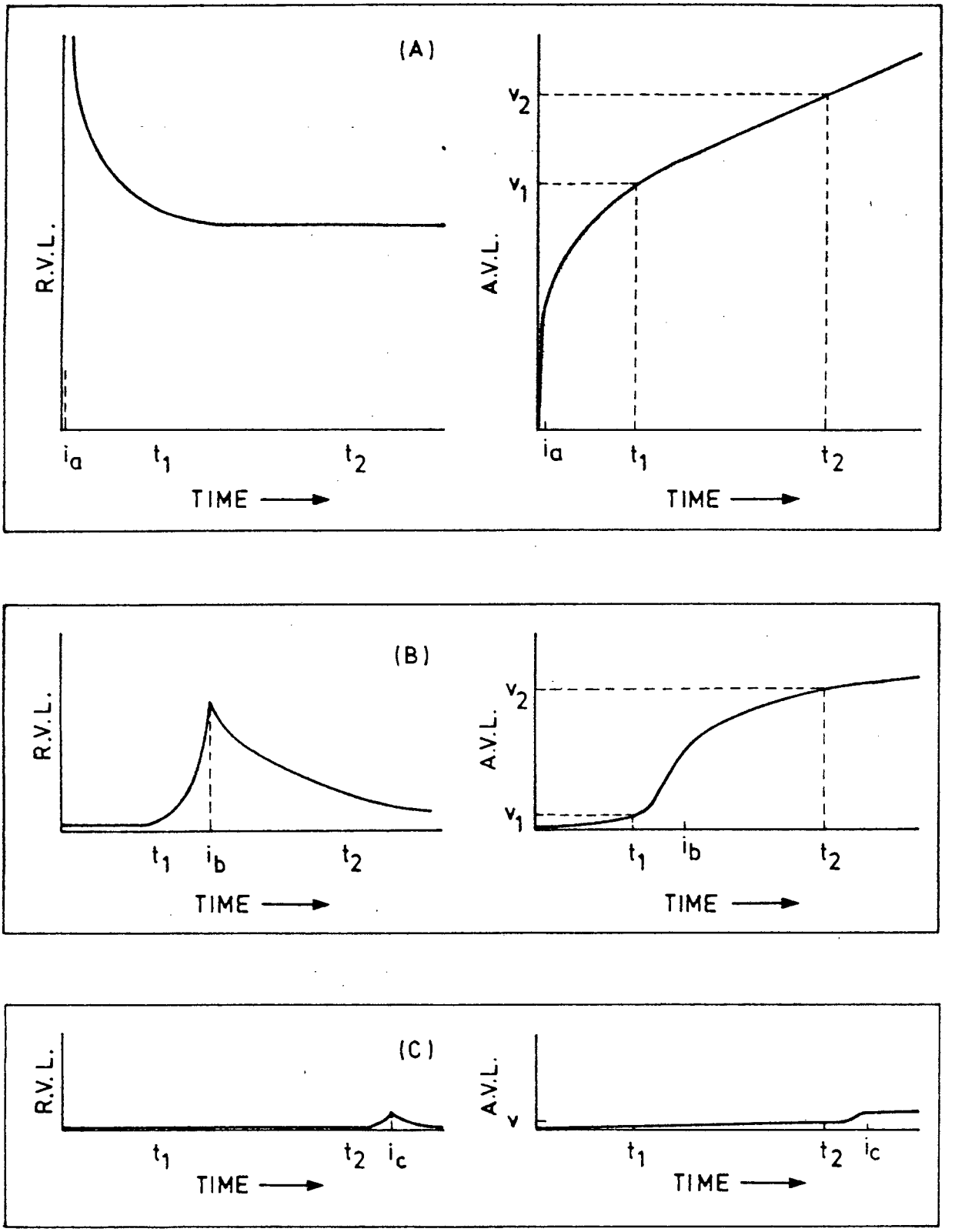

FIGURE 5.17 : Schematic representations of the rate of volume loss by corrosive action (RVL) for three different materials A, B and C in the abraded state under identical corrosive conditions. Integration of the rate gives an accumulative volume loss (AVL) as a function of time. Abrasion stopped at time t=0 thereafter uninterrupted corrosion. (t = time, i = induction period, v = volume)

Fig. 5.17 illustrates how the rate of volume loss due to corrosion as a function of time is related to the induction period. Three situations are possible as a result of a change in the period of uninterrupted corrosion between the abrasive action. The total accumulative volume of material removed can a) increase, b) decrease, or c) remain unchanged.

Case A: Type I, general corrosion. The induction period (i_a) is zero. A thick oxide layer is built up in a period of time (t_1). The rate of volume loss at t_1 approximates to the rate at some latter time, t_2. The difference in accumulative volume loss between the volume at t_1 (v_1) and the volume at t_2 (v_2) is relatively small in comparison to v_1. Consequently, if t_2 is a factor n times greater than t_1 ($t_2=nt_1$) then n times v_1 will be significantly greater than v_2.

Case B: Type II, localised corrosion. The induction period (i_b) falls between t_1 and t_2 (where the period of time, t_2 is n times greater than t_1). The thickening of the oxide layer begins at i_b. Thus the difference in accumulative volume loss between v_1 and v_2 is large in comparison with v_1. As a consequence, n times v_1 remains less than v_2.

Case C: Type III, pitting corrosion. The induction period (i_c) is greater than t_2. The bulk of the surface remains passive and the rate of corrosion is slow but constant in the period before i_c. Thus the accumulative volume loss is linearly proportional to the uninterrupted period of corrosion ($nt_1=t_2$ and $nv_1=v_2$)

The results of the above argument are illustrated in fig. 5.18. Repeated interruptions by abrasive action at the shorter time interval (t_1) can be referred to as a high frequency of abrasion incidents and the longer time interval (t_2) as a low frequency of abrasion.

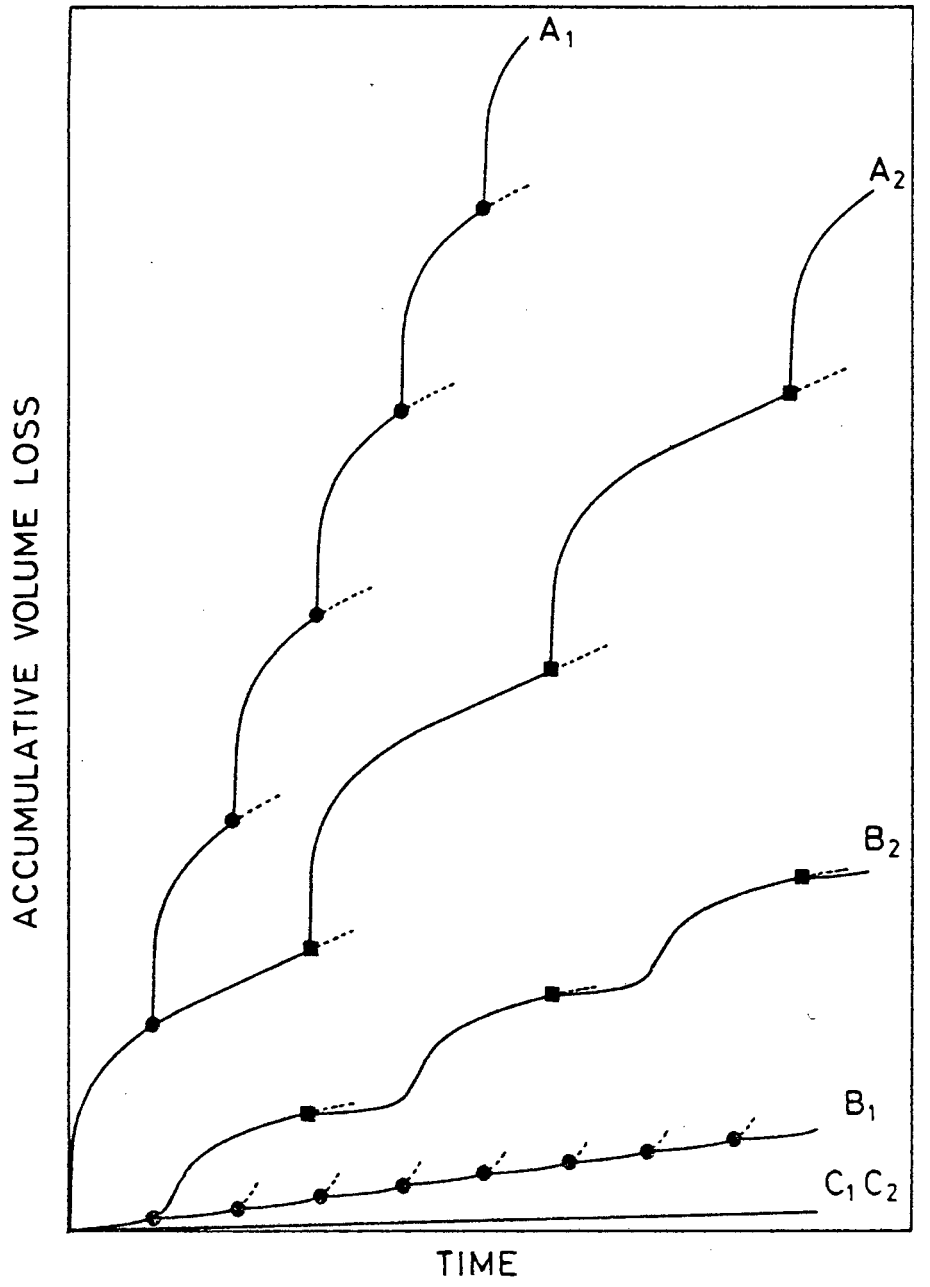

FIGURE 5.18 : Repeated interuptions by abrasive action accelerates the rate of volume loss. (● abrasion after t_1; ■ abrasion after t_2)

Let us now consider the implications of fig. 5.18 on abrasive-corrosive wear resistance by examining the two extreme examples introduced earlier. A semi-continuous abrasive action (high frequency) results in a very short corrosion time. Case A will show a very high rate of material loss while cases B and C will show low volume losses (A_1, B_1 and C_1 of fig. 5.18). As a material with a short induction period (but longer than the corrosion period - case B_1) would perform nearly as well as a stainless material (case C_1), the bulk of the total material wear will be due to abrasive action. It would only be at shut down when the idle period becomes longer than the induction period that the corrosion contribution would become significant.

Materials that are infrequently subjected to intense abrasive action on the other hand would have high corrosion contributions to the total wear rate. The rate of material loss at steady state decreases from case A to B to C (A_2, B_2 and C_2 of fig. 5.18); as does the thickness of the oxide film and the extent of corrosive damage to the surface.

The frequency of light mechanical disruption of the protective oxide layer between incidents of intense abrasion will increase the overall rate of degradation. The relative increase in rate for case B_2 will be greater than for case A_2 although the accumulative volume loss will still remain less. Thus it is predicted that a unexpectedly poor wear performance by a Case B type material may arise if in-service conditions are not critically defined before material selection or there is a marked change away from the operating conditions for which it was designed. The spontaneous repassivation and robustness of the case C type oxide film protects the material from the consequences of incidental disruptions to the protective oxide film and provides a greater safety margin for fluctuating in-service conditions.

All three cases predicted in fig. 5.18 are observed in the experimental results of fig. 4.41. Materials 070M20 and Quatough are covered by case A; the steel WA is case B but because i_b is before t_1 for this material the outcome is as described in case A (type I corrosion behaviour); alloys T820A and UA are covered by case B (type II corrosion behaviour); and case C covers the last four alloys in the diagram (type III corrosion behaviour). The relatively lower abrasion contribution in the low frequency test for alloys WA and T820A (fig. 4.41) is due to the robust, cohesive strength of the thickened oxide film that has built up (fig. 4.43). This oxide, as was demonstrated for 070M20 (fig. 4.44), acts as a dry lubricant but only for a short abrasive path length.

A comparison of the RWRL and RWRL#2 results of figs 4.4, 4.5, 4.6 and 4.7 also demonstrates the outcome of the frequency effect and induction period on accumulative volume loss. Note the change in slope when the evidence of corrosion is not entirely removed by the abrasion. To cite a practical example: It was calculated earlier that the abraded surface of 070M20 has a steady state corrosion rate of 2.8 mm per year. Working from the in-situ results of Noël (1981), the average corrosion contribution to the wear rate of 070M20 is 11.3 mm per year. Thus the synergistic effect of abrasive-corrosive wear has caused a four fold increase in the rate of degradation for this material.

The effect of a change in the corrosion kinetics

The net rate of oxide film growth and of corrosion at steady state is the result of a set of competing chemical reactions. A change in the corrosivity of the mine water will affect the reaction kinetics by changing the chemical activity of the reactants and subsequently the reaction constant, A, of equation (9). Corrosivity as measured by the Saturation Index or Langelier Index does not account for the combined effects of the anions present in mine waters (Higginson and White, 1983; Capendale, 1985) nor the organic and microbial corrosion contributions (Rawat, 1976). The quantitative contribution of these individual constituents is beyond the scope of this study although the effects of microbial corrosion were noted at first hand (Section 3.1.2).

An increase in the concentration of chloride or sulphate ions in neutral or slighlty acidic solutions will increase the rate of oxide dissolution (Burstein and Marshall, 1984; Cieslak and Duquette, 1984). These anions together with nitrates are the aggressive ions found in large quantities in mine waters (Higginson and White, 1983). An increase in the ionic strength of an electrolyte would not change the initial maximum corrosion rate but a slower net rate of oxide film thickening is expected for the general corrosion mechanism (Burstein and Ashley, 1984). Higginson et al. found no correlation between corrosivity and the corrosion rate of unabraded mild steel, although physical factors, like an increase in temperature or flow velocity, did increase the corrosion rate.

The alloyed steels IA 200 and IF 600 which both exhibit general corrosion showed no significant change in cumulative volume loss with an increase in total dissolved solids (fig. 4.45). The corrosion kinetics of thick oxide scales is limited by the diffusion of oxygen through the oxide (Higginson and White, 1983). An increase in dissolved solids will decrease the concentration of dissolved oxygen in the electrolyte and thus decrease the rate of oxide film growth. It will also increase the kinetics of the oxide dissolution process. The expected increase in time to reach steady state conditions is small in comparison to the total test period (fig. 5.14). The net result is no change in volume loss at the end of the 46 hour test period for IA 200 (fig. 4.45).

Steels which rapidly form a chromium enriched oxide film but do not have the alloying content to sustain it (case B of fig. 5.17), show increased anodic activity leading to greater material losses (fig. 4.45). The effect an increase in the oxide dissolution rate has on the rate of corrosion of these materials is described in fig. 5.19 and has features of both the general and pitting corrosion mechanisms. Steels with a passive film show a shorter induction period before breakdown and an increase in corrosion current density (Covino and Rosen, 1984). The increased pitting activity leads to increased material loss at steady state (Fontanta and Greene, 1982). This is observed in the increased corrosion volume losses for those steels with greater than 10 per cent chromium content which normally behave passively for the duration of the standard RWRL test (fig. 4.45). An exception is AISI 316 which is specifically alloyed with molybdenum to resist pitting corrosion (Marshall and Burstein, 1984) and showed no change in volume loss.

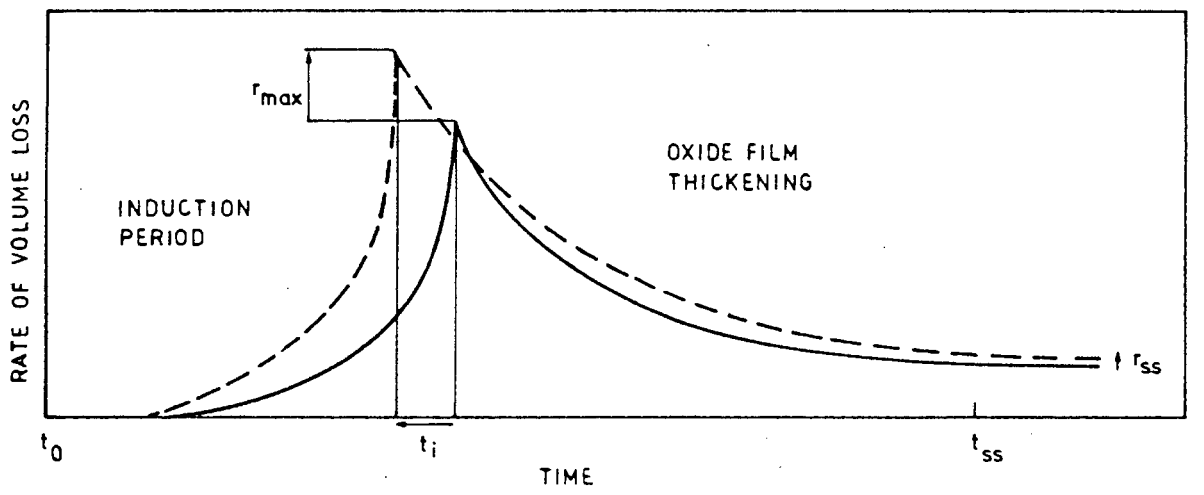

FIGURE 5.19 : Schematic diagram of the change in rate of corrosion (r) of an abraded surface resulting from an increase in the corrosivity of the mine water as a function of the immersion time (t). The case presented here is for a type II material but types I and III can be deduced. (Subscripts: o = newly abraded surface, i = induction, ss = steady state).

5.4 ALLOY SELECTION AND MICROSTRUCTURAL DESIGN

An engineering component can only be expected to give satisfactory performance if the design and the material for its construction are correctly chosen in relation to the anticipated operating conditions. A material selected for use in the gold mines must perform under a unique set of environmental conditions and thus a material with a unique set of properties is required. One that will give optimum performance in relation to its life time cost.

The route for the development of a suitable material for abrasive-corrosive wear resistance is set out in fig. 5.20. Recommendations to improve the wear properties of a microstructure cannot be treated in strict isolation but must take cognisance of the economics of the proposal and whether it will be practical to the end user.

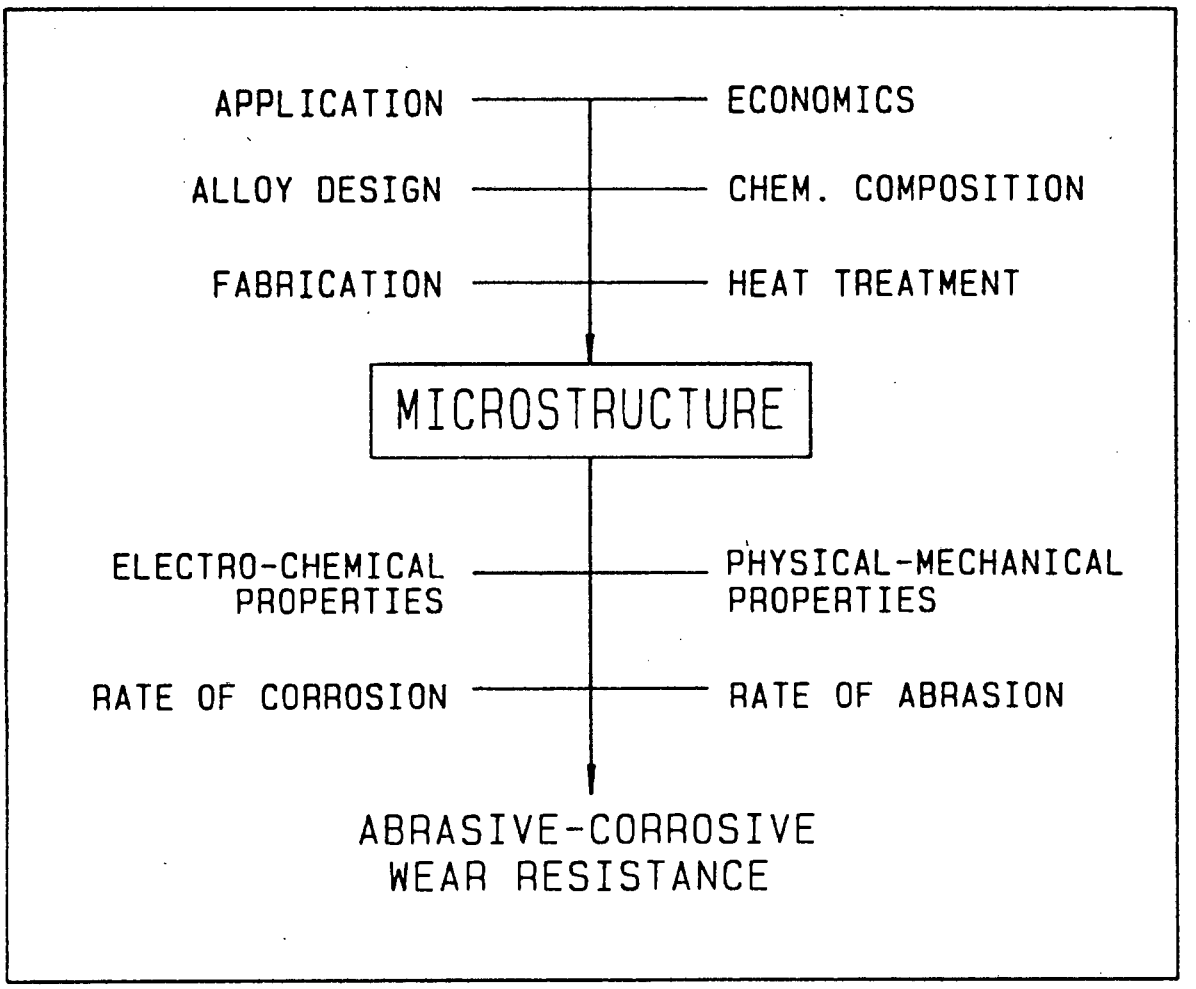

FIGURE 5.20 : Microstructural control is central to the development of an abrasive-corrosive wear resistant steel

Identifying the optimum microstructure for abrasive-corrosive wear resistance

An increase in the bias towards corrosion using the standardized wear tests has shown a separation of the types of microstructure by their common response to wear resistance (figs. 4.9, 4.11 and 4.10). Materials of cognate microstructure and chemical composition have an alike response to wear resistance (fig. 4.16). The austenitic, ferritic and dual phase stainless steels can for example be distinguished from the martensitic experimental alloys (figs 4.10 and 4.16). A brief explanation of the separation would be the superior corrosion resistance of the ferritics and the superior abrasion resistance of the martensitics. The performance within the martensites is separated into the carbon steels, the low chromium steels and the higher chromium alloyed steels (figs. 4.10 and 4.16). The length of the corrosion induction period alone (fig. 5.17) does not account for the trend and due consideration for the effects alloying and microstructure have on work hardening and abrasion resistance must also be given.

The relative importance of the various microstructural and alloying features discussed in Section 5.2 have been evaluated and ranked in ascending order of dry abrasion resistance (fig. 5.21). Solid solution strengthening by increasing carbon or other alloying elements is not a sure way to increase RAR because microstructural phase control has been found to be equally important. The high purity laboratory prepared samples generally have better dry abrasion resistance than the commercially available steels where impurity levels and microstructural inhomogeneities are inevitably higher.

The RAR of the metastable austenites (TRIP steels) are surpassed by the martensitic steels because the maximum hardness achieved during abrasion is insufficient. The former are also strain rate sensitive. The lath martensites as a group are the favoured microstructure for RAR because the precipitation hardened steels fall short on the minimum toughness requirement. A lath martensitic steel with a measurable degree of work-hardening (20%) at the abraded surface in conjunction with a bulk hardness in excess of 500 HV, has superior dry abrasive wear resistant properties. This is the preferred route in alloy design for the development of steels for use in underground equipment in South African gold mines (Protheroe, Ball and Heathcock, 1982; Bee, Peters, Atkinson and Garrett,

1985). A detailed discussion on alloy design is not within the scope of this thesis but a few indications of relevance to this study will be given.

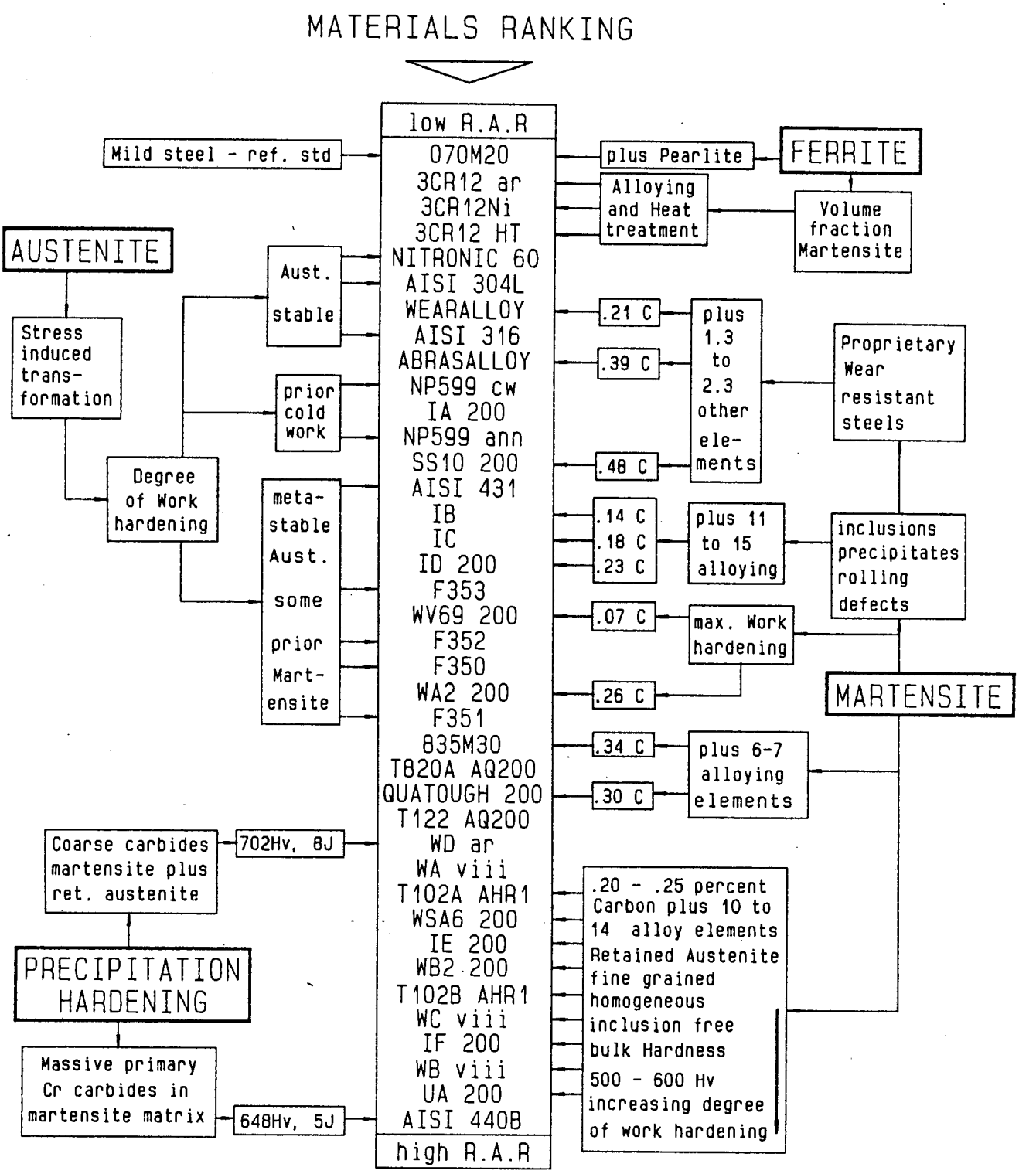

FIGURE 5.21: A ranking of materials with respect to RAR. A synopsis of the main features discussed in Section 5.2 has been linked to the respective materials. Only the optimum micro-structure found for each alloy is included in the table of materials ranking

A suggested chemical composition

The synergistic increase in wear (Section 5.3) has been found to be an integral component of the abrasive-corrosive tribological system. Tailoring a materials corrosion induction period to the in-service conditions is one way of minimising the destructive effect of the environment. The synergistic increase in wear is a maximum for materials that show general corrosion and therefore an essential requirement is sufficient alloying to impart a limited degree of passivity.

A study of fig. 5.21 shows that for the martensitic steels an increase in carbon gives a small increase in dry abrasion resistance. An increase in the total alloying content has a more favourable result provided the quality of the microstructure can be assured. The increase in cost of an alloyed steel would be acceptable if the synergistic increase in abrasive -corrosive wear can be minimised (Protheroe, Ball and Heathcock, 1982).

A minimum chromium content of 10% (fig. 4.35) would provide adequate corrosion resistance. Lesser amounts are possible in an application that involves near continous abrasive action. Increasing the chromium level above 12 or 13% (change from type II to type III corrosion behavior) is not considered justifiable for the abrasive conditions discussed earlier but it may be necessary in more specific applications. For example, to maintain close tolerances of moving parts, or in a highly corrosive environment. Apart from corrosion resistance, chromium also acts as a solid solution strengthener of the martensitic matrix and inhibits the coarsening of Fe_3C precipitates (Honeycombe, 1981). The potentially deleterious effect of chromium on toughness through the promotion of twinned martensite is not relevant at carbon levels of 0.20-0.25% (Protheroe, Ball and Heathcock, 1982; Heathcock, 1983). An increase in carbon above this range would promote twinned martensite while below 0.20%C there is insufficient matrix strength to provide adequate abrasion resistance.

An M_S temperature in the 200-300°C range will promote the formation of meta-stable retained austenite (Rao and Thomas, 1980), an essential microstructural feature for RAR. In the absence of carbon, the elements nickel or manganese are needed to stabilize the austenite phase. Nickel is preferred to manganese because of the ennobling effect of nickel during corrosion while manganese as MnS promotes the earlier breakdown of

passivity (Sedriks, 1984; Capendale, 1985). Greater amounts of nickel (5%) than manganese (2%) can be alloyed to this type of material without a decrease in toughness (Rao and Thomas, 1980). The relative cost of these two alloying elements may force a compromise.

The cleanliness of the steel is of importance. Low sulphur and phosphorous levels (below 0.010%) and an absence of oxygen and hydrogen would minimise inclusions like Al_2O_3 and MnS and avoid intergranular embrittlement. A fine, homogeneous microstructure, free from inclusions, coarse precipitates and other defects introduced during casting and hot rolling, gives a superior work hardening ability and RAR and maximizes the "effective chromium content". The laboratory, vacuum cast steels made from high purity starting material have outperformed the commercial steels which have higher impurity levels. The industrial melt (UA) used an electroslag remelt technique to reduce impurity levels. This direction will have to be followed if optimum wear performance is expected of materials with critical alloying content levels.

Other alloying elements like molybdenum, vanadium and titanium could promote passivity in sufficient quantities but their cost prevents general use. They may however be necessary in small amounts to promote grain refining and dimensional control during cooling or to prevent the formation of $Cr_{23}C_6$ if the absence of carbon from solid solution can be afforded. Copper, aluminium and silicon can also be added in small amounts to control the microstructure but their contribution to corrosion resistance is negligible for the 10% Cr martensitic steels. A summary of the suggested alloying element levels is given in Table 5.3.

TABLE 5.3 : Chemical composition for a martensitic steel anticipated to have superior abrasive-corrosive wear resistant properties.

WEIGHT %	C	Cr	Ni	Mn	S&P	others	Fe
RANGE	0.20-0.25	9.8-10.8	1-4	0-1	0.010 max	as req.	balance

A martensitic alloy with the chemical composition identified in Section 5.2 and Table 5.3 meets many of the requirements for an abrasive- corrosive wear resistant steel. The ideal microstructure prescribes complete chemical homogeneity, a fine-grained austenite (30 micrometres) which has transformed to dislocated lath martensite surrounded by continuous films of retained austenite, the absence of coarse carbides and the maximum quantity of carbon and chromium free in solid solution. Such microstructural control would need a delicate heat treating schedule.

The optimum heat treatment

The optimum heat treatment (section 4.1.3) is an austenite solution temperature of 1100°C followed by an oil quench (Table 4.2). Holding at higher temperatures would cause grain growth and loss of the alloying elements through decarburisation and high temperature oxidation. Air cooling from 1100°C results in coarsening of the carbides (fig. 4.13) and a faster quench is necessary to retain the austenite and get the desired lath martensite. Tempering is necessary to improve the toughness of the quenched structure (fig. 4.12) and in some cases to meet minimum engineering requirements. The optimum wear properties are met on tempering at 200°C (figs 4.12 and 4.14; Table 4.3). This is a general result that holds for other materials of similar microstructure (Appendices A4, A5 and A6).

The RAR decreases above 200°C temper due to the decomposition of retained austenite to Fe_3C. Salesky (1980) reported a sharp drop in the sliding wear of Quatough above 200° temper and showed it was due to the decomposition of retained austenite to Fe_3C. Garrison and Garriga (1983), in studying a 0.4% C UHS steel, found the best RAR was on tempering at 150°C and that RAR decreased sharply above 300°C for the same reason. The drop in RAR (fig. 4.12) corresponding to the decomposition of retained austenite is not dramatic for the experimental steels because the alloying elements act to refine the iron carbide dispertion and restrain the coarsening of Fe_3C to higher tempering temperatures. Thus the hardness and impact toughness are maintained up to 400°C (fig. 4.12) and the work hardening potential is not affected (Bhat, Zackay and Parker, 1978). However, the formation of interlath Fe_3C may have decreased the micro-fracture toughness in the 300°-400°C range (tempered martensite embrittlement, Honeycombe, 1981) and this has been reflected in the RAR

(fig. 4.12). Growth and coarsening of the Fe_3C at 500°C results in a decrease in impact toughness. Further growth and spheroidisation of the iron carbides above 500°C temper results in a further decrease in hardness but toughness increases again due to the disappearance of the crack initiation sites. The decrease in carbon in solid solution decreases the work hardening potential and the tensile strength of the matrix but does not adversely affect RAR because the high alloy content is a second source of precipitation hardening at the higher temperatures (Honeycombe, 1981). However, the presence of alloy carbides (air cooled and above 400°C temper) adversely affects the corrosion resistance of these materials (fig. 4.14) due to the loss of "effective chromium content". El-Koussy, El-Raghy and El-Mehairy (1981) found that tempering decreased the total overall wear resistance of wet grinding media balls (1-12%Cr) especially above 300°C temper due to the decomposition of residual austenite and the formation of carbides. Truman (1976) warns on the temperature and the time at temperature sensitivity to corrosion resistance of a 0.25% C, 13% Cr martensitic steel. Tempering above 400°C was found to deplete the matrix of chromium in the local region about the growing carbide.

Considering alternative microstructures

The idea of using controlled hot-rolling techniques instead of a re--austenite quench and temper should not be discarded as there would be considerable savings in the final cost of the product. A preliminary study (section 4.1.4) has not foreseen any major problems in producing a steel with acceptable wear resistant properties. The alloy T102, which has a chemical composition similar to that in Table 5.3, has good RAR and RWRL values (Tables 4.13 and 4.14). A better control of the phases during the hot rolling sequence would produce a microstructure with excellent wear resistant properties.

The TRIP steels (source F alloys) have great potential as an abrasive-corrosive wear resistant steel. Their dry abrasion performance was overshadowed by the better of the martensitic materials (fig. 5.21) but their abrasive-corrosive wear performance is excellent. The cost factor then puts these materials in a favourable position (Table 4.14), either as an alternative to the 3CR12 type steels in an application that is too abrasive, or as an alternative to the Table 5.3 martensitic steel where corrosion is a problem. If the limiting strength and maximum degree of

work hardening could be improved a nitrogen strengthened TRIP steel with 10% to 12% Cr and an M_s temperature just below room temperature (a fine grained type F351) would be an alternative to the martensitic steel of Table 5.3.

There are however several practical limitations to a TRIP type material. Flame cutting and welding of rolled plate and sections is the preferred technique in the mines. The high amounts of chromium and manganese make it impossible to cut using traditional flame cutting techniques. Alternative methods such as plasma-arc cutting will have to be used. Consumable carbon electrodes with compressed air (gouging) would result in contamination and destroy the corrosion resisting properties therefore tungsten electrodes and plasma gas or an alternative 'clean' method of cutting shall have to be employed. While the martensitic steels can be softened before machining, the TRIP steels work harden during the machining and forming operations. The techniques used in machining tough austenitic stainless steels do not work on these TRIP steels due to the high hardnesses produced. Machining above the M_d temperature (warm machining) would overcome this problem. These alternative fabricating techniques do however add to the final cost of the product. When considering assembly, maintainance and repair underground this material is not compatible with present general mine engineering practice and would not initially meet with largescale approval.

The martensitic alloyed steel with retained austenite of Table 5.3 is thus the best option for abrasive-corrosive wear resistance. The emphasis on microstructural control to achieve optimum wear resistance may impose practical problems in the fabrication of components from this material. The work hardening ability of the quenched martensitic material together with its high initial bulk hardness, necessitates machining to be done in a softened condition. Dimensional stability, hardenability and quench cracking would have to be investigated if heat treatment must follow machining. Flame cutting of steels with above 10%Cr is generally not possible and again plasma-arc cutting would have to be employed. Alternatively, Table 5.3 may have to be revised. The heat-affected zone about a weld or at a flame cut edge would have an adverse effect on wear resistance especially corrosion resistance. This would defeat the purpose of using an alloyed steel and ways to minimise the effect will have to be investigated.

CHAPTER 6

CONCLUSIONS

1. The laboratory wear tests (dry abrasion and abrasive-corrosive wear) give a valid assessment of the potential service life of a material in an underground mining application. The information proved vital in the ranking, further development and selection of materials for the gold mining industry of South Africa.

2. Microstructural control is crucial to the development of superior abrasive-corrosive wear resistant porperties. In the study of microstructures it was found that:

   a) An increase in the hardness and volume fraction of martensite in the dual phase ferritic-martensitic steels, increased their abrasion resistance but not above the proprietary abrasion resistant materials. The corrosion resistance of the dual phase steels however makes their abrasive-corrosive wear resistance superior to that of the proprietry wear resistant steels.

   b) The metastable austenitics have the best abrasion resistance within their class but they have a few disadvantages. The presence of martensite prior to abrasion either due to a high M_S temperature or from prior cold work, reduces the abrasion resistance in proportion to the volume fraction of prior martensite. An increase in the velocity (60-600 mm/sec) resulted in an increase in the volume of material removed per unit path length. The energy absorbing capacity of the transformation to martensite was held accountable for the difference in material response in comparison with a quenched martensitic steel. The good corrosion resistance of the metastable austenitic stainless steels gave these alloys excellent abrasive-corrosive wear resistant properties.

   c) The strength and toughness combination of the martensitic microstructure makes it the most favoured structure for abrasion resistance. The microstructural features necessary to maximise the toughness to strength ratio in martensite are a small volume fraction of inter-lath retained austenite, a homogeneous fine grained structure and the mini-

mum volume fraction of carbides. These features promote a higher degree of work hardening and corrosion resistance in the alloyed martensitic steels.

3. Dry abrasion resistance is considered an energy dissipation process and can be compared to a stress-strain system. A material with a moderate yield strength and a high work hardening rate will have the best advantage. The relative dry abrasion resistance for the tribological system under examination is a function of the bulk hardness plus the work hardening ability of the material. Martensitic steels with a minimum bulk hardness of 500 HV plus the ability to work harden in excess of 10% during abrasion showed excellent relative abrasion resistance. The bulk hardness can be lower if the limiting material strength can be maintained through an increase in the degree of work hardening. The potential of the TRIP steels was seen but they were unable to match the ultimate strength levels of the martensitic steels acheived during dry abrasion.

4. The corrosion kinetics are fastest on a newly abraded metal surface. This is related to the increase in surface roughness, surface area and atomic disorder (which is a maximum at the surface). The net effect of the increased kinetics is an active shift in the free corrosion potential of the bare surface for all metals and the more rapid advancement in the corrosion behaviour with time.

5. Three categories of corrosion behaviour were noted on an abraded metal surface and these are associated with the abrasive-corrosive wear resistance of alloyed steels.

   a) General corrosion resulted in an immediate loss of material and the maximum synergistic increase in abrasive-corrosive wear.

   b) Localised corrosion has an induction period before oxide film thickening results in a synergistic increase in the rate of wear.

   c) Pitting corrosion keeps the surface largely passive so that the contribution of the conjoint action of abrasion and corrosion to the overall wear rate remains minimal.

6. The induction period of the corrosive action (before corrosion is associated with material losses) is an important feature in maximising the corrosion resistance of an otherwise primarily abrasion resistant steel. An increase in the frequency of abrasive action at a corroding metal surface will increase the overall rate of material loss if the corrosion induction period is shorter than the frequency of abrasion. Conversely, a decrease or no change in the overall rate of material loss occurs where the induction period is longer than the frequency of abrasive action. This material property can be tailored to minimize the synergistic increase in abrasive-corrosive wear without resorting to expensive highly alloyed steels.

7. A martensitic alloyed steel with 0.20-0.25% C, 9.8-10.8% Cr, 1-4% Ni, 0-1% Mn and the balance iron as the major constituents is identified to have potentially superior abrasive-corrosive wear resistant properties. The alloy would need to have an M_S temperature between 200 and 300°C. Microstructural phase control is critically important. A quench and tempered heat treatment was found to produce the most favourable microstructural features. A high austenitisation temperature (1100°C) followed by an oil quench to room temperature and a short low temperature (200°C) temper yielded the optimum wear resistant properties for the martensitic alloy. A hot roller quench technique is suggested as a cheaper alternative and a preliminary study shows the same microstructure and wear properties can be expected.

REFERENCES

ABD EL-KADER H., EL-RAGHY S.M. and ABOU EL-HASSEN M.E. (1984) : "Film thickening on abraded 18-10 stainless steel in chloride solutions", British Corrosion Journal, **19** (3), 139-142.

ALLEN C., BALL A. and NOËL R.E.J. (1984) : "The development of 3CR12 type steels to resist corrosive abrasive environments", Proceedings of Inaugural International 3CR12 Conference, Johannesburg, March 1984, 433-453.

ALLEN C., PROTHEROE B.E. and BALL A. (1981) : "The selection of abrasion corrosion resistant materials for gold mining equipment", Journal of the South African Institute of Mining and Metallurgy, **81** (10), 289-297.

ALLEN C., PROTHEROE B.E. AND BALL A. (1981/1982) : "The abrasive-corrosive wear of stainless steel", Wear, **74** , 287-305.

ASM STEELS HANDBOOK (1976) : Source book on stainless steels, American Society of Metals, Ohio.

AVERY H.S. (1974) : "Work hardening in relation to abrasion resistance", Symposium - Materials for the Mining Industry, Barr R.Q. (Ed), Climax Molybdenum Company, 43-76.

BALL A. (1983) : "On the importance of work hardening in the design of wear-resistant materials", Wear, **91** , 201-207.

BALL A. and BÖHM H. (1987) : "The design and performance of steels in an adrasive-corrosive mining environment", IMechE, C189/87, 595-602.

BALL A. and HOFFMAN J.P. (1981) : "Microstructure and properties of a steel containing 12% Cr", Metals Technology, 8 (Sept), 329-338.

BALL A. and WARD J.J. (1985) : "An approach to material selection for corrosive abrasive wear by systematic in-situ and laboratory testing procedures", Trobology International, **18** (6), 347-351.

BARBOSA M. and SCULLY J.C. (1982) : "The role of repassivation kinetics in the measurement of the pitting potential of AISI 304 stainless steel by the scratch method", Corrosion Science, 22 (11), 1025-1036.

BEE J.V., PETERS J.A., ATKINSON M.W. and GARRETT G.G. (1985) : "The development of abrasion-corrosion resistant steels for mining applications", Paper presented at Mintek Conference, Johannesburg, May 1985.

BHAT M.S., ZACKAY V.F. and PARKER E.R. (1979) : "Alloy design for abrasive wear", Proceedings of International Conference on Wear of Materials - 1979, Ludema K.C., Glaeser W.A. and Rhee S.K. (Eds), ASME, New York, 286-302.

BLAU P.J. (1979) : "The use of Knoop indentations for measuring microhardness near worn metal surfaces", Scripta Metallurgica, 13 , 95-98.

BOND A.P. and LIZLOVS E.A. (1968) : "Anodic polarisaion of austenitic stainless steels in chloride media", Journal Electrochemical Society, 115 (11), 1130-1135.

BRINK A.B. (1983) : " The deformation characteristics of a 12% chromium steel", M.Sc thesis, University of Cape Town.

BRUNO R., TAMBA A. and BOMBARA G. (1973) : "Role of the alloying elements at the steel/rust interface", Corrosion - Nace, 29 (3), 95-99.

BRYGGMAN U. (1983) : "Abrasion Resistance of some steels related to mechanisms of gouging wear", Report UPTEC 83 22R, Uppsala University.

BRYGGMAN U., HOGMARK S. and VINGSBO O. (1979) : "Abrasive wear studied in a modified impact test machine", Proceedings of International Conference of Wear of Materials - 1979, Ludema K.C., Glaeser W.A. and Rhee S.K. (Eds), ASME, New York, 292-303.

BUCHANAN R.A., TURNER G.D., GRAY P.D., MELENDEZ J.G., TALBOT T.F. and McDONALD J.L. (1983) : "A new apparatus for synergistic studies of corrosive wear", Corrosion - Nace, 39 (9), 377-378.

BURSTEIN G.T. and ASHLEY G.W. (1984) : "Kinetics of repassivation of scratch scars generated on iron in aqueous solutions", Corrosion - Nace, 40 (3),110-115.

BURSTEIN G.T. and MARSHALL P.I. (1984) : "The coupled kinetics of film growth and dissolution of stainless steels repassivating in acid solutions", Corrosion Science, **24** (5), 449-462.

BURSTEIN G.T. ASHLEY G.W. and MARSHALL P.I. (1983) : "Reactivity of metals in aqueous solutions under conditions of abrasion", Proceedings of 36th International Conference on Industrial Water Treatment and Conditioning, Cebedeau-Liege, 53-65.

BURSTEIN G.T., ASHLEY G.W., MARSHALL P.I. and MISRA R.D.K. (1983) : "Corrosion of metals under conditions of erosive wear", Proceedings 6th International Conference on Erosion by Liquid and Solid Impact, 49/1-49/8.

CAPENDALE A.E. (1985) : "The influence of water composition on the pitting behaviour of a stainless steel", M.Sc thesis, University of Cape Town.

CHASTELL D., DOIG P., FLEWITT P.E.J., and RYAN K. (1979) : "The influence of stress on the pitting susceptibility of a 12% CrMoV martensitic stainless steel", Corrosion Science, **19** , 335-341.

CHEN W.Y.C. and STEPHENS J.R. (1979) : "Anodic polarisaion behavour of austenitic stainless steel alloys with lower chromium content", Corrosion - Nace, **35** (10), 443-451.

CIESLAK W.R. and DUQUETTE D.J. (1984) : "Properties of the passive films formed on ferritic stainless steels in Cl^- solutions", Corrosion - Nace, **40** (10), 545-550.

CONTROLLING CORROSION HANDBOOK (1978) : Committee on corrosion, Department of Industry, London.

COVINO Jnr B.S. and ROSEN M. (1984) : "Induction time studies of Fe18Cr and 430 SS under open circuit conditions in chloride-containing sulfuric acid", Corrosion - Nace, 40 (4), 140-146.

DEVINE T.M. and RITTER A.M. (1983) : "Sensitization of 12 wt pct chromium, Titanium-stabilized ferritic stainless steel", Metallurgical Transactions A, **14A** , 1721-1728.

DIESBURG D.E. and BORIK F. (1974) : "Optimising abrasion resistance and toughness in steels and irons for the mining industry", Symposium - Materials for the Mining Industry, Barr R.Q. (Ed), Climax Molybdenum Company, 15-41.

DRIVER R. and MEAKINS R.J. (1977) : "Effect of surface oxide on inhibition of acid corrosion of mild steel and pure iron", British Corrosion Journal, **12** (2), 115-117.

DUNN D.J. (1985) : "Metal removing mechanisms comprising wear in mineral processing", Proceedings of International Conference on Wear of Materials - 1985, Ludema K.C. (Ed), ASME, New York.

EL-KOUSSY R., EL-RAGHY S.M. and EL-MEHAIRY A.E. (1981) : "Effect of heat treatment conditions and composition on the wear resistance of some chromium steels", Tribology International, December, 323-328.

ELAYAPERUMAL K., DE P.K. and BALACHANDRA J. (1972) : "Passivity of type 304 stainless steel - Effect of plastic deformation", Corrosion - Nace, **28** (7), 269-273.

FLEMING J.R. and SUH N.P. (1977) : "Mechanics of crack propogation in delamination wear", Wear, **44** , 39-56.

FLOREEN S. (1982) : "An examination of chromium substitution in stainless steels", Metallurgical Transactions A, **13A** , 2003-2013.

FONTANA M.G. and GREENE N.D. (1982) : Corrosion Engineering, Series in Material Science and Engieering, 2nd Ed, McGraw-Hill, New York, 297-346.

FURZE A. (1987) : "Editorial", Journal of the South African Stainless Steel Development Association, 23 (5), 17-24.

GARRISON Jnr W.M. (1987) : "Abrasive wear resistance: The effects of ploughing and the removal of ploughed material", Wear, **114** , 239-247

GARRISON Jnr W.M. and GARRIGA R.A. (1983) : "Ductility and the abrasive wear of an ultra high strength steel", Wear, 85 , 347-360.

GLOVER G.J.(1980) : "The brittle and plastic responce of quartz", PhD thesis, University of Cape Town.

GRASSIANI M. (1978) : "The effect of cold work on the corrosion behaviour of ferrous alloys", Israel Journal of Technology, **16** , 169-175.

GREENE N.D. (1962) : "Predicting behaviour of corrosion resistant alloys by potentiostatic polarisation methods", Corrosion - Nace, **18** , 136t-142t.

GREENE N.D. and WILDE B.E. (1970) : "Variable corrosion resistance of 18Cr-8Ni stainless steels: Influence of environmental and metallurgical factors", Corrosion - Nace, **26** (12), 533-538.

HARRIS J.B. (1983) : "An investigation of wear and the performance of steels in the gold mining industry", M.Sc thesis, University of Cape Town.

HARTY B. (1988) : "Corrosion fatigue of engineering alloys", PhD thesis, University of Cape Town.

HASHIMOTO K., ASAMI K., NAKA M. and MASUMOTO T. (1979) : "The role of alloying elements in improving the corrosion resistance of amorphous iron base alloys", Corrosion Science, **19** , 857-867.

HEATHCOCK C.J. (1983) : "The influence of the sloping environment on the operation and reliability of mining machines", Internal report of the Research Organisation of the Chamber of Mines of South Africa.

HEIDEMEYER J. (1981) : "Influence of the plastic deformation of metals during mixed friction on their chemical reaction rate", Wear, **66** , 379-387.

HIGGINSON A. (1984) : "The effect of physical and chemical factors on the corrosivity of a synthetic mine water", Mintek report M140, Council for Mineral Technology, Randburg, South Africa.

HIGGINSON A. and WHITE R.T. (1983) : "A preliminary survey of the corrosivity of water in gold mines", Mintek report No M65, Council for Mineral Technology, Randburg, South Africa.

HINTERMANN H.E. and TRÜMPER G. (1967) : "188 - Zur kenntis des electrochemischen verhaltens aufgedampfter silberschichten", Helvetica Chemica Acta, **50** (7), 1819-1831.

HIRTH J.P. and RIGNEY D.A. (1976) : "Crystal plasticity and the delamination theory of wear", Wear, 39 , 133-141.

HONEYCOMBE R.W.K. (1981) : Steels - metallurgy and materials science, Edward Arnold Publishers, London.

HORNBOGEN E. (1975) : "The role of fracture toughness in the wear of metals", Wear, 33 , 251-259.

HSU K.L., AHN T.M. and RIGNEY D.A. (1980) : "Friction, wear and microstructure of unlubricated austenitic stainless steels", Wear, 60 , 13-37.

JOUGHIN N.C. (1975) : "Potential for the mechanisation of stoping in gold mines", Journal of the South African Institute for Mining and Metallurgy, **76** (6), 285-300.

JOUGHIN N.C. (1978) : "Progress in the development of mechanised stoping methods", Journal of the South African Institute for Mining and Metallurgy, **78** (8), 207-217.

KIM K.Y., BHATTACHARYYA S. and AGARWALA V. (1981) : "An electrochemical polarization technique for evaluation of wear-corrosion in moving components under stress", Proceedings of Conference on Wear of Materials - 1981, Rhee S.K., Ruff A.W. and Ludema K.C. (Eds), ASME, New York, 772-778.

KWOK C.K.S. (1982) : "Two-body, dry abrasive wear of Fe/Cr/C experimental alloys - Relationship between microstructure and mechanical properties", M.Sc thesis, University of California.

LARSEN-BASSE J. (1968) : "Influence of grit diameter and specimen size on wear during sliding abrasion", Wear, 12 , 35-53.

LARSEN-BASSE J. and TANOUYE P.A. (1978) : "Strain rate effects in low speed two-body abrasion", Journal of Lubrication Technology, 100 (4), 181-184.

LENEL U.R. and KNOTT B.R. (1986) : "Wear resistance of steels designed for use in severe abrasion-corrosion conditions", Paper presented at International Conference on Wear of Materials - 1987, Ludema K.C. (Ed), ASME, New York, 635-643

LOKHVITSKII Y.L., ANAN'EVSKII V.A., KROKHMAL Y.N., KOLESNIKOV V.M. and STEPANENKO N.M. (1979) : "Corrosion-Mechanical wear in alkali solutions", Translated from Fiziko-Khimicheskaya Mekhanika Materialov, 15 (5), 86-89, Plenum Publishing Corp., 0038-5565/79/1505-0502.

LUNARSKA E., SZKLARSKA-SMIALOWSKA Z. and JANIK-CZACHOR M. (1975) : "Susceptibility of Cr-Ni-Mn stainless steels to pitting in chloride solutions", Corrosion - Nace, 31 (7), 231-234.

MACMILLAN J.W.M. and FLEWITT P.E.J. (1975) : "Assessment of methods for cleaning oxide from fracture surfaces for examination in a scanning electron microscope", Micron, 6 , 141-146.

MARSHALL P.I. and BURSTEIN G.T. (1984) : "Effects of alloyed molybdenum on the kinetics of repassivation on austenitic stainless steels", Corrosion Science, **24** (5), 463-478.

MOKKEN A.H. (1977) : "The viability of the gold mining industry in relation to the rational use of materials of construction and protection", The Professional Engineer, Journal of Federation of Societies of Professional Engineers of South Africa, 6 (3), July 1977.

MOORE J.J., IWASAKI I., NATARAJAN K.A., PEREZ R. and ADAM K. (1984) : "The effect of grinding ball composition and mineral slurry environment on grinding media wear", IMechE, C352/84, 215-226.

MOORE M.A. (1974) : "A review of two-body abrasive wear", Wear, 27 , 1-17.

MOORE M.A. (1979) : "Energy dissipation in abrasive wear", Proceedings of International Conference on Wear of Materials - 1979, Ludema K.C., Glaeser W.A. and Rhee S.K. (Eds), ASME, New York, 636-638.

MOORE M.A. (1980) : "Abrasive Wear", Paper presented at the Fundamentals of Friction and Wear of Materials, Materials Science Seminar, American Society of Metals, Pittsburgh, Pennsylvainia.

MOORE M.A. and DOUTHWAITE R.M. (1976) : "Plastic deformation below worn surfaces", Metallurgical Transactions A, 7A , 1833-1839.

MOORE M.A., RICHARDSON R.C.D. and ATTWOOD D.G. (1972) : "The limiting strength of worn metal surfaces", Metallurgical Transactions, 3 , 2485-2491.

MORELAND P.J. and HINES J.G. (1979) : "The concept and development of corrosion monitoring", Materials Performance - Nace, Feb 1979, 65-70.

MULHEARN T.O. and SAMUELS L.E. (1962) : "The abrasion of metals: A model of the process", Wear, 5 , 478-498.

MURRAY M.J., MUTTON P.J. and WATSON J.D. (1979) : "Abrasive wear mechanisms in steels", Proceedings of International Conference on Wear of Materials - 1979, Ludema K.C., Glaeser W.A. and Rhee S.K. (Eds), ASME, New York, 257-265.

MUTTON P.J. and WATSON J.D. (1978) : "Some effects of microstructure on the abrasion resistance of metals", Wear, **48** , 385-398.

NOËL R.E.J. (1981) : "The abrasive-corrosive wear behaviour of metals", M.Sc (Eng) thesis, University of Cape Town.

NOËL R.E.J. and BALL A. (1983) : "On the synergistic effects of abrasion and corrosion during wear", Wear, 87 , 351-361.

NOËL R.E.J., ALLEN C. and BALL A. (1984) : "The development and use of in-situ and laboratory tests as a guide to the selection of materials for the gold minig industry", IMechE, C358/84, 23-28.

PEARCE J.T.H. (1983) : "The use of transmission electron microscopy to study the effects of abrasive wear on the matrix structure of a high chromium cast iron", Wear, **89** , 333-344.

PECKNER D. and BURNSTEIN I.M. (1977) : Handbook of Stainless Steels, McGraw-Hill Inc., New York.

PESSAL N. and LUI C. (1971) : "Determination of critical pitting potentials of stainless steels in aqueous chloride environments", Corrosion Science, **16** , 1987-2003.

PETERS J.A. (1983) : "A microstructural approach to alloy design for superior corrosion-abrasion wear resistance", M.Sc thesis, University of the Witwatersrand.

PICKERING F.B. (1983) : Physical metallurgy and the design of steels, Applied Science Publishers, London.

POSTLETHWAITE J. AND HAWRYLAK M.W., (1975) : "Effect of slurry abrasion on the anodic dissolution of iron in water", Corrosion - Nace, 31 (7), 237-239.

POSTLETHWAITE J., TINKER E.B. and HAWRYLAK M.W. (1974) : "Erosion-corrosion in slurry pipelines", Corrosion - Nace, 30 (8), 285-290.

POUPBAIX M. (1966) : Atlas of electrochemical equilibria in aqueous solutions, Pergamon Press, Brussels.

POWELL G.L.F. (1972) : "Wear in the mineral industry - An evaluation of research requirements", Amdel bulletin, 14 ,Oct, 9-16.

PROTHEROE B.E. (1979) : "The causes of metallic wear in hard rock mining conditions with some solutions", Paper presented at Conference on Fracture, University of Witwatersrand, Johannesburg.

PROTHEROE B.E., BALL A. and HEATHCOCK C.J. (1982) : "The development of wear resistant alloys for the South African gold mining industry", Proceedings of International Conference on Recent Developments in Speciality Steels and Hard Materials, Comins N.R. and Clarke J.B. (Eds), CSIR, Pretoria, 289-298.

PROTOPAPPAS E. (1983) : "The phase equilibria and microstructure of the dual phase steel 3CR12", M.Sc thesis, University of Cape Town.

RAWAT N.S. (1976) : "Corrosivity of underground mine atmospheres and mine waters: A review and preliminary study", British Corrosion Journal, 11 (2), 86-91.

RICE S.L., NOWOTNY H. and WAYNE S.F. (1982) : "The role of specimen stiffness in sliding and impact wear", Wear, 77 , 13-28.

RICHARDSON R.C.D (1967) : "The maximum hardness of strained surfaces and the abrasive wear of metals and alloys", Wear, 10 , 353-382.

RIGNEY D.A. and GLAESER W.A. (1977) : "Wear Resistance", Revised paper for Structural Materials and Tribology, Service Characteristics section, Bettlelle Colombus Laboratories, 597-638.

ROA B.V.N.and THOMAS G. (1980) : "Structural property relations and the design of Fe4CrC base structural steels for high strength and toughness", Metallurgical Transactions A, **11A** , 441-453.

SALESKY W.J. (1980) : "Sliding wear, toughness and microstructural relationships in high strength Fe/Cr/C experimental steels", M.Sc thesis, University of California.

SALESKY W.J. and THOMAS G. (1981): "Design of medium carbon steels for wear applications", Proceedings of Conference on Wear of Materials - 1981, Rhee S.K., Ruff A.W. and Ludema K.C. (Eds), ASME, New York, 298-305.

SALVAGO G., FUMAGALLI G. and SINIGAGLIA D. (1983) : "The corrosion behaviour of AISI 304L stainless steel in 0.1M HCl at room temperature - II The effect of cold work", Corrosion Science, **23** (5), 515-523.

SCHUMACHER W. (1985) : "Corrosion wear synergy of alloy and stainless steels", Proceedings of International Conference on Wear of Materials - 1985, Ludema K.C. (Ed), ASME, New York.

SEDRIKS A.J. (1982) : "Corrosion resistance of austeritic Fe-Cr-Ni-Mo alloys in marine environments", International Metals Review, **27** (6), 321-353.

SEDRIKS A.J. (1984) : "Metallurgical aspects of passivation of stainless steels", Paper presented at Conference on Stainless Steels, Göteburg, Sept 1984, 125-133.

SHAMSELDIN A.M., ABD EL-KADER J.M., ABD EL-WAHAB F.M., and HEGAZY H.S. (1983) : "Effect of cold work on anodic polarization of low carbon steel", Journal of Materials Science, **18** , 2732-2742.

SHETTY H.R., KOSEL T.H. and FIORE N.F. (1983) : "A study of abrasive wear mechanisms in cobalt-based alloys", Wear, **84** , 237-343.

SYMONS R. (1986) : Private Communication, Metallurg South Africa, May 1986.

TAMURA I. (1982) : "Deformation-induced martensitic transformation and transformation-induced plasticity in steels", Metal Science, **16** (5), 245-253.

THOMAS C.R. (1981) : "SX 3CR12 - a material for abrasion-corrosion control", Journal of the South African Institute of Mining and Metallurgy, October 1981.

TORRANCE A.A. (1980) : "The correlation of abrasive wear tests", Wear, 63 , 359-370.

TRUMAN J.E. (1976) : "Corrosion resistance of 13% chromium steels as influenced by tempering temperature", British Corrosion Journal, 11 (2), 92-96.

TRUMAN J.E. and PIRT K.R. (1979) : "The resistance to localised corrosion of some stainless steels", Corrosion Prevention and Control, (12), 12-22.

TURNBULL A. (1983) : "The solution composition and electrode potential in pits, crevices and cracks", Corrosion Science, 23 (8), 833-870.

UETZ H. and FÖHL J. (1979) : "Wear as an energy transformation process", Paper presented at the Fourth International Abrasion Colloquium, Grenoble: France, May 1979.

UHLIG H.H. (1979) : "Passivity in metals and alloys", Corrosion Science, 19 777-791.

UHLIG H.H. and REVIE R.W. (1985) : Corrosion and Corrosion Control, John Wiley & Sons, New York, Chap. 7.

VERHOEVEN J.D. (1975) : Fundamentals of physical metallurgy, John Wiley & Sons., New York, 287.

VINGSBO O. (1979) : "Wear and wear mechanisms", Paper presented at International Conference on Wear of Materials - 1979, Ludema K.C., Glaeser W.A. and Rhee S.K. (Eds), ASME, New York, 620-635.

VINGSBO O. and HOGMARK S. (1984) : "Single-pass pendulum grooving - a technique for abrasive testing", Wear, 100 , 489-502.

WU YANG, RUI-CHENG NI, HUI-ZHONG HUA and POURBAIX A. (1984) : "The behaviour of chromium and molybdenum in the propogation process of localized corrosion of steels", Corrosion Science, 24 (8), 691-707.

ZACKAY V.F., PARKER E.R., FAHR D.and BUSCH R. (1967) : "The enhancement of ductility in high-strength steels", Transactions of the ASM, **60** , 252-259.

ZUM-GAHR K.H. (1981/1982) : "Formation of wear debris by the abrasion of ductile metals", Wear, **74** , 353-373.

ZUM-GAHR K.H. and DOANE D.V. (1980): "Optimizing fracture toughness and abrasion resistance in white cast irons", Metallurgical Transaction A, **11A** , 613-620.

APPENDIX

CALCULATED M_s AND M_d TEMPERATURES FOR THE EXPERIMENTAL ALLOYS

A number of empirical equations are available to predict the temperature at which austenite will start to transform to martensite on cooling (M_s). These all use weight per cent element content as parameters but are generally only applicable over a limited range.

$$M_s\ (°C) = 502 - 810C - 1230N - 13Mn - 30Ni - 12Cr - 54Cu - 46Mo$$

(ref. Pickering, 1983; based on austenitic stainless steels)

$$M_s\ (°C) = 539 - 423C - 30.4Mn - 17.7Ni - 12.1Cr - 7.5Mo$$

(ref. Andrews, cited Honeycombe, 1981; based on carbon and alloyed steels)

$$M_s\ (°C) = 561 - 474C - 33Mn - 17Ni - 17Cr - 21Mo$$

(ref. Steven and Haynes, cited Verhoeven, 1975; based on low alloyed steels)

$$M_s\ (°C) = 659 - 474C - 23Cr - 30Ni$$

(ref. Peters, 1983; adapted for quaternary alloys)

The Andrews equation is favoured by the martensitic experimental alloys since Peters has left out the contribution of Mn. The low carbon, highly alloyed austenitics are covered by the Pickering equation. Pickering (1983) also gave a formula for the temperature below which martensite will form on undergoing 30% plastic deformation (M_{d30}) again based on austenitic stainless steels.

$$M_{d30}\ (°C) = 497 - 462(C+N) - 9.2Si - 8.1Mn - 13.7Cr - 20Ni - 18.1Mo$$

TABLE A1 : Predicting the M_S temperature

MATERIAL	MEASURED M_S (°C)	CALCULATED M_S (°C)			
		PICKERING	ANDREWS	STEVEN	PETERS
Quatough	338	172	302	284	424
WA	288	114	294	272	286
WB	220	72	253	214	211
WC	234	108	266	215	228
WD	179	-135	161	82	114
UA	272	90	267	236	251
T820A	357	222	331	303	388
T820B	768	222	331	303	389
T102A	392	196	304	265	337
T102B	346	187	300	260	332
T122	361	162	274	224	283
3CR12	456	291	347	310	360
3CR12Ni	389	268	339	300	332
WV69	420	242	335	296	303
F350		- 35	8		310
F351		- 58	- 16		264
F352		- 32	45		264
F353		6	136		264
WSA6			268		266
WA2			285		274
WB2			242		196
ID			240		226
IF			215		180
Nit60		-425			
AISI 316		-199			
NP 599		-131			
AISI 304		- 53			
AISI 304L		- 34			
AISI 431		75	195		

CALCULATION OF COST FACTORS FOR EXPERIMENTAL ALLOYS

The cost factor is the sum of the cost of the alloying elements that make up the final chemical composition as analysed. Losses during melting and all fabrication costs are not considered. The alloy prices are based on Ferro alloy concentrates except for iron, nickel and copper which is based on market price for clean scrap (Symons, 1986). Naturally the prices change with market forces.

TABLE A2 : Retail price (Rands) for alloying elements per kilogram content (Symons, May 1986).

SCRAP	PRICE per kg
Steel, mild	0.18
Nickel	10.45
Copper	3.60
Aluminium	2.80
FERRO-ALLOY	**PRICE per kg**
Chrome (LC)	3.26
Chrome (HC)	2.20
Silicon	2.22
Molybdenum	25.36
Manganese (HC)	1.08
Manganese (MC)	1.98
Tungsten	53.40
Niobium	43.16
Titanium	15.60

COMPOSITE TABLE OF WEAR TEST RESULTS

The Table A3 overleaf includes all the materials in their heat treated conditions that are covered in this dissertation. Where more than one result was available from repeat tests, only the most representative or mean value is tabulated. Zero values and gaps mean either no information is available, no test results were obtained or, for some of the corrosion results, a weight loss of zero was recorded. Only the results from tests conducted under standardized conditions are tabulated. Tables A4, A5 and A6 are the materials classified with respect to Toughness and Tables A7 and A8 with respect to Cost Factor and all ranked according to their relative resistance to wear.

TABLE A3 : Material wear results (c.f. Table 3.5 for description of heat treatment codes)

No.	MATERIAL AND CONDITION	HARDNESS HV30 L	HARDNESS HV30 T	TOUGHNESS CHARPY(J) L	TOUGHNESS CHARPY(J) T	CHEMICAL COMPOSITION %C	CHEMICAL COMPOSITION %Cr	MICROSTR ORIGIN DENSITY	RAR abr	RAR RAR	RWRL abr	RWRL corr	RWRL RWRL	RWRL#2 abr	RWRL#2 corr	RWRL#2 RWRL#2
1	070M20	143	149	0.0	119.0	.15	.02	1K 7.86	.0097	1.00	.0099	.0693	1.00	.0398	.0662	1.00
2	835M30	0	530	0.0	55.0	.34	1.35	1P 7.83	.0055	1.72	.0067	.0496	1.41	.0309	.0470	1.35
3	SS10/200	775	0	0.0	2.0	.42	.02	1P 7.83	.0065	1.49	.0068	.0556	.94	.	.	0.00
4	ABRASALLOY	433	436	0.0	25.0	.39	.43	1P 7.85	.0069	1.36	.0071	.0759	1.06	.0375	.0498	1.21
5	WEARALLOY4	461	406	0.0	66.0	.21	.02	1P 7.85	.0070	1.34	.0071	.0611	1.16	.	.	0.00
6	AISI 304L	245	206	0.0	178.0	.04	18.80	5S 7.90	.0073	1.29	.0070	.0002	11.02	.0371	.	2.86
7	AISI 316	0	210	0.0	172.0	.08	16.60	5S 7.90	.0069	1.36	.0071	.0002	10.81	.	.	0.00
8	AISI 431	0	496	0.0	72.0	.16	16.14	2S 7.70	.0068	1.56	.0056	.0003	13.48	.0292	.	3.75
9	AISI 440B	0	648	0.0	5.0	.88	17.45	7S 7.80	.0046	2.27	.0045	.0016	12.92	.	.	0.00
10	QUATOUGHar	0	285	41.6	31.1	.30	4.00	1T 7.80	.0082	1.19	.0126	.0569	1.27	.	.	0.00
11	QUATOUGH T	0	546	0.0	47.6	.30	4.00	1T 7.80	.0054	1.73	.0105	.0579	1.29	.0292	.0311	1.75
12	WA ar	527	514	0.0	22.8	.24	7.08	4W 7.80	.0061	1.54	.0073	.0076	3.11	.	.	0.00
13	WA iv	470	473	0.0	48.8	.24	7.08	4W 7.80	.0068	1.38	.0079	.0120	2.40	.	.	0.00
14	WA vi	540	543	0.0	67.5	.24	7.08	4W 7.80	.0058	1.61	.0058	.0083	3.21	.0246	.0088	3.15
15	WA viii	459	561	0.0	62.5	.24	7.08	4W 7.80	.0053	1.78	.0063	.0063	3.71	.	.	0.00
16	WB ar	614	606	0.0	11.3	.24	10.30	4W 7.80	.0051	1.85	.0063	.0037	4.63	.	.	0.00
17	WB vi	573	575	0.0	27.0	.24	10.30	4W 7.80	.0048	1.95	.0040	.0009	10.12	.0210	.	5.11
18	WB viii	594	602	0.0	26.0	.24	10.30	4W 7.80	.0045	2.07	.0047	.0008	9.02	.	.	0.00
19	WC ar	606	618	0.0	7.0	.25	12.30	4W 7.80	.0057	1.66	.0052	.0004	8.86	.	.	0.00
20	WC vi	614	639	0.0	16.0	.25	12.30	4W 7.80	.0048	2.01	.0042	.0001	11.53	.	.	0.00
21	WC viii	610	610	0.0	15.5	.25	12.30	4W 7.80	.0057	1.97	.0049	.0002	10.40	.	.	0.00
22	WD ar	680	705	0.0	8.0	.43	12.20	7W 7.80	.0054	1.78	.0051	.0022	4.91	.	.	0.00
23	WD i	462	465	0.0	11.0	.43	12.20	7W 7.80	.0061	1.53	.0061	.0032	5.73	.	.	0.00
24	WA2 ar	554	550	0.0	18.0	.26	7.18	4W 7.80	.0066	1.81	.0076	.0100	2.82	.	.	0.00
25	WA2 AC	435	514	0.0	27.0	.26	7.18	4W 7.80	.0071	1.70	.0064	.0112	2.53	.	.	0.00
26	WA2 200	546	508	0.0	56.0	.26	7.18	4W 7.80	.0071	1.70	.0078	.0091	2.93	.0245	.0079	3.25
27	WA2 300	503	467	0.0	61.0	.26	7.18	4W 7.80	.0085	1.41	.0085	.0094	2.77	.	.	0.00
28	WA2 400	484	459	0.0	50.0	.26	7.18	4W 7.80	.0080	1.51	.0067	.0102	2.62	.	.	0.00
29	WA2 500	456	454	0.0	35.0	.26	7.18	4W 7.80	.0075	1.60	.0090	.0125	2.31	.	.	0.00
30	WA2 600	268	289	0.0	141.0	.26	7.18	4W 7.80	.0093	1.29	.0112	.0171	1.75	.	.	0.00
31	WB2 ar	604	602	0.0	13.0	.27	10.40	4W 7.80	.0056	1.88	.0046	.0052	5.05	.	.	0.00
32	WB2 AC	412	631	0.0	10.0	.27	10.40	4W 7.80	.0056	1.88	.0058	.0050	4.88	.	.	0.00
33	WB2 200	509	554	0.0	47.0	.27	10.40	4W 7.80	.0057	1.85	.0052	.0025	6.43	.0261	.0008	3.91
34	WB2 300	491	484	0.0	52.0	.27	10.40	4W 7.80	.0068	1.55	.0061	.0030	5.44	.	.	0.00
35	WB2 400	472	499	0.0	66.0	.27	10.40	4W 7.80	.0070	1.50	.0062	.0033	5.21	.	.	0.00
36	WB2 500	425	523	0.0	24.0	.27	10.40	4W 7.80	.0065	1.62	.0061	.0050	4.46	.	.	0.00
37	WB2 600	299	321	0.0	126.0	.27	10.40	4W 7.80	.0088	1.20	.0067	.0062	3.32	.	.	0.00
38	WBA6 ar	550	547	0.0	12.0	.25	8.00	4W 7.80	.0075	1.42	.0064	.0076	3.54	.	.	0.00
39	WBA6 200	532	511	0.0	34.0	.25	8.00	4W 7.80	.0057	1.65	.0069	.0073	3.49	.0251	.0043	3.58
40	IA DQ	350	336	0.0	5.0	.12	6.00	3I 7.80	.0076	1.29	.0083	.0133	2.30	.0360	.0141	2.10
41	IA 200	320	334	0.0	10.0	.12	6.00	3I 7.80	.0076	1.29	.0079	.0149	2.18	.0409	.0179	1.79
42	IA 300	354	337	0.0	10.0	.12	6.00	3W 7.80	.0071	1.48	.0103	.0259	1.37	.	.	0.00
43	IA 600	300	297	0.0	22.0	.12	6.00	3I 7.80	.0089	1.19	.0110	.0200	1.60	.	.	0.00
44	IB	503	493	0.0	52.0	.14	8.71	4I 7.80	.0062	1.56	.0065	.0016	6.70	.0220	.	4.79
45	IC	502	518	0.0	59.0	.18	9.00	4I 7.80	.0061	1.58	.0060	.0019	6.94	.0230	.0072	3.49
46	ID DQ	620	675	0.0	6.0	.23	9.06	4I 7.80	.0061	1.72	.0066	.0242	1.51	.	.	0.00
47	ID 200	562	554	0.0	27.0	.23	9.06	4I 7.80	.0067	1.59	.0062	.0068	3.31	.0278	.0010	3.66
48	ID 300	503	493	0.0	36.0	.23	9.06	4I 7.80	.0072	1.48	.0067	.0097	3.02	.	.	0.00
49	ID 600	523	381	0.0	4.0	.23	9.06	4I 7.80	.0086	1.24	.0062	.0288	1.34	.	.	0.00
50	IE 300	520	502	0.0	36.0	.20	10.40	4I 7.80	.0057	1.85	.0059	.0004	7.87	.0254	.0004	4.38

TABLE A3 (conti) : Material wear results

No.	MATERIAL AND CONDITION	HARDNESS HV30 L	HARDNESS HV30 T	TOUGHNESS CHARPY(J) L	TOUGHNESS CHARPY(J) T	CHEMICAL COMPOSITION %C	CHEMICAL COMPOSITION %Cr	MICROSTR ORIGIN DENSITY	RAR abr	RAR RAR	RWRL abr	RWRL corr	RWRL RWRL	RWRL#2 abr	RWRL#2 corr	RWRL#2 RWRL#2
51	IF QQ	570	602	0.0	5.0	.22	10.80	4I 7.80	.0057	1.85	.0046	.0015	8.13	.	.	0.00
52	IF 200	524	561	0.0	25.0	.22	10.80	4I 7.80	.0051	2.07	.0055	.0011	7.51	.0253	.	4.18
53	IF 300	483	490	0.0	36.0	.22	10.80	4I 7.80	.0067	1.59	.0061	.0008	7.19	.	.	0.00
54	820A AQ200	465	470	0.0	57.3	.20	7.66	4T 7.80	.0070	1.72	.0081	.0075	3.18	.0282	.0051	3.16
55	820A AHR1	465	470	0.0	50.3	.20	7.66	4T 7.80	.0059	1.60	.0064	.0105	2.93	.0278	.0025	3.48
56	820A AHR1T	459	452	0.0	67.7	.20	7.66	4T 7.80	.0062	1.51	.0056	.0110	2.99	.	.	0.00
57	820A AHR2	476	478	0.0	53.0	.20	7.66	4T 7.80	.0055	1.71	.0079	.0189	1.85	.	.	0.00
58	820B AQ200	457	457	0.0	62.0	.20	7.61	4T 7.80	.0077	1.56	.0057	.0065	4.06	.0281	.0019	3.51
59	820B AHR1	406	470	0.0	48.7	.20	7.61	4T 7.80	.0076	1.59	.0087	.0158	2.02	.	.	0.00
60	820B AHR1T	473	454	0.0	69.0	.20	7.61	4T 7.80	.0078	1.54	.0099	.0127	2.19	.0268	.0102	2.85
61	820B AHR2	470	459	0.0	52.0	.20	7.61	4T 7.80	.0070	1.71	.0076	.0107	2.71	.0300	.0027	3.22
62	820B AHR2T	467	457	0.0	70.2	.20	7.61	4T 7.80	.0077	1.56	.0076	.0081	3.16	.	.	0.00
63	102A AQ200	520	502	0.0	64.3	.20	9.85	4T 7.80	.0053	1.77	.0060	.0010	7.08	.0233	.0005	4.42
64	102A AHR1	517	511	0.0	34.5	.20	9.85	4T 7.80	.0066	1.81	.0069	.0135	2.43	.	.	0.00
65	102A AHR1T	451	462	0.0	92.5	.20	9.85	4T 7.80	.0075	1.59	.0084	.0052	3.65	.0285	.0061	3.04
66	102B AHR1	481	540	0.0	38.5	.21	9.86	4T 7.80	.0063	1.90	.0069	.0048	4.24	.	.	0.00
67	102B AHR1T	505	511	0.0	91.1	.21	9.86	4T 7.80	.0072	1.66	.0077	.0052	3.34	.0283	.0050	3.16
68	122 AQ200	470	490	0.0	57.5	.21	12.00	4T 7.80	.0068	1.76	.0056	.0018	6.70	.0252	.0012	3.99
69	122 AHR1	504	550	0.0	25.7	.21	12.00	4T 7.80	.0060	1.30	.0058	.0007	7.63	.	.	0.00
70	122 AHR1T	499	481	0.0	64.3	.21	12.00	4T 7.80	.0072	1.68	.0060	.0012	6.89	.0280	.0007	3.67
71	F350	0	223	40.0	0.0	.05	10.00	5F 7.80	.0057	1.69	.0061	.	11.11	.0213	.	4.97
72	F351	0	225	40.0	0.0	.05	12.00	5F 7.80	.0056	1.71	.0040	.	14.90	.0213	.	4.94
73	F352	0	230	40.0	0.0	.05	12.00	5F 7.80	.0058	1.68	.0050	.0001	11.59	.0186	.0011	5.35
74	F353	0	465	40.0	0.0	.05	12.00	5F 7.80	.0059	1.63	.0053	.0004	10.44	.0154	.0064	4.83
75	3CR12 ar	143	153	0.0	80.0	.02	11.33	3M 7.74	.0094	1.03	.0089	.0030	7.41	.	.	0.00
76	3CR12 HT	228	250	0.0	75.5	.02	11.33	3M 7.74	.0077	1.23	.0066	.0013	8.96	.0453	.	2.33
77	3CR12Ni HT	0	308	270.7	159.0	.03	11.71	3M 7.74	.0087	1.08	.0082	.0003	10.43	.0436	.	2.45
78	WV69 ar	0	413	90.0	0.0	.07	12.00	4W 7.80	.0072	1.33	.0066	.0001	13.07	.	.	0.00
79	WV69 200	0	379	175.0	0.0	.07	12.00	4W 7.80	.0057	1.66	.0076	.0034	8.01	.0370	.	2.87
80	UA 200	0	559	0.0	78.5	.23	8.65	4U 7.80	.0045	2.10	.0056	.0116	4.62	.0227	.0160	4.33
81	NP599 ann	0	206	0.0	107.0	.10	16.30	5B 7.70	.0068	1.42	.0116	.0004	6.80	.0227	.0016	4.33
82	NITRONIC60	0	231	0.0	40.0	.10	17.00	5B 7.62	.0079	1.22	.0132	.0005	5.80	.	.	0.00
83	NP599 cw	0	313	0.0	87.0	.10	16.00	5B 7.64	.0070	1.37	.	.	0.00	.	.	0.00

L = longitudinal orientation of specimen to rolling direction
T = transverse orientation of specimen to rolling direction
%C = weight per cent carbon
%Cr = weight per cent chromium
abr = accumulative gram weight loss for abrasion portion
corr = accumulative gram weight loss for corrosion portion
RAR = Relative Abrasion Resistance
RWRL = Relative Abrasive-Corrosive Wear Resistance (Lab)
RWRL#2 = Relative Abrasive-Corrosive Wear Resistance (alternative test conditions)

TABLE A4 : Materials classified with respect to toughness and ranked according to their dry Relative Abrasion Resistance (RAR) (c.f. TABLE 4.9)

R.A.R

ROW
1 Z
2 1.8
3 1.6
4 1.4
5 0

TOUGHNESS

COLUMN
A 80
B 60
C 40
D 20
E 0

	A	B	C	D	E
1		UA 200 2.1 78.5		IF 200 2.07 25	AISI 440B 2.27 5
				WB viii 2.07 26	WC vi 2.01 16
2			WB2 200 1.85 47	WB vi 1.95 27	WC viii 1.97 15.5
				102B AHR1 1.9 38.5	WB2 AC 1.88 10
				IE 300 1.85 36	WB2 ar 1.88 15
				WSA6 200 1.85 34	IF OQ 1.85 5
				102A AHR1 1.81 34.5	WB ar 1.85 11.3
					WA2 ar 1.81 18
3	WV69 200 1.66 175	WA viii 1.78 62.5	122 AQ200 1.76 57.5	WA2 AC 1.7 27	WD ar 1.78 8
	102B AHR1T 1.66 91.1	102A AQ200 1.77 64.3	QUATOUGH T 1.73 47.6	WB2 500 1.62 24	ID OQ 1.72 6
		122 AHR1T 1.68 64.3	820A AQ200 1.72 57.5	WA2 500 1.6 35	WC ar 1.66 7
		WA vi 1.61 67.5	835M30 1.72 55		
			F351 1.71 40		
			820B AHR2 1.71 52		
			820A AHR2 1.71 53		
			WA2 200 1.7 56		
			F350 1.69 40		
			F352 1.68 40		
			F353 1.63 40		
			820A AHR1 1.6 50.3		
4	102A AHR1T 1.59 92.5	820B AHR2T 1.56 70.2	820B AHR1 1.59 48.7	IF 300 1.59 36	WD i 1.53 11
	NP599 ann 1.42 107	820B AQ200 1.56 62	IC 1.58 59	ID 200 1.59 27	SS10 200 1.49 2
		AISI 431 1.56 72	IB 1.56 52	WA ar 1.54 22.8	IA 300 1.48 10
		820B AHR1T 1.54 69	WB2 300 1.55 52	122 AHR1 1.5 25.7	WSA6 ar 1.42 12
		820A AHR1T 1.51 67.9	WA2 400 1.51 50	ID 300 1.48 36	
		WB2 400 1.5 66			
		WA2 300 1.41 61			
5	NP599 cw 1.37 87	WEARALLOY4 1.34 66	WA iv 1.38 48.8	ABRASALLOY 1.36 25	IA 200 1.39 10
	AISI 316 1.36 172	3CR12 HT 1.23 75.5	NITRONIC60 1.22 40	IA 600 1.19 22	IA OQ 1.39 5
	WV69 ar 1.33 90			QUATOUGHar 1.19 31.1	ID 600 1.24 4
	WA2 600 1.29 141				
	AISI 304L 1.29 178				
	WB2 600 1.2 126				
	3CR12Ni HT 1.08 159				
	3CR12 ar 1.03 80				
	070M20 1 119				

TABLE A5 : Materials classified with respect to toughness and ranked according to their Corrosive-Abrasive Wear Resistance (RWRL) where the emphasis is on corrosion of an abraded surface (c.f. TABLE 4.10)

R.W.R.L

ROW

1	11
2	7
3	4
4	2
5	0

TOUGHNESS

COLUMN

A	80
B	60
C	40
D	20
E	0

	A			B			C			D			E		
1	WV69 ar	13	90	AISI 431	13.4	72	F351	14.9	40				AISI 440B	12.9	5
	AISI 304L	11	178				F352	11.5	40				WC vi	11.5	16
							F350	11.1	40						
2	AISI 316	10.8	172	3CR12 HT	8.9	75.5	F353	10.4	40	WB vi	10.1	27	WC viii	10.4	15.5
	3CR12Ni HT	10.4	159	102A AQ200	7	64.3				WB viii	9	26	WC ar	8.8	7
	WV69 200	8	175							IE 300	7.8	36	IF OQ	8.1	5
	3CR12 ar	7.4	80							122 AHR1	7.6	25.7			
										IF 200	7.5	25			
										IF 300	7.1	36			
3	NP599 ann	6.8	107	122 AHR1T	6.8	64.3	IC	6.9	59	WB2 500	4.4	24	WD i	5.7	11
				WB2 400	5.2	66	122 AQ200	6.7	57.5	102B AHR1	4.2	38.5	WB2 ar	5	15
				UA 200	4.6	78.5	IB	6.7	52				WD ar	4.9	8
				820B AQ200	4	62	WB2 200	6.4	47				WB ar	4.6	11.3
							NITRONIC60	5.8	40				WB2 AC	4.5	10
							WB2 300	5.4	52						
4	102B AHR1T	3.8	91.1	WA viii	3.7	62.5	820A AQ200	3.1	57.5	WSA6 200	3.4	34	WSA6 ar	3.5	12
	102A AHR1T	3.6	92.5	WA vi	3.2	67.5	820A AHR1	2.9	50.3	ID 200	3.3	27	WA2 ar	2.8	18
	WR2 600	3.3	126	820B AHR2T	3.1	70.2	WA2 200	2.9	56	WA ar	3.1	22.8	IA OQ	2.3	5
				820A AHR1T	2.9	67.9	820B AHR2	2.7	52	ID 300	3	36	IA 200	2.1	10
				WA2 300	2.7	61	WA2 400	2.6	50	WA2 AC	2.5	27			
				820B AHR1T	2.1	69	WA iv	2.4	48.8	102A AHR1	2.4	34.5			
							820B AHR1	2	48.7	WA2 500	2.3	35			
5	WA2 600	1.7	141	WEARALLOY4	1.1	66	820A AHR2	1.8	53	IA 600	1.6	22	ID OQ	1.5	6
	070M20	1	119				835M30	1.4	55	QUATOUGHar	1.2	31.1	IA 300	1.3	10
							QUATOUGH T	1.2	47.6	ABRASALLOY	1	25	ID 600	1.3	4
													SS10 200	.9	2

TABLE A6 : Materials classified with respect to toughness and ranked according to their Resistance to Abrasive- Corrosive Wear (RWRL #2). The emphasis is on abrasion resistance coupled with a resistance to corrosion (c.f. TABLE 4.11)

R.W.R.L #2

ROW

1	4
2	3.5
3	3
4	2
5	0

TOUGHNESS

COLUMN

A	80
B	60
C	40
D	20
E	0

	A	B	C	D	E
1	NP599 ann 4.33 107	102A AQ200 4.42 64.3	F352 5.35 40	WB vi 5.11 27	
		UA 200 4.33 78.5	F350 4.97 40	IF 200 4.18 25	
			F351 4.94 40	IE 300 4.08 36	
			F353 4.83 40		
			IB 4.79 52		
2		AISI 431 3.75 72	122 AQ200 3.99 57.5	ID 200 3.66 27	
		122 AHR1T 3.67 64.3	W82 200 3.91 47	WSA6 200 3.58 34	
		820B AQ200 3.51 62			
3	102B AHR1T 3.16 91.1	WA vi 3.15 67.5	IC 3.49 59		
	102A AHR1T 3.04 92.5		820A AHR1 3.48 50.3		
			WA2 200 3.25 56		
			820B AHR2 3.22 52		
			820A AQ200 3.16 57.5		
4	AISI 304L 2.88 178	820B AHR1T 2.85 69			IA 00 2.1 5
	WV69 200 2.87 175	3CR12 HT 2.33 75.5			
	3CR12Ni HT 2.45 159				
5	070M20 1 119		QUATOUGH T 1.75 47.6	ABRASALLOY 1.21 25	IA 200 1.79 10
			835M30 1.35 55		

TABLE A7 : Classification with respect to the cost factor of the materials and ranked according to dry abrasion resistance, RAR (c.f. TABLE 4.13)

R.W.R.L

COST FACTOR

ROW	
1	11
2	7
3	4
4	2
5	0

COLUMN	
A	0
B	400
C	600
D	800
E	1000

	A	B	C	D	E
1			F351 14.9 720	AISI 431 13.4 910	AISI 440B 12.9 1030
			MV69 ar 13 700		AISI 304L 11 1690
			F352 11.5 690		
			MC vi 11.5 660		
			F350 11.1 660		
2		122 AHR1 7.6 560	F353 10.4 630	MB vi 10.1 830	AISI 316 10.8 2350
		102A AQ200 7 510	3CR12Ni HT 10.4 710	MB viii 9 830	IF OQ 8.1 1250
			MC viii 10.4 660		IF 200 7.5 1250
			3CR12 HT 8.9 640		IF 300 7.1 1250
			MC ar 8.8 660		
			MV69 200 8 700		
			IE 300 7.8 760		
			3CR12 ar 7.4 640		
3		122 AHR1T 6.8 560	IC 6.9 680	MB2 200 6.4 830	NP599 ann 6.8 1050
		122 AQ200 6.7 560		MB2 300 5.4 830	IB 6.7 1020
		102B AHR1 4.2 500		MB2 400 5.2 830	NITRONIC60 5.8 1790
		820B AQ200 4 430		MB2 ar 5 830	MD i 5.7 1170
				MB ar 4.6 830	MD ar 4.9 1170
				UA 200 4.6 810	
				MB2 AC 4.5 830	
				MB2 500 4.4 830	
4		102B AHR1T 3.8 500	MA viii 3.7 720	MB2 600 3.3 830	ID 200 3.3 1140
		102A AHR1T 3.6 510	MSA6 ar 3.5 760		ID 300 3 1140
		820A AQ200 3.1 470	MSA6 200 3.4 760		
		820B AHR2T 3.1 430	MA vi 3.2 720		
		820A AHR1T 2.9 470	MA ar 3.1 720		
		820A AHR1 2.9 470	MA2 200 2.9 730		
		820B AHR2 2.7 430	MA2 ar 2.8 730		
		102A AHR1 2.4 510	MA2 300 2.7 730		
		IA OQ 2.3 450	MA2 400 2.6 730		
		820B AHR1T 2.1 430	MA2 AC 2.5 730		
		IA 200 2.1 450	MA iv 2.4 720		
		820B AHR1 2 430	MA2 500 2.3 730		
5	QUATOUGH T 1.2 340	820A AHR2 1.8 470	MA2 600 1.7 730		ID OQ 1.5 1140
	QUATOUGHar 1.2 340	IA 600 1.6 450	835M30 1.4 680		ID 600 1.3 1140
	WEARALLOY4 1.1 210	IA 300 1.3 450			
	ABRASALLOY 1 310				
	070M20 1 190				
	S510 200 .9 230				

TABLE A8 : Classification with respect to the cost factor of the materials and ranked according to the corrosive- abrasive wear resistance, RWRL (c.f. TABLE 4.14)

R.A.R

ROW	
1	1.9
2	1.7
3	1.5
4	1.3
5	0

COST FACTOR

COLUMN	
A	0
B	400
C	600
D	800
E	1000

	A	B	C	D	E
1		102B AHR1 1.9 500	WC vi 2.01 660	UA 200 2.1 810	AISI 440B 2.27 1030
			WC viii 1.97 660	WB viii 2.07 830	IF 200 2.07 1250
				WB vi 1.95 830	
2	QUATOUGH T 1.73 340	102A AHR1 1.81 510	IE 300 1.85 760	WB2 AC 1.88 830	IF QQ 1.85 1250
		102A AQ200 1.77 510	WSA6 200 1.85 760	WB2 ar 1.88 830	WD ar 1.78 1170
		122 AQ200 1.76 560	WA2 ar 1.81 730	WB2 200 1.85 830	ID QQ 1.72 1140
		820A AQ200 1.72 470	WA viii 1.78 720	WB ar 1.85 830	
		820B AHR2 1.71 430	B35M30 1.72 680		
		820A AHR2 1.71 470	F351 1.71 720		
			WA2 200 1.7 730		
			WA2 AC 1.7 730		
3		122 AHR1T 1.68 560	F350 1.69 660	WB2 500 1.62 830	IF 300 1.59 1250
		102B AHR1T 1.66 500	F352 1.68 690	AISI 431 1.56 910	ID 200 1.59 1140
		820A AHR1 1.6 470	WV69 200 1.66 700	WB2 300 1.55 830	IB 1.56 1020
		102A AHR1T 1.59 510	WC ar 1.66 660	WB2 400 1.5 830	WD i 1.53 1170
		820B AHR1 1.59 430	F353 1.63 630		
		820B AHR2T 1.56 430	WA vi 1.61 720		
		820B AQ200 1.56 430	WA2 500 1.6 730		
		820B AHR1T 1.54 430	IC 1.58 680		
		820A AHR1T 1.51 470	WA ar 1.54 720		
		122 AHR1 1.5 560	WA2 400 1.51 730		
4	SS10 200 1.49 230	IA 300 1.48 450	WSA6 ar 1.42 760		ID 300 1.48 1140
	ABRASALLOY 1.36 310	IA 200 1.39 450	WA2 300 1.41 730		NP599 ann 1.42 1050
	WEARALLOY4 1.34 210	IA QQ 1.39 450	WA iv 1.38 720		NP599 cw 1.37 1050
			WV69 ar 1.33 700		AISI 316 1.36 2350
5	QUATOUGHar 1.19 340	IA 600 1.19 450	WA2 600 1.29 730	WB2 600 1.2 830	AISI 304L 1.29 1690
	070M20 1 190		3CR12 HT 1.23 640		ID 600 1.24 1140
			3CR12Ni HT 1.08 710		NITRONIC60 1.22 1790
			3CR12 ar 1.03 640		

Note to readers

As a consequence of this and other studies certain steels have been produced in greater quantities and are presently under reveiw by COMRO for wide scale application in the gold mines of South Africa.

The materials made available to the author and presented herein have, in most cases, originated from 50 kg experimental melts. Since then the industrial melts have been produced and material designations have been standardised. I have used the original material designation (for example : 351) and prefix it with the supplier (in this case Fulmer) so that F351 is what is now refered to as 1210.

It would not be entirely correct to rename the early laboratory melts with the present industrial melt designation because of the small differences in chemical composition and method of fabrication. These differences have influenced the microstructure and properties. The table below presents the old and new names with their corresponding chemical compositions.

TABLE A9 : Comparison of the experimental alloyed steels presented in this thesis with their corresponding industrial scale melts

MATERIAL DESIGNATION		CHEMICAL COMPOSITION							MECHANICAL PROPERTIES			HEAT TREATED CONDITION
THESIS	COMRO	C	Mn	Si	Cr	Ni	Mo	N	HV	CJ	RAR	
UA 200	825	.25 .23	.02 .35	.03 .32	8.0 8.65	3.0 3.33	.01 .02	- -	530 559	63 78	1.8 2.1	1100°0Q T200° 1100°0Q T200°
T102A	102A	.20 .20	1.0 1.01	.018 .018	10.0 9.85	.007 .007			513 462	57 92	2.0 1.6	1100°0Q T200° AHR(1) T200°
T122	122	.20 .20	1.00 1.00	.018 .018	12.0 12.0	.008 .08			513 481	57 64	1.5 1.7	1100°0Q T200° AHR(1) T200°
F351	1210	.10 .05	10.0 10.0		12.0 12.0			.17 .2	500 225	150 ?	1.6 1.7	as rolled annealed
IB	927	.15 .14	.6 .7	.2	9.0 8.71	2.0 1.93	.07 .01		478	52	1.5	unknown unknown

AUG 1988